Adaptive Hand Neuroprosthesis Using Inertial Sensors for Real-Time Motion Tracking

vorgelegt von
Christina Salchow-Hömmen
M. Sc.
ORCID: 0000-0001-5527-9895

an der Fakultät IV - Elektrotechnik und Informatik
der Technischen Universität Berlin
zur Erlangung des akademischen Grades

Doktorin der Ingenieurwissenschaften
-Dr.-Ing.-

genehmigte Dissertation

Promotionsausschuss:

Vorsitz:	Prof. Dr. Benjamin Blankertz
Gutachter*innen:	Prof. Dr.-Ing. Jörg Raisch
	Prof. Dr. Alessandra Pedrocchi
	Dr. Thierry Keller

Tag der wissenschaftlichen Aussprache: 17. Januar 2020

Berlin 2020

Abstract

People suffering from upper limb impairments after a stroke or spinal cord injury are not only restricted in their independence but also in their inclusion in professional and social life. The increasing number of patients and the resulting rise in timely and monetary rehabilitation expenses lead to strong demands for new, effective therapies. Neuroprostheses based on functional electrical stimulation (FES) have been found to influence motor recovery positively. Electrical pulses are applied to peripheral nerves in the forearm and hand to generate functional hand motions. However, noninvasive hand neuroprostheses (HNPs) for rehabilitation face several challenges in clinical practice. The limited selectivity of transcutaneous FES yields difficulties in achieving fine hand movements by stimulating the muscle-rich forearm. Inter-subject variability in neuroanatomy and tolerance of the FES make an individual adjustment of spatial and temporal stimulation parameters obligatory. Furthermore, strategies are required for a quick and easy adaptation of stimulation parameters in real-time, as the neuromuscular system is subject to time-variant changes.

In this thesis, new concepts and methods are presented on the road to a novel, adaptive HNP based on automation, closed-loop control, and user-centered design. The HNP features a new, modular hand sensor system for accurate real-time motion tracking of FES-induced movements. In contrast to glove-based approaches, the proposed solution maintains the sense of touch. Algorithms for measuring segment orientations, wrist and finger joint angles, and fingertip positions from up to 17 micro inertial sensors were developed for application in patients with severe motor impairment of the hand. The methods avoid extensive calibration movements performed by the patients and work robustly in magnetically disturbed environments, i.e., indoors. The sensor system was evaluated with four healthy subjects in different validation settings before it was applied in clinical studies.

Selective and individual stimulation of hand motion was assured by utilizing electrode arrays for the HNP together with user-centered identification strategies. An effective search for suitable virtual electrodes, formed by multiple, active array elements, is essential for clinical acceptance and practicability of HNPs. Semi-automatic and automatic methods for identifying stimulation positions and intensities were developed, realizing different levels of user integration. The semi-automatic approach allows caregivers to continuously modify virtual electrodes via a touchscreen while the stimulation intensities are automatically controlled to achieve desired wrist extension. Both identification methods were evaluated in five stroke survivors and yield suitable stimulation setups for hand opening and closing in patients who could tolerate the FES, with the semi-automatic approach being 25% faster than the automatic.

A static parameter setup throughout a therapy session does not account for changes in the muscular response. For example, the rotation of the forearm during reach-and-grasp tasks leads to a change in FES response due to the relative transition between the skin and underlying neuromuscular tissues. An automatic real-time adaptation strategy of virtual electrodes and stimulation intensity in electrode arrays was investigated for a secure grasp during forearm movements. The novel method facilitates dynamic repositioning of electrodes and optional closed-loop control of the stimulation intensity. The hand sensor system was used to estimate grasping strength when using elastic objects. Experiments in four able-bodied volunteers revealed that the automatic electrode adaptation generates a strong, stable grasp force regardless of the rotational state of the forearm, in contrast to static electrodes.

In summary, the presented concepts and methods in this thesis contribute to a higher degree of automation and adaptation of HNPs, which in the long run will enhance the use of FES-based technology in rehabilitation and, thereby, promote the motor recovery of patients.

Zusammenfassung

Menschen mit Lähmungserscheinungen in den oberen Extremitäten nach einem Schlaganfall oder einer Rückenmarksverletzung sind sowohl in ihrer Unabhängigkeit als auch in ihrer beruflichen und sozialen Integration eingeschränkt. Wachsende Patientenzahlen und der damit verbundene Anstieg des zeitlichen und finanziellen Aufwands für die Rehabilitation führen zu einer starken Nachfrage nach neuen Therapien. Neuroprothesen basierend auf funktioneller Elektrostimulation (FES) können das Wiedererlangen motorischer Fähigkeiten positiv beeinflussen. Funktionelle Handbewegungen werden durch elektrische Anregung der peripheren Nerven im Unterarm erzeugt. Nicht-invasive Handneuroprothesen (HNPs) stehen jedoch in der Praxis vor diversen Herausforderungen. Die eingeschränkte Selektivität der transkutanen FES gestaltet die Erzeugung feinmotorischer Bewegungen durch Stimulation am muskelreichen Unterarm schwierig. Variabilität in Neuroanatomie und Toleranz gegenüber FES machen eine individuelle Anpassung der Stimulationsparameter erforderlich. Darüber hinaus sind Strategien zur schnellen, einfachen Adaption der FES in Echtzeit notwendig, da das neuromuskuläre System zeitvariablen Veränderungen unterworfen ist.

In dieser Dissertation werden neue Konzepte und Methoden für eine neuartige, adaptive HNP vorgestellt basierend auf Automatisierung, Regelung und benutzerzentriertem Design. Die HNP verfügt über ein neues, modulares Handsensorsystem für die Erfassung FES-induzierter Bewegungen in Echtzeit. Im Gegensatz zu handschuhbasierten Ansätzen bewahrt die vorgeschlagene Sensorik den Tastsinn. Für die Anwendung bei Patienten mit schweren motorischen Beeinträchtigungen der Hand wurden Algorithmen zur Messung von Orientierungen, Hand- und Fingergelenkwinkeln sowie Positionen der Fingerspitzen durch bis zu 17 Inertialsensoren entwickelt. Die Verfahren vermeiden komplexe Kalibrierungsbewegungen, die von den Patienten ausgeführt werden müssen, und arbeiten robust in magnetisch gestörten Umgebungen, d. h. auch in Innenräumen. Das Sensorsystem wurde mit vier gesunden Probanden in unterschiedlichen Set-ups validiert, bevor es in den folgenden Studien zum Einsatz kam.

Eine selektive und patienten-individuelle Stimulation von Handbewegungen wurde durch die Verwendung von Elektrodenarrays und benutzerfreundlichen Identifikationsstrategien in der neuen HNP erreicht. Eine effektive Suche nach geeigneten virtuellen Elektroden, die aus aktiven Array-Elementen bestehen, ist für die klinische Akzeptanz und Praktikabilität entscheidend. Es wurden halb- sowie voll-automatische Methoden zur Identifikation von Stimulationspositionen und -intensitäten entwickelt, um verschiedene Ebenen der Benutzerintegration zu realisieren. Der halb-automatische Ansatz ermöglicht es dem Anwender, virtuelle Elektroden über einen Touchscreen kontinuierlich zu modifizieren, während die Stimulationsintensitäten automatisch geregelt werden. Beide Identifikationsmethoden wurden in fünf Schlaganfallpatienten evaluiert und geeignete virtuelle Elektroden für Handöffnen und -schließen gefunden, sofern die Patienten die FES tolerierten. Der halb-automatische Ansatz war 25 % schneller als der automatische.

Bei Verwendung statischer Parametereinstellungen während einer Therapiesitzung werden Änderungen in der Muskelantwort nicht berücksichtigt. Beispielsweise beeinflusst die Drehung des Unterarms die FES-induzierte Handbewegung aufgrund der relativen Verschiebung zwischen Haut und darunter liegendem neuromuskulären Gewebe. In der Arbeit wird eine automatische Echtzeitadaption für virtuelle Elektroden und FES-Intensität in Elektrodenarrays vorgestellt, um einen sicheren Griff bei Unterarmbewegungen zu gewährleisten. Das neue Verfahren ermöglicht die dynamische Neupositionierung von aktiven Elektroden und optional die Regelung der Stimulationsintensität. Mit dem neuen Handsensorsystem wird die Greifkraft bei Verwendung elastischer Objekte abgeschätzt. Experimente mit vier gesunden Probanden ergaben, dass die automatische Adaption im Gegensatz zu statischen aktiven Elektroden eine stabile Greifkraft unabhängig vom Rotationszustand des Unterarms erzeugt.

Zusammenfassend ermöglichen die vorgestellten Konzepte und Methoden einen höheren Grad an Automatisierung und Anpassung von HNPs, was langfristig den Einsatz dieser Technologie in der Rehabilitation und dadurch die motorische Genesung fördern kann.

Acknowledgements

I would like to express my sincere thanks to all the people who have supported me along the long path of this thesis, who motivated, questioned and promoted me and my actions with courage and passion.

First and foremost, my gratitude belongs to my supervisors Prof. Dr.-Ing. Jörg Raisch and Dr. Thomas Schauer, who introduced me to the interesting field of functional electrical stimulation and have shown a large and consistent interest in my project during the times. I would also like to thank all my colleagues from the Control Systems Group at Technische Universität Berlin, especially my "roommate" Markus Valtin and Dr.-Ing. Thomas Seel for sharing their expertise and their friendship. Furthermore, it was a pleasure to work with Astrid Bergmann, Daniel Laidig, Philipp Müller, Arne Passon, and Constantin Wiesener—thank you for the mutual support. I thank the Technische Universität Berlin for granting me the promotion completion scholarship to finish this thesis.

Most of this work was conducted within the innovation cluster *BeMobil* funded by the Federal Ministry of Education and Research. Within this project, the clinical evaluation was made possible by Sebastian Böttcher, Dr. med. Frank Dähne, and Uri Shiri from Unfallkrankenhaus Berlin. Thank you for your medical advice and for screening and recruiting suitable patients. Moreover, I would like to thank my friend Natalie Jankowski from Humboldt Universität zu Berlin and Laura Schönijahn for support in the user-centered analysis. Many thanks also to the people who have participated in the experiments.

Deepest thanks go to my family, who always believed in me during all these times. I also would like to thank my dear friends who accompanied me along the way. In particular, the exchange with Leonie, Natalie, and Tina to the ups and downs of a Ph.D. have always given me new courage. Last but not least, I am forever grateful for my husband Peter for his understanding, endless patience, and encouragement when it was most required. Thank you!

Christina Salchow-Hömmen
Berlin, August 2019

Table of Contents

Title Page i

Abstract v

Zusammenfassung vii

Acknowledgements ix

List of Figures xv

List of Tables xvii

Abbreviations xix

Symbols xxi

1 Introduction 1

1.1 Motivation . . . 1
1.2 The Human Hand . . . 4
1.3 Neurophysiology of Motion . . . 8
1.4 Functional Electrical Stimulation . . . 10
1.5 Hand Motion Tracking . . . 15
1.6 Aim and Contributions of the Thesis . . . 18
1.7 Thesis Outline . . . 19
1.8 Related Publications of the Author . . . 19
1.9 Related Student Projects Supervised by the Author . . . 20

2 State of the Art in Hand Neuroprostheses 23

2.1 Overview . . . 23
2.2 Goals and Requirements . . . 24
2.3 First Generation of Hand Neuroprostheses . . . 25
2.4 From Single Electrodes to Electrode Arrays . . . 28
2.5 Control of Hand Neuroprostheses . . . 43
2.5.1 Introduction . . . 43
2.5.2 Signals for Control of Hand Neuroprostheses . . . 45
2.5.3 Open- and Closed-Loop Control . . . 51
2.6 Conclusion . . . 62

3 Concept of the New Hand Neuroprosthesis 65
3.1 Overview . . . 65
3.2 Stimulator and Parameters . . . 66
3.3 Electrode Arrays . . . 67
3.4 Hand Sensor System . . . 70
3.5 Control Unit and Interface . . . 72

4 Real-Time Hand and Finger Motion Tracking with Inertial Sensors 75
4.1 Overview . . . 75
4.2 Motivation . . . 76
4.3 Methods for Joint Angle and Fingertip Position Estimation . . . 78
4.3.1 Biomechanical Hand Model . . . 78
4.3.2 Introduction to Quaternions and Dual Quaternions . . . 81
4.3.3 Hand Sensor System Algorithms . . . 84
4.4 Simulations and Experimental Validation . . . 87
4.4.1 Overview . . . 87
4.4.2 Simulations . . . 88
4.4.3 Idealistic Setting with Optical Reference System (Setting 1) . . . 89
4.4.4 Realistic Setting Exploiting Characteristic Hand Poses (Setting 2) . . . 92
4.5 Results . . . 93
4.5.1 Simulative Results . . . 93
4.5.2 Results under Idealistic Conditions (Setting 1) . . . 94
4.5.3 Results under Realistic Conditions (Setting 2) . . . 94
4.6 Discussion . . . 96
4.7 Conclusions and Future Research . . . 99

5 Identification of Suitable Stimulation Sites in Electrode Arrays 101
5.1 Overview . . . 101
5.2 Motivation . . . 102
5.3 Methods . . . 104
5.3.1 Semi-Automatic Search Strategy . . . 104
5.3.2 Automatic Search Strategy . . . 109
5.4 User-Centered Validation . . . 113
5.4.1 Participants . . . 113
5.4.2 Setup . . . 113
5.4.3 User-Centered Evaluation . . . 114
5.4.4 Procedure . . . 115
5.4.5 Data Analysis . . . 117
5.5 Results . . . 117
5.6 Discussion . . . 126
5.7 Conclusions and Recommendations . . . 130

6 Real-Time Adaptation of Virtual Electrodes for Safe Grasping 131
6.1 Overview . . . 131
6.2 Motivation . . . 132
6.3 Method . . . 133
6.4 Experimental Validation . . . 136
6.5 Results . . . 138
6.6 Discussion . . . 141
6.7 Conclusions and Future Research . . . 143

7 General Discussion and Conclusion 145
7.1 Summary . . . 145
7.2 General Discussion . . . 146
7.3 General Conclusions and Future Research . . . 149

References 151

Appendix A Range of Hand Motion 183

Appendix B Stimulator RehaMovePro 185

Appendix C Hand Model for Simulations 187

Appendix D Feedback Controller Experiments 189

Appendix E Influence of the Upper Arm Position 193

List of Figures

1.1 Examples of available neuroprostheses and robots for rehabilitation 3
1.2 Anatomy of the human hand: bones and joints 5
1.3 Physiology of the human hand: movements 6
1.4 Anatomy and function of the forearm muscles: extensors 7
1.5 Anatomy and function of the forearm muscles: flexors 7
1.6 Six functional grasp types 8
1.7 Neurophysiology of movement: CNS and MUs 9
1.8 Principle of transcutaneous FES and pulse shapes 11
1.9 Exemplary EMG recording during FES 15
1.10 Examples of motion tracking systems for the hand 17

2.1 Examples of commercially available EMG-triggered FES systems 28
2.2 Example: INTFES stimulation system 30
2.3 Example: electrode array design 41
2.4 Principle structure of open-loop control for neuroprostheses 44
2.5 Principle structure of closed-loop control for neuroprostheses 45
2.6 Overview of suggested signals for FES control in HNPs 46
2.7 Temporal relation of EEG, EMG, and motion tracking 51
2.8 Example: vEMG proportional control 53
2.9 Example: contralateral FES control 59

3.1 Schematic illustration of the HNP 66
3.2 Stimulator and charge control scheme 67
3.3 Electrode arrays with 35 elements 68
3.4 Electrode array layout 69
3.5 Modular IMU-based hand sensor system 71
3.6 Real-time visualization of the measured hand posture 72
3.7 GUI for the HNP 73

4.1 Modeled bones and joints of the human hand 79
4.2 Coordinate systems of the biomechanical hand model 80
4.3 Hand sensor system algorithms 85
4.4 Simulation of different functional finger length ratios 88
4.5 Idealistic setting with optical reference system 90
4.6 Marker positions of the optical reference system 90

4.7 Validation setting under realistic conditions . . . 92
4.8 Points of contact on the fingertip . . . 93
4.9 Overview of experiments in Setting 2 . . . 94
4.10 Results: HSS evaluation under idealistic conditions . . . 95
4.11 Results: exemplary position time series and errors for Setting 1 . . . 96
4.12 Results: HSS evaluation under realistic conditions . . . 97
4.13 Results: exemplary time series of a pinch motion in Setting 2 . . . 98

5.1 Virtual electrode and virtual electrode model . . . 105
5.2 Weight functions of the circular virtual electrode model . . . 106
5.3 Closed-loop control within the semi-automatic search . . . 107
5.4 Proof-of-concept of the closed-loop semi-automatic search . . . 108
5.5 Flow chart of the semi-automatic search . . . 110
5.6 Flow chart of the automatic search . . . 112
5.7 Experimental setup with the HNP . . . 114
5.8 Overview of the user-centered evaluation procedure . . . 116
5.9 Results: Identified VEs with the two search methods for each patient . . . 119
5.10 Cost function scale for hand opening and closing . . . 120
5.11 Results: exemplary grasp-and-release cycle . . . 121
5.12 Results: exemplary time course of the semi-automatic search . . . 122
5.13 Results: average duration of the VE serach . . . 124
5.14 Results: patients' perception . . . 125

6.1 States of forearm rotation . . . 133
6.2 Principle of the automatic VE adaptation . . . 134
6.3 Block diagram for feedback control of the grasping strength . . . 136
6.4 Utilized sensor setup for the automatic VE adaptation . . . 137
6.5 Results: identified VEs for grasping for three forearm states . . . 139
6.6 Results: comparison of constant VE versus real-time VE adaptation . . . 140
6.7 Results: correlation range between grasp force and grasp index . . . 141
6.8 Results: step response and identified first-order model . . . 142
6.9 Results: closed-loop control in pronation . . . 142

C.1 Exemplary visualization of the Simulink hand model . . . 188

D.1 RehaStim stimulator and customized demultiplexer . . . 190
D.2 Electrode array with 24 elements . . . 190
D.3 Virtual electrode paths for the controller experiments . . . 191

E.1 Evaluated upper arm positions . . . 194
E.2 Example: recorded wrist angles and analysis window . . . 195

List of Tables

1.1 Overview of hand motion tracking systems 16

2.1 Overview of electrode arrays and identification methods in literature 31

4.1 Ratios of the funcional finger segment lengths 81
4.2 Average thickness of soft tissue at the fingertip 81
4.3 Overview of experiments in Setting 1—idealistic conditions 91
4.4 Overview of experiments in Setting 2—realistic conditions 93
4.5 Results: HSS evaluation in Setting 1 95
4.6 Results: HSS evaluation in Setting 2 97

5.1 Reference joint angles for the automatic search 117
5.2 Results: parameters of the identified VEs 118
5.3 Results: cost function values for each identified VE 120
5.4 Results: used options in the VE identification experiments 123

6.1 Results: static VE stimulation versus automatic VE adaptation 139

A.1 Range of motion of the human hand. 183

B.1 Technical details of the RehaMovePro stimulator 185

C.1 Assumed finger length in the Simulink hand model 187

D.1 Technical details of the RehaStim stimulator 189

E.1 Results for the influence of the upper arm position 195

Abbreviations

3D Three-dimensional/three dimensions 70

9D Nine-dimensional 70

A Abduction/adduction 91

ADL Activities of daily living 2

AF Abduction/adduction with extension/flexion 91

ANN Artificial neural network 37

AP Action potential 8

ARAT Action research arm test 52

B Baseline method of the HSS algorithms 84

BCI Brain-computer interface 47

BGS Belgrade grasping system 26

BI Bioimpedance 47

CI Confidence interval 81

CNS Central nervous system 1

DIP Distal interphalangeal (joint; Articulatio interphalangealis distalis) 5

DOF Degree of freedom 3

EA Electrode array 28

EEG Electroencephalopgraphy 14

eEMG Electrically evoked electromyogram 14

EMG Electromyography/electromyogram 14

ERD Event-related desynchronization 47

ES Electrical stimulation 2

F Flexion/extension 91

F1 Thumb (digit one) 5

F2 Index finger (digit two) 5

F3 Middle finger (digit three) 5

F4 Ring finger (digit four) 5

F5 Little finger (digit five) 5

FEM Finite element model 36

FES Functional electrical stimulation 2

FFC Flexible flat cable 69

FNS Functional neuromuscular/neural stimulation 2

FSR Force-sensitive resistor 50

GUI Graphical user-interface 41

HNP Hand neuroprosthesis 4

HSS Hand sensor system 66

ILC Iterative learning control 39

IMU Inertial measurement unit 17

ISB International Society of Biomechanics 78

M1 Method one of the HSS algorithms 84

M2 Method two of the HSS algorithms 84

MAS Modified Ashworth scale 56

MCP Metacarpalphalangeal (joint; Articulatio metacarpo-phalangealis) 5

MEMS Micro-electromechanical system 17

MN Motor neuron 8

MPC Model predictive control/controller 57

mRS Modified Rankin scale 113

MU Motor unit 8

NMES Neuromuscular electrical stimulation 2

P1 Experiment one of the HSS validation 93

P2 Experiment two of the HSS validation 93

P3 Experiment three of the HSS validation 93

P4 Experiment four of the HSS validation 93

PC Personal computer 38

PCB Printed circuit board 29

PCE Point of complete enclosure 138

PID Proportional-integral-derivative 54

PIP Proximal interphalangeal (joint; Articulatio interphalangealis proximalis) 5

RMSE Root-mean-square error 77

SCI Spinal cord injury 1

SSVEP Steady-state visual evoked potentials 47

T-CMC Thumb base (joint; Articulatio carpometacarpalis pollicis) 5

T-IP Thumb interphalangeal (joint; Articulatio interphalangealis pollicis) 5

T-MCP Thumb metacarpalphalangeal (joint; Articulatio metacarpalphalangealis pollicis) 5

TAM Technology acceptance model 115

USB Universal serial bus 66

VE Virtual electrode 29

vEMG Volitional electromyogram 14

VR Virtual reality 16

WCS Wrist coordinate system 80

Symbols

a Accelerometer readings (3D) 84

$\bar{a}_j$ Averaged joint angle of joint j 111

$a_{j,\mathrm{ref}}$ Reference joint angle of joint j 111

α Wrist joint angle describing extension/flexion 106

β Wrist joint angle describing radial/ulnar deviation 108

C Grasp index 135

C_{ref} Grasp index reference for closed-loop control 136

c Center of rotation of the wrist joint 80

d Dual part of a dual number 82

dip DIP joint angle 114

$\mathbb{D}$ Set of dual quaternions 82

$\mathbb{D}_0$ Set of dual quaternions with a real part equal to one and a dual part with zero scalar part 83

$\mathcal{D}$ Bijective operator on vectors 83

e Fed-back error 106

ϵ Dual unit 82

F Grasp force 135

F_{ref} Grasp force reference for closed-loop control 136

f_{s} Stimulation frequency 12

f_{t} Sampling frequency 84

G Index for global coordinate systems 80

G First-order model 107

g Angular rates of 3D gyroscope 84

g_j Weight of a joint j in the cost function J or in the grasp index function C 111

γ Rotation angle of the forearm 133

γ_z Rotation angle of state z of the forearm rotation 134

h Diameter of the virtual electrode model 105

I Maximum current of a stimulation pulse 11

$I_{\max}$ Maximum allowed current intensity 53

$I_{\min}$ Minimum allowed current intensity 67

I_{norm} Normalized current 67

ipa Index for initial-pose-aligned quaternions 86

J Cost function of the automatic search 109

K PID controller function 106

K_D Differential gain of a PID controller 107

K_I Integral gain of a PID controller 107

K_P Proportional gain of a PID controller 107

k Gain of a first-order model 107

L Minimum cost function value per tested virtual electrode of the automatic search 111

l_{d} Functional length of the distal finger segment 80

l_{h} Functional length of the palm 79

l_{m} Functional length of the middle finger segment 80

l_{p} Functional length of the proximal finger segment 80

m Magnetometer readings (3D) 84

m Number of active elements in a virtual electrode 118

mcp_α Extension/flexion angle of the MCP joint 114

mcp_β Abduction/adduction angle of the MCP joint 114

N Neutral state of the forearm rotation 133

opt Index for coordinate systems defined within the optical system in the HSS validation 89

P Pronation state of the forearm rotation 133

p Fingertip position (3D) 80

p_a Parameter set of the applied VE 134

pip PIP joint angle 114

pw Pulse width of a stimulation pulse (one phase) 11

$pw_{\max}$ Maximum allowed pulse width 58

$pw_{\min}$ Minimum allowed pulse width 67

pw_{norm} Normalized pulse width 67

p_z Parameter set of a virtual electrode for forearm state z 134

Q Dual quaternion 82

$\mathbf{Q}^*$ Conjugate of a dual quaternion 82

q Quaternion 81

$\mathbf{q}^*$ Conjugate of a quaternion 82

q_0 Scalar part of a quaternion **q** 81

q Charge of a stimulation pulse 11

$q_{\max}$ Maximum allowed charge 67

q_{mec} Mechanical threshold for electrical stimulation 12

$q_{\min}$ Minimum allowed charge 67

q_{mot} Motor threshold for electrical stimulation 12

q_{sen} Sensory threshold for electrical stimulation 12

q_{tol} Tolerance level (stop threshold) for electrical stimulation 12

r Real part of a dual number 82

$\mathbb{R}$ Set of all real numbers 81

ρ Angular bound for discrete forearm rotation states 135

S Supination state of the forearm rotation 133

s Shape of the virtual electrode model 105

std Standard deviation 95

$\mathbb{S}$ Set of all modeled body segments 85

σ Size (diameter) of a symmetric electrode array element in mm 105

T Time constant of a first-order model 107

T_d Time constant describing the dead time of a first-order model 107

tip TIP joint angle 135

t_{s} Stimulation period 12

Δt Sampling interval 85

u Normalized charge of a stimulation pulse 67

u_C Stimulation threshold given in normalized charge marking complete enclosure of an object 136

u_{mot} Motor threshold for electrical stimulation given in normalized charge 106

u_{step} Stimulation intensity used for recording step responses 106

u_{tol} Tolerance level (stop threshold) for electrical stimulation expressed in normalized charge u 107

$\hat{u}$ Global stimulation intensity of the virtual electrode 105

$\hat{u}_{\text{CL}}$ Global stimulation intensity applied in closed-loop 108

$\hat{u}_{\text{OL}}$ Global stimulation intensity applied in open-loop 108

VE_1 Virtual electrode position one for wrist and finger extension 115

VE_2 Virtual electrode position two for wrist extension 116

VE_3 Virtual electrode position three for finger flexion 116

$\mathbf{v}$ Vector in $\mathbb{R}^3$ 83

w Weight function of the virtual electrode model 105

y Controlled joint angle within the semi-automatic search 106

y_{ref} Reference joint angle within the semi-automatic search 106

$\tilde{\mathbf{y}}$ Vector of non-controlled joint angles within the semi-automatic search 106

$\mathbf{z}$ Center point of the virtual electrode model 105

z State of the forearm rotation 134

$\mathbb{Z}_+^*$ Set of all positive integer numbers not including zero 111

ζ Angle between MCP joint center of F3 and the T-CMC joint center in the biomechanical hand model 79

1 Introduction

1.1 Motivation

Movement disabilities have a significant impact on the quality of life of the affected people. Depending on the level of impairment, patients are not only limited in their independence but also in their inclusion in professional and social life. Stroke is one of the major causes of disability in adulthood, worldwide and in Germany [1, 2, 3, 4]. A stroke is defined as an acute episode of focal dysfunction of the brain (or retina, or spinal cord) due to infarction or bleeding in the relevant part, which comes with a loss of focal neurological function [5]. As a result of the demographic change and aging populations in Europe[1], the absolute number of patients suffering a stroke will most likely increase in the future from 1.1 million per year in 2000 to more than 1.5 million per year in 2025 [1, 2, 5, 6]. Approximately 40 % of the stroke survivors are left permanently disabled or paralyzed [1]. Neurological rehabilitation aims to recover the movement skills of the patient that are lost when a part of the brain was damaged. The human brain has the ability to relearn the functions lost due to stroke, which is known as brain plasticity [7]. The complexity of the brain allows compensation of lost functions, such as motor control of innervated limbs, via other parts of the brain. This reorganization or relearning process benefits from incremental movement training, starting with simple and externally supported tasks and leading to independently controlled sensomotoric interactions [8]. Focused and specific repetitive training has been shown to result in enhanced limb function [9, 10]. Individually adapted intensity and frequency of the therapeutic training have a significant impact on the possible rehabilitation success [8, 11]. Nowadays, manual treatment methods provided by therapists are the most common form of therapy in clinical praxis [12]. Therefore, the success of the physical rehabilitation of individuals depends on the availability of personnel and monetary resources.

A second large group of people with severe motor impairments due to injuries of the central nervous system (CNS) are patients suffering from spinal cord injury (SCI). A harm of the spinal cord may lead to complete or incomplete loss of sensory and motor function below the

[1] EU countries, Iceland, Norway, and Switzerland

level of lesion [13]. In Germany, more than 17,000 people suffer from paraplegia or tetraplegia due to SCI (as of 2015, [14]). Tetraplegic patients have paralysis in the lower and upper extremities as a result of a higher neurological lesion in the spinal cord [13]. However, in many cases, residual hand and arm function are present to some extent (lesion below cervical level C4). Early treatment of those patients aims at promoting compensatory movements with the remaining functionality of hand and arm to manipulate objects and regain some level of independence in everyday life [15]. Furthermore, early treatments aim to prevent the partly innervated muscles from wasting and weakness [16]. Conservative treatment includes among others strengthening programs for all voluntary muscles, and extensive, repetitive training in activities of daily living (ADL) provided by skilled physical and occupational therapists [17]. Besides, surgical techniques have been established to increase upper extremity function for tetraplegics, such as tendon transfer for voluntary extension of the elbow and the wrist [18, 19].

The growing number of affected people, and subsequently the rise in timely and monetary rehabilitation expenses lead to strong demands for new therapeutic approaches to improve the effectiveness and efficiency of neurorehabilitation [20]. Furthermore, the number of scientific evidence stating that high intensity and high frequency of therapy can enhance movement recovery increases [21, 22]. Therefore, and due to the rapid process in modern technologies, for example, in integrated circuits, wireless communications, and physiological sensing, the development of sophisticated technical aids in the field of physical rehabilitation has expanded massively over the last twenty years [23]. The range of applications is wide. The repetitive character of movement therapy calls for automated systems. Two main research fields in rehabilitation engineering are the evolution of rehabilitation robots and neuroprostheses.

"Neuroprostheses [...] are artificial systems that in a broad sense bridge interrupted or damaged neural connections between the brain and [lower or] upper extremity muscles using a technique called functional electrical stimulation (FES)." [24, p. 14] In literature, FES may also be referred to as neuromuscular electrical stimulation (NMES), functional neuromuscular/neural stimulation (FNS), or simply electrical stimulation (ES). A frequency of short electrical impulses is applied via implanted or surface electrodes to artificially evoke action potentials in the underlying neural and muscular tissue with the goal to produce muscle contraction and finally functional movements [25]. This method requires intact motor neurons that connect the spinal cord with the target muscles [26]. One treatment aspect is to enhance the use of and strengthen the remaining muscular tissue. Applications in physical rehabilitation range from the restoration of reaching and grasping skills of the upper limb (e.g., [27, 28, 29]) to standing, walking, and cycling support in the lower limb (e.g., [30, 31, 32, 33, 34]. Examples of commercially available systems are shown in Fig. 1.1. The goal of neuroprostheses can be to support relearning (*therapy*), for example, in stroke survivors, or to assist persons who have a chronic disability to accomplish ADL (*assistance*) [35]. In all applications, the imitation of the natural control of human movements with a neuroprosthesis requires extensive knowledge of the individual human system as well as a high reactivity of the technical system, and therefore it is still subject of research.

Besides neuroprostheses, the second main research area in rehabilitation engineering are (partly) automated robots. In most cases, these systems allow for robot assistance in movement initiation, guidance of the movement, weight compensation, and high-intensity,

(a) *NESS H200 Wireless* (Bioness Inc., Valencia, CA, USA) neuroprosthesis with orthosis for the upper limb (Photo: © Bioness)

(b) *MyGait* (Otto Bock, Duderstadt, Germany) neuroprosthesis for assistance in drop foot (Photo: © by Ottobock)

(c) *Amadeo* (Tyromotion GmbH, Graz, Austria) for end-effector-based, robotic hand training (Photo: © Tyromotion)

Figure 1.1: Examples of commercially available neuroprostheses and robots for rehabilitation.

iterative training with accurate feedback [23, 36]. The movement is either completely or partly performed by the robot to assist the patient, or the robot can restrict the voluntary motion of the patient by providing resistivity, e.g., for muscle strengthening [36]. According to their mechanical properties, rehabilitation robots can be classified into three main groups with either active or passive implementation: a) exoskeletons, b) end-effector-based (also known as manipulators), and c) cable-driven robots [37]. An example of an end-effector-based system for upper limb rehabilitation is shown in Fig. 1.1. Robotic rehabilitation devices require proximity or contact with the patient and therefore face many challenges, for example, regarding the possible degrees of freedom (DOFs), safety, command and control, wearability, transport, as well as mimicking the flexibility of a human therapist [22, 38].

Numerous developments in the field of rehabilitation robots and neuroprostheses address hand and upper limb support after stroke or SCI (e.g., [39, 40, 41, 42]). Impairments of the hand and upper limb function have a significant influence on the patient's independence in everyday life. The hand is the human body's most precise and useful tool to manipulate objects and perform ADL, such as personal hygiene. The rehabilitation and support of the hand function are therefore of crucial importance for affected patients. Eighty percent of stroke survivors suffer a paresis in hand and upper extremity [8]. Tetraplegic SCI patients stated that regaining arm and hand function is their highest priority [43]. The broad variety of hand movements is a consequence of the complex anatomy of the hand, with numerous bones, joints, and muscles, and the precise motor control via the human brain. This complexity and

high functionality make the support of hand function via technical aids and therapy systems a challenge with high research attention.

Studies show that the application of FES and rehabilitation robots can assist the therapist in promoting rehabilitation to individuals and can help to intensify the therapy, which may increase chances of recovery or may accelerate the rehabilitation progress [23, 44, 45]. However, the grand challenge for assistive, enabling technologies is that each patient shows individual—almost unique—disability characteristics. A technical solution for one person will not necessarily work for another, even if their disabilities appear clinically similar [22]. In general, robotic devices have among other things the disadvantages of being cost intensive, having large dimensions, and limited flexibility (DOFs, communication) [38]. The application of mechanical systems to support hand and finger movements is additionally complicated by the comparatively small dimensions and extensive functionality of this body part. Therefore, by today, neuroprostheses have a greater potential to be successfully used in the two application scenarios *therapy* and *assistance* of the hand in a clinical as well as in a home environment.

Current research in the field of rehabilitation with hand neuroprostheses (HNPs) focuses on automation and control concepts along with strategies of actively engaging the patients in the training session. A particularly challenging task is the realization of adaptive behavior of the HNP, which should adapt easily and quickly to the individual anatomy, movement capabilities, and control abilities of each patient. Furthermore, the training with the neuroprostheses should integrate and promote the residual voluntary activity of the patient to improve the outcome of motor rehabilitation. New methods aim at increasing practicability and thus the use of FES-based therapy in clinical rehabilitation. Progress in these research questions require knowledge and ideas in different areas of medicine (physiology, psychology, biomechanics), engineering (electrical, computer, mechanical), and rehabilitation science. Suitable solutions in this interdisciplinary research field can only be achieved by intensive cooperation of engineers, physicians, therapists, and patients. This dissertation proposes a novel adaptive hand neuroprosthesis using transcutaneous FES technology that aims at enhancing the outcome and acceptance of HNPs in clinical practice.

1.2 The Human Hand

To understand to what extent FES in the form of neuroprostheses can be used to provide restoration of hand function, it is necessary to review the anatomy and physiology of hand and forearm. The hand and forearm build a complex mechanical system with 31 bones and more than 17 joints and ligaments, resulting in over 23 DOFs [46, 47]. The forearm has two bones, radius and ulna, which can be moved relative to each other yielding a rotation of the forearm and hand (one DOF). The hand is anatomically divided into three parts: the carpus (wrist), the metacarpus, and the phalanges (fingers). Figure 1.2 shows all the joints and bones of the hand.

The carpus consists of multiple bones, which allow for small internal shifts versus each other. However, in common biomechanical models of the hand, the DOFs of the wrist are often simplified to two, namely extension/flexion and ulnar/radial deviation [48, 49]. Those movement directions are displayed in Fig. 1.3. The palm consists of the metacarpal bones of the

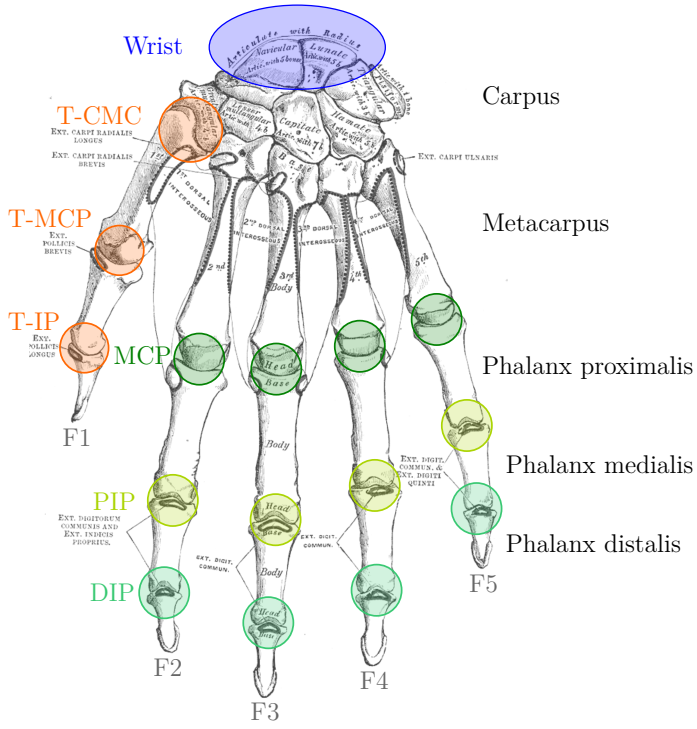

Figure 1.2: Bones and joints of the human hand illustrated for the left hand in posterior (dorsal) view adapted from [50]. The thick gray lines with black dots mark the muscle attachment points. The joints considered in this thesis, namely wrist, T-CMC, T-MCP, T-IP, MCP, PIP, and DIP joint, are marked by colors.

fingers F2–F5 (index (F2), middle (F3), ring (F4), and little finger (F5)). The metacarpals are connected with the carpal bones of the wrist via strong restricted joints, allowing only minimal shifts. An exception is the metacarpal of the thumb (F1), which is connected to the carpus via a saddle joint (*Articulatio carpometacarpalis pollicis*, T-CMC) allowing for three restricted, functional DOFs. The proximal phalanges follow the metacarpal bones. For fingers F2–F5, the connecting metacarpalphalangeal joint (MCP) allows two DOFs, namely extension/flexion and abduction/adduction, as seen in Fig. 1.3. Again, the thumb metacarpalphalangeal joint (T-MCP) represents an exception because it is a hinge joint and provides only one DOF. The proximal interphalangeal joints (PIP) between proximal and middle phalanx for fingers F2–F5 and between proximal and distal phalanx for the thumb (interphalangeal joint, T-IP) represent hinge joints with one DOF. The middle phalanx and distal phalanx of fingers F2–F5 are connected via the distal interphalangeal joint (DIP), a hinge joint with one DOF. Anatomical and mechanical constraints restrict the range of motion of each joint. A table with the average ranges of motion for healthy individuals can be found in *Appendix* A (Table A.1).

Numerous skeletal muscles actuate the described skeletal structures of the hand by contraction and stretching. They can be distinguished into intrinsic and extrinsic muscles [52]. Intrinsic muscles originate and terminate in the hand. Extrinsic muscles are located in the forearm and can be grouped into flexors and extensors for bending and extending of wrist and fingers. The extensors are mainly situated on the dorsal side of the forearm, whereas the flexors are mainly located on the ventral side. Both extrinsic muscle groups and functions of individual muscles are illustrated in Figs. 1.4 and 1.5. That the muscles and innervating nerves overlap and form layers is a problem in transcutaneous FES, as the electric field strength might

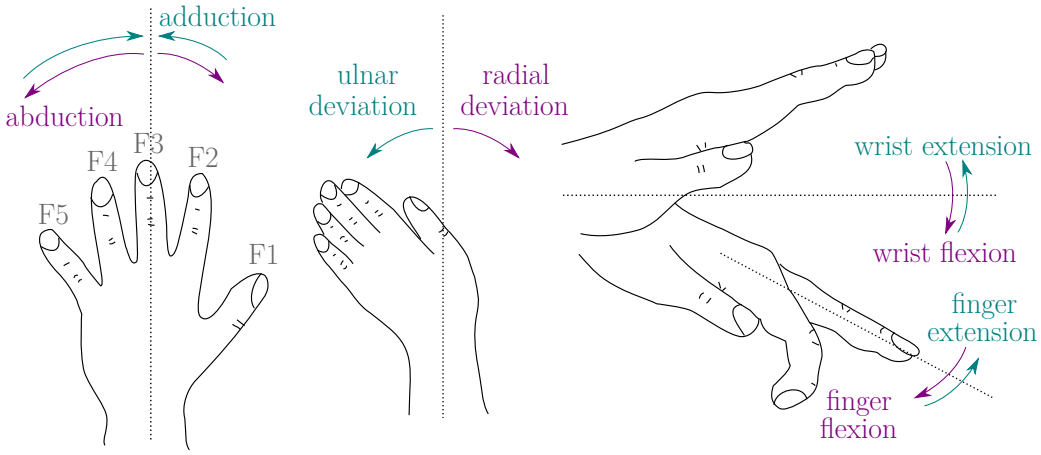

Figure 1.3: Definition of hand and finger movements, illustrated for the left hand. Ulnar/radial deviation is also known as ulnar/radial abduction or wrist abduction. Finger abduction in the MCP joints describes the movement away from the center of the extremity, whereas finger adduction refers to the move toward the center of the extremity. Reproduction from [51], under CC BY 4.0 [2], with modifications.

not be high enough at deep-lying target muscles and instead causes unwanted contractions in surface muscles. Furthermore, some muscles (e.g., *M. flexor digitorum superficialis*, *M. flexor digitorum profundus*) are multi-tendoned muscles, which can be considered to have sub-compartments for selective activation of individual digits [53, 54].

Each movement sequence of the hand includes the synchronous contraction and stretching of several, intrinsic and extrinsic muscles [46, 55]. Selective voluntary activation of individual fingers often leads to movements or forces in neighboring fingers, known as the enslaving effect [54, 56]. This effect exists for motion as well as force production. Reasons for this include the neurological coupling (e.g., neighboring areas in the motor cortex of the brain; cf. next *Section* 1.3) and common tissues between muscles and tendons [54, 57]. For the index finger (F2), the most independent voluntary motility is reported, whereas the middle finger (F3) shows the strongest coupling with movements of other fingers [58].

The muscle activation pattern for an object manipulation task of the hand, for example, a grasp-and-release task with an object, can be divided into the following main steps: As the hand reaches out to grasp an object, the hand aperture and fingers inlcuding the thumb (F1–F5) gradually evolve into a posture that matches the shape and intended use of the object [59, 60]. This natural preparation movement usually also involves an extension or rather stabilization of the wrist, achieved through co-activation of the corresponding extensor and flexor muscles [52]. In the case of a spherical grasp, all fingers will then flex around the object through contraction of the finger flexor muscles, such that the object is fixated between fingers and palm. The wrist usually remains in its stabilized posture. This hand posture is maintained during the transport phase [59]. For the release, the fingers extend. In literature, six basic types of prehension are classified which dominate in activities of daily living, namely lateral grasp, power (cylindrical, palmar) grasp, tripod pinch grasp, tip pinch, extension grasp, and spherical grasp [52, 54, 61, 62], all depicted in Fig. 1.6. Please refer to [62] for a detailed overview.

[2] `https://creativecommons.org/licenses/by/4.0/`

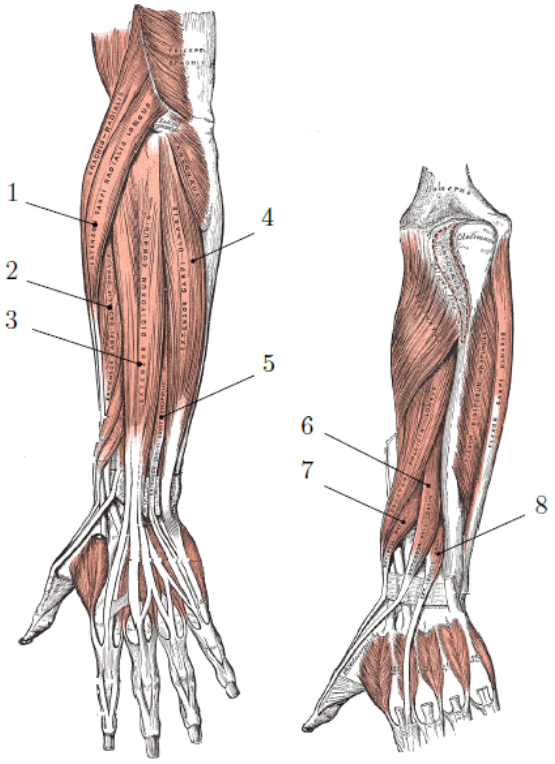

(a) Surface layer **(b)** Deeper layer

	Extensor muscles
1	*M. extensor carpi radialis longus*: Extension and radial deviation of the wrist
2	*M. extensor carpi radialis brevis*: Extension and radial deviation of the wrist
3	*M. extensor digitorum*: Extension of fingers II–V
4	*M. extensor carpi ulnaris*: Extension and ulnar deviation of the wrist
5	*M. extensor digiti minimi*: Extension of the little finger (V)
6	*M. extensor pollicis longus*: Extension of the thumb
7	*M. extensor pollicis brevis*: Extension of the thumb
8	*M. extensor indicis*: Extension of the index finger (II)

Figure 1.4: Anatomy and function of surface and deep extensor muscles in the left forearm (anterior) adapted from [50].

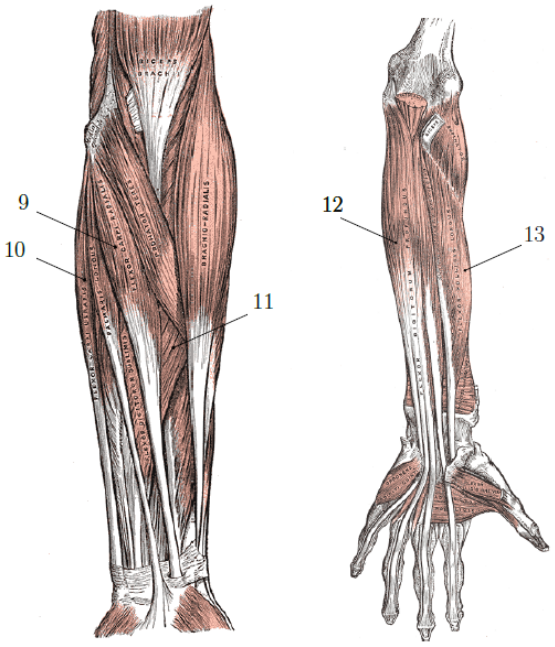

(a) Surface layer **(b)** Deeper layer

	Flexor muscles:
9	*M. flexor carpi radialis*: Flexion and radial deviation of the wrist
10	*M. flexor carpi ulnaris*: Flexion and ulnar deviation of the wrist
11	*M. flexor digitorum superficialis*: Flexion of all fingers but the thumb
12	*M. flexor digitorum profundus*: Flexion of fingers II–V
13	*M. flexor pollicis longus*: Flexion of the thumb

Figure 1.5: Anatomy and function of surface and deep flexor muscles in the left forearm (posterior) adapted from [50]. Tendons and tendon sheaths of the flexor muscles are bundled in the *carpal tunnel* proximal to the wrist joint.

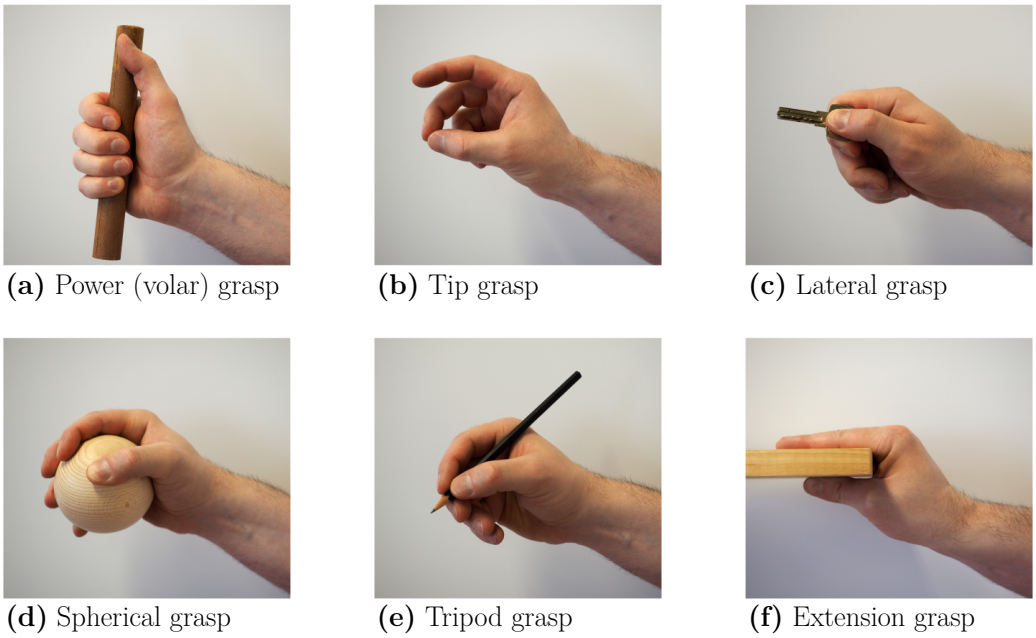

(a) Power (volar) grasp **(b)** Tip grasp **(c)** Lateral grasp

(d) Spherical grasp **(e)** Tripod grasp **(f)** Extension grasp

Figure 1.6: Six functional grasp types that dominate daily activities according to [54, 61]. The figure is adapted from [61].

1.3 Neurophysiology of Motion

In this subsection, a summary of the neurophysiological mechanisms of movement generation in the human body is given. For a deeper understanding of the physiology, please refer to [63] and [64].

The central nervous system consists of the brain and spinal cord in the narrow sense [65]. It receives information, coordinates and controls the activity of all parts of the human body. Efferent nerves from and afferent nerves to the CNS allow for precise control of the locomotor system [63]. Efferent nerve fibers are the descending, activating connections from the brain to the muscles, while the afferent nerves provide sensor information from the periphery to the CNS. The communication within the nervous system takes place through *action potentials* (APs). APs are short electrical spikes or impulses (around 1 ms) elicited through depolarization at the nerve cell membrane [66]. Their generation follows the *all-or-nothing* principle [64]: If the depolarization at the efferent nerve crosses the threshold, an action potential is evoked. The amplitude and activation threshold of the AP is consistent for cells of the same type.

In a neurologically intact individual, voluntary skeletal muscle contractions and therefore movements are first initiated by APs in the motor cortex of the brain [67]. Those action potentials are transmitted via circuits to the upper *motor neuron* (MN) in the spinal cord, where they are forwarded to the lower MN via interneurons or synapses. The lower MN innervates 5–1000 muscle fibers and transmits the electrical control signals via depolarization at the motor end plate [24]. Each muscle fiber consists of multiple single muscle cells (myofibrils). The muscle fibers that are innervated by one lower MN form a *motor unit* (MU) [65]. A single muscle consists of 100–2000 MUs [24]. Figure 1.7 shows the described pathway from the brain to muscle fibers.

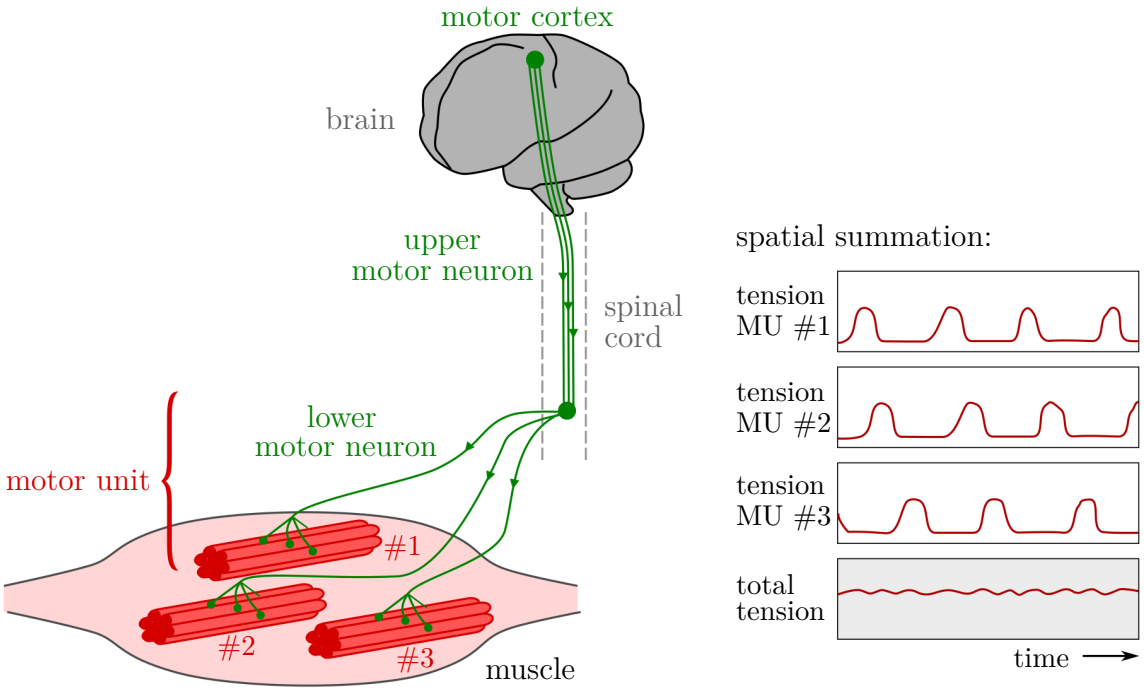

Figure 1.7: Recruitment of skeletal muscles via the CNS. This simplified illustration is based on the representations in [67] and [68]. The right part shows the spatial summation of the tension of single motor units of a muscle which sum up to a smooth, total tension of that muscle as shown in the plot at the bottom.

A single AP along a lower MN elicits a single contraction in the innervated muscle fibers. A muscle contraction is defined as a shortening of muscle fibers that leads to a reduction of the active muscle length and thereby actuates/moves the connected skeleton [47]. The generated muscular force is controlled via the number of recruited MUs (*spatial coding*; see Fig. 1.7) and the frequency of action potentials (*temporal coding*). Starting from an AP frequency of 10 Hz, single muscle contractions fuse to a tetanic contraction in a motor unit [67].

The MUs and their corresponding muscle fibers can be classified regarding contraction velocity and fatigue resistance [67]. Type I muscle fibers are smaller in diameter and contract at a lower velocity but are therefore more resistant against fatigue (*slow-twitch fibers*). Type II muscle fibers feature a faster contraction velocity but also fatigue faster (*fast-twitch fibers*) and have a larger diameter. The ratio between fast-twitch and slow-twitch fibers in a muscle varies depending on its function and condition [69]. Muscles that are involved in gross movements, such as walking, have few motor units, where each includes a large number of muscle fibers. Muscles involved in fine movements, such as single finger actuation, have many motor units, where each contains only a small number of muscle fibers [68]. The physiological MU recruitment follows the Henneman's size principle [70, 71]. According to the principle, small forces are generated by activating slow-twitch type I muscle fibers. For stronger forces, fast-twitch type II muscle fibers are recruited in addition [65]. For moderate forces, the motor units usually contract asynchronously. Single MUs are activated at frequencies between 5–10 Hz [72]. Spatial summation of several MUs emerges tetanic muscle contractions, as illustrated in Fig. 1.7. This strategy of natural muscle recruitment is optimized to reduce fatigue.

Lesions of the upper MN, for example, in the brain during stroke or in the spinal cord through an injury, lead to a paralysis of the connected motor units. In many cases, spasticity occurs together with the paralysis. Spasticity refers to the presence of increased muscle reflexes, disinhibition of extraneous reflexes, and pathological reflexes [67]. Furthermore, damages to the afferent nerves may lead to a loss of sensory perception. Muscles that are paralyzed and thereby do not receive regular exercise suffer from disuse atrophy and the proportion of fast-twitch fibers becomes higher than in active muscles [68, 73]. Especially in SCI patients, the phenomenon of disuse atrophy can be observed. However, muscle atrophy is often a reversible process, and physical rehabilitation can help to regain slow-twitch fibers to some extent [68].

1.4 Functional Electrical Stimulation

The paralysis in stroke patients and in the majority of SCI patients has its origin in missing communication of the CNS with the peripheral nervous system, due to damages to the relevant cortex areas or the upper MN in the spinal cord[3]. However, the lower MNs are often intact, and the muscles themselves retain their ability to contract and actuate the skeletal system [76]. Functional electrical stimulation can be applied to the lower MNs to replace the missing signals from the CNS.

In FES, sequences of short electrical impulses are applied via electrodes to evoke action potentials and thereby muscle contractions [26, 77]. The electrodes are either placed on the skin for transcutaneous stimulation, through the skin (percutaneous) or are implanted, either directly onto the muscle (epimysial) or around the innervating nerve (cuff electrodes) [54]. The principle of AP generation through FES is the same for all electrode types [67]. The sequence of electrical impulses yields an electric field between the anode (+) and cathode (–) electrode [67], as illustrated in Fig. 1.8. This electric field leads to relative ion-concentration changes along the underlying cellular membranes. Underneath the cathode, each impulse adjusts the cell membrane potential toward positive values (depolarization). Once the all-or-nothing threshold of the transmembrane potential of an excitable cell is crossed, an AP is evoked and propagates in both directions along the axon [26, 77]. On one end, the AP elicits a muscle contraction in the innervated muscle fibers [26].

As the excitation thresholds and hence stimulation amplitudes are typically significantly higher for muscle fibers than for the corresponding motor neurons, most FES applications target the MNs or the motor points [54, 78, 79]. *Motor points* are defined as the site of (transcutaneous) electrical stimulation that produces the strongest and most isolated contraction at the lowest level of ES [26, 80]. This is most likely the point where the MN branches and innervates the target muscle fibers [81]. In transcutaneous, monopolar electrode setups, in which a small electrode is combined with a comparatively larger electrode as depicted in Fig. 1.8, the smaller electrode is usually placed above or closer to the motor point. The electric field is higher beneath the small electrode compared to the larger one. In bipolar setups, both electrodes have the same size.

[3] In SCI, the upper MN, the lower MN, or both can be damaged. In the latter two cases, artificial activation of the muscles through ES of the innervating MN is not possible. The direct stimulation of denervated muscles to treat their degeneration and the associated decay of joints and skin will not be considered further in this work. Please refer, for example, to [74] and [75] for more information.

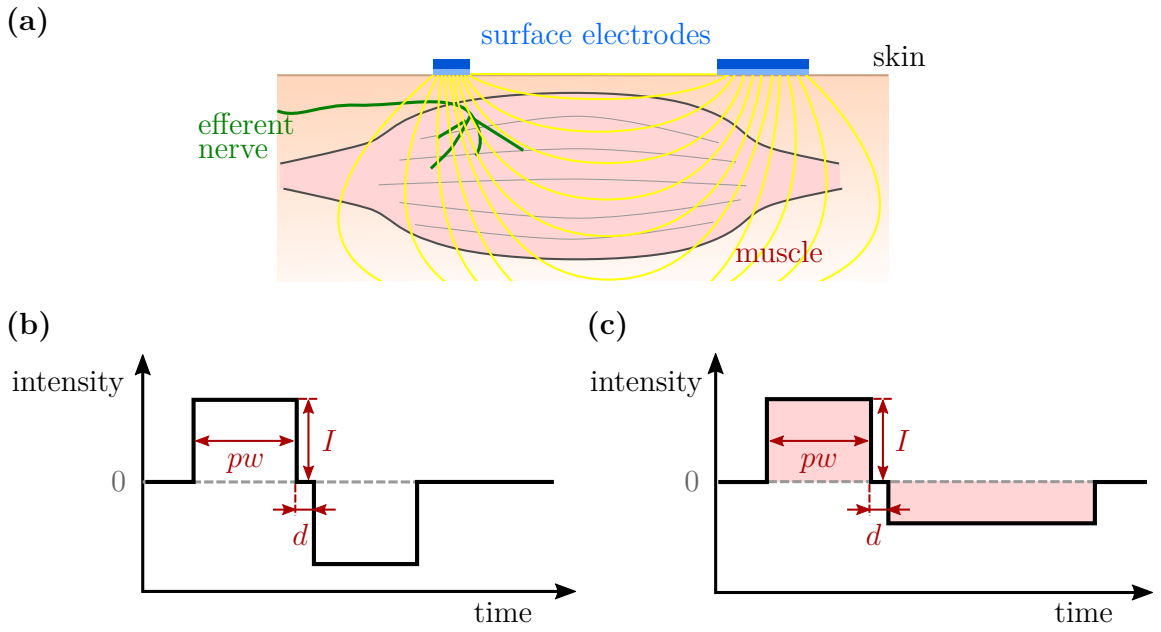

Figure 1.8: The principle of transcutaneous functional electrical stimulation with a monopolar electrode setup and typical electrical pulse shapes with parameter definitions (adapted from [71]). (a) The resulting electric field lines are illustrated in yellow. The closer the field lines are, the higher is the electric field strength leading to a depolarization around the innervating nerve. (b) Symmetric, charge-balanced bi-biphasic pulse. (c) Asymmetric, charge-balanced bi-biphasic pulse.

The stimulation pattern commonly used to excite motor neurons through ES is a sequence of rectangular impulses. To prevent the formation of electrochemical products that might interact with the electrodes or the underlying tissue, charge-balanced biphasic waveforms are often applied [67, 82]. Shape and parameters of the rectangular biphasic waveform are illustrated in Fig. 1.8. When applying biphasic pulses, the polarity of the electrodes changes from the first to the second phase. In the following, the electrode which is closer to the motor point and smaller in size will be referred to as the *active electrode* (in Fig. 1.8a the left electrode); the one further away from the motor point and larger will be referred to as the *counter electrode*. In general, the active electrode serves as a cathode (–) for the first phase of the biphasic pulse.

The applied pulse width pw depends on the FES application, namely on the muscle (group) that should be activated. It ranges between 10 µs and 1000 µs [25]. When the electric charge is sufficiently high, an AP will be generated in the MNs within the resulting electric field [83]. The impulse charge q, in the following also referred to as *stimulation intensity*, is defined as the product of electrical current I and pulse width pw.

$$q = I \cdot pw \tag{1.1}$$

For biphasic impulses, these scales relate to the positive phase of the impulse. The pause d in between the two phases is supposed to avoid diminished electrical excitation due to the reversal of the polarity at the electrodes [71, 82], see Fig. 1.8. The impulse charge q and the resulting electric field size and strength in the underlying tissue affect the number of recruited motor units and thereby the evoked muscle force as described in the previous section (*spatial summation*) [76].

Regarding the stimulation intensity, the following individual thresholds are differentiated in this thesis. The sensory threshold q_{sen} describes the stimulation intensity, where the stimulated individual first perceives the stimulation [84]. The motor threshold q_{mot} in FES marks the stimulation intensity, where first contractions of the target muscles or movements of the target system can be visually observed [84]. The workspace of the FES ranges from q_{mot} to stop threshold q_{tol}, which is the highest intensity an individual tolerates [84], or the mechanical threshold q_{mec}, where the mechanical system has reached the end of its range of movement. The individual thresholds vary significantly between humans and the body area of application [85].

Despite the pulse shape and stimulation intensity, the contraction pattern and the resulting muscle force are modulated by the *stimulation frequency* f_{s}, which is the number of electrical impulses applied in a second (*temporal summation*) [25, 76]. The *stimulation period* t_{s} is defined as $1/f_{\text{s}}$. Low stimulation frequencies ($f_{\text{s}} < 15\,\text{Hz}$) produce singular muscle contractions (twitches) rather than smooth, tetanic contractions as in physiologically generated movements [76]. The minimum frequency for evoking natural contractions of skeletal muscles varies between different muscles in the body [86]. To achieve continuous contractions of hand and arm muscles (tetanization), the stimulation frequency has to be at least 16 Hz or more [39]. Applications to other muscle groups benefit from higher frequencies, for example, in FES for drop foot correction with 60 Hz [34]. Furthermore, higher frequencies are generally reported to be more comfortable due to a smoother contraction rather than a tapping effect of lower stimulation frequencies [25, 87]. However, with increasing frequencies, the recruited muscle fibers fatigue faster during prolonged, synchronous stimulation [26, 88]. The relationship and effects between stimulation frequency, pulse shape, and intensity on the one hand and resulting force, fatigue, and perception, on the other hand, are still subject to research [25].

In the field of rehabilitation with neuroprostheses, transcutaneous functional electrical stimulation is dominant. Although percutaneous and implanted electrodes achieve a higher stimulation selectivity through precise placement and the necessary electrical charge applied is significantly lower compared to surface electrodes, they come with an invasive risk and challenges regarding biocompatibility and long-term stability [39, 71]. Transcutaneous FES is applied via self-adhesive or nonadhesive electrodes which are relatively low cost, noninvasive, comparatively easy to apply, and can be reconfigured for different functional requirements [26, 54]. Pairs of electrodes are usually placed on the skin in the vicinity of the estimated motor points of the target muscle [39, 73, 81], as illustrated in Fig. 1.8.

Finding the *optimal stimulation position* on the skin that generates the desired contraction in the target muscle(s) and strength at minimal stimulation intensity is very critical in transcutaneous FES and requires skill and patience [89]. Despite individual differences in anatomy and responsiveness toward FES, the localization of the electrodes is aggravated by the unknown electric pathways due to inhomogeneities in the skin and the unique structure of the underlying fat and muscle tissue [90]. Skin resistivity, necessary stimulation intensity to activate the target muscles, and tolerated stimulation intensity characterize and limit the outcome of the transcutaneous ES. Especially the selective activation of deeper structures (e.g., activation of the *M. flexor digitorum profundus* in the forearm) is delicate, as it requires high stimulation intensities and more superficial structures are activated as well (e.g., *M. flexor carpi radialis*) [26]. A higher selectivity in activation of neighboring muscles in the same layer

can be achieved using smaller electrode sizes [91]. *Electrode arrays* were introduced consisting of multiple, small elements, that can be activated separately and thereby offer a variety of stimulation options [92, 93, 94]. However, the electrode size affects not only the selectivity of the stimulation but also the choice of the stimulation parameters, the perceived comfort, and force generation associated with electrically induced excitatory responses [84].

Portable electrical stimulators are utilized to apply transcutaneous FES in practice. Available stimulators can be classified into constant-voltage regulated or constant-current regulated stimulators [79]. In a constant-voltage regulated stimulator, the effective stimulation depends on the impedance of the underlying tissue and the electrode-tissue-interface. Constant-current regulated stimulators provide a stable current over large impedance changes. However, they suffer from the risk of causing tissue damage in case the electrode-tissue impedance becomes partially very high yielding a high current densities at locations with lower impedance [24]. Commercially available stimulators usually come with preprogrammed protocols from which the users can choose [25]. Parameters can be adjusted, and some systems allow the design of custom ES programs.

Discomfort during transcutaneous ES limits the use of FES systems [89]. As the generated electric field propagates through and along the skin, cutaneous and subcutaneous pain receptors are activated as well leading to an uncomfortable, sometimes painful perception of the FES [95]. Inhomogeneities in the skin and electrode edge effects can lead to localized high current densities causing additional discomfort or even skin burns [90]. The applied current density at the electrode-skin-interface also depends on the size of the electrode, with smaller electrodes leading to higher current densities presumably leading to more discomfort than a larger electrode at the same stimulation parameters [91].

A major problem of transcutaneous FES is the different recruitment and activation of electrically stimulated muscles compared to physiological recruitment, resulting in faster muscle fatigue [67]. The artificial recruitment of MUs does not follow the Henneman's size principle. Instead, electrical stimulation at low intensities first activates fast-twitch type II muscle fibers, as the corresponding motor neurons have a lower threshold than type I fibers. Only with increasing stimulation intensity slow-twitching, fatigue-resistant type I fibers are recruited [79]. Furthermore, the motor units are activated synchronously via FES instead of asynchronously as in physiological activation [96]. Besides, the frequency of recruitment by electrical stimulation is significantly higher (16–100 Hz) compared to the firing rate of the MUs during voluntary contractions (5–10 Hz) [72, 97]. These factors prevent the recovery of the muscle fibers during the movement generation, and muscle fatigue develops rapidly. Several strategies were introduced to reduce muscle fatigue in electrically stimulated muscles, for example, via imitation of natural recruitment patterns through stochastically modulating the interpulse interval, or asynchronous stimulation at low frequencies (10–16 Hz) via a number of stimulation electrodes or elements of an electrode array spread over the target muscle [72, 86, 98, 99]. These methods help to delay but not prevent muscle fatigue.

Despite these limitations, FES is widely used in therapeutic and assistive interventions in various applications [34, 54, 100, 101]. In the motor rehabilitation of stroke patients, FES aims to reduce motor impairment by promoting sensorimotor re-learning through extensive exercise [35, 102]. Studies have shown that neuromuscular electrical stimulation activates

both efferent and afferent pathways, and thus also activates the somatosensory cortex of the CNS [103, 104]. Other effects of FES such as muscle strengthening, spasticity prevention, and physiological aspects (e.g., motivation), may additionally have a positive therapeutic impact on the motor rehabilitation of a patient [35]. There exists evidence that voluntary reaching and grasping function can improve in hemiplegic patients through repetitive, task-oriented FES interventions [45, 102, 105, 106, 107]. In SCI patients, FES attempts to assist with motor control and muscle strength in tetraplegic or paraplegic patients [100, 108]. Besides motor recovery and assistance in body motility, various other applications utilize FES: for treating dysphagia, assistance with respiration, restoring gastric function, supporting micturition, and pain management [71].

One of the many challenges in using FES as a neuroprosthesis for the upper limb is the synchronization of stimulation with the remaining, voluntary muscle activity. Synchronized biofeedback is proven to maximize the benefits of FES therapy [35]. A popular physiological approach to control FES is the registration of and synchronization with the remaining muscle activity via surface electromyography (EMG), see for example [24, 109, 110]. Electromyography measures muscle activity via the derivation of electrical potentials. When measuring with surface electrodes, mainly the sum of action potentials of the motor units located below and between the electrodes is detected [67].

Two different types of electromyograms can be observed from an electrically stimulated muscle: an FES-evoked EMG (eEMG) and a patient-induced, voluntary[4] EMG (vEMG) [13, 111]. The most characteristic feature of the eEMG activity is the *M-wave*, which occurs 3–6 ms after the impulse. The simultaneous activation of several motor units by a stimulation impulse yields this large wave (mV) in the EMG due to the superposition of many APs [67]. Some FES control approaches use the amplitude or area under the M-wave as a measure of the degree of muscle activation by FES [112]. However, EMG measurement during active ES is not trivial and requires advanced techniques [67]. The second part of the EMG recording, the patient-induced EMG activity, reflects the physiological muscle activation. Due to the asynchronous activation of MUs, this proportion is significantly smaller with an amplitude in the μV range and is related to the strength of the voluntary muscle contraction [113]. The vEMG appears as a rather noise-like signal with frequency components in the range of 30–300 Hz [114]. An example of surface EMG signals measured with voluntary contractions during active FES is presented in Fig. 1.9. Via signal processing including pattern recognition (M-wave) and high-pass filtering (vEMG), the two EMG components—FES–evoked and patient-driven—can be separated (e.g. [115, 116]). If the vEMG signal is continuously extracted, it can be used to modulate the strength of the ES delivered to paralyzed muscles (vEMG proportional control) [117, 118]. Besides the usage for control and synchronization the stimulation with the voluntary activity of an individual, the EMG measurements can be used to study muscle fatigue [119]. In addition to the EMG, other biological, for example, electroencephalography (EEG), and non-biological signals, such as force measurements or motion tracking, as well as multi-modal approaches were introduced to trigger and control the onset and strength of ES (e.g., [120, 121, 122, 123, 124]).

[4]The term *voluntary* assumes that reflex activity and spasticity can be neglected.

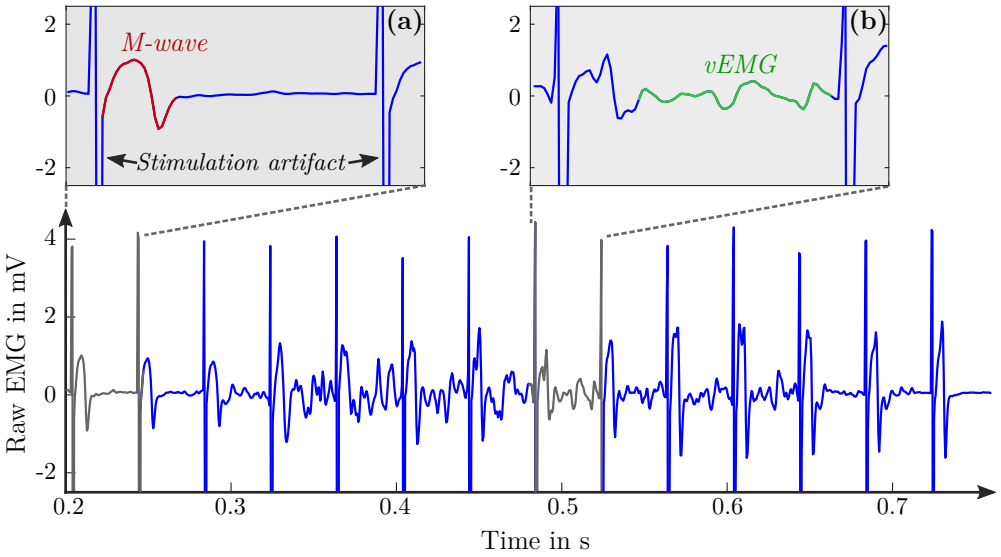

Figure 1.9: Exemplary surface EMG recording from the lower arm during active stimulation with a stimulation frequency of 25 Hz. Separate transcutaneous electrodes were used for stimulation and EMG recording of wrist and finger extensors. Sub-figure (a) shows a stimulation period with almost no volitional muscle activity. The *M-wave* induced by the FES as well as the stimulation artifact of each impulse are visible. In (b), a stimulation period with moderate patient-driven muscle activity is displayed. This figure is adapted from [13].

In summary, generating functional movements with transcutaneous FES in (partly) paralyzed limbs is not a trivial task. The outcome depends, among other things, on proper positioning of the electrodes, on the general muscular condition, on the stimulation pattern, on the correct synchronization with remaining activity and on the occurrence of internal and external disturbances [71]. Commercially available FES systems apply the electrical stimulation in open-loop: A predefined stimulation pattern is applied with predefined intensities at static stimulation positions. Closed-loop control of FES has the potential to improve the effectiveness and the usefulness of the therapy significantly: The stimulation parameters are adjusted according to the observed system status (feedback-loop). The positive effects of closed-loop FES have been demonstrated for gait support (e.g., [125, 126, 127]) as well as for arm motion support (e.g., [128]). However, as the human hand is a complex, highly nonlinear, coupled, and time-variant system [68], the development of practical closed-loop solutions for HNPs arises numerous challenges. They range from reliable, easy-to-attach sensors for feedback, over adaptive controllers for compensating the time-variant muscle response, to a user-friendly operation of such sophisticated systems. Therefore, closed-loop control strategies have not gained ground in clinical applications of HNPs yet [68].

1.5 Hand Motion Tracking

Besides biological signals, such as the EMG, the tracking of voluntary and generated movements has been widely used to control neuroprostheses [123, 129, 130, 131]. Furthermore, motion analysis is utilized in modern monitoring strategies to measure grasping performance, e.g., improvement in rehabilitation after stroke [132]. The tracking of hand movements presents a particular challenge due to the large number of finger segments and the resulting numerous degrees of freedom. Moreover, the field of rehabilitation imposes some specific demands on the

Table 1.1: Overview of suggested hand motion tracking systems for clinical applications. This list does not claim to be complete and rather shows examples. The advantages and disadvantages refer to the application in closed-loop FES for grasp-and-release tasks.

System Type		Examples	Advantages and Disadvantages
Optical systems	with markers	*Vicon* (Vicon Motion Systems, Oxford, UK)	(+) accurate (−) extensive setup by expert, expensive, line-of-sight restriction, stationary
	without markers	*Kinect V2* (Microsoft, Redmond, WA, USA) [131], *Leap Motion* (Leap, San Francisco, CA, USA)	(+) contactless, affordable (−) model-based accuracy, line-of-sight restriction
Data gloves	with bend sensors / optical fibers	*5DT Data Glove Ultra* (5DT, Orlando, FL, USA), *Cyperglove III* (CyberGlove Systems, San Jose, CA, USA)	(+) quick setup (−) less sense of touch, glove not suitable for spastic hand, hygienically problematic, measures only angles (no accelerations/ velocities/positions)
	with IMUs	*Cobra Glove* (Synertial, Lewes, UK), *PowerGlove* [133, 134, 135]	(+) quick setup, detailed measurements (−) less sense of touch, glove not suitable for spastic hand, hygienically problematic, calibration motions necessary, magnetic disturbances

design of a hand motion tracking system, such as ease of use, portability, and preservation of the sense of touch.

The Table 1.1 summarizes and compares available types of measurement systems for real-time hand movement data acquisition. They can be classified into two main categories according to the utilized sensor technology [83]: optical, vision-based systems and data gloves (resistive bend sensors, inertial sensors).

Optical systems work camera-based and detect an object by its contours [136] or by optical markers applied to the object, as seen in the examples of Fig. 1.10. Erol et al. [137] give a detailed overview of vision-based hand pose estimation. Motion tracking with optical markers is the gold standard in human motion capturing, with which new methods are usually compared [138]. However, the application of numerous, small markers on each segment of the hand is too time-consuming for daily hand tracking, and the camera system is usually stationary and expensive [139]. Therefore, marker-free optical motion capturing devices have become popular within the last years [140, 141]. Although computer gaming and virtual reality (VR) are the main drivers for this rapid evolution, the practical application in health care, for example, in robots of physical rehabilitation, is suggested and explored frequently [83, 142, 143]. These strongly model-dependent approaches face limited accuracy—depending on the lighting conditions—and line-of-sight restrictions when used for hand motion tracking [138]. For example, they can only track finger segments that are inside the observation volume and are not hidden by other segments or objects. In FES-elicited hand movements, which do sometimes not fit expected natural gestures, these restrictions become especially problematic.

Wearable, glove-based systems represent one of the most important technologies for acquiring hand movement data [144]. Gloves appear to be well suited for ambulatory use because they are portable, wearable, and supposedly easy to attach, as seen in Fig. 1.10c.

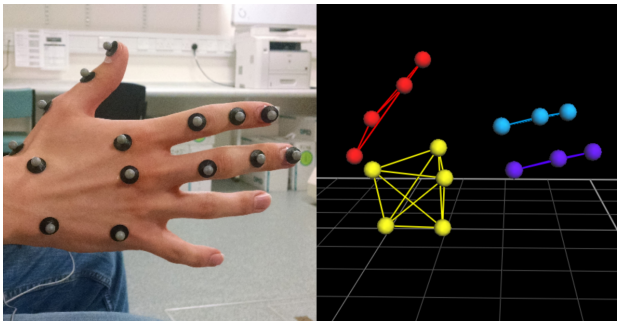

(a) Camera-based motion tracking with markers (©2018 Dimitra Blana)

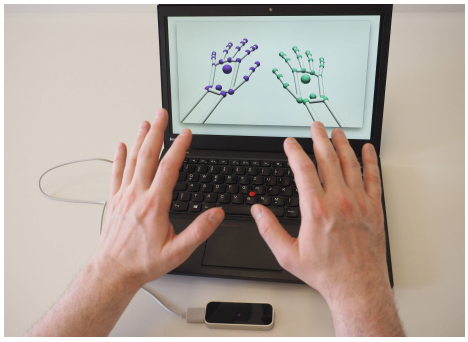

(b) *Leap Motion* for marker-free, camera-based motion tracking (Leap, San Francisco, CA, USA)

(c) *Cobra Glove* with 16 IMUs (Synertial, Lewes, UK; Photo: © AiQ-Synertial 2019)

Figure 1.10: Examples for motion tracking systems for the human hand.

However, gloves have the distinct disadvantage of being difficult to put onto motor-impaired or even spastic hands of stroke and SCI patients. They must be customized to individual hand sizes, lead to a reduced sense of touch, and cleaning and disinfecting is challenging. The available gloves differ in the way kinematic information is obtained [133]. Resistive bend sensors or optical-fiber sensors are placed in gloves of different material to cover the joints of interest [145]. This positioning makes them prone to mechanical wear, and it entails the need for a thorough calibration. Moreover, these sensors quantify joint angles and are not capable of measuring an absolute orientation of the finger segments (cf. Table 1.1).

The process in micro-electromechanical system (MEMS) technology resulted in the availability of tiny and low-cost inertial measurement units (IMUs), which can also be integrated into gloves for human hand motion tracking [146, 147]. IMUs typically consist of a combination of multi-dimensional gyroscopes, accelerometers, and often magnetometer sensors allowing the estimation of joint angles, segment and joint angle velocities, as well as position and orientation in space via sensor fusion techniques [148]. For hand motion tracking, the sensors are usually placed on single finger segments in a glove (e.g., [133, 149]). The current drawbacks of motion tracking with IMUs include the need for extensive initial sensor-to-segment calibration movements and the occurrence of measurement errors when measuring with magnetometers in magnetically-disturbed environments, such as indoor environments containing electronic devices and objects of ferromagnetic material [150].

Many of the mentioned systems offer a high tracking accuracy for healthy hands and are optimized for the various applications in virtual and augmented reality. However, there

are unsolved problems when it comes to the application in physical rehabilitation. These shortcomings are well reflected in the small number of existing studies that propose systems for closed-loop FES based on real-time sensing of hand motions (e.g., [42, 151, 152, 153]). In summary, there exist very few previous contributions that propose solutions for real-time hand motion tracking with respect to the requirements of motor rehabilitation in stroke and SCI patients.

1.6 Aim and Contributions of the Thesis

The previous, brief introduction to the basics of hand neuroprostheses highlighted the complexity and interdisciplinarity that a holistic approach requires. The challenges include the variety and dynamics of the neuromuscular system in the forearm and the hand, as well as the limitations of transcutaneous electrical stimulation regarding selectivity, muscle recruitment, and pain perception. Besides, intuitive interfaces between user and neuroprosthesis for synchronization and control of the system's behavior are needed.

The general objective of this thesis is the development of new adaptive strategies and concepts for a hand neuroprosthesis that address these challenges in a clinically relevant context. The primary goal, however, is not to establish a mature product, but much more to develop an improved set of rehabilitation tools in terms of customization of electrical stimulation, automatic control, and user-friendly operation. This work focuses on solutions for FES support of hand function, such as grasp restoration, and neglects the support of motion in the shoulder and elbow joint. The new methods aim at patients with preserved voluntary upper arm function, or might be combined with existing rehabilitation systems for the upper arm (FES, robotic) in the future.

With respect to the state of the art in HNPs for rehabilitation, the contributions of this dissertation are the following:

1. Detailed literature overview on HNPs, electrode arrays, and open- and closed-loop control of stimulation parameters,

2. New hardware concept for a HNP including a jointly developed novel hand sensor system for tracking kinematic data based on inertial sensors, and new electrode array designs,

3. Development of novel algorithms for real-time hand motion tracking with inertial sensors for application in patients with severe motor impairment of the hand, and evaluation in different environmental settings,

4. Conception and user-centered practicability analysis of two identification strategies for suitable stimulation points in electrode arrays for inducing arbitrary hand movements with FES, and

5. Development of a new control strategy for automatic real-time adjustment of electrode positions depending on the posture of the forearm to ensure sufficient grasping strength under varying forearm conditions.

1.7 Thesis Outline

Following the introduction, this thesis consists of six further chapters. The state of the art in HNPs is presented in *Chapter* 2. It highlights the demands, expectations, and resulting challenges of the application in rehabilitation and assistance.

Chapter 3 introduces the structure of the developed HNPs. The main components, such as electrical stimulator, electrode arrays, and the hand motion tracking system, are explained in detail.

Reliable motion tracking is a crucial factor for adaptive neuroprostheses. The developed hand sensor system is outlined in detail in *Chapter* 4. It includes the concept and the evaluation of the system for hand posture and joint angle estimation.

New approaches for identifying suitable stimulation sites in electrode arrays on the forearm are presented in *Chapter* 5. Identification methods with different levels of user integration were compared and evaluated by patients and health professionals in a user-centered study.

In *Chapter* 6, novel strategies for adaptive stimulation with the hand neuroprosthesis are described. They include an automatic adaptation and closed-loop control of stimulation parameters, such as position and intensity, to compensate forearm movements occurring in grasp-and-release tasks.

Finally, the thesis ends with an overall discussion and conclusions of the achieved results in *Chapter* 7. Recommendations for future research are provided.

1.8 Related Publications of the Author

This doctoral dissertation is based in part on the publications listed below. The entries are arranged chronologically.

Salchow-Hömmen, C., Callies, L., Laidig, D., Valtin, M., Schauer, T., Seel, T. “A Tangible Solution for Hand Motion Tracking in Clinical Applications”, *Sensors*, 19(1):208, 2019. DOI: 10.3390/s19010208.

Salchow-Hömmen, C., Jankowski, N., Valtin, M., Schönijahn, L., Böttcher, S., Dähne, F., Schauer, T. “User-centered practicability analysis of two identification strategies in electrode arrays for FES induced hand motion in early stroke rehabilitation”, *Journal of NeuroEngineering and Rehabilitation*, 15:123, 2018. DOI: 10.1186/s12984-018-0460-1.

Salchow-Hömmen, C., Thomas, T., Valtin, M., Schauer, T. “Automatic control of grasping strength for functional electrical stimulation in forearm movements via electrode arrays”, *at – Automatisierungstechnik*, 66(12):1027–1036, 2018. DOI: 10.1515/auto-2018-0068.

Thomas, T., Salchow, C., Valtin, M., Schauer, T. “Automatic real-time adaptation of electrode positions for grasping with FES during forearm movements”, In *Automed Workshop*, Villingen-Schwenningen, March 2018.

Salchow, C., Dorn, A., Valtin, M., Schauer, T. “Intention recognition for FES in a grasp-and-release task using volitional EMG and inertial sensors”, *Current Directions in Biomedical Engineering*, 3(2):161–165, 2017. DOI: 10.1515/cdbme-2017-0034.

Valtin, M., Salchow, C., Seel, T., Laidig, T., Schauer, T. “Modular finger and hand motion capturing system based on inertial and magnetic sensors”, *Current Directions in Biomedical Engineering*, 3(1):19–23, 2017. DOI: 10.1515/cdbme-2017-0005.

Jankowski, N., Schönijahn, L., Salchow, C., Ivanova, E., Wahl, M. “User-centred design as an important component of technological development”, *Current Directions in Biomedical Engineering*, 3 (1):69–73, 2017. DOI: 10.1515/cdbme-2017-0015.

Salchow, C., Valtin, M., Seel, T., Schauer, T. “Development of a Feedback-Controlled Hand Neuroprosthesis: FES-Supported Mirror Training”, In *Automed Workshop*, Wismar, September 2016.

Salchow, C., Valtin, M., Seel, T., Schauer, T. “A new semi-automatic approach to find suitable virtual electrodes in arrays using an interpolation strategy”, *European Journal of Translational Myology*, 26(2):6029, 2016. DOI: 10.4081/ejtm.2016.6029.

1.9 Related Student Projects Supervised by the Author

Many of the experimental results that are described and discussed within this dissertation have been obtained with the valuable support of students whose Bachelor/Master thesis or projects the author supervised or co-supervised. Again, the entries are arranged chronologically.

Callies, L. “Development and evaluation of quaternion-based methods for hand posture estimation via inertial sensors”, Master Thesis, 2018 (supervised together with T. Seel)[5].

Szabo, G., Thomas, T., Pannen, C. “Untersuchung des Einflusses der Armhaltung auf FES-induzierte Handbewegungen” (engl.: *Examination of the influence of arm posture on FES-induced hand movements*), Project, 2017.

Schönijahn, L. “Funktionelle Elektrostimulation in der Schlaganfallbehandlung: Nutzerzentrierte Entwicklung einer grafischen Benutzeroberfläche” (engl.: *Functional electrical stimulation in stroke rehabilitation: User-centered development of a graphical user-interface*), Master Thesis, 2017 (collaboration with supervision by M. Minge and N. Jankowski).

Dorn, A. “Sensor fusion for intention recognition and FES-control in a hand neuroprosthesis”, Master Thesis, 2017.

Nguyen, A. “Extension of the automatic search for virtual electrodes for grasping”, Project, 2016.

Jirasek, R. “Entwicklung und Evaluierung eines automatisierten Identifikationsverfahrens zur Regelung einer Handneuroprothese” (engl.: *Development and evaluation of an automated identification method for control of a hand neuroprosthesis*), Master Thesis, 2016.

Nguyen, A. “Development and validation of a test frame in SimMechanics for simulation of an inertial measurement unit based handsensory”, Project, 2016 (supervised together with T. Seel).

[5] Awarded the *Clara-von-Simson* prize of the Technische Universität Berlin (third place)

Smadi H. “Optische Bewegungsanalyse und entkoppelte Regelung mit Einzelelektroden für eine Handneuroprothese” (engl.: *Optical motion analysis and decoupled control with single electrodes for a hand neuroprosthesis*), Bachelor Thesis, 2016.

Bias A. “Design and implementation of a controlled, manual array electrode element search with virtual interface”, Final-year Project at University of Glasgow, 2016.

2

State of the Art in Hand Neuroprostheses

2.1 Overview

This chapter summarizes the state of the art of hand neuroprostheses based on FES. In *Section* 2.2, the goals and requirements for the behavior and characteristics of an ideal HNP for recovery or replacement of grasp function are elaborated. It will be shown that there exist conflicting demands, making the development of HNPs that mimic physiological movement abilities especially challenging. These considerations are the basis for evaluating the available neuroprostheses and approaches reviewed in the following.

Section 2.3 provides a chronological overview of early successful systems, which were termed hand neuroprostheses. In this dissertation, the focus is on noninvasive, transcutaneous systems. The use of single surface-electrodes posed some problems, for example, due to insufficient selectivity of stimulation and anatomical and physiological differences between individuals. As a result, the electrode array technology reviewed in *Section* 2.4 has been widely applied in research over the last decades. The identification of suitable active electrodes within electrode arrays is a central topic in array technology for grasping and is therefore examined in detail.

Assuming that a sufficient electrode setup on the forearm was established, the subsequent question arises on how to generate movement by FES such that it supports the residual motor activity and needs of the patient. Consequently, *Section* 2.5 reviews approaches on synchronization of FES with the patient's intention and opportunities for real-time adaptation of stimulation parameters. Different biological and non-biological signals for driving HNPs as well as existing methods for open- and closed-loop control of FES-grasping are discussed.

The identified open problems and challenges for the practical application of HNPs are then summarized in *Section* 2.6. The main research questions, which were addressed in this thesis, are explained.

2.2 Goals and Requirements

The goal of almost all presented and available HNPs is the improvement or assistance of the grasp function. The hand function shall be supported with FES in a physiological way, such that the resulting motion resembles a natural limb function and allows the performance of ADL [39]. The ideal behavior of a HNP would be that the FES activates the same nerves/muscles which the patient's body is recruiting or would recruit for the desired movement if volitional activity existed. This requires that all hand and forearm muscles can be activated separately by the FES. Thereby, the patient should be able to achieve the whole range of possible movements of the human hand and the resulting forces with the help of the HNP. Furthermore, an ideal HNP should be able to provide this behavior regardless of the individual pathology of the patient. For example, if a patient possesses partial volitional grasp function, the objective of an HNP is to only augment the remaining grasp function by FES [35]. The residual voluntary activity of affected patients can range from zero to almost just single muscle weakness. Besides, not all parts of the arm and hand are affected to the same degree. Regardless of the remaining volitional function of the individual and how the neuroprosthesis is used to assist grasp, the HNP should never interfere with the patient's preserved motor capabilities while supporting the hand function [39]. Therefore, HNPs need to provide various grasping and command strategies to adapt to the individual needs and therapy goals of a patient.

The generation of complex hand movements requires the control and synchronization of several stimulation channels in a fast and straightforward yet reliable way [39]. It is desirable that the neuroprosthesis reacts as fast as the natural activation via the human motor pathways (see *Chapter* 1) would respond; in other words, the neuroprostheses should have the same time delays as the human system to allow for quick movements.

At last, the system should also be easy and fast to use by all user groups to gain acceptance in clinical practice. In this context, essential user groups, that encounter the HNP, are patients with paralysis (stroke, SCI), clinicians (physiotherapists, occupational therapists, physicians), and persons who take care of patients (e.g., relatives). Each user group—and maybe also each user—has a different knowledge background and different expectations regarding the system's behavior and mode of operation. Moreover, there exist different application scenarios regarding the environment, in which the HNP should be applied (clinical setup, home setup), and the objective of the application (therapy or technical aid), each coming with further specific requirements toward the device. However, a short setup time of the hand neuroprosthesis is essential for all applications. As paid therapy sessions are limited in time, the complete setup of a HNP should ideally take no longer than five minutes. The HNP should be easy and fast to put on and take off. Quick initialization of the system can only be realized by a high degree of automation and storage and recall of previous settings of an individual patient. In addition to these functional requirements and desirable behavior of HNPs, there exist further demands, such as hygiene aspects, recyclability of system components (e.g., electrodes), and monetary aspects.

It is unlikely that the described ideal behavior can be achieved with a single HNP system. Many of the stated requirements exclude each other. For example, to achieve a short setup time, it would be useful to have a hardware setup with a small number of components. On the

other hand, a high degree of automation to allow automatic initialization and adaptation can only be realized with information from large sensor networks of different types. Furthermore, the muscle recruitment with FES differs from physiological muscle recruitment (cf. *Section* 1.4). Therefore, an FES activated muscle cannot have the same dynamic characteristics as a naturally recruited muscle (e.g., time delays). However, the above paragraphs give an overview of the ideal behavior of HNPs and also to some extent reflect the expectations and hopes of the users. Those should be kept in mind when reviewing the achievements of published and available FES systems. Many HNPs have been introduced over the last years, each taking a further step toward reliable, user-independent, and adaptive HNPs by presenting a solution for parts of the problem, such as the generation of a specific grasp type, a setup for a particular application scenario, or a distinct control strategy of the stimulation. The following review summarizes the most popular approaches and highlights the current research in the field of hand rehabilitation with FES technology.

2.3 First Generation of Hand Neuroprostheses

Past and existing hand neuroprostheses can be classified into invasive and noninvasive approaches, depending on their application of electrical stimulation via implanted or surface electrodes [154]. The first commercially available invasive system was the *Freehand system* from NeuroControl Inc. (1997), developed in Cleveland (OH, USA) by the team of Peckham/Mortimer/Keith [18, 27, 155]. Stimulation was applied via implanted epimysial electrodes and an implantable eight-channel stimulator and controlled by a shoulder position transducer mounted on the contralateral shoulder. Extrinsic muscles on the forearm and intrinsic hand muscles were stimulated (cf. *Section* 1.2). It was an open-loop system, meaning the system used a one-way communication direction, from an external controller box to the implant. The position transducer monitored two axes of shoulder motion, where one axis (usually protraction/retraction) was used to control hand opening and closing, and the other axis (usually elevation/depression) was used for logical commands, for example, holding a stimulation level [24]. It was possible to adjust the control strategy to different shoulder motion capabilities of the individual patients. The target user group was tetraplegic SCI patients, in specific individuals with chronic hand impairment regarding grasping and holding. They used the system—if necessary in combination with tendon transfer on the upper arm for elbow extension (reaching)—as a permanent assistive device to perform ADL [18].

The major drawback from the economic perspective of invasive systems such as the *Freehand system* is that the potential user group of SCI patients is relatively small, whereas the setup costs of the system including surgery, as well as the development costs, were comparatively high. Consequently, the commercial distribution of the *Freehand system* was ceased in 2002 [154]. However, invasive systems with a similar setup but support of hand, elbow, and shoulder function are under investigation in current research [156, 157, 158]. Stroke patients are the larger patient group compared to SCI. Stroke rehabilitation has the primary goal to regain full recovery of hand motor function, which requires the development of HNPs for temporary use in therapy rather than for permanent assistance as provided by implanted systems. Especially the application of FES in the early phase of rehabilitation, which is suggested, needs flexible

systems [39]. Therefore, this thesis and the following literature review exclusively focuses on noninvasive FES systems.

Noninvasive FES systems apply the stimulation transcutaneously, usually via self-adhesive surface electrodes, as described in *Section* 1.4. The first generation of noninvasive systems for restoring hand function are the *Handmaster* from NESS Ltd. (Israel) [28], and the *Bionic Glove* from the University of Alberta [159]. Based on previous research results regarding the applicability of FES on the forearm and the design of stimulation setups [160, 161], the *NESS Handmaster* became commercially available in 1994 [24]. It combines a forearm orthosis with FES to restore simple grasps [28]. Adjustable electrodes are placed in the inner surface of the orthosis, such that they stimulate the finger flexors and extensors and the thenar muscle group via three stimulation channels. The stimulation patterns are fixed, and only the stimulation currents can be adjusted manually. The user controls the stimulation via a simple push-button connected via cable. The orthosis can be mounted without voluntary finger activity by the patient itself and is therefore applicable for home use. Limiting factors of this system are the solid construction of the orthosis that restricts the range of motion, the fixed stimulation patterns, and the limited space for electrode positioning, which sometimes inhibits suitable stimulation of all desirable muscle groups (e.g., finger flexors) [24]. The first successor system *NESS H200* was presented by the company Bioness Inc. (USA), which nowadays provides the newest version *NESS H200 Wireless*[6] (see Fig. 1.1a in *Chapter* 1). In both follow-up systems, the original functionality did not change. Minor modifications were applied regarding the fit and design of the orthosis, and the latest version has a wireless control unit.

The *Bionic Glove*, marketed as *Tetron Glove* by Neuromotion (Canada) until 1999, stimulated the same muscle groups as the *Handmaster*, but had a different design and control strategy [24]. The neuroprosthesis aimed at improving/strengthening the functional tenodesis grasp and release in patients with voluntary control over wrist flexion and extension [39]. Tenodesis refers to the (passive) opposition of the thumb and index finger via voluntary extension of the wrist due to mechanical coupling [162]. This grasp type is beneficial for SCI patients with functional C6–C7 level and stroke patients with active wrist [24]. The *Bionic Glove* provides electrical stimulation via three active electrodes over the motor points and one common counter electrode placed in a neoprene sleeve, which also holds connectors, wires, and the stimulator [159]. The control unit and the stimulator were integrated into the sleeve (or fingerless glove), making the *Bionic Glove* a wireless and portable system. An integrated position transducer over the wrist was used to detect voluntary movement in this joint according to preset trigger angles. Once the system recognizes a wrist extension, the finger flexors are stimulated to provide hand closure. Vice versa, when the wrist flexes, a hand opening was stimulated. The *Bionic Glove* was built very compact focusing on usability. However, the exposed position of the stimulator and control unit as well as unreliable electrode contacts were some of the disadvantages of this system [24].

Another available system at that time was the *Belgrade Grasping System* (BGS) proposed by Popović et al. in 1998, which was developed based upon clinical experience with the *Bionic Glove* [54]. The BGS was the first noninvasive system which simultaneously stimulated grasping and reaching. In the first version, the BGS consisted of four stimulation channels with

[6] `https://www.bioness.com/Products/H200_for_Hand_Paralysis.php` Accessed on January 16th, 2018

single electrodes, where three channels were used for grasping function, and the fourth channel stimulated the triceps brachii muscle in the upper arm for augmenting elbow extension [163]. A predefined stimulation pattern, which was derived from physiological movement synergies observed in healthy volunteers, was triggered via a push-button [164]. The stimulation system was subsequently marketed as the *Actigrip CS* and was used in future systems [54, 92].

Keller [24] presented in his thesis a neuroprosthesis for grasping for SCI based on a portable, programmable system named *Compex Motion*. The system was designed to be used in a wide range of FES applications since stimulation patterns (stimulation amplitude, frequency, and pulse width) could be freely chosen and changed in real-time. As each patient shows an individual pathology and a specific reaction to the electrical stimulation, a flexible stimulator system marked an important, necessary step toward the fulfillment of the requirements of an adaptive, user-independent neuroprosthesis. The author also presented different control strategies between which it was possible to choose for the individual patient. A push-button, voice control, and surface EMG recordings, registered from consciously recruited muscles from the contralateral limb, were available for an event-triggered stimulation. This control paradigm allows the initiation of the stimulation (onset), the switching between hand closure and hand opening, and, in the case of voice control, also realizes an adjustment of the stimulation intensity. Additionally, a sliding potentiometer and the EMG signal were utilized for continuous control of the stimulation parameters. Depending on the position of the slider or the ratio between the EMG of two muscles, hand opening or closing is commanded, and the stimulation intensity is set proportionally. Because the EMG is a biological signal, the usage of EMG allows a more natural way to control the neuroprosthesis, but it is also less robust to (environmental) disturbances and more challenging to handle than the other strategies [24].

All five control strategies were applicable with the portable *Compex Motion* FES system [24]. The neuroprosthesis for grasping was tested in ten SCI patients with varying levels of impairment with the focus on its suitability as a technical aid in ADL. In six subjects (C4–C7) the neuroprosthesis was able to generate the desired function, such that the patient could perform ADL with the neuroprosthesis they could not complete without it. All implemented control strategies were applied, indicating that a variety of control methods should be offered by HNP systems to fit the patient's needs. Issues with the developed system were the long donning time of the prototype of approximately 5–10 minutes [24]. Although the technical setup allowed a dynamic change of stimulation parameters, a feedback-control of the electrical stimulation was not presented.

Besides those specialized hand systems, multi-purpose EMG-triggered FES systems are commercially available for the treatment of stroke patients in a clinical or home environment. Examples are the *Automove 800* (Danmeter-Canada, Surrey, BC, Canada), as well as the *NeuroMove NM 900* (Biomation, Amonte, ON, Canada), or the *STIWELL med4* (MED-EL, Innsbruck, Austria), as seen in Fig. 2.1. In the training with those systems, patients have to use their voluntary residual muscle activity to exceed an individually set EMG threshold. If the threshold is reached, a predefined stimulation pattern is applied. Audio and visual feedback is provided for motivation purposes. However, those systems lack tracking and feedback of the stimulation outcome (e.g., motion tracking, eEMG) and, therefore, these systems do not meet the demands for adaptive, controlled stimulation.

(a) *NeuroMove NM 900* (Biomation, Amonte, ON, Canada; Photo: ©Biomation)

(b) *STIWELL med4* (MED-EL, Innsbruck, Austria; Photo: ©MED-EL)

Figure 2.1: Examples of commercially available EMG-triggered FES systems.

2.4 From Single Electrodes to Electrode Arrays

Common problems in the application of single surface electrodes for generating wrist and precise finger movements in HNPs are the limited selectivity resulting in unwanted movements and the time-consuming process of finding suitable stimulation sites. The high density of muscles in the forearm, responsible for complex hand and finger movements of 23 DOFs, make a selective activation of target muscles essential for generating functional grasps (cf. *Chapter* 1). Because of the inter-human variances in anatomic structures and the inability to precisely predict the pathways of the electrical charge, it requires a lot expertise and patience of the users to place single electrodes in the optimal position for the function to be performed [92]. The standard, manual procedure for finding suitable electrode positions is to place the electrodes on a first guess, apply stimulation at increasing intensities, observe the evoked motion, and judge the outcome qualitatively. Then the often self-adhering electrodes are taken off and repositioned at a different location on the skin until a satisfying movement is generated. As it becomes obvious that this process can be time-consuming, it gets even more difficult when different electrode sizes are available and can be tested [92]. Moreover, suitable electrode sites can overlap for different muscles making a selective, independent activation with single electrodes of available shape impossible. The integration of individually arranged, multiple electrodes and corresponding wires into a garment (e.g., as suggested by Rupp et al. [29]) or orthosis (e.g., *Bioness H200*) can help to accelerate the donning and positioning of the neuroprosthesis but does not always improve a highly selective activation of target muscles [54]. Another observed problem occurs through the relative movement between the skin surface and the underlying muscular and neural tissue during rotation of the forearm, namely pronation or supination. The forearm rotation may result in a shift of the stimulation point, which can change the evoked movement as other muscles are stimulated [92]. Hence, a dynamic adjustment of the stimulation point is necessary to support ADL with FES, which is not possible when using static, single surface electrodes.

Electrode arrays (or *multi-pad electrodes*) were introduced for HNPs as an alternative solution to overcome some of the problems in surface electrical stimulation [92, 165, 166]. Electrode arrays (EAs) consist of multiple, small single electrode elements or pads, which can be activated separately. Usually, the elements are arranged on a flexible printed circuit

board (PCB) or integrated into a textile. In PCB-based EAs, skin contact is usually provided through a sticky hydrogel layer [90]. Either each element receives a single gel-pad (e.g., [167], see Fig. 2.2) or all elements are covered by a common hydrogel layer (e.g., [42], see Fig. 2.3). In most applications, a monopolar electrode setup was utilized, with the active electrode element(s) in the array above the motor point and a common, larger single electrode as counter electrode (see *Section* 1.4). By activating multiple elements in a defined temporal pattern (synchronously/asynchronously), so-called *virtual electrodes* (VEs) can be formed [166, 168, 169]. VEs can evoke an electric field with almost arbitrary shape, which can be changed in position and time. In the technical realization, one channel of a conventional stimulator is usually expanded with a controllable demultiplexer that connects with the EA(s) and splits the current to the selected elements. Usually, the elements are connected in parallel.

Lawrence et al. [166], who introduced the term *virtual electrode*, combined the *Compex motion* stimulator with a customized demultiplexer to distribute the stimulation on up to 16 channels and a novel, customized, fabric EA with 16 elements. When searching for selective stimulation of finger flexors (index, ring, and little finger), they observed different forces for various VE configurations and placements on the array. One conclusion was that EAs with a high number of small elements are required to achieve sufficient selectivity in stimulation through precise placement of VEs.

A new challenge arising from the application of electrode arrays is the exponentially increasing number of possible VEs resulting from a rising number of electrode elements. Over the last decades, extensive research has been performed on developing and optimizing identification strategies for determining suitable VEs in electrode arrays for HNPs (e.g., [151, 170, 171, 172]). Numerous FES systems were introduced that differed in electrical stimulator technology, electrode array design including material, element shape, element size, number of elements and their gel-layer's layout, the applied VE identification strategies, as well as the additional sensors utilized for (partly) automation of the electrode configuration and stimulation parameters. The following paragraphs hold a chronological and EA-sorted overview of suggested FES systems with transcutaneous EA technology for HNPs. The electrode arrays and VE identification strategies are summarized in Table 2.1, in the same order as they appear in the text.

In literature, a recent review on EA technology for the application to the upper and lower extremities can be found in [173]. Furthermore, the electrical behavior of stimulation via electrode arrays with different characteristics (e.g., layout, element size, surface conductivity) was analyzed via current density modeling and measurements in multiple studies (e.g., [90, 91, 174, 175]). The characteristics of the applied gel-layer (resistivity, coverage single/common) and the gap between elements turned out to be essential factors regarding selectivity, comfort, and current distribution. When using a common gel-layer, the spread of the electric field and thereby the selectivity of the stimulation is regulated by the gel resistivity[7] and the gap size between elements [174]. The use of single gel-pads for the EA offers a selective stimulation implicitly, but might yield a more painful stimulation due to increased current densities [91, 176]. Furthermore, the pads can be difficult to handle in clinical practice, as they need to

[7] A low electrical resistivity of the gel leads to a more focal electric field beneath the electrode and vice versa.

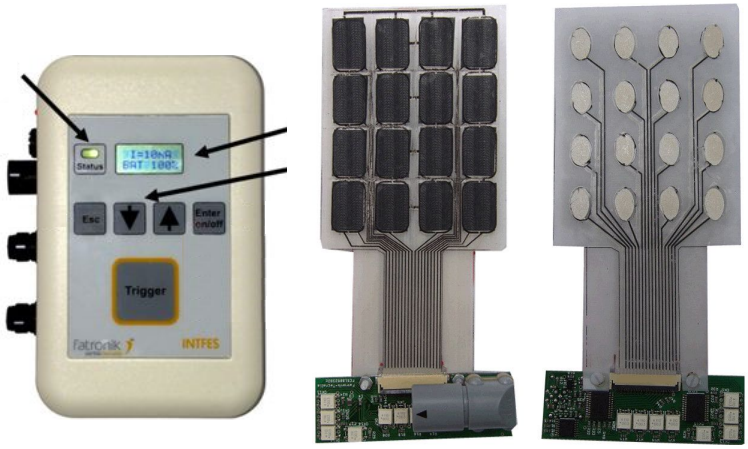

Figure 2.2: The *INTFES* system consists of the stimulator and the multi-pad electrode including a stimulation channel multiplexer board. The electrode is shown in top-view (left) with the pressure sensor layer and in bottom-view (right) with the contact layer covered with hydrogel pads. The system was first introduced by Velik et al. [167]. The figure is a reproduction with modifications from Malešević et al. [177], used under CC BY 2.0 [8].

be changed frequently. Keller & Kuhn [90] suggest gap sizes below 3 mm for EAs and list corresponding gel resistivities for different gap sizes with a common gel-layer.

Bijelić et al. [92] were the first to introduce an interactive interface for the array configuration together with a 24-element electrode array. The so-called *Actitrode* array was combined with a programmable stimulator (*Actigrip CS*; Neurodan, Aalborg, Denmark) and a switcher box, which consisted of 24 push-button switches that matched the layout of the conductive fields on the flexible substrate electrode array. Two electrode arrays were positioned at the dorsal and volar side of the forearm, with a common counter electrode above the carpal tunnel (cf. Fig. 1.5). The setup was tested in three post-stroke hemiplegic patients and the FES response was evaluated by recording six joint angles on the index and ring finger as well as the wrist using flexible goniometers (Biometrics, Gwent, UK). The authors reported that suitable VE configurations in the electrode array for finger flexion and extension were changing with respect to the position of the sensory and motor nerves when the forearm was pronated and supinated. A major conclusion for future developments was that the VE form and position have to dynamically fit the relative movement of the stimulated structures and the skin contact [92]. However, Bijelić et al. did not present a solution for this real-time adaptation of the VEs. Furthermore, they found different electrode configurations for each patient, revealing that it is necessary to investigate the array for every patient individually. The proposed concept with the manually switchable interface appeared user-friendly due to its intuitive usage but yielded a slow identification process making it impossible to test all available element combinations.

[8] https://creativecommons.org/licenses/by/2.0/

Table 2.1: Overview of electrode arrays, stimulation setup, and VE identification methods for HNPs.

Authors	**Electrode array**			**Stimulator**	**Anode**	**Identification strategy**			
and year	Number of elements, name	Shape, size, layout	Material	Name, number of channels		Degree of automation	Utilized sensors	Criteria	Tested on patients?
Bijelić et al. 2004 [92]	24, *Actitrode*	round, $\emptyset$ 1 cm, 6×4	plastic flexible substrate, micro-fiber textile patches, no hydrogel	*Actigrip CS* (Neurodan, Aalborg, Denmark), 4	single electrode	manual	push-button controller box	strongest finger flexion/ extension without coupling of the wrist	yes (stroke)
Popović-Bijelić et al. 2005 [178]				*Actigrip CS* (Neurodan, Aalborg, Denmark), 4	single electrode	manual	push-button controller box	grasp: sufficient finger flexion with wrist deviation $< 15°$; release: sufficient finger extension with wrist deviation $< 15°$	yes (SCI)
Popović & Popović 2009 [170]				*UNA-FET* (Unasistemi, Belgrade, Serbia), 4	single electrode	automatic	eletrogoniometer (7 joint angles)	sufficient strong grasp with wrist deviation $< 15°$	yes (SCI)
O'Dwyer et al. 2006 [179]	single electrode matrix	round, $\emptyset$2.5 cm, 2×2	x	*NeuroTech NT2000* (BMR, Galway, Ireland), 2	matrix of 2 single electrodes	automatic	data glove with goniometers and flex sensors	match between measured and ideal reaching motion (wrist= $15° \pm 5°$, finger flexion $<$ threshold; wrist deviation $<$ threshold)	no
Keller et al. 2006 [93, 180]	60	rectangular, 1 cm^2, 10×6	garment sleeve, no hydrogel reported	*Compex Motion* (Compex Medical SA, Ecublens, Switzerland), 4	single electrode, elements of the EA	automatic	force sensor [181]	strongest force in that finger with minimal coupling to the other fingers	no

The reviewed publications on electrode arrays on the forearm are listed in the order of appearance in the text, which is based on the date of publication and the utilized EA.

Table 2.1: Overview of electrode arrays, stimulation setup, and VE identification methods for HNPs (continued).

Authors	**Electrode array**			**Stimulator**	**Counter**	**Identification strategy**			
and year	Number of elements, name	Shape, size, layout	Material			Degree of automation	Utilized sensors	Criteria	Patients?
Schill et al. 2009 [182]	single electrode matrix	round, $\emptyset 2.5\,\mathrm{cm}$, 3×3	x	*Motionstim 8* (Krauth & Timmerman, Hamburg, Germany), 8	single electrode	semi-automatic	3 bending sensors	correlation of magnitudes between recorded movement and reference movement	no
Malešević et al. 2010 [183, 184]	16, *INTFES*	oval, $1.0\,\mathrm{cm}^2$, 4×4	plastic flexible substrate, separate hydrogel pads	not named	single electrode	semi-automatic	flexible goniometers (wrist, MCP F3–F4)	ANN to distinguish between different waveform classes and define correlation of each pad and activated muscle beneath	no
Hoffmann et al. 2012 [151]			common hydrogel layer	*INTFES* [167], 1	single electrode	automatic	VR data glove (*DG5 Vhand 2.0*)	maximal movement amplitudes of single elements together with four different combination strategies	no
Malešević et al. 2012 [177]				*INTFES* [167], 1	single electrode	manual / automatic	6 flex sensors (wrist (2), F2–F5)	grasp quality via cost function: weighted flexion amplitudes of fingers and wrist for different desired hand postures	yes (stroke)
Popović-Maneski et al. 2013 [94]	23	rectangular, varying, [2; 4; 3; 4; 3; 4; 4]	plastic flexible substrate, common gel-layer	*INTFES* [167], 1	single electrode	manual	flex sensors (wrist, F1–F4)	sufficient strength of contraction can be generated in the target muscles with minimum overflow to non-synergistic muscles	yes (stroke)

The reviewed publications on electrode arrays on the forearm are listed in the order of appearance in the text, which is based on the date of publication and the utilized EA.

Table 2.1: Overview of electrode arrays, stimulation setup, and VE identification methods for HNPs (continued).

Authors	**Electrode array**			**Stimulator**	**Counter**	**Identification strategy**			
and year	Number of elements, name	Shape, size, layout	Material			Degree of automation	Utilized sensors	Criteria	Patients?
Exell et al. 2013 [171], Freeman 2014 [153]	40	oval, unknown, 5×8	flexible PCB, probably common gel-layer	*Odstock* (Odstock Medical, Salisbury, UK), 4	single electrode	automatic	14 joint angles with data glove (*5DT 14 Ultra*) plus 2 electrogoniometers	Newton-based iterative-learning control: minimize quadratic difference between measured and desired hand pose	no
Kutlu et al. 2016 [185]	24	oval, unknown, 4×6	flexible PCB, common gel-layer	*Odstock* (Odstock Medical, Salisbury, UK), 4	single electrode	automatic	wrist and finger joint angles via optical motion tracking with *Kinect* and *PrimeSense* (cf. *Section* 2.5.2)	Newton-based iterative-learning control (see above, [153, 171])	yes (stroke)
Pedrocchi et al. 2013 [40] (*MUNDUS*)	unknown number of elements	rectangular, varying size, 6 separate EAs	flexible PCB, probably 1 common gel-layer per EA	*RehaStim* (Delta Version [186]; HASOMED, Magdeburg, Germany), 8	3 single electrodes	automatic	customized data glove with bend sensors over MCP+ PIP joints and force sensors on fingertips and palm	not described	yes (SCI and multiple sclerosis)

The reviewed publications on electrode arrays on the forearm are listed in the order of appearance in the text, which is based on the date of publication and the utilized EA.

Table 2.1: Overview of electrode arrays, stimulation setup, and VE identification methods for HNPs (continued).

Authors	**Electrode array**			**Stimulator**	**Counter**	**Identification strategy**			
and year	Number of elements, name	Shape, size, layout	Material			Degree of automation	Utilized sensors	Criteria	Patients?
Crema et al. 2017 [42]	78, *HandNMES*	rectangular, 12×16 mm and 14×18 mm, 6 separate EAs	plastic flexible substrate, 1 common gel-layer per EA	*RehaStim* (Delta Version [186]; HASOMED, Magdeburg, Germany), 8	single electrode(s)	semi-automatic	*Vicon Bonita* (optoelectronic motion capture system) with hand model for wrist and F1–F5 plus force sensors on the fingertips	match between induced movement and library of desired movements plus feedback from the subject (perception); ranking criteria: limited wrist motion, effective grasping kinematics, and comfort of stimulation	no
Crema et al. 2017 [187] (*Helping Hand*)	59	unknown shape and size, 5 separate EAs (layout 4×4 and 2×2)	flexible PCB, probably one common gel-layer per EA	*INTFES* (customized) [167], 1	unknown	manual	none	adjustment of VE via GUI	yes (stroke)
Molteni et al. 2018 [188], Crema et al. 2018 [189] (*RETRAINER*)	16×3 EAs	rectangular, unknown size, 4×4	flexible PCB, several gel-patches each covering several elements	*RehaMovePro* (HASOMED, Magdeburg, Germany) [190]	unknown	manual	for control: force and inertial sensors)	adjustment of VE via GUI (cf. above [187])	yes (stroke)

The reviewed publications on electrode arrays on the forearm are listed in the order of appearance in the text, which is based on the date of publication and the utilized EA.

Table 2.1: Overview of electrode arrays, stimulation setup, and VE identification methods for HNPs (continued).

Authors	**Electrode array**			**Stimulator**	**Counter**	**Identification strategy**			
and year	Number of elements, name	Shape, size, layout	Material			Degree of automation	Utilized sensors	Criteria	Patients?
De Marchis et al. 2016 [172]	15+12 (proximal + distal block)	oval, $1.12\,\mathrm{cm}^2$, $[4;4;3;4]$ + 3×4	unknown, separate hydrogel pads	*RehaStim2+* (HASOMED, Magdeburg, Germany)	integrated in the EA (6+6)	automatic (offline)	EMG (3 channels)	M-wave analysis of three target muscles: optimal stimulation pattern for a muscle if the peak-to-peak of the median M-wave was at least twice as a high as the median M-wave	no
Popović-Maneski et al. 2016 [191]	40	round, $\emptyset\,0.8\,\mathrm{cm}$, 8×5	magnetic pads in textile, separate hydrogel pads	2 stimulators (prototype from [192]), each 4 channels	2 single electrodes	semi-automatic (offline)	EMG via two 24-element EAs with two 24-channel amplifiers	comparison of EMG maps recorded during the performance of defined motions with the paretic and non-paretic hand; missing muscle activity in the paretic forearm was identified and stimulation positions were selected close to these areas	yes (stroke)
Yang et al. 2018 [193]	24, *e-sleeve*	oval, unknown, 6×4	plastic flexible substrates, textile	customized stimulator	single electrode(s)	automatic	*Kinect V2*	Newton-based iterative-learning control (see above, [153, 171])	yes (stroke)

O'Dwyer et al. [179] presented the idea of not only using a matrix of elements for the active electrode site but also for the counter electrode position (bipolar electrode setup; cf. *Section* 1.4). This concept was evaluated in a reduced setup with small single surface electrodes (∅ 2.5 cm), where four electrodes were arranged as a matrix above the hand extensor muscles, close to the elbow joint, and two electrodes were placed at the dorsal end of those muscles, close the wrist. The setup was inspired by the electrodes in the *Bionic Glove* sleeve [159]. The identification procedure aimed at finding the best electrode pair for a balanced contraction of wrist and finger extensors. For this purpose, a customized sensor garment (glove) was utilized to measure wrist extension and abduction angles as well as finger flexion angles via accelerometer-based goniometers and flex sensors. An exhaustive search was performed comparing the measured, generated angles by the stimulation of each possible electrode pair with reference values from the literature. The authors reported that an "ideal" electrode configuration was identified for each of the ten tested healthy individuals, which varied from volunteer to volunteer [179]. Although the idea of configuring bipolar electrode setups with electrode arrays seemed promising, it also raised new challenges. Extending this approach to larger arrays would nonlinearly increase the number of possible element configurations. Consequently, the duration of the suggested exhaustive search would become infeasibly long for clinical applications. Furthermore, FES systems would need to be developed which realize programmable multiplexing of both, active and counter array. These might be the reasons why attempts of this kind were the exception in recent HNPs.

Keller et al. [93] presented a system with an EA consisting of 60 textile embedded electrode pads, which facilitated spatial and temporal variations of the electrical stimulation in real-time. Each pad of the array had a separate cable, which made the system bulky. They evaluated the selectivity of the ES using finite element model (FEM) simulations and measurements in non-disabled volunteers and stroke patients. Force [181] of and joint angles (*P5 data glove*; Essential Reality Inc., Mineola, NY, USA) in single fingers were recorded. The FEM simulations showed that neighboring, active elements appeared as one electrode regarding the neural activation if the gap between the elements was 2 mm or less, supposedly for the case with a connecting gel-layer. Furthermore, the results revealed that selective stimulation of wrist and finger extensors was possible to some extent. In [180], a first automatic identification approach for selective stimulation of finger flexors was presented with the same system. The force was measured via a customized device [181] during sequential stimulation of each pad with fixed stimulation parameters. The best pad for each finger was defined as the pad generating the strongest force in that finger with minimal coupling to the other fingers. Once, the activation region was determined, a Hammerstein model[9] was identified to adjust the stimulation intensity during the following stimulation. Thereby, Keller et al. presented the first approach toward closed-loop control of FES with electrode arrays [180]. However, they also mentioned that separate activation zones could not be identified for all fingers.

In 2009, Popović & Popović [170] suggested an automatic search strategy for generating palmar and lateral grasps (cf. *Section* 1.2, Fig. 1.6) in tetraplegic SCI patients using two *Actitrode* arrays presented in [92] positioned on the dorsal and volar side of the forearm. In addition, two single electrode pairs were placed to stimulate the thumb muscles. An automatic

[9]The model comprises a nonlinear static input function followed by a linear transfer function.

search in the electrode array was realized through the iterative evaluation of joint angle recordings with electrogoniometers from the index finger, ring finger, wrist, and forearm for the stimulation of each array pad. This sensor setup was not practical for clinical use due to the bulky and motion restrictive nature of the sensors (cf. *Section* 2.5.2). A VE was assumed to be "optimal" when fingers, wrist and forearm movements were most similar to the trajectories of healthy individuals when grasping (aggregate error). The authors [170] reported durations of the identification procedure of about 10 minutes. Furthermore, once the VEs were determined in the tetraplegic patient, they observed that the VEs remained unchanged when tested on different days.

In the same year, Schill et al. [182] presented a semi-automatic adaptation strategy for active wrist joint stabilization in an electrode array consisting of nine single, self-adhesive electrodes arranged as a matrix. The generated movement by the ES of each pad was compared to reference movements and, in a second step, up to 30 combinations of electrodes were built and tested. The stimulation response was recorded with bend sensors. Magnitude and dynamic criteria were developed to assess the stimulation outcome automatically in comparison with a given reference. The authors observed that the generated movement of an electrode combination did not equal a simple superposition of the responses evoked by every single electrode of the combination due to interference effects. As a limiting fact, they tested their approach only in one healthy test person.

To speed up the identification process in electrode arrays, Malešević et al. suggested the evaluation of individual muscle twitch responses instead of continuous stimulation for identification of suitable array pads for hand motion [183, 184]. A muscle twitch refers to a single contraction of muscles following a single electrical impulse. Previous studies showed that muscle twitch responses correlate with the elicited muscle forces when stimulating with electrical pulse trains [194]. Besides, Malešević et al. suggested the usage of three MEMS accelerometers for recording the twitch responses in wrist, middle finger, and ring finger. Joint acceleration during wrist or finger flexion/extension was used to train an artificial neural network (ANN) to distinguish between different waveform classes, namely activation of wrist flexors and activation of finger flexors, and thereby define the correlation of each pad with the activated muscle groups. A new multi-pad electrode was utilized named *INTFES*, consisting of 4×6 oval pads with one gel-layer per pad. The twitch protocol contained nine pulses presented at 2 Hz with individually fixed stimulation current and pulse width. The results were compared with a continuous stimulation protocol at 30 Hz of 2 s duration, where joint angles were recorded via goniometers. The rule-based ANN classification using accelerometers signals was in line with the ranking using the goniometer data and continuous ES for more than $96 \pm 2\%$ of the pads. The authors concluded that muscle twitch responses could be utilized to accelerate the identification process of useful electrode pads and allow the testing of multiple stimulation parameters (500 ms per twitch response). However, a separate ANN had to be trained for each tested volunteer to allow correct classification, when a minimal sensor setup (one sensor) shall be used. Thereby, the clinical feasibility of this concept remained questionable.

The portable, one-channel stimulator *INTFES* (INTelligent Functional Electrical Stimulation) together with a corresponding *INTFES* electrode array (4×6 oval) with integrated

multiplexer board was introduced by Velik et al. [167] (cf. Fig. 2.2). The EA was explicitly designed for usage on the forearm for the support of wrist and finger function. The INTFES system could be either controlled by a personal computer (PC) via Bluetooth or in a manual adjustment mode without the necessity of a PC. Due to these features, the system has been used in various publications for FES via electrode arrays on the forearm (e.g., [72, 151, 177]).

Hoffmann et al. [151] utilized the *INTFES* system with two multiplexers and two electrode arrays (common hydrogel layer per EA) for developing an automatic identification algorithm for VEs and corresponding stimulation intensities. Their goal was to find VEs that generate stability in the wrist joint and simultaneous extension and flexion of the fingers. The proposed algorithm consisted of two phases, stimulating single pads in the first phase and pad combinations in the second phase. The muscular response to the ES trains (50 Hz) was recorded in the form of joint angles gathered from a VR data glove (*DG5 Vhand 2.0*; DGTech Engineering Solutions, Bazzano, Italy). The best pad or best pad combination was defined by the smallest Euclidean distance between measured and desired joint angles. The method by Hoffmann et al. [151] represents an advanced solution for EAs: It included measurements from the wrist and all five fingers and identified VE locations as well as stimulation parameters. However, drawbacks of the approach are that it was only evaluated in non-disabled volunteers, the joint angle estimation with the *DG5* data glove did not cover all DOFs of the hand, and the algorithm just tested a small set of predefined stimulation intensities.

Malešević et al. [177] presented a different automatic approach with the *INTFES* system for identifying VEs for grasping with a touchable electrode array. There, all EA pads were activated iteratively via twitch stimulation with different amplitudes (brute-force). The responses were recorded with a customized sensor garment, consisting of six bend sensors: two for the wrist, one sensor per finger F2–F5. A cost function was determined to judge the grasp quality based on the weighted flexion amplitudes of fingers and wrist such that minimal wrist movement and large joint deviations were rewarded (no reference data needed). As an alternative to the automatic approach, the authors additionally provided a *manual protocol* for selecting suitable VEs, which might be used by trained health professionals. For that, the EA was extended by a pressure sensor layer that allowed the independent activation of a pad via push on its backside. The authors tested the proposed methods in three stroke patients, revealing that the *INTFES* electrode was not large enough to cover all relevant hand muscle activation points. Nevertheless, Malešević et al. [177] provided a complete stimulation concept for EAs on the forearm that, in theory, would allow closed-loop control and the dynamic adjustment of active electrode configurations depending on the forearm rotation (pronation, supination). Yet, they did not provide experiments and results for those advanced aspects of their system.

Triggered by the conclusions of Malešević et al. [177], Popović-Maneski et al. [94] designed a new electrode array for grasping. Shape and size of the EA were determined from forearm measurements with single electrodes in seven hemiplegic patients. In each patient, experienced therapists defined *functional points*, where sufficient strength in the target muscle(s) for a grasp could be generated with minimum activation of non-synergistic muscles via surface FES. The resulting surface stimulation map revealed that there exist overlaps between functional points of the target muscles. The derived EA consisted of 24 elements, probably owed to the stimulation system, and had rectangular elements with different electrode sizes from the

elbow (larger) to the wrist (smaller), covering a large area on the forearm. The identified functional points and the new EA were evaluated with the bend sensor garment from [177] and a pressure measurement device, which captured the force of each finger (F2–F5). The authors reported that functional grasps could be generated in all patients when activating the determined functional points [94]. Furthermore, they demonstrated that an adaptation of the VEs was necessary depending on the forearm rotation because otherwise, the stimulation led to significantly reduced grasp force. An automatic solution for this behavior was still missing.

A popular research question addressed in many studies is the possible advantage of using asynchronous activation versus synchronous (simultaneous) activation of EA elements involved in the VE to delay fatigue in the stimulated muscles. In synchronous stimulation, all elements of a VE are simultaneously activated (one impulse) per stimulation period t_s (cf. *Section* 1.4). Conversely, in asynchronous stimulation, each element of the VE is activated with an individual impulse during each stimulation period t_s with a defined temporal distribution. As FES recruits larger motor units prior to smaller and more fatigue-resistant units, unlike voluntary muscle recruitment, and uses higher frequencies compared to physiological activation, muscle fatigue develops faster in FES supported training [72, 195] (cf. *Section* 1.4). Asynchronous stimulation within EAs was introduced to mimic the physiological activation pattern [196]. Popović-Maneski et al. [72] presented results for stimulation of finger flexors, where surface-distributed low-frequency asynchronous stimulation via electrode arrays doubled the time interval before the onset of fatigue compared with conventional synchronous stimulation. Furthermore, regarding discomfort, asynchronous ES was preferred over synchronous ES when stimulating hand and finger extensors in 15 healthy volunteers [66]. From the results of these studies, it can be concluded that asynchronous stimulation is the preferred activation paradigm so far with EAs [66, 177].

A research group from the UK suggested the use of feedback-control strategies for the optimization of VEs in EAs for hand movements [153, 171]. They claimed that previously proposed methods lack in speed and dimensionality since they do not take into account the underlying dynamic model linking FES and induced motion. Exell et al. [171] combined a Newton-based iterative learning control (ILC) scheme with an identification strategy. They formulated the identification problem as follows: Find a stimulation parameter set (active EA elements, intensity on a 0–5 scale) which minimizes the quadratic difference between measured and desired hand pose. The iterative procedure starts with a step-wise stimulation of a start configuration and in the following variations of the start configuration. Based on the results, a new configuration is calculated, and the procedure is repeated. The search ends after a limited number of iterations. A 40-element EA (5×8; Tecnalica, Spain) was used to apply FES over the extensor muscle groups in the forearm. Fourteen joint angles were measured via a fiber-optic bend-sensor based data glove (*5DT 14 Ultra*; 5DT, Orlanda, FL, USA) and two electrogoniometers. The authors demonstrated their approach in two healthy volunteers for three hand postures: pointing, pinching, and hand opening. The results showed that the error between stimulated configuration and desired hand posture decreased with each iteration, and the use of a restricted input space could reduce the duration of the identification procedure to approximately 8 minutes per posture [153]. This duration is still too long for clinical applications. Furthermore, no results were provided showing the evoked hand posture

nor joint angle time series, which makes it difficult to judge the approach's performance. Moreover, the chosen hand posture "pinching" of index finger and thumb seems difficult to be generated via stimulation of an EA placed over the forearm extensors only. Instead, the extension of middle, ring and little finger was stimulated.

The identification methods by [153, 171] were integrated into a holistic approach for upper limb rehabilitation combining passive arm weight support and ES via single electrodes on the shoulder and upper arm muscles (triceps) as well as an EA over the wrist and finger extensors ([185]; *GO-SAIL* [83]). The previously used data glove was replaced by contact-free motion tracking of wrist and finger joint angles with *Kinect* (Microsoft, Redmond, WA, USA) and *PrimeSense* (PrimeSense, Tel-Aviv, Israel). The system was tested with unimpaired participants and four stroke patients. The utilized control scheme will be reviewed in more detail in *Section* 2.5.

In the project *MUNDUS*, an assistive framework for the support of arm and hand functions was established [40]. An exoskeleton on the arm was combined with FES on the upper arm and forearm. For generating hand motion, an EA design was suggested consisting of six different arrays for stimulation of finger flexors (two EAs) and extensors (two EAs) in the forearm as well as intrinsic finger muscles (two EAs on the hand; cf. *Section* 1.2). All arrays were embedded in a textile garment. A customized sensor glove with bend sensors over MCP and PIP joints and force sensors on the fingertips and palm was used for an automatic VE identification, which was not further described in [40], and control of the movement (see *Section* 2.5.3). The system was evaluated in patients with SCI and multiple sclerosis.

As a further development of the EA in [40], Crema et al. [42] suggested a modular EA design consisting of 78 elements in total. Again, the elements were distributed on six separate EAs covering extensor and flexor muscles on both sides of the forearm (four EAs) and intrinsic finger muscles (two EAs), as shown in Fig. 2.3. All the sub-arrays connect to one central, rigid PCB to minimize the number of cables and are placed in an arm cuff. In [42], a motion capture system (Vicon Motion Systems Ltd., Oxford, UK) with optical markers glued to a glove was used in combination with force sensors on the fingertips for identifying VE configurations. The described identification procedure consisted of open-loop ES of each element and emoticon-coded sensation feedback from the stimulated user. The ranking of the responses was based on the following criteria: limited wrist motion, effective grasping kinematics (comparison with library of desired movements), and comfort. In a second phase of the procedure, the stimulaton parameters of the selected element(s) were optimized via closed-loop control using the force sensors. This procedure appeared time-consuming considering the high amount of EA elements, even though the duration was not explicitly stated [42].

In the follow-up project *RETRAINER* (S2), a HNP was developed for rehabilitation and assistance after stroke [188]. The system combines a splint to lock the wrist joint in extension with ES via three EAs, each with 16 independent active elements, to activate extrinsic forearm muscles for finger flexion and extension [189]. Those EAs were previously suggested to be combined with two other arrays for stimulating intrinsic hand muscles as well (seven-element array for intrinsic hand flexors, four-element array for thenar muscle group) in the so-called *Helping Hand* system [187]. In both systems, *RETRAINER* and *Helping Hand*, the authors use a manual search for suitable VE positions and sizes via a reactive graphical user-interface

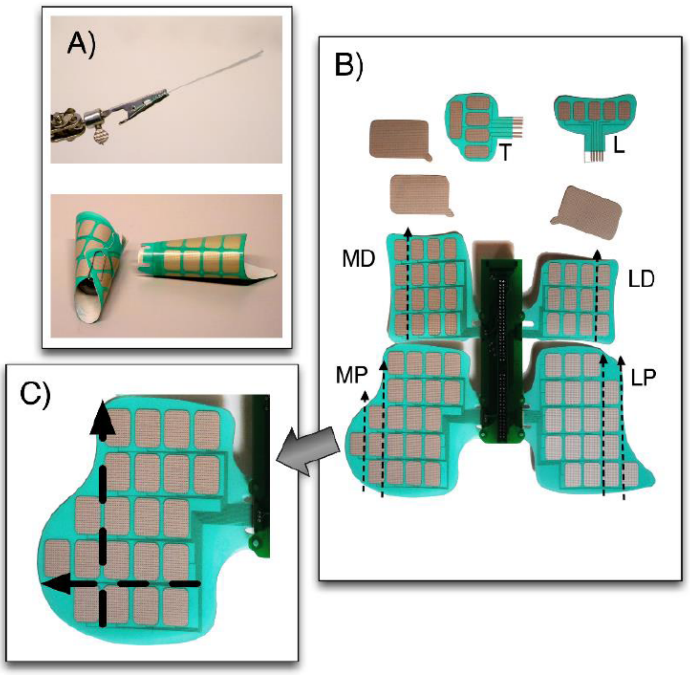

Figure 2.3: Modular electrode array by Crema et al. [42] with 78 electrode elements in total. Each array unit is covered by a single hydrogel layer. Reproduction from [42] (© 2017 IEEE).

(GUI). The VE centroid can be moved on a virtual grid and the size of the active electrode can be modified. Through the integration of previously defined VEs for a patient in subsequent sessions, a search duration of 2–3 minutes is reported [189].

De Marchis et al. [172] introduced an identification approach utilizing the FES-induced EMG response for suitable VE determination in the forearm. They applied a novel EA consisting of 15 stimulation elements (active), and 12 return elements (counter), where each stimulation element could be combined with each return element. Three surface EMG channels were recorded from three extensor muscles (*E. digitorum communis*, *E. carpi radialis*, *E. carpi ulnaris*). The scanning procedure included the testing of every possible configuration of two elements (180 in total) at different current intensities and offline EMG-analysis afterward. The algorithm analyzed the peak-to-peak value of the FES-characteristic M-wave (cf. *Section* 1.4) for each tested configuration and EMG-channel. The procedure was evaluated by kinematic recordings with a data glove (*DG5 Vhand 3.0*; DGTech Engineering solutions, Bazzano, Italy) measuring all five fingers and wrist motions. The results of eight non-disabled volunteers revealed that the selected VEs were suitable for eliciting functional hand opening with selective muscle recruitment. Although this electro-physiologically based identification approach yielded reliable results, problems were the long setup and search times due to multiple electrodes and devices, which will further increase when grasp movements—consisting of extension and flexion—shall be generated. A possible improvement might be achieved through the recording of EMG via another EA, as suggested in [197] for the lower leg.

Popović-Maneski et al. [191] developed a method for selecting VE positions based on the comparison of EMG maps from both forearms, recorded during the performance of defined motions with the paretic and non-paretic hand. Their idea was to mimic the patient-individual activation map of the non-paretic arm for stimulation on the paretic side. The method comprises two phases of operation: (1) EMG with two 24-channel arrays is recorded while the

patient performs target movements, namely hand opening, and grasping. The EAs for the EMG deviation were first positioned on the dorsal and volar side of the non-paretic forearm. Then, the procedure was repeated for the impaired forearm. Areas where the differences between the EMG maps obtained from both arms were above a threshold were identified as the stimulation sites. In phase (2), the stimulation setup is installed comprising two EAs on the dorsal and volar side of the paretic forearm and two wearable stimulators with four output channels each [192]. Each EA consisted of 40 elements with magnetic contacts on the back. Selected elements were connected with the stimulator's channels via leads with magnetic tips. The EAs were placed approximately over the previously identified positions, although the layouts of EMG-arrays and FES-arrays were different. The maximum stimulation intensity for each identified VE was adjusted manually. The stimulation pattern was derived from the timing observed in the EMG maps.

Popović-Maneski et al. [191] evaluated their method in three sub-acute stroke patients. The voluntary motion with the nonparetic hand and the voluntary and FES-induced motion with the paretic one were assessed via tracking joint angles (goniometers) and recording grasp force (custom-made dynamometer). The authors reported an improvement in hand function via FES at the selected stimulation areas. The idea of studying the complex physiological activity of the unimpaired limb for the stimulation of impaired muscles appears sophisticated. In addition to VE positions, other aspects such as the physiological stimulation profiles for the simultaneous activation of agonists and antagonists, i.e., extensors and flexors, can be identified with the suggested method. Nevertheless, the approach is technologically laborious and time-consuming. The EMG system must first be applied to one arm and then to the other arm. Afterward, the actual FES setup needs to be applied. Suitable electrode positions are selected semi-manually based on the maps; associated stimulation intensities are tuned manually. Whether recording and evaluating the EMG maps is necessary for every FES session was not discussed by the authors [191]. If so, future implementations of this method would require EMG recordings and electrical stimulation with the same device and the same EAs, albeit not parallel.

Malešević et al. [168] analyzed the temporal and spatial variability of surface motor activation zones via EAs in 20 FES sessions in twelve hemiplegic patients after stroke. They utilized an updated version of the *INTFES* stimulator (v2, Tecnalia, Derio, Spain) and a new EA with 16 separate pads (4×4) of different size. The study considered VEs corresponding to wrist extension, finger extension, and thumb extension movements. Suitable VEs were identified through visual inspection of separate ES of each pad at different intensities. Previous publications stated that size and shape of identified VEs remained the same from day to day in the same patient if the EA was placed at the same forearm position (e.g., [170, 177]), which would immensely reduce the FES setup time in daily repetitive training. However, Malešević et al. [168] found that adaptation of the VE configurations for wrist, finger, and thumb extension were required each session for all patients. The authors concluded that an experimental (re-)calibration procedure is necessary in each therapy session. The results of the previous session might be used as a priori knowledge in the following session(s). These findings should be kept in mind when developing new EA identification strategies, even though

Malešević et al. [168] did not present quantitative measurements of the stimulation response and only relied on subjective assessments.

Besides the mentioned EA systems and identification approaches, other FES systems with EAs have been introduced for the generation of hand movements with minor modifications of the presented studies (e.g., [198, 199]). Current research in EA technology deals with the integration of arrays in everyday fabrics, such as it is the goal of the *SMARTmove* project [193, 200], and personalization, as suggested in the *MoreGrasp* project for SCI patients [41].

2.5 Control of Hand Neuroprostheses

2.5.1 Introduction

The establishment of a suitable electrode setup with EAs, which allows more or less selective activation of the target muscles in the forearm, is only one problem to be solved in the field of HNPs. The second, probably even more challenging part is the control and command concept for the electrical stimulation to generate functional movements. This concept should include how stimulation parameters (e.g., stimulation intensity, active VE) are adjusted to the individual patient, the muscular state, and the desired movement, and how the FES is synchronized with the patient's intention and residual movement capabilities (e.g., on- and offset of the ES). *Adaptation* and *synchronization* of the ES are two crucial factors for the successful application of neuroprostheses in motor rehabilitation and are often summarized under the term *control*.

Movement generation through FES is a highly nonlinear, dynamic process [13, 68]. Consequently, the control of FES based on measured quantities, that are subject to uncertainties, is a non-trivial task. The stimulation effect depends on the positioning of the electrodes, muscular condition (e.g., fatigue, posture), voluntary contributions to the movement through residual motor activity, external and internal disturbances such as spasticity [67]. Furthermore, the system's characteristics in terms of stimulation parameters and muscular response vary significantly between individuals, as well as in the same individual on a day-to-day basis [92, 168]. The time-variant nature of FES makes manual adjustment of multi-channel FES systems very time-consuming and prone to achieving the optimal stimulation effect. Therefore, intense use of multi-channel FES systems in clinical and home applications cannot be observed up to now [13].

Open- and closed-loop control approaches have been studied for decades to create patient- and situation-specific solutions through adaptation and synchronization of the ES [13]. Both attempts require manual input and/or (wearable) sensor systems to gather information about the status of the plant—here the stimulated neuromuscular system—as well as to detect the intention of the patient in real time [129].

The principle of *open-loop* control for neuroprostheses is illustrated in Fig. 2.4. The key of an open-loop controller is that it will always output the same, precomputed stimulation pattern (controller output) for the same reference (controller input) regardless the status of the actual plant (cf. black boxes and arrows in Fig. 2.4) [164]. Advanced open-loop systems allow to incorporate system information, for example, on the intention of the patient, to change the input reference of the controller and enable synchronization to some extent (cf. gray

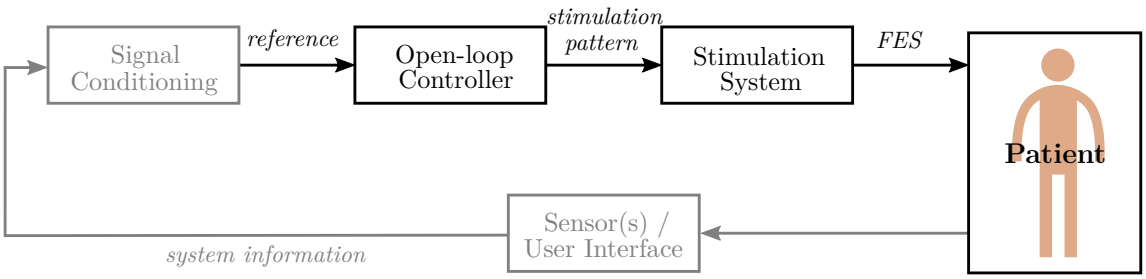

Figure 2.4: Principle structure of open-loop control for an FES-based neuroprosthesis inspired by [129]. The controller outputs a stimulation pattern depending on the given reference and forwards it to the actuator, here the stimulation system. Optionally, a sensor or some kind of user interface (e.g., push-button) is used to gather information on the patient demands, see the gray path. For example, in the case of a HNP, the information might verify whether the patient wants to have a grasp or release motion stimulated. Through signal conditioning (e.g., a state machine or an input-output map) the reference can be adjusted.

boxes and arrows in Fig. 2.4). However, open-loop control does not involve a direct feedback of the actual state of the system, meaning that the generated movement through ES is not evaluated, and stimulation parameters are not adjusted to changing conditions such as muscle responsiveness and posture [68, 129]. Currently available, commercial FES systems operate in an open-loop modality and usually require a manual re-adjustment of stimulation parameters during a therapy session longer than 10 minutes.

Closed-loop control is based on minimizing the difference (error) between desired reference and observed value [164]. Therefore, a sensor or sensor network is essential to track the actual status (e.g., motion, muscle contraction) of the system. Figure 2.5 shows this principle of closed-loop control in neuroprostheses. Ideally, the stimulation pattern can be adjusted automatically through closed-loop control to the patient's needs in order to delay the onset of fatigue and to induce and synchronize movements in an optimal way [13]. The controller design requires detailed knowledge on the system dynamics and reliable real-time monitoring of physiological signals. When it comes to controlling multiple DOFs, as it is the case in HNPs for grasping, the controller design, as well as the measurement strategy, becomes highly intricate [129]. Therefore, current research focuses on the development of portable/wearable measurement systems for real-time tracking of the controlled signals and on the implementation of advanced control algorithms to stimulate movements from ADL with multiple DOFs.

The choice of the utilized signal(s) for the adaptation and synchronization of the ES depends, among other things, on the availability and robustness of sensors for tracking the relevant signal(s) as well as the patient's capabilities. The sensors incorporated in neuroprostheses face various requirements concerning functional and usability aspects [129]. The measurement needs to provide stable signals over time, that ideally are reproducible over subsequent sessions, and are available at suitable resolutions to track the required dynamics [129]. The utilized sensors need to be compact, easy to use and to mount, portable, should allow natural interaction and fulfill hygienic standards [201]. Furthermore, signal processing and advanced algorithms (e.g., for sensor fusion and pattern recognition) are required for extracting the relevant signal information for the control system.

The variety of available physiological and kinematic signals, methods for data processing, and the resulting range of proposed open- and closed-loop control approaches for hand

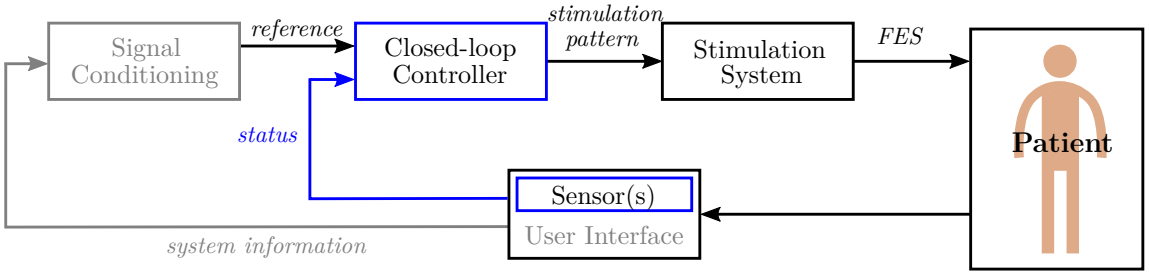

Figure 2.5: Principle structure of closed-loop control (feedback-control) for an FES-based neuroprosthesis. The controller adjusts the stimulation pattern based on a comparison of reference (desired value) and measured status (actual value). This feedback-loop is highlighted in blue. Optionally, additional sensors or user interfaces can be used to synchronize the control-loop behavior with the patient's intention (gray path).

neuroprostheses are systematically reviewed in the remainder of this chapter. In the next section, biological and non-biological signals and corresponding sensor technologies are briefly introduced concerning their (potential) application in HNPs. *Section* 2.5.3 summarizes available open- and closed-loop command and control approaches for adjustment and synchronization of the ES with the focus on hand rehabilitation.

2.5.2 Signals for Control of Hand Neuroprostheses

In the previous *Section* 2.4 on electrode arrays, different sensors and signals were utilized for electrode and parameter identification which shall now be reviewed regarding their potential in generating command signals and their use in feedback control. According to Ambrosini et al. [129], sensors for neuroprostheses can be divided into two categories: (1) sensors of *biological signals*, and (2) sensors of *non-biological signals*. Biological signals, such as the EMG or EEG, are capable of providing information on the system's status and intention of the user in a natural manner. Non-biological signals, such as applied force on a grasped object, mainly contribute information on the current state of the system [129]. The selection of suitable signal(s) to control a hand neuroprosthesis is not definite, and depends on many aspects, for example, on the specific task to be controlled, on the abilities of the patient, or on the environment where the system shall be applied. Figure 2.6 summarizes the available biological and non-biological signals for HNP control, which are considered in the following starting with biological signals.

Electromyography

The electrical activity of motor units recorded via surface EMG can be used as a biological control signal for various kinds of neuroprostheses [164], in its continuous form or translated into events. The principle of EMG measurements for FES applications has already been introduced in *Section* 1.4. From this, it can be derived that the EMG signal can be utilized for assessing the residual volitional muscle activity (vEMG)—and thereby the patient's intention—to trigger and control the ES (open-loop), as well as for determining the quality of muscle responses to the applied ES to track and control the recruitment of motor units via the eEMG (closed-loop) [13]. Additionally, EMG recordings can be used to monitor the patient's muscular condition

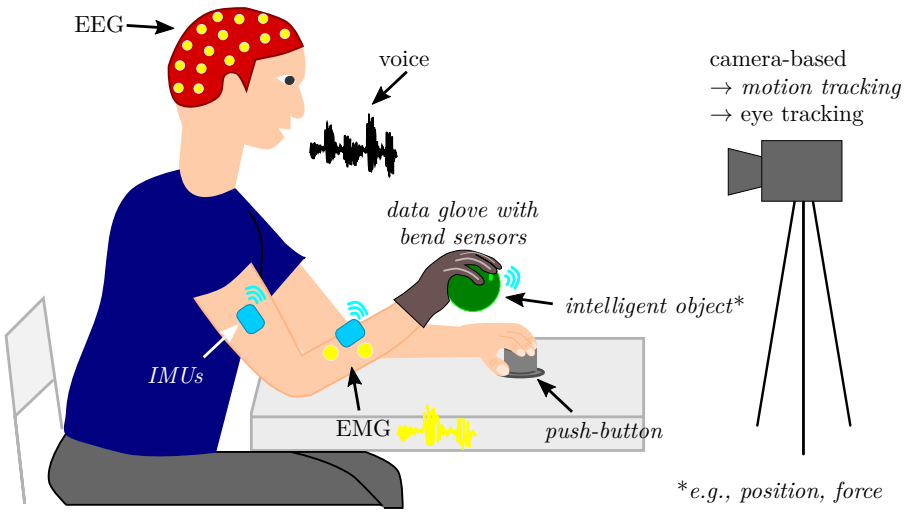

Figure 2.6: Overview of suggested biological and non-biological signals and corresponding sensors for command and control of hand neuroprostheses. Non-biological signals/sensors are labeled in italic. This illustration does not claim to show all available signals or sensor technologies.

and coordination. It was shown that the EMG signal is related to the produced muscle force, although this relation is neither direct nor reliable [164, 202]. The continuous measurement of the EMG provides a high temporal resolution. Among others, the quality of the EMG signal depends on the utilized hardware (amplifier, electrodes), the skin, and the time-varying contact impedances [109].

With the current technologies, the EMG signals can be evaluated either from muscles that are not involved in the movement, from muscles that are involved in the movement but are not stimulated, or that are both involved in the movement and artificially activated with ES [129]. Using the EMG signal(s) from the muscle(s) to be stimulated is the most promising way of controlling stimulation in a physiological manner through volitional intent via EMG [35]. The challenges in the case of closed-loop control with EMG are manifold. It is obvious that the usage of patient-induced EMG for triggering and adaptation of the ES relies on the patient's ability to activate the target muscle(s). The technical setup and signal processing have to allow a robust measurement of the vEMG with and without stimulation. Furthermore, amplitude changes in the vEMG were reported after the onset of the ES, possibly due to collision blocking of the descending nerve impulses or other inhibitory effects [35].

Nevertheless, multiple approaches have been proposed for open-loop control of stimulation parameters, such as current amplitude and pulse width, via the amplitude of the vEMG (e.g., [111, 115, 118]; cf. *Section* 2.5.3). Besides, EMG-triggered FES has turned out to be a robust method for simple control of the stimulation and indicated that the incorporation of the patient-induced movement may be important in motor re-learning (e.g., [35, 203, 204]).

Electroencephalography

Electroencephalography measures potentials from electrical activity in the human brain through surface electrodes on the scalp. EEG signals in combination with ES have been suggested to bridge the interrupted connection between the CNS and the motor units in paralyzed patients. The use of EEG signals for control of human-made systems is generally referred

to as *brain-computer interface*[10] (BCI). Besides their utilization in neuroprostheses, BCIs were proposed for various applications, for example, for controlling robots [205] or navigating in virtual realities [206]. A detailed review of BCI technology and applications for assistive devices and rehabilitation can be found in [207] and [208].

The central element of each noninvasive BCI system is the translation from EEG potentials from the user into a command or feedback signal for a technical device via signal processing and classification [129]. BCI systems distinguish different patterns of brain activity, each being associated with a particular intention or mental task/state of the user [208]. Several EEG phenomena have been suggested to be used in open-loop control: evoked potentials such as the event-related P300 component in response to visual oddball events (e.g., [40]) or steady-state visually evoked potentials (SSVEP; e.g., [209]), and spontaneous signals like rhythmic activity in specific frequency ranges (e.g., [210]) and event-related desynchronization (ERD) of those rhythms (e.g., [209, 211]). All of these phenomena require training of the users, in which they learn to modulate their brain signals, as well as training of patient-individual classifiers for the extraction of control commands (e.g., with the support of machine learning techniques) [208]. This preparation may result in long setup times of several weeks or month (e.g., [120]) before the patient is able to control the device, especially if motor imagery shall be used. Therefore, BCIs were mainly applied to control neuroprostheses in an assistive manner (motor substitution) via discrete commands. SCI is the primary target group. Current research focuses on the classification of natural brain patterns for different grasp types to reduce the need for exhaustive training [212]. The aesthetic and cosmetic appearances of noninvasive EEG technologies are further issues for user acceptance of BCI-based assistive technologies [213].

BCIs can also be combined with other biological or non-biological control signals (*hybrid BCI*), where at least one EEG channel is used [208]. The use of the EEG has the advantage that no residual (hand) motor function is necessary for the control, unlike in natural control via the EMG. Hence, BCIs were suggested as a good opportunity to access the motor system and rehabilitation at all stages of stroke recovery [208, 214]. However, the combination of FES with BCI for stroke therapy, with the goal to facilitate motor recovery, still needs further investigation [215]. Marquez-Chin et al. [216] provide a detailed literature review of the usage of BCI for enhancing FES.

Other Biological Signals

Bioimpedance (BI) was suggested to access movements and muscle contractions in real-time for the control of FES systems (e.g., drop-foot neuroprosthesis [217]). Impedance describes the relation of voltage to current in terms of amplitude and phase. The BI signal is a complex variable depending on the passive electrical properties of the tissue, measured by the voltage drop caused by an artificially applied alternating current flow through tissue [13]. Nahrstaedt & Schauer [218] showed that BI could assess FES-induced gripping force. However, due to the comparably high effort for the measurement setup—including measurement and stimulation electrodes, amplifier and another stimulation channel—, the application of BI has not yet prevailed amongst HNPs.

[10] Please note that the term *brain-computer interface* generally refers to all concepts that translate the user's brain activity into commands, regardless whether the activity was measured via noninvasive techniques (EEG) or invasive methods, such as electrocorticography.

The *electroneurogram* is an electrical signal generated by the activity of peripheral nerves [129]. It requires the implementation of nerve cuff electrodes and is therefore only suitable for permanent, assistive FES systems and not for rehabilitation treatment.

Eye tracking was employed for communication purposes in patients with a high-level disability. Several techniques are available for collecting gaze and eye movement data, such as electrooculography via measurement electrodes on the face or nowadays more frequently used contact-free video-based tracking [219]. For FES, eye tracking offers a possibility for command-control of the neuroprosthesis, for example, the target object which the user would like to grasp can be communicated, and a matching stimulation strategy is selected and triggered (e.g., [40]). However, gaze and eye tracking can only be used as command signals within a physiological user interface if the user's regular eye and hand behavior are not restricted [129].

The same accounts for speech recognition in *voice control* of neuroprostheses. So far, simple vocal commands, such as "stimulation on/off" or "grasp", were tested as user-interfaces in an open-loop control of neuroprostheses for the upper limb (e.g., [161, 181]). A big challenge in speech recognition is the correct differentiation between the user's voice and the background noise captured by the microphones to avoid erroneously triggering of the stimulation [129].

Movement Tracking

The movement of the body in the form of non-biological signals, such as joint angles, velocities, and positions, has been suggested in many approaches for controlling neuroprostheses of the upper and lower limb in open- or closed-loop (e.g., [123, 127, 220]). In patients with remaining volitional activity, body kinematics can be used to synchronize the stimulation with the user's intention [129]. For feedback-control, the tracking of the FES-induced movement is employed for real-time adaptation of the stimulation parameters (e.g., [32, 221]). However, hand motion tracking comes with several challenges due to the high number of DOFs and short segment length (cf. *Section* 1.5).

Various types of sensors have been exploited for assessing hand motion in neuroprosthesis. Especially for wrist motion tracking, *electrogoniometers* were frequently applied (e.g., [171, 183]). They measure angles in one or two planes of movement: The two ends of the electrogoniometer are attached to the two body segments connected by the joints; a flexible transducer (e.g., *bend sensor*) in between measures joint angles through bending and stretching [129]. Electrogoniometers are easy to use, but they can limit the range of motion of the measured joint and an application for multiple DOFs might be impractical (wearability, calibration procedures) [129]. Various *bend sensors*, also known as *flex sensors*, have been integrated into commercially available data gloves, such as the *5DT 14 ultra* (5DT, Orlando, FL, USA) or the *DG5 Vhand 2.0* (DGTech Engineering Solutions, Bazzano, Italy), to track multiple joints of the human hand. In FES-based rehabilitation, data gloves have mainly been applied for the optimization of virtual electrodes in electrode arrays (e.g., [151, 171]; cf. Table 2.1).

Inertial sensors have become popular for motion tracking over the last decades, as advances in MEMS technology have led to decreased size, weight, power consumption, and costs of MEMS-based inertial sensors [133]. Accelerometers, gyroscopes, and magnetometers are used individually or combined as *inertial measurement units* to assess joint angles, velocities, and

segment orientations (e.g., [201, 220]). *Accelerometers* measure the one-, two-, or three-dimensional specific force, which is the sum of (1) the linear acceleration, i.e., the translation- or rotation-related instantaneous change of velocity, and (2) the gravitational acceleration, which is approximately $9.81\,{}^{\mathrm{m}}/_{s^2}$ in vertical direction near the surface of earth [129]. Double integration of the linear acceleration in an inertial frame, in theory, yields the position of the accelerometer sensor. When the (long-time average of the) linear acceleration is negligible, the inclination of the sensor can be determined. However, the sensor placement must be known to infer the body segment orientation, and the orientation around the vertical axis (heading) cannot be determined. *Gyroscopes* provide the one-, two-, or three-dimensional angular velocities of the body segment to which they are attached [129]. Segment orientations and joint angles can be determined by integration of these angular rates if initial values are known and measurement biases are removed. However, the biases of MEMS-based gyroscopes are temperature-dependent and time-varying, which makes it difficult to estimate them during movements [222].

To overcome the disadvantages of both sensor types, accelerometers and gyroscopes, additional magnetometers are often included in *IMUs* to correct heading errors. Heading describes the angle of the sensor with respect to the magnetic north. In a magnetically undisturbed environment, magnetometers measure this component as well as a vertical component of the local earth magnetic field [223]. However, these readings are typically noisy and affected by magnetic disturbances originating from objects containing ferromagnetic material or emitting magnetic fields [13].

Through sensor fusion of the different measurement signals, the real-time orientation of an attached IMU—in fact, of the local coordinate system that is aligned with the housing of the sensor—can be estimated with respect to a three-dimensional inertial reference coordinate system [13]. If IMUs are rigidly attached to two body segments that are connected via a joint, the orientation of each sensor can be related to the orientation of the body segment, and joint angles can be determined. Yet, this approach requires knowledge of the sensor-to-segment orientation of each sensor [13]. Among the most significant challenges in using inertial sensors for hand rehabilitation are (1) sensor-to-segment calibration, which may require the performance of movements that are not feasible for disabled patients, (2) concepts for a quick, functional sensor attachment, (3) the need for advanced sensor fusion algorithms, and (4) measurement artifacts resulting from soft-tissue motion.

With the launch of affordable, non-contact depth cameras, such as the *Kinect* (Microsoft, Redmond, WA, USA), the *RealSense* (Intel, Santa Clara, CA, USA) or the *Leap Motion* sensor (Leap, San Francisco, CA, USA), camera-based motion tracking has become relevant within rehabilitation technology. Infra-red light-sources and sensors are used to calculate position data of objects in three-dimensional space [83]. Combined with pattern recognition, landmarks of interest, such as limb segments or joint centers, can be tracked and used for the control of FES systems (e.g., [221, 224]). Currently available systems offer a high tracking accuracy for non-paralyzed hands and are optimized for the various applications in virtual and augmented reality. However, problems for their use in control of FES are that motion of paralyzed hands might not match the modeled behavior and line-of-sight restrictions may occur when it comes to manipulation of objects (cf. *Section* 1.5).

Force and Pressure Sensors

In hand rehabilitation, the use of force or pressure sensors was proposed to measure the subject's interaction with the environment and rehabilitation tools [129]. The assessment of the applied force is crucial for a reliable grasping of objects, for example, to control that an object does not slip out of the hand (force too small) and neither is crushed (force too big) [118]. Mostly force-sensitive resistors (FSRs) and strain gauges are applied to record these non-biological signals. Strain gauges change their resistance when strain is applied. Problems for their use in neuroprostheses are among others a high power consumption and temperature variability [164]. FSRs change their resistance in response to an externally applied force. They have a low power consumption, are thin, lightweight, and relatively sensitive to small physical force, although they often show a nonlinear relation [225, 226]. Challenges in their application in HNPs are that FSRs restrict the sense of touch when placed in the palm or at the finger tips, and that depending on the manipulated object different contact points exist and need to be tracked.

Other Non-Biological Signals

Another idea in upper limb rehabilitation setups is to utilize information measured from the objects to be manipulated instead of biological or non-biological signals from the human user. So-called *intelligent objects* are equipped with sensors such as, for example, strain gauges to measure their deformation and thereby indirectly the applied grasp force (e.g., [227]), or visual markers for position tracking and object identification (e.g., [209]). The use of intelligent objects has the advantage that fewer sensors need to be mounted on the user, but it also limits the training modalities. To overcome these problems, in the project *RETRAINER*, objects belonging to the patient were equipped with radio-frequency sensitive tags [228]. The distance between the object and an antenna placed on the back of the patient's hand was measured and evaluated together with the tag identification.

Despite the described control signals, input devices such as push-buttons, switches, manual slider or joysticks serve as user-interfaces in many proposed FES systems for commanding/triggering the stimulation (e.g., *NESS Handmaster* [28], or [229]), and should, therefore, be mentioned in this context. Ideas from other areas, such as the control of a powered wheelchair via myoelectric auricular signals—in other words, by wiggling ears—[230] or via magnetically-tracked tongue movements [231] for tetraplegic subjects, could also be integrated into future FES systems for hand rehabilitation.

Sensor Fusion

All the reviewed signals come with advantages and disadvantages regarding their usability for FES applications. In this context, also the temporal relation of the signals to the process of physiological motion generation should be considered [232]. While the EEG provides information from the CNS at the cortical level, the EMG describes the resulting muscle activation at peripheral level, and motion tracking ultimately evaluates the resulting motion, as illustrated in Fig. 2.7. The general delay in synchronization between intended and FES-induced movement is the highest for using motion tracking. However, the measurement noise in tracking

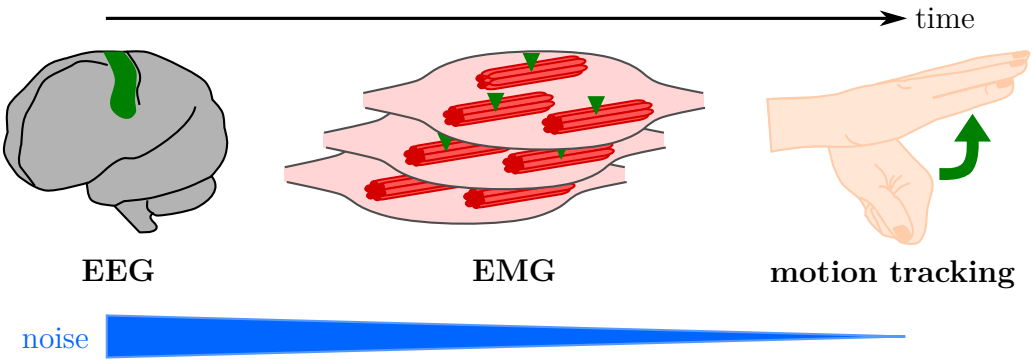

Figure 2.7: Temporal relation of EEG, EMG, and motion tracking in the course of physiological movement generation from CNS to the periphery. The measurement noise is decreasing with being the highest for measuring neural activity via EEG and the lowest for tracking body segments.

muscular (EMG) and neural activity (EEG) induces artificial delays through signal processing, which is necessary to increase the signal reliability.

One way to improve the accuracy of information regarding human intention, muscular state, and movement is to fuse the continuous and discrete data from multiple, different modalities (*sensor fusion*) [233]. Further, the term *hybrid control* or *hybrid system* was introduced relating to the fusion of various control signals, for example, in their individual decisions regarding the user's intent or status (e.g., posture, movement) by weighting the contribution of each modality [208, 234]. Benefits from the use and fusion of multiple sensors are that those sensors can provide redundant information, which might reduce uncertainty and thereby increase reliability in case of a sensor failure, and/or they provide complementary information [233]. For example, Fougner et al. reduced the classification error of EMG pattern recognition for movement control by including the information from upper limb position tracking with accelerometers [235]. Through sensor fusion, more features from the user and the environment could be obtained using multiple sensors, which is of high interest for the intricate control problem in automated HNPs.

2.5.3 Open- and Closed-Loop Control

In the development of a suitable strategy for intuitive control and automatic adaptation of the FES, many of the described signals in *Section* 2.5.2 have been tested and combined in various ways. The proposed control strategy depends crucially on the target user group—SCI or stroke—and their capabilities as well as the target movement and function—assistance or therapy (motor learning). Although many feedback-control strategies have been employed to control FES-induced movement in large joints, such as the elbow (e.g., [221, 236, 237, 238]) or ankle (e.g., [125, 127]), the majority of HNPs applied FES in open-loop to support wrist and finger motion (e.g., [29, 109, 120, 159, 201, 209]). Command-control and (sequential) triggering of the stimulation are the most common approaches, and there exists evidence on their clinical relevance in rehabilitation [220, 239, 240]. However, acceptance by patients and treating health professionals can only be achieved through control strategies close to physiological control, which induce the expected motion at the intended time and ideally to not interfere with other activities, such as motion in other body parts or communication (cf. *Section* 2.2).

One of the first closed-loop strategies for FES-generated hand motion was presented by Crago et al. [241]. They suggested a combination of force and position feedback to regulate grasp, defined as a sequence of hand opening (finger extension) and hand closing (finger flexion). The authors considered that position feedback shall be used for hand opening and until the object is touched (feedback-loop with stiffness controller), when force feedback becomes dominant (force-feedback loop with muscle activation controller). Two antagonist muscles were stimulated via a co-contraction map allowing a continuous change between single muscle activation and co-activation. Controller and mapping parameters were manually adjusted for each subject. The general feasibility of this approach was shown in SCI individuals without voluntary control of hand muscles [241]. Limitations were the choice of the position reference signal for the case of using various objects, the fixed design of the co-contraction map, the restriction to a single joint, and the laboratory sensor setup. "External" disturbances, such as voluntary movements in patients with residual muscle activity, could not be compensated with this method.

The following control-approaches focused on utilizing and strengthen the residual muscle activity of stroke and SCI patients. Saxena et al. [109] were among the first to investigate the feasibility of an EMG-controlled FES system for grasping applied to persons with SCI. Their goal was to restore simple grasps by stimulating finger and thumb flexor muscles and trigger the FES via surface EMG from the wrist (on-off control with manual threshold). Volitional wrist extension is synergistic with grasping [118, 159]. The system by [109] was evaluated in six SCI patients with some residual wrist extension. The authors observed muscle fatigue during the 30-minute test session, such that the peak of the integrated, rectified EMG signal dropped to about 60% compared to its value at the beginning. This change indicated the need for closed-loop control with automatic adjustment of the trigger threshold relying on a measurement of the stimulation outcome.

Thorsen et al. [118] also used the volitional EMG from the wrist extensor muscle but suggested a continuous, proportional control of the FES. In the established system, named MeCFES system (myoelectrical controlled functional electrical stimulator), wrist extension either controlled wrist extensor stimulation or thumb flexor stimulation. The proportional gain between vEMG and FES for piecewise linear control as well as offset and maximum stimulation intensity were determined manually via trial and error for each tested patient [242]. This method is illustrated in Fig. 2.8. Thorsen et al. evaluated their system clinically in SCI (enhancement of tenodesis grasp) [243] and stroke patients (wrist and finger extension) [244]. They found an immediate as well as a therapeutic effect for the intervention with the MeCFES neuroprosthesis in 27 SCI patients, but state that only 9% of the cervical SCI population might be candidates for their technique [243]. The results within the stroke cohort indicated that more than one FES channel is necessary for supporting multiple hand movements, such as required in the performed *Action Research Arm Test*[11] (ARAT) [244]. In all papers [118, 243, 244], the authors did not elaborate possibilities for automatic tuning and adaptation of the controller gain. The manual, individual identification of the gain is very time-consuming

[11]The ARAT is a performance test to access upper limb function in patients with motor impairments [245]. It consists of four sub-tests—*grasp*, *grip*, *pinch*, and *gross movements*—comprising 19 movements (tasks) in total. In the first three sub-tests, the ability to grasp, manipulate, and release objects differing in size, weight, and shape (e.g., wooden blocks, marbles) is tested [246]. The performance of each task is rated on a four-point scale (0 = no movement possible; 3 = movement performed normally) [246].

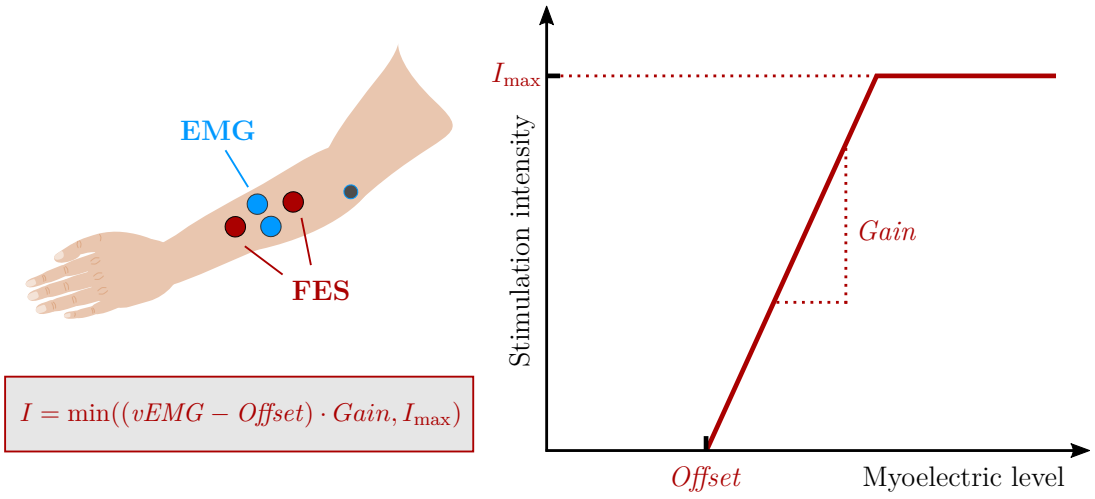

Figure 2.8: Principle of vEMG proportional control of wrist extension as suggested by Thorsen et al. [118, 242, 244]. A piecewise linear function was defined by vEMG-offset, gain, and maximally tolerated intensity $I_{\max}$ to adjust the stimulation intensity in relation to the myoelectric level (vEMG). The figure is adapted from [118] and [242].

and not practical when it comes to the control of multiple FES channels via multiple EMG channels. It should be noted that the MeCFES system is one of the few HNPs that was evaluated in a multicenter randomized controlled trial with 45 stroke patients to promote restoration of movements during task-oriented therapy [110]. No adverse events or negative outcomes were reported.

Keller et al. [24] proposed the use of surface EMG from two muscles of the contralateral upper limb. Triggered and continuous open-loop EMG control were tested in ten SCI patients to restore palmar and/or lateral grasp function (cf. *Section* 2.3). Depending on the ratio between the EMG of two muscles, hand opening or closing is commanded, and the stimulation intensity is set proportionally. Salbert et al. [247] developed an EMG-triggered state machine, which enabled the user to control the motion sequence of hand opening and closing via vEMG measurements of the hand extensors and flexors. However, first experiments with patients revealed that their assumption of a higher vEMG in the hand extensors compared to flexors during the attempt of hand opening and vice versa did not always hold due to a strong co-activation of muscle groups. Besides, different electrode placement, shifting contact resistances, as well as measurement noise led to varying vEMG-quality in each trial.

Shalaby [111] suggested the use of a new four-channel EMG system (*StiMyo*) which allows the measurement during ES from the stimulation electrodes itself resulting in a reduced setup. The system was utilized for vEMG-proportional control of the stimulation of finger and wrist extension and evaluated in healthy volunteers. The results revealed that subjects need to generate sufficiently smooth EMG profiles to profit from EMG-proportional FES; otherwise, this control scheme may result in oscillations in the resulting motion. Furthermore, the author stated that continuous control of the ES via EMG is only possible if spasticity is moderate or absent. As an alternative, so-called EMG-carried stimulation was investigated where the ES is active as long as the low-pass filtered volitional EMG exceeds a predefined threshold. However, this type of EMG-triggered stimulation did not allow modulation of the FES intensity.

The previously discussed EMG control strategies suffer from a static mapping of EMG to FES and laborious manual parameter tuning. But the results revealed that the system behavior changes over longer periods of use [109]. Therefore, static thresholds and gains might not be sufficient. Colgoni et al. [248] were among the first to suggest automation of parameter identification for EMG-proportional control through the use of an additional sensor. EMG was measured and FES (one channel) was applied via the same electrodes over the wrist extensors and the wrist angle was tracked via one IMU on the hand back. The authors suggested iterative learning of the piecewise-linear relationship between vEMG and FES via parallel tracking of the EMG-level and the corresponding wrist angle. Two iterations were necessary to determine the relationship, which was then utilized in a closed-loop EMG-based control to realize an "*assist-as-needed*" principle.

The term *assist-as-needed* refers to the level of support in conventional and technology-assisted motor training: The patient performs the movement autonomously until the degree possible in his/her neurological state, and the therapist or technical device (e.g., FES and/or robotic) only supports the remaining level necessary to complete the training task [249]. The term "patient-cooperative" is used as a synonym (e.g., [250]). The assist-as-needed principle in rehabilitation technology is the answer to the results of multiple studies showing that active movements help to promote rehabilitation more effectively than passive, high-repetitive exercise (e.g., [251, 252]).

Colgoni et al. [248] fed back the measured wrist angle to a controller and the angular reference was derived from the vEMG via the established relationship. A proportional-integral-derivative (PID) controller with anti-windup[12] for stimulation intensity was implemented. The controller parameters were chosen via trial and error. The authors only showed preliminary results with an unknown number of healthy volunteers and stroke patients [248]. The authors concluded that iterative learning should continue during operation with the neuroprosthesis to adapt for changes in spasticity, muscle tone and fatigue [248]. Furthermore, recalibration of parameters such as the maximal vEMG activity should be performed from time-to-time as they observed changes for the evaluated stroke patients. Although the approach by Colgoni et al. [248] seems very promising, as it realized closed-loop control, this type of direct mapping of an ES/EMG channel to one joint angle appears not to be applicable to manifold multi-DOF motions.

The mentioned EMG-based approaches focus on training of a single movement, such as wrist extension, that is promoted through EMG-triggered or EMG-proportional FES on a single muscle (group). However, functional tasks performed with the hand in ADL involve complex temporal and spatial coordination of multiple muscles on the forearm [254]. The use of surface EMG for the control of several muscle groups faces unsolved challenges regarding the technique and usability (e.g., multiple EMG-channels necessary, which possibly yields in more electrodes and wires). Zhou et al. [254] recently suggested controlling FES on the paralyzed limb via contralateral EMG-mapping from the healthy side in hemiplegics. Their so-called EMG bridge for real-time control aimed at mimicking the movements of the contralateral hand. Wireless communication was realized between EMG and FES module to reduce the

[12] *Anti-windup* is a strategy to limit the integration of a controller to the given limits of the controller output [253]. Since the controller output of real-life systems is usually bounded (e.g., lower and upper limit of the stimulation intensity), an anti-windup is used to avoid undesired closed-loop behavior in case of saturation.

number of wires [255]. Each target muscle of the paralyzed limb has its own source muscle in the contralateral limb. Through EMG pattern classification based on linear discriminant analysis, the motion status is classified, and a mapping of EMG detection channel to the corresponding stimulation channel controls the applied ES intensity. The classifier needs to be trained individually in a separate phase. The method was validated in healthy subjects only, using motion tracking of both hands with the *Leap Motion* sensor (Leap, San Francisco, CA, USA). The approach by [254] allows the training of multiple movements achievable through four stimulated muscle groups and facilitates bilateral training. However, the assumed static EMG to FES mapping cannot be expected to be valid throughout a training session of 10 minutes and more.

Gandolla et al. [256] suggested a cascade ANN to classify hand grasp intentions and movements of multiple DOFs from surface EMG. They recorded the EMG from ten bipolar electrodes arranged in a circular configuration around the forearm. Three functional grasp types were evaluated in healthy volunteers and stroke patients: pinching, grasping an object, and hand closing. The ANN detected the volunteer's motion intention within the time window starting from the EMG activity onset to movement onset. The authors reported precision rates of $76 \pm 14\%$ [256]. As the classifier was designed to be used with robotic assistive devices, the interference of electrical stimulation with the EMG signal remains to be investigated.

Ambrosini et al. [115] combined FES with a passive upper-limb exoskeleton and controlled both modalities via EMG with adaptive filtering for assistive and rehabilitative purposes. Although this approach certainly addressed the critical issue of arm support for reach-and-grasp motions, the FES for generating hand motion remained triggered (on/off-control), and no new control strategy for grasping was presented.

For persons suffering from amputation, the EMG pattern recognition has been extensively investigated to control multiple DOFs electro-mechanical prostheses [254, 257]. Also for myoelectric control of neuroprostheses and rehabilitation robots various approaches for pattern recognition of EMG were investigated (e.g., [258, 259, 260]). Lee et al. [261] presented myoelectric pattern classification via ten surface electrodes on the hand and forearm to differentiate six functional tasks in stroke survivors with moderate to severe impairment. The authors concluded that a subject-specific EMG classification paradigm is necessary, which is also depending on the target task and the corresponding EMG electrode placement [261]. The need for individualization of the classification and the large electrode setup hinder the integration of such methods in FES systems due to practical reasons (e.g., time, costs).

For the same reasons, EEG-based BCI-control of FES has mainly been evaluated for command-control of hand motion in SCI patients. As neuroprostheses for SCI mostly aim at providing a long-term assistive function for the user, long training times for an individual adjustment of control interfaces seem more feasible. A first, single-case demonstration of noninvasive restoration of grasp function in tetraplegic SCI by EEG (two channels) and FES via surface electrodes was presented by Pfurtscheller et al. [120]. After several months of training, the patient was able to mentally induce oscillations in the beta frequency band to trigger a sequential transition between different, predefined stimulation states for a lateral hand grasp. Rohm et al. [262] suggested the use of a motor-imagery BCI for a hybrid neuroprosthesis, which combines a semi-active orthosis with FES for restoration of hand, finger, and elbow

function. In a single-case study with one SCI tetraplegic, the BCI performance for triggering the FES remained at about 70% after one year of training. Therefore, new concepts aim at combining BCI with other modalities, such as IMUs and force sensors [41].

Savic et al. [209] suggested a two-stage BCI approach for command control of the ES: A SSVEP-based selection of the appropriate grasp pattern for the intended object was followed by an ERD-based triggering of the stimulation through motor imagery. For the SSVEP, three objects were equipped with flickering LEDs at different frequencies. The application of motor-imagery triggered FES through the use of ERD is a promising idea for rehabilitation. However, the adjustment of FES parameters was not addressed, and the method was only demonstrated in healthy volunteers so far [209]. Likitlersuang et al. [263] combined a single-channel EEG-based BCI for FES-triggering with a computer vision system for selecting grasp types and corresponding stimulation patterns for eight predefined target objects. The configuration of the BCI and the exercise with the new system were conducted in one session. Results in five able-bodied volunteers and one SCI patient revealed a computer vision accuracy of 87.5% (SCI) and long average latencies of 5.9 ± 1.5 seconds for the BCI. Daly et al. [215] showed in a single-case study that motor imagery could be used in FES-assisted movement training to improve finger extension in stroke. Until today, BCI-controlled FES-systems remain in research and are not ready for the user to operate them independently at his/her home [240].

With increasing miniaturization of sensing technology, the use of residual motion for FES control of grasping was investigated in several setups. An early approach was the previously described *Bionic Glove* [159] that used data from a wrist position sensor to control stimulation of hand and wrist muscles in SCI patients (cf. *Section* 2.3). Command-control with inertial sensors on the upper limb was proposed by Tong et al. [201]. Bi-axial accelerometers and gyroscopes were placed in pairs at the shoulder, upper arm, forearm, and hand back. A rapid forward-and-backward movement of hand and arm was evaluated as a command signal to possibly trigger FES, with success rates of up to 97% in SCI patients [201]. Mijovic et al. [121] trained an ANN with dual-axis accelerometers to predict forearm motion. Pairs of two accelerometers were placed on the upper arm and forearm and five arm motions were performed in seven healthy volunteers. The trained ANN could discriminate between the different motions (Pearson's correlation coefficient > 0.91) and might be suitable for selecting grasp types in command control.

Accelerometer-triggered FES was suggested by Mann et al. [220] for the elbow, wrist, and finger extensors to enhance functional task practice in chronic stroke patients. Only one bi-axial accelerometer was used, integrated into the stimulator attached on the upper arm. The 15 participants of this pilot study showed an increase in ARAT score and in the *Modified Ashworth Scale*[13] (MAS) after two weeks of intervention. Like EMG-triggered stimulation, movement-triggered ES seems promising to enhance task-oriented training and therefore arm rehabilitation after stroke. However, it requires reasonable volitional shoulder and elbow motor control.

[13]The *Modified Ashworth Scale* grades spasticity on a scale from 0–4. The modified version differentiates "1" and "1+" for a more gradual classification of slight increases in muscle tone [264]. By manually moving a limb through its range of motion to passively stretch various muscle groups, the examiner rates the muscle tone according to the MAS.

Tresadern et al. [265] demonstrated a similar approach with acceleration-based triggering of FES for wrist and finger extension. Again, the stimulator hosted an integrated bi-axial accelerometer but was mounted on the forearm. The authors presented a framework for tuning a patient-individual finite-state-machine-based controller via automatic parameter identification and user input. For this, the state machine's structure (order of states) is defined by the user via a GUI. For parameter optimization of the state machine, the patient first needs to perform the desired movement multiple times. In each repetition, the clinician has to mark instants in time where state transitions—and therefore stimulation—should occur. The system then automatically identifies classifiers (thresholds) by analyzing the recorded data to discriminate the different states. How the stimulation parameters are selected remains unclear. Although the approach of Tresadern et al. [265] tackles the important aspect of adapting FES-control to the individual patient, the methodology reveals some weaknesses in the clinical practice. It is questionable whether affected (stroke) patients can repetitively perform the desired movement without FES to generate appropriate training data. Furthermore, the effect of the FES on movement execution and thereby on the classification is not discussed.

Closed-loop control of finger joint angles in grasping, holding, and releasing objects was investigated by Westerveld et al. [152]. The authors compared a model predictive controller (MPC) with a proportional feedback controller for tracking reference trajectories. Hand and thumb positions were measured with a marker-based motion capture system, and finger flexion angles were calculated. For the proportional controller, isometric thumb force was additionally measured in two directions via a customized setup. For the MPC, a second order linear dynamic polynomial model (ARX) with nine inputs (number of stimulation electrodes) and five outputs was utilized. In an automated identification procedure, where step responses are recorded for all inputs, model parameters are determined. Proportional controller gains were set empirically based on observation of the finger movement. In two healthy volunteers, step responses and the performance in grasping of objects from the ARAT were evaluated. The authors reported average steady-state tracking errors of 1–24 deg and preferred the MCP controller due to the automated identification in their setup [152]. Although the musculoskeletal system has a complex nature, the model-based MPC did not outperform the simple proportional controller. Limitations of this study are the laboratory, impracticable setup for measuring thumb force and hand motion and the validation in healthy volunteers only. In [266], the MPC approach for ES of finger muscles was combined with an end-effector-based robotic arm. An evaluation with severe chronic stroke patients revealed low success rates in grasp-and-release tasks of the ARAT. Especially the hand opening had a small success rate ($< 25\%$), and no complete movements could be made [266]. The positioning accuracy of the robot with respect to the object position was named as the most critical part for the overall performance.

The *Kinect* (Microsoft, Redmond, WA, USA) has been utilized for object and grasp type classification for FES control on the forearm by several groups (e.g., [123, 267, 268]). The concept of artificial perception aims at mimicking human perception during prehension and grasping. Štrbac et al. trained an ANN to differentiate eight objects and assigned corresponding grasp types generated through FES [123]. Through real-time hand motion tracking, the onset of the stimulation was triggered depending on the distance to the target object. ES was applied via the *INTFES* multi-pad electrode (cf. *Section* 2.4), where individual positions and

stimulation patterns were determined at the beginning of an experiment. Despite a mentioning of possible fine tuning of the ES amplitude during hand opening, a concept for closed-loop adaptation of the stimulation intensity was not presented. After the user grasped the object, the system automatically activated the stimulation pattern for hand opening (release) after a predefined period. The authors reported accuracies in grasp type selection / object classification of 90% [123]. In [267], a classifier was proposed for detecting the intended grasp type of the user from hand motion tracking instead through object identification. Simonsen et al. [268] did not classify different grasp types with the *Kinect* but automatically determined the on- and offset for stimulating hand opening. Although these approaches seem promising for intention recognition on a large scale, it remains unclear how the phases of object manipulation and changes in the neuromuscular system can be addressed in closed-loop with this camera-based approach.

Knutson et al. [269] applied motion-based contralaterally controlled FES for home-based rehabilitation of elbow extension and hand opening after stroke. The principle of contralateral control via motion tracking is illustrated in Fig. 2.9. In [269], the movement of the non-paralyzed, contralateral hand and arm was used for proportional control of the stimulation. A customized data glove with three, one-directional bend sensors (Images SI, Staten Island, NY, USA) was attached, measuring the flexion of fingers F2–F4. An elbow cuff was equipped with a single bend sensor to assess elbow flexion. The triceps in the upper arm was stimulated for elbow extension; hand opening was induced by stimulating the extensor digitorum communis and the extensor pollicis longus (three channels). Movement-proportional control was realized via pulse-width modulation: The stimulator increased pw of each stimulation channel from zero to $pw_{\max}$ in proportion to the amount of opening of the contralaterally worn control glove (hand/forearm electrodes) or elbow cuff (triceps electrode). In a pilot case-study, four chronic stroke patients with moderate to severe impairment were treated for twelve weeks of bi-lateral training (home-based as well as therapist-supervised laboratory-based). Photographs of the suitable electrode positions were given to the participants assisting them in the electrode-setup at home. The authors reported that all participants were able to use the system at home—independently or with minimal assistance from a caregiver—and increased their scores in clinical assessments. The approach by Knutson et al. [269] demonstrated the feasibility of home-based FES-therapy and contralateral open-loop control. The FES-induced motion and problems such as muscle fatigue were, however, not addressed.

Sun et al. [270] proposed a "flexible upper-limb FES system" controlled in open-loop via a finite-state machine previously presented in [271]. They aimed to increase the degree of automation in comparison to existing systems and provide flexibility for individual adjustments in patient-specific upper-limb therapy. The suggested state machine represents a sequence of movement phases, where each phase implements the ramping toward and holding of ES channels at their respective targets [271]. The transition between movement phases occurs based on clinician-defined rules. Those rules can be based on data from inertial sensors (one placed over the sternum, one on the forearm), an instrumented object (detects grasp/release), a button-press, or on a counter. A transition rule can be created by a maximum of two Boolean conditions combined via AND or OR. ES is applied through a programmable 5-channel stimulator. A tablet with a GUI guides the clinician through the system setup. The setup consisted of

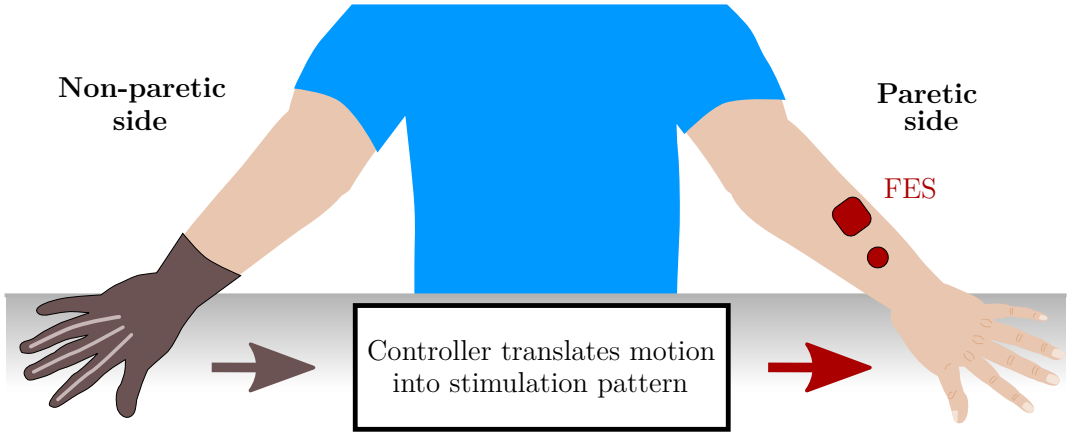

Figure 2.9: Principle of contralateral control via motion tracking for patients with hemiparesis. In this example, the voluntary motion of fingers F2–F4 from the non-paralyzed hand is translated into a stimulation pattern for FES on the forearm on the paretic side. The illustration is inspired by Knutson et al. [269].

five stages [270]: (1) selection/modification/creation of training activities, (2) placement of electrodes on selected muscles and sensors, (3) tuning stimulation parameters/profiles for each movement phase, (4) definition of transition rules, (5) selection of patient instructions and biofeedback. Although not all steps need to be performed in subsequent training sessions of one patient, as they can be stored, the setup process seems quite time-consuming. The system was clinically tested by nine therapists for FES-supported activities with 22 stroke patients with upper-limb impairment in three centers [270, 272]. Face-to-face, semi-structured interviews were included to gain the clinicians' perception on the system's usability [273]. The authors reported an efficiency[14] of the system of below 40% on average over eight therapy sessions [270]. The presented approach showed, therefore, that the demands for flexible therapeutic FES-frameworks and effective arm and hand rehabilitation regarding costs—quick and easy to use—and benefit compete with each other and create a major problem in individual FES therapy. Nevertheless, Sun et al. [270] provided a step toward user-centered FES-aided therapy, where patients and clinicians are in focus. Their framework might be improved by integrating closed-loop control of the ES and automatic parameter identification (e.g., [265]).

Further attempts were published, focusing on single joint control via motion signals. For example, Reinert et al. [274] suggested a state machine for adjusting the pulse width to control single finger flexion. Recently, Hodkin et al. [275] proposed open-loop control of ES via triggering with a custom-made slide rail with integrated proximity sensors to train reach-and-grasp. The rail comprised a cube (5 cm) fastened to the end, which was tethered by a spring-loaded reel [275]. The training tasks consisted of pulling the cube; on release, it automatically returned to the start position. Proximity sensors with a 10 cm range at either end of the rail provided information on the cube and hand position. FES for hand opening (extensor digitorum communis) and arm extension (anterior deltoid) was delivered by a 2-channel stimulator (Odstock Medical; cf. Table 2.1). At the start of each trial, auditory and visual cues announced that the patient should reach toward the block, hand and arm extension were stimulated. The proximity signal triggered the further stimulation pattern.

[14]The authors defined efficiency as the total practice time in a therapy session divided by the total therapy time multiplied with 100, though ranging from 0 to 100% [270].

The authors reported modest functional improvements in clinical interventions of 1–2 weeks with four stroke and seven SCI patients, where one session consisted of 200 repetitions [275]. Muscle fatigue was not reported, although it can be expected in such high repetition rates. The approach lacks an automatic identification and closed-loop adjustment of stimulation parameters as well as automatic sensor calibration since all those settings need to be made manually by the clinician.

Force control of FES generated movements was addressed by Westerveld et al. [276] and Crema et al. [42]. The latter proposed closed-loop grasp control using a force sensor positioned at the thenar eminence in the palm as a feedback signal [42]. VEs and corresponding current intensities were identified prior via an open-loop identification protocol (cf. *Section* 2.4). Grasp force was then controlled using pulse-width modulation and a PID controller with anti-windup. Preliminary results in healthy subjects were presented for a static measurement setup (no forearm movements; neutral pronosupination), presumably showing that the controller was able to elicit the desired force. However, after 150 s, muscle fatigue occurred in the untrained subjects. Westerveld et al. [276] aimed at controlling two directions of thumb force evoked by FES applied to three thumb muscles[15]. Recruitment curves were defined for all three muscles. A linear vector summation was assumed for the resulting forces, acting around the same joint. Via load sharing, the redundancy of the inverse problem was solved where three actuators control the thumb force in two directions. In the experimental setup, a custom-built apparatus measured the thumb forces with two single-axis load cells with pre-loaded springs. The forearm was fixated, and the thumb was connected to the springs. The method was tested in five able-bodied volunteers and five stroke patients. Under feedback control, the authors report a similar performance in force accuracy of the two groups. The work of Westerveld et al. [276] nicely demonstrated that feedback-controlled FES could induce precise forces in the human hand. Yet, a manifold and bulky measurement setup is necessary to achieve this degree of precision, making it inappropriate for clinical practice.

Several systems and methods were introduced for combining FES with passive or active arm support through exoskeletons and orthoses (e.g., [115, 224, 277]). The idea is that task-oriented training of reach-and-grasp movements relies on sufficient residual motor activity of the upper arm, which is not the case in many stroke and SCI patients. Sensor fusion was suggested for controlling such functionally complex upper limb systems, for example, in the *MUNDUS* project [40, 278]. Multiple modalities, namely motion tracking via *Kinect*, an exoskeleton with position sensors, an EEG-based BCI, as well as interactive objects, were combined for feedback control of arm movements (shoulder and elbow joint) with possible hand function support. The detection method for the user's intention depends on the user's residual capabilities, which was assigned to three application scenarios[16] [40]. Additionally, a sensorised glove with bend sensors (MCP and PIP joint) plus force sensors (fingertip and palm) was designed and applied for monitoring and control of the induced movement. A closed-loop controller adjusted the stimulation intensity on shoulder and upper arm muscles according to the reference joint angles of a central state machine [278]. However, hand motion remained controlled in open-loop.

[15] *Abductor pollicis longus*, *opponens pollicis*, *flexor pollicis brevis* (cf. Figs. 1.4 and 1.5)

[16] (1) Present but weak residual functional control of arm and/or hand muscles; (2) no residual functional control of arm and hand but full control of neck muscles, gaze fixation possible; (3) neither full control of arm and hand nor eye muscles.

Researchers from the UK suggested a system based on ILC termed *SAIL*[17] in which closed-loop stimulation is applied to the triceps [279] and anterior deltoid on the shoulder [280] to support specified reaching activities (VR tasks) in combination with a robotic work station. A biomechanical model of the arm was employed to describe the movement in response to the stimulation for identification and ILC [281]. Specific tasks of finite duration are performed repeatedly starting from an initial arm position. After each iteration, the controller uses the performance error from each trial to update the stimulation parameters. The next iteration is initiated automatically after 20 s of rest time [83]. In a further development (*GO-SAIL*[18]), FES for wrist and finger extension was added to support functional tasks with real-world objects [83, 282]. The ILC scheme was adapted to the wrist/finger extensor muscles with motion tracking of shoulder, elbow, and wrist joints via the *Kinect* (cf. *Section* 2.5.2) and an electrogoniometer over the wrist joint [224, 282]. Averaged reference trajectories for each joint were determined from kinematic data of 14 unimpaired adults performing the training tasks. First results with single electrodes on the forearm revealed that more selective finger movement was required to increase the task performance [282]. An electrode array replaced the existing stimulation setup on the forearm, and additional hand and wrist joint angles were measured via *PrimeSense* in the *GO-SAIL+* system [83, 283]. A touch table screen was integrated to present VR tasks. Kutlu [83] showed promising results regarding reference joint angle tracking, but also mentioned the issues of long set-up times (components, controller settings) as well as the insufficient long-term stability of initial identification results. Time-variant physiological changes, such as fatigue and spasticity, could not be compensated adequately by this model-based approach. To address the request for home-based rehabilitation, a compact version of the system was presented in [131]. Recently, Freeman et al. [284] proposed a new, adaptive ILC framework that automatically adapts reference trajectories with regard to the residual capability of the user and simultaneously ensures convergence to the intended task. Beyond simulations, results with this approach are still pending.

Grimm & Gharabaghi [277] presented a closed-loop rehabilitation device for reach-to-grasp assistance via multi-channel ES and a multi-joint arm exoskeleton for anti-gravity support. Seven DOFs on the shoulder, elbow, and wrist were supported, and kinematics plus grip force were measured with the Armeo Spring robot arm exoskeleton (Hocoma, Swiss Federal Institute of Technology, Zurich, Switzerland). ES was applied at sub-threshold level ($q < q_{\mathrm{mot}}$) to seven muscles via single electrodes to encourage shoulder, elbow, and finger (extension/flexion) movement. The timing of the stimulation was adjusted in real-time with a delay of 2 s according to a biomechanical movement model based on vector positions of the virtual arm and the target direction. The target direction was derived from the presented VR task (i.e., a ball had to be grasped in virtual space and transferred to a basket). The authors compared two training sessions, one with and one without ES, in 18 severely affected chronic stroke patients. The results showed increased performance in exoskeleton-based training through the sub-threshold ES [277]. Although the idea of preserving the participants' engagement by applying sensory stimulation, the clinical relevance regarding facilitating motor learning of the additional ES remains unclear. Furthermore, the presented adaptation strategy will not work for FES-supported movements due to the massive delay.

[17] Stroke assistance through iterative learning
[18] Goal-oriented stroke assistance through iterative learning

2.6 Conclusion

Evidenced by the high number of publications on this topic, the field of FES-assisted rehabilitation and support of hand motion is of enormous interest when it comes to regaining mobility and independence in stroke and SCI. Artificial movements performed with FES observed in the reviewed papers involved wrist and finger extension/flexion, pronation and supination of the forearm, as well as grasping with or without holding objects [240]. However, each system only supports a particular range of movements. Besides, current challenges are the possibility of quick customization of the application to the individual patient, flexibility in control strategies and level of support with regard to the patient's capabilities, as well as continuous adaptation of the ES during operation to guarantee the completion of movements and motivate the user. Furthermore, the use of existing neuroprostheses depends on available engineering support due to lack of automation and usability concepts.

Problems with the existing stimulation systems are among others exhaustive setup and search times with single electrodes and electrode arrays, limited ways of control, and non-user-evaluated interfaces. Further drawbacks are the limited number of subjects, in which the EA methods were tested, and short intervention periods [173]. The main reason for this might be that most of the FES systems with EAs contain prototype components, which are usually produced at a small-scale. Often only one to a maximum of two functional prototypes of a research system exist. Therefore, the number of people that can be treated with the device is limited. Besides, although mentioned in the outlook of many publications (e.g., [94, 118]), there are currently no studies that include stimulation systems with EAs that account for real-time control of the ES and dynamic EA reconfiguration [173]. The mentioned necessity of automatically adjusting VE locations to forearm movements was not solved in the reviewed literature. Moreover, the current automatic VE selection approaches disregard the existing expertise of the users, as the individual opinion of the treating health professional and the patient's sensing regarding stimulation comfort is often not reflected sufficiently in the decision process of the algorithms [169]. All those factors may lead to poor acceptance of EA-based hand neuroprostheses in clinical practice.

All mentioned feedback signals and suggested control strategies come with certain restrictions and unsolved problems, yielding specific systems which are only helpful for carefully selected groups of patients and specific application scenarios [242]. Simple methods (e.g., command control via push-button) lack sufficient involvement and intuition, whereas physiological approaches based on EMG and EEG usually require high costs regarding adaption and training with the individual patient [285]. The utilization of biological signals further faces varying signal qualities, due to different electrode placements from session to session, shifting contact resistances, as well as measurement noise. Motion tracking is a promising approach for closed-loop control of FES as it is able to track the user's intention—although delayed with respect to volitional activation originating from the CNS—and the resulting movement from ES (e.g., [83, 152]). However, real-time hand motion tracking is a challenging task due to the large number of finger segments and degrees of freedom of the joints between them. Moreover, the field of rehabilitation imposes some specific requirements regarding, for example, portability, setup, hygienic aspects, and reliability. These shortcomings are well

reflected in the small number of existing studies that propose systems for closed-loop FES based on continuous, real-time sensing of hand motions and biological signals [51].

The lack in synchronization and adaptation of the ES in the sense of a natural motor control yields limited acceptance of HNPs by affected patients. Not all patients benefit from the suggested systems because they do not reach the eligible criteria [240]. A combination and fusion of sensors and signal types in the form of hybrid control seems necessary to address this complex problem. The balance between the resulting technical effort and the ease-of-use can only be solved with a high degree of automation. Additionally, self-adaptation is necessary such that the user can dynamically choose the best interaction signal at any time [208].

In this thesis, several of the mentioned drawbacks in current HNPs are addressed. As reliable, wearable sensors were identified as a key element of automated FES systems, new methods for hand motion tracking with inertial sensors were developed and evaluated for their use in a realistic clinical environment (cf. *Chapter* 4). This technology was utilized in a feedback-controlled search strategy for suitable EA configurations (see *Chapter* 5). Treated stroke patients and health professionals were interviewed to gain insights into the acceptance of those methods. Automatic real-time control of the ES and dynamic EA reconfiguration were investigated for compensating forearm motions (cf. *Chapter* 6). All those new methods aim at increasing the degree of automation and adaptation of HNPs, and thereby promoting the outcome and acceptance of this technology in neurorehabilitation.

3

Concept of the New Hand Neuroprosthesis

3.1 Overview

Within this dissertation, a new hand neuroprosthesis was designed with novel hard- and software components. As the hardware setup is utilized throughout the thesis, it is presented in detail in this chapter.

Figure 3.1 gives an overview of the HNP design. Since the literature review has shown that electrode arrays are more promising than single electrodes on the forearm regarding placement times, selectivity, and dynamic adjustment of stimulation positions for wrist and finger movement, two EAs are integrated in the system to stimulate grasp and release: one for stimulating wrist and finger extensor muscles, one for finger flexors. The utilized stimulator is connected with a demultiplexer to enable the use of up to 59 active EA elements [190]. For open- and closed-loop control as well as intention recognition, hand motion tracking via a novel IMU-based hand sensor system is employed. A portable computer with touch display controls the HNP and serves as a user interface. A push-button can be integrated for additional user input. These components of the developed HNP are described thoroughly in the following sections.

Copyright Statement: The HNP and its components have been previously published in multiple publications of the author [51, 169, 285, 286, 287, 288]. Therefore, parts of the text and figures in this chapter are extracted from those publications. Specifically, Fig. 3.1 of this section was adapted from [169], and both Figs. 3.5 and 3.6 are taken from [51] without modifications according to the Creative Commons license[19]. *Section* 3.4 is also based on [51] with slight modifications and additions in the text.

[19] CC BY 4.0: `https://creativecommons.org/licenses/by/4.0/`

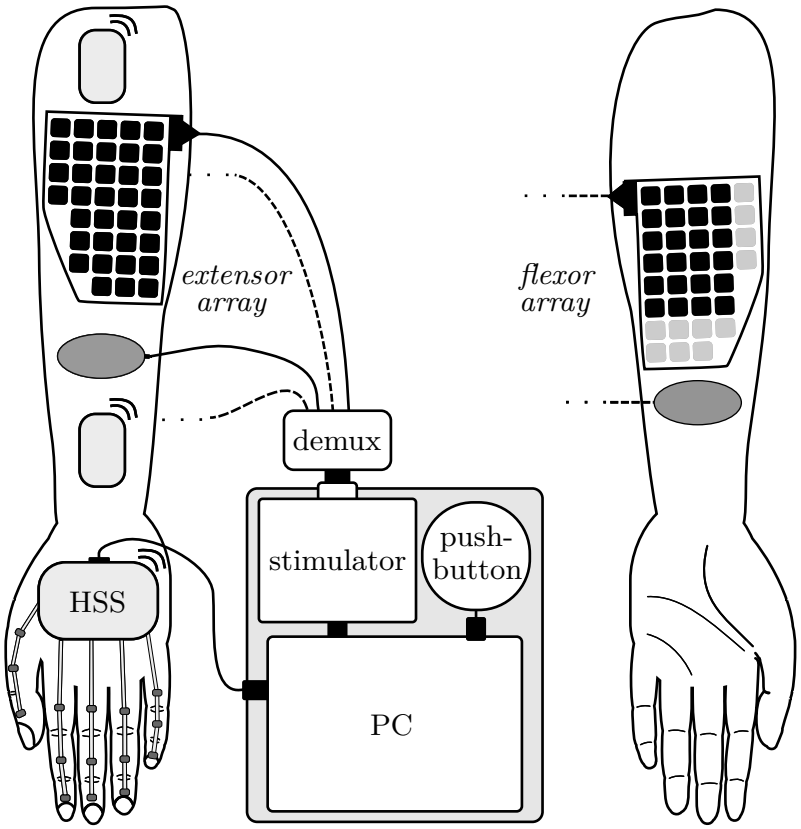

Figure 3.1: Schematic illustration of the hand neuroprosthesis on the left arm. Only the black array elements are available in this setup. The hand sensor system for motion tracking is abbreviated with HSS, the demultiplexer with demux.

3.2 Stimulator and Parameters

For ES, the *RehaMovePro* stimulator (HASOMED, Magdeburg, Germany) with science adapter and demultiplexer [190] is utilized, as seen in Fig. 3.2. The battery-powered stimulator features four current-controlled stimulation channels. When using all four channels, the maximum possible stimulation frequency is 190 Hz [190]. A universal serial bus (USB) connection to a computer allows command control of the stimulation via a customized *Matlab/Simulink* (MATLAB R2016b; MathWorks, Natick, MA, USA) interface (cf. *Section* 3.5). Current amplitude and pulse width can be changed between every applied pulse enabling a quick, dynamic adjustment of these parameters. Technical specifications on the stimulator are listed in *Appendix* B (Table B.1). The additional feature of the stimulator that enables the adjustment of the stimulation pulse shape beyond the various predefined options was not utilized in this work. Instead, biphasic and charge-balanced pulses of asymmetric shape (pw, I) were applied (cf. Fig. 1.8 in *Section* 1.4).

The utilized demultiplexer (cf. Fig. 3.2) is connected to one stimulation channel and supports EAs with up to 59 elements. From these elements, 48 are active elements, and eleven can be addressed as active or counter elements (see definition in *Section* 1.4). Two contacts are available for counter EA-elements or separate counter electrodes.

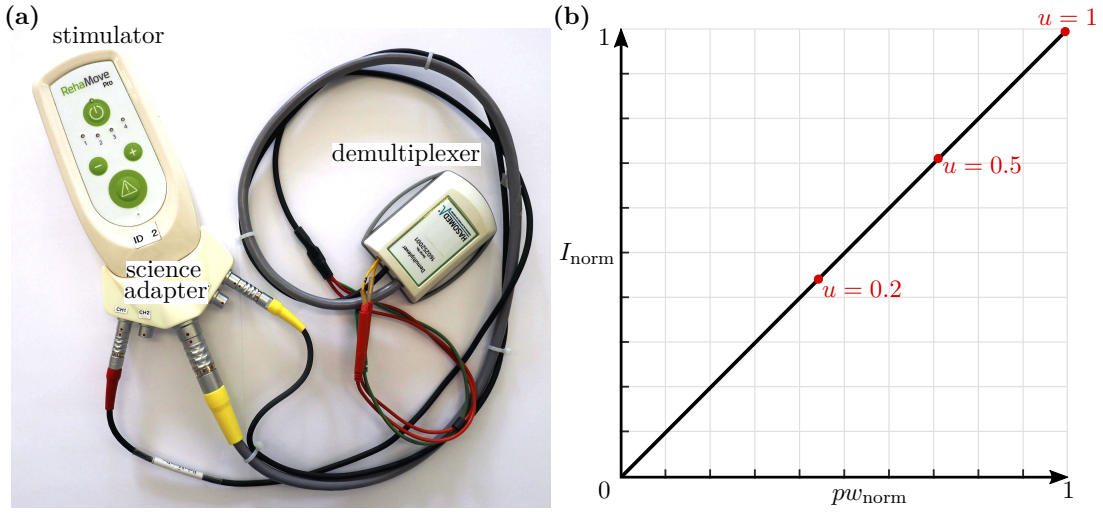

Figure 3.2: *RehaMovePro* stimulator with science adapter and demultiplexer (a), and applied relationship between current I and pulse width pw for the charge control scheme (b). I_{norm} is the normalized stimulation intensity, and pw_{norm} is the normalized pulse width. The resulting normalized charge u is marked exemplarily at three points in red.

To reduce the number of free parameters in the control paradigm, a fixed, but manually adjustable stimulation frequency between 25 Hz and 33 Hz was used, and only the pulse charge q was dynamically manipulated. For a given charge q, the values of pulse width and stimulation current are automatically determined by using a predefined relation between pw and I. This scheme was introduced by Shalaby [111] under the term *charge control*. Due to residual sensation of stroke patients, which is the target group of the HNP, only a current in the range of $I_{\text{min}} = 0\,\text{mA}$ to $I_{\text{max}} = 80\,\text{mA}$ and a pulse width in the range of $pw_{\text{min}} = 10\mu\text{s}$ to $pw_{\text{max}} = 500\mu\text{s}$ is applicable. These limits correspond to a charge ranging from $q_{\text{min}} = 0$ to $q_{\text{max}} = 40\mu\text{C}$. For the charge control scheme, the charge and the corresponding quantities pw and I are normalized to the range from zero to one:

$$I_{\text{norm}} = \frac{I - I_{\text{min}}}{I_{\text{max}} - I_{\text{min}}}, \tag{3.1}$$

$$pw_{\text{norm}} = \frac{pw - pw_{\text{min}}}{pw_{\text{max}} - pw_{\text{min}}}, \tag{3.2}$$

$$u = \frac{q - q_{\text{min}}}{q_{\text{max}} - q_{\text{min}}} = I_{\text{norm}} \cdot pw_{\text{norm}}, \tag{3.3}$$

where u refers to the normalized charge. In this thesis, a linear relationship between pw_{norm} and I_{norm} is assumed where both quantities are equally distributed. Figure 3.2 shows the resulting quantized relationship for the usage with the *RehaMovePro*, as applied in the following experiments.

3.3 Electrode Arrays

In the previous chapter, the concept and benefits of using EAs for FES-induced hand motion have been widely discussed (see *Section* 2.4). Especially in early stroke rehabilitation, the

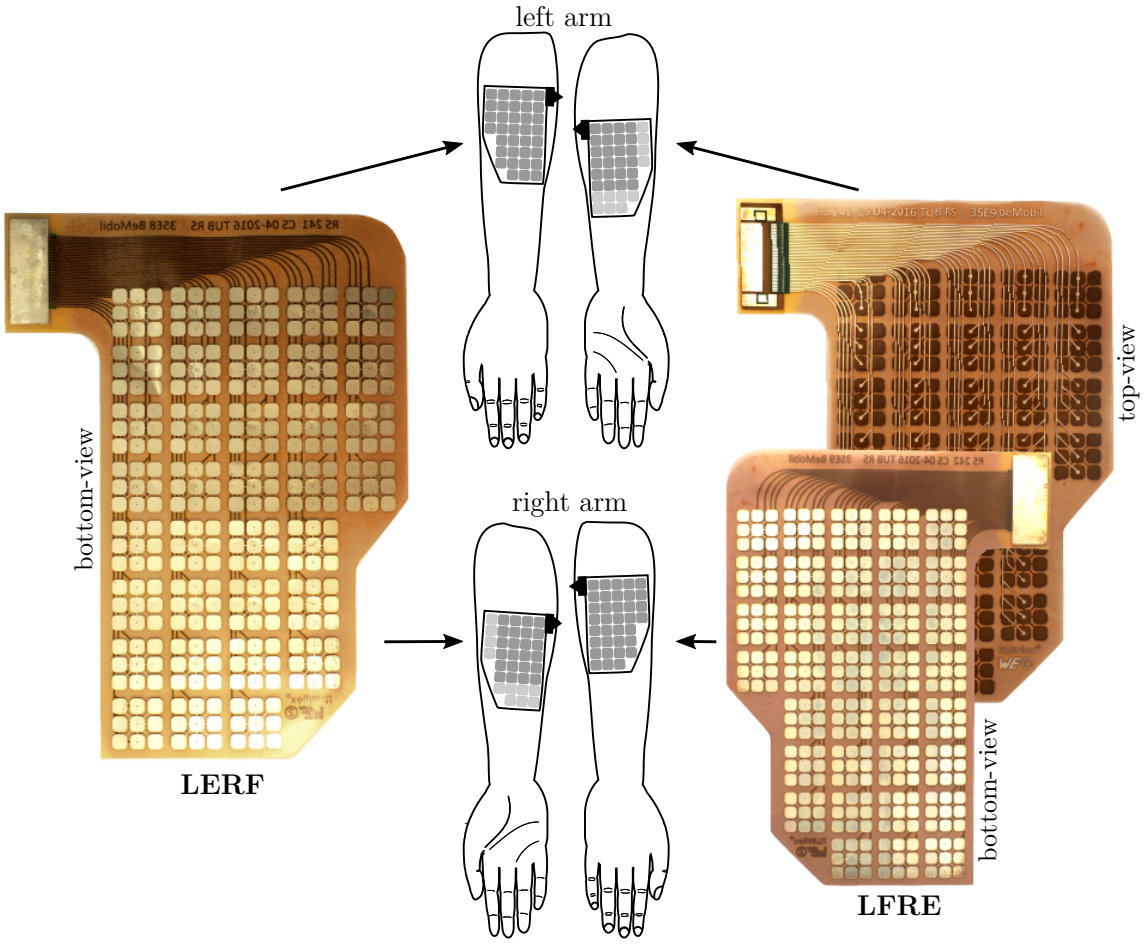

Figure 3.3: New electrode arrays with 35 elements for the HNP. The two EAs, LERF and LFRE, have a mirrored layout, allowing them to be used on either the left or right forearm. On the right, the electrode array is displayed in top-view as well, showing the connector and outer appearance.

electrode setup needs to be adjusted frequently to the changing neurological status due to spontaneous recovery [289]. Therefore, the new HNP utilizes EAs to stimulate wrist and finger extensors/flexors in the forearm for generating wrist and finger extension (hand opening) and grasping. The stimulation of intrinsic hand muscles, as suggested by others (e.g., [40, 42]), is omitted to avoid a restriction of perception and guarantee the full range of motion in the paralyzed hand. Usability was an essential aspect during the design of the EAs.

Two customized electrode arrays were designed with a mirrored layout, as shown in Figs. 3.3 and 3.4. The EAs are interchangeable: One EA, named LERF, is assigned for stimulating extension when placed on the dorsal side of the left forearm (→ *extensor array*), and the other EA, named LFRE, is then placed on the ventral side to stimulate finger flexors (→ *flexor array*; cf. Fig. 3.1). In case of stimulating the right forearm, the two array layouts are used the other way around. This array design allows manufacturing only two different layouts serving both, stimulation of the left and right arm. Each EA consists of 35 elements. As the utilized demultiplexer provides 59 active outputs, not all 70 elements of both EAs can be used in the same setup. In accordance with others (e.g., [94, 187]), more elements—specifically, all 35 elements of one EA—and therefore a larger surface area are assigned for the stimulation of the wrist and finger extensors. Only 24 elements remain for the stimulation of the finger flexors, as indicated in Fig. 3.1.

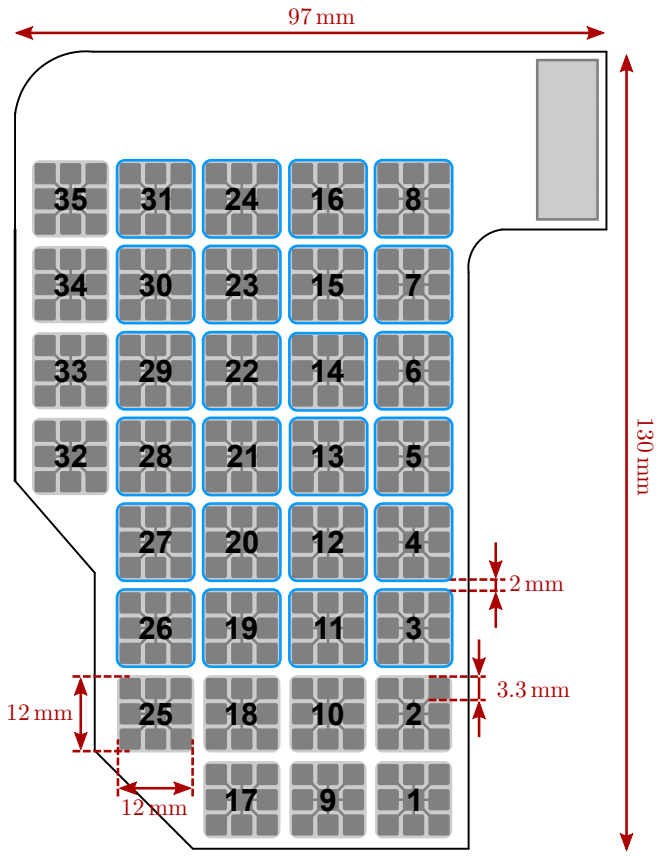

Figure 3.4: Electrode array layout LERF, which is either used on the dorsal side of the left forearm or the ventral side of the right forearm. In the latter case, only the 24 highlighted elements are connected with the demultiplexer. The EA is displayed in top view with the gel layer at the bottom.

The element size in both arrays is $12 \times 12\,\mathrm{mm}^2$ with a gap of 2 mm between elements [90]. The elements itself comprise nine connected sub-elements, each with a size of $3.3 \times 3.3\,\mathrm{mm}^2$ (see Fig. 3.4). In this way, the deformability of the array elements and thereby the flexibility and comfort of the whole electrode array is increased. The EAs were manufactured as flexible PCB (TWINflex; Würth Elektronik, Niedernhall, Germany). Flexible flat cables (FFC) of 1.2 m length connect each EA with the demultiplexer. Therefore, an FFC connector (35 pins, 0.5 mm pitch) is soldered to each EA.

Skin contact and impedance matching are established by a hydrogel layer. Although single hydrogel pads for each element would yield a higher selectivity of the electric field [91], they are impractical when it comes to the necessary frequent change of the hydrogel layer. The donning and doffing stress, as well as the dehydration require a gel layer replacement after approximately ten hours of stimulation [42]. If the same EA is used for multiple persons, the gel layer needs to be changed for each user. Hence, a single hydrogel layer (AG702 stimulating gel with a volume resistivity of $1500\,\Omega\mathrm{cm}^2$; Axelgaard Manufacturing, Fallbrook, CA, USA) for each EA is applied in the new HNP. The gel is cut to match the shape of each EA such that it covers all array elements. In the experiments in this work, a new gel layer was used for each subject; the EAs were disinfected between measurements.

In the application of the HNP, the EAs serve as the active electrodes and two additional single electrodes (oval, 4×6.4 cm; ValuTrode, Axelgaard Manufacturing, Fallbrook, CA, USA)

are placed as counter electrodes at approximately 1 cm distance in distal direction from the EAs on both sides of the forearm (see Fig. 3.1). It was decided not to integrate the counter electrodes into the EAs to keep flexibility for different arm lengths and varying anatomy. The EAs and counter electrodes are attached via the self-adhesive gel layers and fixed via a custom-made cuff (see Fig. 5.7 in *Chapter* 5).

3.4 Hand Sensor System

At the Control Systems Group at Technische Universität Berlin, a novel, portable IMU-based hand sensor system (HSS[20]) has been developed for real-time motion tracking of wrist and finger joint angles and fingertip positions. The development was necessary as available systems for hand motion tracking did not meet the high requirements for rehabilitation purposes (see review in *Section* 1.5 and *Section* 2.5.2). A system was required that is easy to put onto spastic hands (for example, of stroke patients), is not disturbed by the proximity of electronic devices, is not subject to line-of-sight restrictions, and requires only a minimum of calibration effort [51]. The hardware setup was inspired by Kortier et al. [133] and was previously published by Valtin et al. [287] and Salchow-Hömmen et al. [51].

The developed HSS is composed of a mandatory base unit, which is placed on the back of the hand, and up to five sensor strips, which are placed on the segments of the fingers, and an optional wireless inertial sensor for the forearm to track the wrist angles if desired, as depicted in Fig. 3.5. The system is compact and portable as well as modular in the sense that sensor strips can be removed and replaced arbitrarily. These characteristics increase the flexibility in different therapy settings and for multiple hand sizes, making the system more practical and easier to maintain compared to commercial data gloves.

To capture hand motions in high accuracy and precision, the sensor system is able to measure the translational and rotational motion of each finger segment and the hand back. The base unit is a custom printed circuit board placed in a three-dimensional (3D) printed shell ($6.1 \times 4.0 \times 1.1$ cm). It includes a nine-dimensional (9D) inertial sensor (MPU9259, InvenSense Inc., San Jose, CA, USA; footprint 3×3 mm), comprising a 3D accelerometer, a 3D gyroscope, and a 3D magnetometer, as well as five connectors for the sensor strips. A USB-connection to the computer facilitates power supply and data transfer. Each sensor strip connects three 9D inertial sensors (MPU9259; see above) through a 19 cm long flexible PCB. One IMU is attached to each of the three segments of the finger, as seen in Fig. 3.5. The strips at the thumb, index, and middle finger have additional connectors for integrating optional pressure sensors at the finger end segment, which can be taped to the fingertip to measure grasp strength.

Data transfer between the sensor strips and the unit is provided by a serial peripheral interface bus. Sensor data can be sampled at frequencies of up to 1 kHz for accelerometers and gyroscopes, whereas the magnetometers are limited to 100 Hz. The sensor for the forearm

[20] ***Author's contribution***: The author's contribution to this system consists of (a) the principle design of the sensor network (e.g., number of sensors, placement, length of finger strips), (b) the mounting concept, and (c) the development and evaluation of algorithms for joint angle and fingertip position estimation (cf. *Chapter* 4). The contributions (a) and (b) were made in close collaboration with Markus Valtin; for part (c), the author cooperated closely with Dr.-Ing. Thomas Seel and Leonie Callies. The hardware concept and realization as well as the software interface for the HSS was contributed by Markus Valtin.

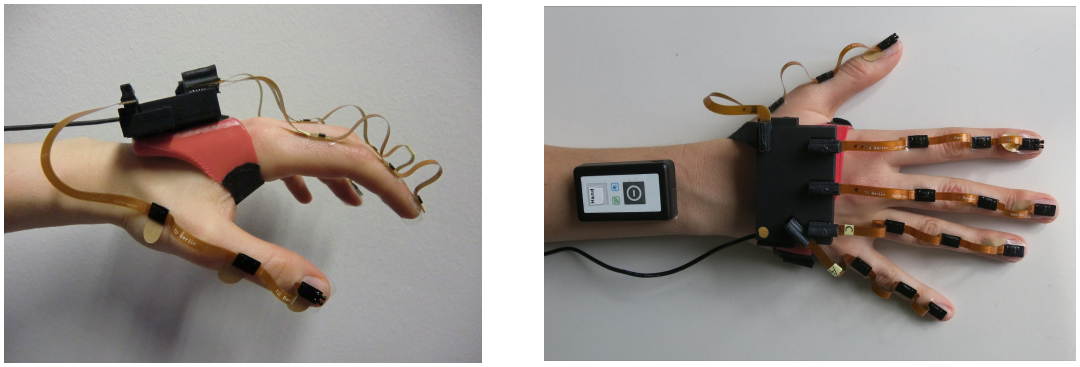

Figure 3.5: Modular hand sensor system for real-time motion tracking of wrist and finger joints as well as fingertip positions. The system consists of a base unit on the hand back, a wireless IMU on the forearm, and up to five sensor strips, each equipped with three IMUs appearing as black rectangles.

(HASOMED GmbH, Magdeburg, Germany) is independent of the base unit and sends its data via Bluetooth (3.0 high data rate) directly to the computer at the same frequency (100 Hz) and with a latency of approximately 10 ms. The forearm sensor is necessary for tracking wrist joint angles in various arm positions. Processing of the raw IMU data is done in *Matlab/Simulink*.

Focusing on stroke and SCI patients, the system was not embedded into a glove. Instead, individual sensor strips are attached adhesively to the finger segments using skin-friendly tape. In this way, the system does not further impair the patient's sense of touch, which is important when relearning to manipulate objects. A silicon fixture was designed that attaches the base unit of the system to the hand back. The mounting of the HSS by another person takes approximately 2 minutes. While the suggested setup may not be superior in sports or VR applications, it is particularly suitable for clinical use with paralyzed hands, as it can be mounted on closed hands (e.g., if a voluntary extension is impeded due to high muscle tone). The complete system measures a total weight of 50 g (25 g base unit + 15 g silicon fixture + 2 g per sensor strip), which equals approximately 10% of the average human hand [290].

Calibration of all sensors was performed using a custom-built calibration robot by Valtin (Control Systems Group, Technische Universität Berlin) to automate the process and to ensure a consistent calibration quality [291]. The bias, a linear scaling correction factor, a rotation matrix that ensures the orthogonality of the sensor axes, and a second rotation matrix, which assures that all three sensor coordinate systems (accelerometer, magnetometer, gyroscope) are aligned, were determined. This type of sensor calibration is performed once every three months to compensate possible bias fluctuations over time.

The proposed motion estimation method is based on the mathematical framework of dual quaternions and aims at avoiding extensive calibration motions and at meeting the requirements of clinical rehabilitation practice. A set of algorithms, the underlying biomechanical hand model, as well as validation results are presented in *Chapter* 4. To monitor the hand motion in real time, an animated 3D visualization has been developed using *Matlab/Simulink* for real-time data processing and BabylonJS[21] as a 3D engine. An example of the visualization is shown in Fig. 3.6.

[21] `github.com/BabylonJS`

Figure 3.6: Example of the 3D real-time visualization of the measured hand posture with the HSS.

3.5 Control Unit and Interface

The (control) algorithms and software were initially developed in *Matlab/Simulink* (MATLAB R2016b; MathWorks, Natick, MA, USA) on a regular PC using a modified Linux ERT target [292]. The executable program can then be run to any (portable) computer, as long as all the necessary libraries and drivers for the hard- and software are installed. In this work, the stimulator, the HSS, and optionally a push-button were connected via USB with a laptop having a touch display.

The GUI was realized in *Python* (version 1) and in *HTML5* (version 2). Version 2 is a further development based on the findings by Schönijahn [293], who optimized the GUI version 1 using usability engineering methods such as user testing. Examples from both versions are displayed in Fig. 3.7. The user navigates through the settings via the touch display, or alternatively via mouse-clicks. An external push-button (PowerMate; Griffin Technology, Nashville, TN, USA) could be integrated for direct user input: It was given to the patient, such that she/he could interrupt the stimulation at any time.

Besides the mentioned hard- and software components, it is possible to integrate an EMG amplifier in the setup to measure EMG via separate electrodes during FES [285].

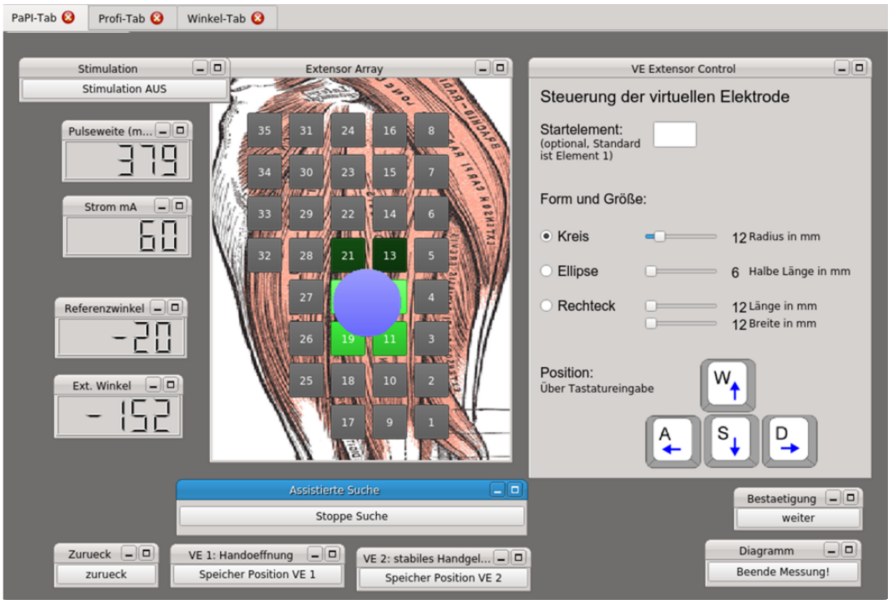

(a) Version 1 for the semi-automatic search presented in *Chapter* 5

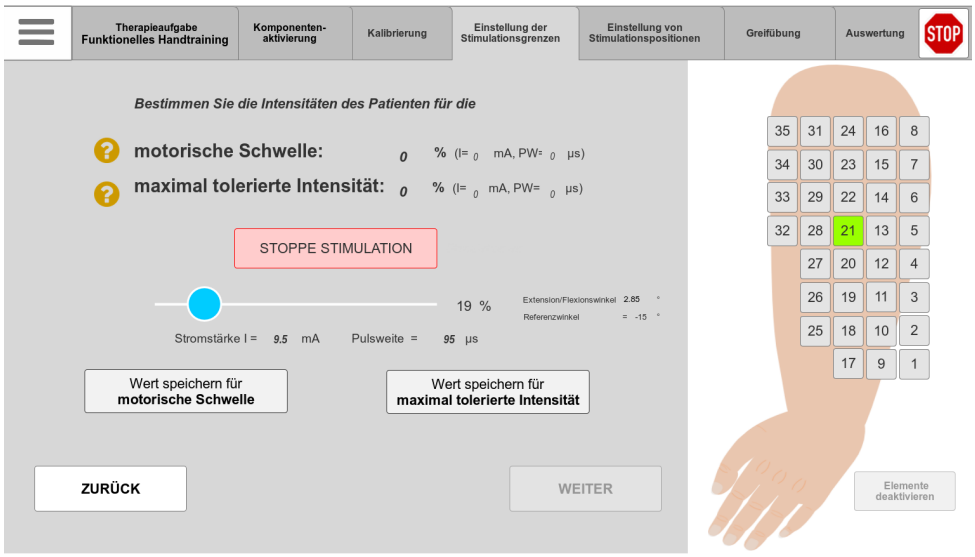

(b) Version 2

Figure 3.7: Exemplary screens of the implemented GUI for the HNP. The GUI was designed in the German language since studies and experiments were exclusively performed in Germany.

4

Real-Time Hand and Finger Motion Tracking with Inertial Sensors

4.1 Overview

To overcome drawbacks of existing systems for hand motion tracking, a novel IMU-based sensor system for real-time tracking of wrist plus finger motion was established (see *Section* 3.4). This chapter presents dual-quaternion-based methods for assessing finger segment orientations, joint angles, and fingertip positions from the raw IMU data. The proposed approach in this thesis addresses the specific requirements of clinical applications in two ways: (1) In contrast to glove-based approaches, the established solution maintains the sense of touch. (2) In contrast to previous work, the proposed methods avoid the use of extensive calibration procedures, which means that they are suitable for patients with severe motor impairment of the hand, such as stroke survivors. To overcome the limited significance of validation in lab environments with homogeneous magnetic fields, the proposed HSS was validated using functional hand motions in the presence of severe magnetic disturbances as they appear in realistic clinical settings.

In the following, *Section* 4.2 briefly reviews the requirements for hand motion tracking in physical rehabilitation, and existing IMU-based systems are discussed. *Section* 4.3 describes the mathematical approach from the underlying biomechanical hand model to the dual-quaternion-based algorithms. A compact introduction to quaternions and dual quaternions is provided. *Sections* 4.4 and 4.5 contain the setup and the results of the simulative and experimental validation, respectively. The results are discussed in *Section* 4.6. Conclusions and possible starting points for future work are given in *Section* 4.7.

[51] Salchow-Hömmen, C., Callies, L., Laidig, D., Valtin, M., Schauer, T., Seel, T. "A Tangible Solution for Hand Motion Tracking in Clinical Applications", *Sensors*, 19(1):208, 2019. DOI: 10.3390/s19010208.[22]

The text and figures in this chapter are extracted from [51], available under the Creative Commons license[23]. More specifically, Figs. 4.1–4.3 and Figs. 4.6–4.13 are reprinted with modifications; Fig. 4.5 is included without modifications. The HSS model for simulations presented in *Section* 4.4 and the corresponding results in *Section* 4.5.1 were added in this thesis.

4.2 Motivation

Objective real-time assessment of hand motion is crucial for closed-loop FES-control in HNPs. Furthermore, motion tracking can be used as a valuable tuning modality for the identification of virtual electrodes in electrode arrays (e.g., [151, 171, 183]; cf. *Section* 2.4). Beyond those applications, objective motion tracking facilitates, for example, real-time biofeedback of hand motion and would yield valuable measurement information for robotic assistive devices [294].

As stated in *Section* 1.5, real-time hand motion tracking is a non-trivial task due to the large number of joints, the resulting multiple degrees of freedom, as well as the specific requirements for the application in motor rehabilitation. Therefore, motion tracking devices need to be portable to allow the application in various clinical environments or even in the context of supervised home rehabilitation. Complicated calibration procedures must be avoided to make the system suitable for patients with severe motor impairment of the hand. For the same reason attaching the system to the hand must be easy and non-restrictive. For example, while gloves may be preferred in gaming applications, they are not a feasible solution for spastic hands. Furthermore, hygienic aspects and individual hand sizes have to be considered, primarily if more than one patient uses the system. A reduced sense of touch should also be avoided to facilitate all aspects of physical rehabilitation.

Lastly, rehabilitation is typically performed in indoor environments and the proximity of electronic devices and objects (e.g., tables, chairs, hand tools) containing ferromagnetic material such as steel. Therefore, the assumption of a homogeneous magnetic field is not fulfilled in a realistic rehabilitation setting, which is a problem when it comes to motion tracking with IMUs using magnetometers. If such an IMU passes by a ferromagnetic object, this induces a short-time magnetic disturbance that can be detected and treated by adjusting the sensor fusion weight of the magnetometer. However, if the IMU-equipped hand is placed near an electronic device or grasps a ferromagnetic object for an extended period, the disturbance does not disappear quickly, and the magnetometer readings are useless during the entire time. This severely impedes the usability of most existing sensor fusion schemes [295, 296]. A reliable system for hand motion tracking must measure joint angles and fingertip positions despite these challenges.

[22] ***Author's contribution***: The author's contribution to [51] includes reviewing the literature, development of the novel methods, overseeing the algorithm implementation, the experiments, and the data evaluation, discussion of the results, visualization of methods and results, writing the manuscript, and revising the manuscript based on annotations and suggestions of the co-authors.

[23] CC BY 4.0: https://creativecommons.org/licenses/by/4.0/

Available types of measurement systems for hand motion tracking in clinical applications were summarized and compared in Table 1.1 (see *Section* 1.5). In short, marker-free camera-based motion tracking is promising for rehabilitation purposes, due to being contact-free and becoming affordable [83]. However, these strongly model-dependent approaches face problems when tracking FES-elicited hand movements, which sometimes do not match expected natural gestures. Furthermore, line-of-sight restrictions may occur, especially when interacting with objects [138]. Although camera-based motion tracking became portable in the sense that they can be quickly set-up in clinical and home environments, they are not wearable and suitable in assistive devices in contrast to data gloves. Gloves with integrated bend sensors quantify joint angles but are not capable of measuring an absolute orientation of the finger segments. Therefore, portable and small IMU-technology was suggested for assessing hand motion in clinical, ambulatory settings [133].

Kortier et al. [133] were among the first to present an IMU-based glove system. They applied IMUs consisting of a 3D gyroscope and a 3D accelerometer to all finger segments and three locations on the back of the hand. In addition, 3D magnetometers were placed at the fingertips and on the back of the hand. Multiple extended Kalman filters were used to fuse the sensor readings and biomechanical constraints to estimate the orientation of every sensor. Each measurement is preceded by a calibration protocol that consists of prescribed poses and precisely defined finger motions, which are used to determine the axes of rotation of all joints. The authors compared their estimation to an optical system in trials with pinching movements of the thumb and index finger [133, 135]. All results were obtained in a laboratory environment under the assumption of a perfectly homogeneous magnetic field. Such conditions are rarely found in clinical practice, and a large number of neurological patients will be unable to perform the required precise calibration poses and motions properly.

Connolly et al. [149] presented an IMU-based data glove that aims at measuring finger and thumb joint movements accurately in patients with rheumatoid arthritis, who are capable of donning a glove. The system includes inertial sensors connected via stretchable substrate material to calculate joint angles and angular velocities. The inertial sensor fusion is based on magnetometers, which will yield false measurements in realistic therapy environments. The motion estimation method requires an initial calibration pose. The description of the specific algorithm is very brief, contains no equations, and indicates that joint angle calculation depends on measured gravitational accelerations. The latter implies that the method becomes highly inaccurate if the joint axis is close to the vertical axis. Under laboratory conditions, the system exhibited root-mean-square errors (RMSEs) of 6° when placed on wooden blocks cut to specific angles.

Choi et al. [297] proposed a wireless data glove with IMUs in a modular design and a new orientation estimation algorithm. The algorithm relies on undisturbed magnetometer data and requires a time-consuming calibration procedure. Their evaluation lacks real-time measurements in realistic conditions and numeric results with human hands. Recently, Lin et al. [298] presented a similar design. They report a mean error in joint angles under ±3° for a 15 minutes measurement of extension and flexion. However, they evaluated the system on a customized measurement platform, allowing only extension and flexion of finger joints, in a laboratory environment under the assumptions of a perfectly homogeneous magnetic field and

with stable sensor biases. It remains unclear how the system performs on the human hand, where many joints have more than one degree of freedom.

In summary, further developments for hand motion tracking are needed to fulfill the requirements of motor rehabilitation in stroke and SCI patients. The proposed system in this chapter aims at being used with any kind of paralyzed hands (e.g., spastic hands), measuring hand motion reliably in indoor environments, and requiring only a minimum of calibration effort. Its accuracy and precision is evaluated for functional motions like pinching and grasping objects in a realistic environment with substantial and permanent magnetic field disturbances.

4.3 Methods for Joint Angle and Fingertip Position Estimation

4.3.1 Biomechanical Hand Model

Inertial measurement units can be used to determine the orientation of body segments in a global coordinate frame via sensor fusion [296]. However, to track finger segment orientations, joint angles, and fingertip positions, a biomechanical model of the hand that describes the relations between segment orientations and positions is required [299]. The following hand model is employed to map the anatomy and the new HSS, which was described in the previous *Section* 3.4.

Degrees of Freedom

Various biomechanical models for the hand are found in the literature, and they differ significantly in their degree of complexity. Cobos et al. [48, 49] give an overview of proposed hand models with 26, 24, 23 and 20 DOFs for the fingers. In this work, the hand is modeled as a kinematic chain with 21 rotational DOFs for the finger joints and two DOFs for the wrist (in total 23 DOFs).

In preparation of the subsequent explanations, it is necessary to recall a few terms from the introduction to the hand's anatomy (see *Section* 1.2). The five fingers are denoted by F1 to F5, where F1 indicates the thumb and F5 the little finger (cf. Fig. 1.2). Fingers F2–F5 consist of three phalanges (segments), namely *distal*, *middle*, and *proximal* phalanx. The considered joints and corresponding DOFs of the utilized model are depicted in Fig. 4.1. The model simplifies the wrist by replacing it with a saddle joint. This implies that the palm of the hand is assumed to be flat and rigid. The position of the MCP joints can be obtained by pure and constant translation along the palm. The T-CMC joint, linking the thumb's metacarpal bone to the wrist, is modeled as a spheroidal ball joint that has three DOFs. This assumption guarantees that the opposition of the thumb to the palm can be modeled. Please refer to Fig. 1.3 for the definitions of hand and finger movements.

Definition of Local Coordinate Systems

The International Society of Biomechanics (ISB) has proposed a set of coordinate systems to be used when reporting kinematic data of the human body [300]. For hand and forearm, the authors introduce a coordinate system with an x-axis pointing in dorsal (left hand) or

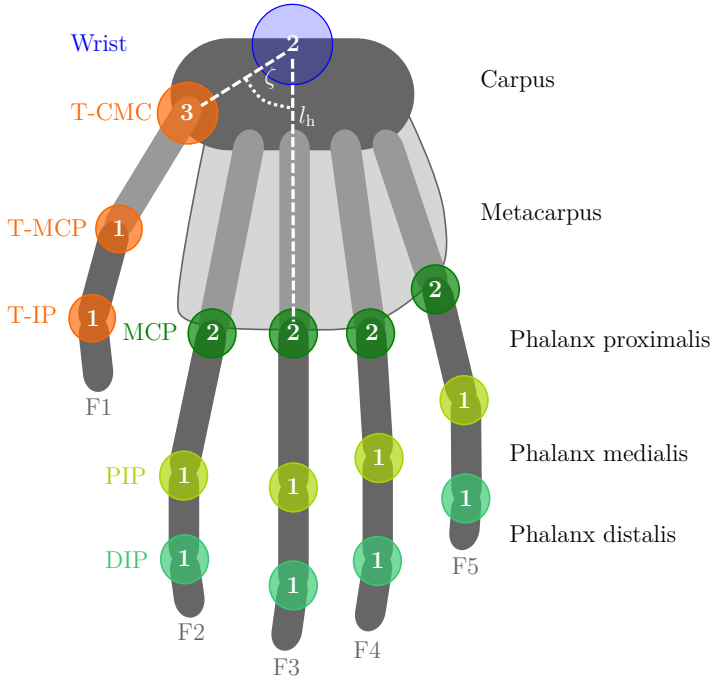

Figure 4.1: Modeled bones and joints of the human hand. The joints are illustrated as colored circles with numbers indicating the considered degrees of freedom. The metacarpal segments (light gray) of F2–F5 form the palm, which is treated as flat and rigid in this model. The white dotted line from the wrist to the MCP joint of the middle finger marks the length of the palm l_h, which needs to be measured for the model. The remaining joint center positions of MCP and T-CMC are deviated via constant ratios and angles, as exemplarily shown for the thumb with angle ζ =58°.

palmar (right hand) direction. The y-axis coincides with the longitudinal axis of the bone and is directed distally for the left hand and proximally for the right hand. The z-axis is added to form a right-handed coordinate system.

This is only one possible definition of coordinate systems. Goislard de Monsabert et al. [301] have compared and tested two different approaches. They call the second concept *functional axes*. The z-axis of this approach is the actual axis of flexion and extension in the finger joints which does not necessarily coincide with the z-axis of the ISB convention. It is used, for instance, by Kortier et al. [133]. This axis is not constant during flexion of the finger [301, 302]. Goislard de Monsabert et al. [301] conclude that the functional axes facilitate the interpretation of the results, but that the differences in the angles about the two varying z-axes are minor, namely always less than 7° for the same movement. It is more complicated to identify and use functional axes because it requires complex calibration movements. Therefore, the authors do not give a strong recommendation. Consequently, the HSS employs coordinate systems according to the ISB recommendations.

The established biomechanical hand model associates each bone with a coordinate frame that has the same orientation as the rigidly connected IMU but lies on the longitudinal axis of the bone at the distal center of rotation (or fingertip in the case of the distal phalanges). The axes x, y, and z are named according to the ISB definitions. These coordinate systems are illustrated in 4.2 for the example of the middle finger F3. In the following, they will be denoted by the segment index $j \in \mathbb{S} = \{$forearm, hand, F1p, F1m, F1d, F2p, F2m, F2d, F3p, F3m, F3d, F4p, F4m, F4d, F5p, F5m, F5d$\}$.

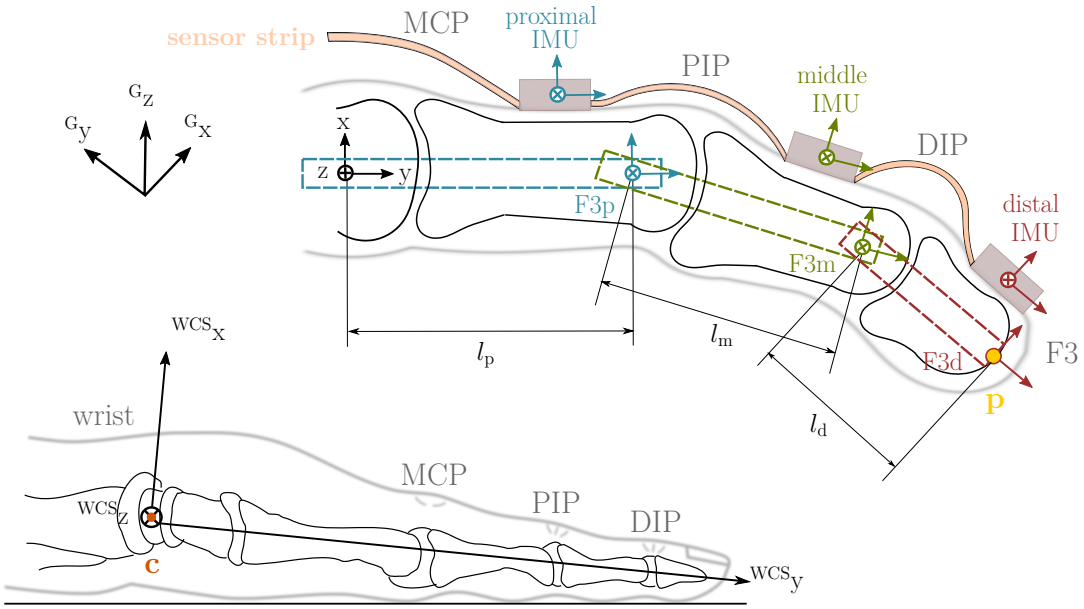

Figure 4.2: Hand model terms for the exemplary finger F3 of a left hand and location of coordinate frames. Top: IMU frames as well as bone frames (both no index) are located in the centers of rotation and the inertial global coordinate frame (index G). The IMU and bone frames are assumed to differ only by a constant translational offset. l_p, l_m, and l_d denote the functional lengths of the proximal, middle, and distal phalanges. The point **p** marks the fingertip position of interest. Bottom: The wrist coordinate system (WCS) is located in the center **c** of rotation of the wrist for the left hand.

The coordinate frame in which the fingertip positions are determined has its origin in the center of rotation of the wrist (**c**) and has a constant, fixed orientation with respect to the forearm, as depicted in Fig. 4.2 (bottom). It is denoted wrist coordinate system (WCS). The y-axis coincides with the middle finger and points distally when the arm and hand lie flat on a horizontal surface and the abduction angle of the wrist joint is zero. This pose is defined as the neutral pose. It implies that the y-axis is slightly tilted downward and the x-axis deviates by a few degrees from the vertical axis. Therefore, the y-axis is not precisely aligned with the longitudinal axis of the forearm.

Lengths of the Phalanges

The lengths of the bones complete the kinematic hand model. Several studies on relative lengths of the phalanges have been conducted [303, 304, 305, 306]. The use of relative lengths has the advantage that only a small number of characteristic quantities must be measured for accurate tracking of an individual hand rather than measuring each phalanx individually. This reduces the required time and lowers the risk of additional measurement errors. The studies mentioned above distinguish between ratios of bone lengths and ratios of functional lengths. The latter describe distances between the centers of rotation of the bones and are the lengths that are of interest in this case. The results presented in [303, 304, 305, 306] are summarized in Table 4.1; they agree well with each other. Therefore, these ratios were used in the model to calculate functional segment length from hand length measurement in the following.

Buryanov & Kotiuk [306] have also examined the amount of soft tissue at the fingertip. Average thicknesses are provided in Table 4.2. These values are subtracted from the measured

Table 4.1: Ratios of the functional lengths of the proximal (l_p), middle (l_m) and distal (l_d) phalanges according to Hamilton & Dunsmuir [304] (F2–F5), Buchholz et al. and Buryanov & Kotiuk [303, 306] (F1). The 95% confidence intervals (CI) observed by [304] are also included.

	F1	**F2**		**F3**		**F4**		**F5**	
	$l_\mathrm{p}/l_\mathrm{d}$	$l_\mathrm{p}/l_\mathrm{m}$	$l_\mathrm{m}/l_\mathrm{d}$	$l_\mathrm{p}/l_\mathrm{m}$	$l_\mathrm{m}/l_\mathrm{d}$	$l_\mathrm{p}/l_\mathrm{m}$	$l_\mathrm{m}/l_\mathrm{d}$	$l_\mathrm{p}/l_\mathrm{m}$	$l_\mathrm{m}/l_\mathrm{d}$
Ratios	0.98	1.86	1.24	1.72	1.36	1.70	1.29	1.91	1.06
95% CI		0.018	0.018	0.013	0.016	0.016	0.016	0.022	0.022

Table 4.2: Average thickness of soft tissue at the fingertip in mm (mean ± standard deviation) according to Buryanov & Kotiuk [306].

F1	**F2**	**F3**	**F4**	**F5**
5.67 ± 0.61	3.84 ± 0.59	3.95 ± 0.61	3.95 ± 0.60	3.73 ± 0.62

lengths of the fingers before the ratios are applied to determine the functional segment lengths in the hand model.

Likewise, the length of the palm needs to be measured from the wrist to the MCP joint of F3. Constant angles and ratios are used to determine the position of the thumb's T-CMC joint and the MCP joints of the remaining fingers respectively, as illustrated in Fig. 4.1. Thereby, the proposed model for the HSS only requires a minimum effort of body measurements.

4.3.2 Introduction to Quaternions and Dual Quaternions

The estimation of segment orientations and fingertip positions is based on the concept of quaternions, which enable an elegant and gimbal-lock-free[24] description of rotations in $\mathbb{R}^3$. Beyond that, the extension to dual quaternions facilitates a description of both rotations and translations in $\mathbb{R}^3$ that exhibits no singularities and is more compact than other representations [307]. The remainder of this subsection provides a brief introduction to the mathematical concept of dual-quaternions. For a deeper understanding of the basic principles, please refer to Leclercq et al. [308] and references therein.

A *quaternion* is defined as

$$\mathbf{q} = q_0 + q_1\mathrm{i} + q_2\mathrm{j} + q_3\mathrm{k} \tag{4.1}$$

with the three imaginary units $\mathrm{i}, \mathrm{j}, \mathrm{k}$, which satisfy the Hamilton identity [309]

$$\mathrm{i}^2 = \mathrm{j}^2 = \mathrm{k}^2 = \mathrm{ijk} = -1. \tag{4.2}$$

The set of all quaternions is denoted by $\mathbb{H}$. The imaginary units can be interpreted as an orthonormal basis of $\mathbb{R}^3$ with $\mathrm{i} = [1,0,0]^T$, $\mathrm{j} = [0,1,0]^T$ and $\mathrm{k} = [0,0,1]^T$. Thus, the quaternion can be written as the sum of a scalar q_0 and a vector part

$$\mathbf{q} = q_0 + \begin{bmatrix} q_1 \\ q_2 \\ q_3 \end{bmatrix} \tag{4.3}$$

[24] "Gimbal-lock" refers to a mathematical problem in three-dimensional descriptions, in which rotations with respect to specific axes can no longer be realized with the aid of rotary operators for predetermined axes.

and use common vector operations on the vector part. It follows from Eq. (4.2) that multiplication of two quaternions $\hat{\mathbf{q}}$ and $\mathbf{q}$ yields the quaternion

$$\hat{\mathbf{q}}\,\mathbf{q} = \hat{q}_0 q_0 - \begin{bmatrix}\hat{q}_1\\ \hat{q}_2\\ \hat{q}_3\end{bmatrix} \cdot \begin{bmatrix}q_1\\ q_2\\ q_3\end{bmatrix} + \hat{q}_0 \begin{bmatrix}q_1\\ q_2\\ q_3\end{bmatrix} + q_0 \begin{bmatrix}\hat{q}_1\\ \hat{q}_2\\ \hat{q}_3\end{bmatrix} + \begin{bmatrix}\hat{q}_1\\ \hat{q}_2\\ \hat{q}_3\end{bmatrix} \times \begin{bmatrix}q_1\\ q_2\\ q_3\end{bmatrix}, \tag{4.4}$$

where $\cdot$ denotes the scalar product and $\times$ denotes the cross product. The *conjugate* of a quaternion is defined as

$$\mathbf{q}^* = q_0 - q_1\mathrm{i} - q_2\mathrm{j} - q_3\mathrm{k}, \tag{4.5}$$

and the *quaternion norm* of $\mathbf{q}$ is

$$\|\,\mathbf{q}\| = \sqrt{\mathbf{q}\,\mathbf{q}^*} = \sqrt{q_0^2 + q_1^2 + q_2^2 + q_3^2}. \tag{4.6}$$

A quaternion with $\|\,\mathbf{q}\| = 1$ is called *unit quaternion*. As the quaternion norm is multiplicative, the multiplication of two unit quaternions always yields a unit quaternion.

A *dual number* is defined to be $z = r + \epsilon d$, where $r, d \in \mathbb{R}$. ϵ is called the *dual unit* and fulfills the condition $\epsilon^2 = 0$ with $\epsilon \neq 0$ [308]. In analogy to complex numbers, r is called the real part and d the dual part of z.

Combining the two aforementioned concepts, a *dual quaternion* is defined as

$$\mathbf{Q} = \mathbf{q}_\mathrm{r} + \epsilon\,\mathbf{q}_\mathrm{d} \tag{4.7}$$

with $\mathbf{q}_\mathrm{r}$, $\mathbf{q}_\mathrm{d} \in \mathbb{H}$ [310]. The set of dual quaternions is called $\mathbb{D}$.

To distinguish dual from regular quaternions (which are denoted by lowercase letters), dual quaternions will be denoted by uppercase letters. Multiplication of two dual quaternions $\mathbf{Q}_A$ and $\mathbf{Q}_B$ can be expressed by quaternion multiplications of the real and dual parts and results in

$$\begin{aligned}\mathbf{Q}_A\,\mathbf{Q}_B &= (\,\mathbf{q}_\mathrm{Ar} + \epsilon\,\mathbf{q}_\mathrm{Ad})(\,\mathbf{q}_\mathrm{Br} + \epsilon\,\mathbf{q}_\mathrm{Bd})\\ &= \mathbf{q}_\mathrm{Ar}\,\mathbf{q}_\mathrm{Br} + \epsilon(\,\mathbf{q}_\mathrm{Ar}\,\mathbf{q}_\mathrm{Bd} + \mathbf{q}_\mathrm{Br}\,\mathbf{q}_\mathrm{Ad}).\end{aligned} \tag{4.8}$$

The conjugate of a dual quaternion can be defined in multiple ways depending on the application. For the calculation of rigid body transformations, the following definition is useful. The dual quaternion

$$\mathbf{Q}^* = \mathbf{q}_\mathrm{r}^* - \epsilon\,\mathbf{q}_\mathrm{d}^* \tag{4.9}$$

is called the *conjugate* of $\mathbf{Q}$, where $\mathbf{q}_\mathrm{r}^*$ and $\mathbf{q}_\mathrm{d}^*$ are quaternion conjugates according to Eq. (4.5).

A dual quaternion is called *unit* dual quaternion if

$$\|\,\mathbf{q}_\mathrm{r}\| = 1, \tag{4.10}$$

$$\mathbf{q}_\mathrm{r}\,\mathbf{q}_\mathrm{d}^* + \mathbf{q}_\mathrm{d}\,\mathbf{q}_\mathrm{r}^* = 0. \tag{4.11}$$

Furthermore, the set of dual quaternions with a real part equal to one and a dual part with zero scalar part is denoted by $\mathbb{D}_0$. Both the set $\mathbb{D}_0$ and the set of unit dual quaternions are necessary to describe 3D kinematics with dual quaternions.

Describing rotations and translations of objects in $\mathbb{R}^3$ by dual quaternions requires a relationship between the vectors and dual quaternions. Following Leclercq et al. [308], in this work, a unique dual quaternion $\mathbf{Q} \in \mathbb{D}_0$ is assigned to each vector $\mathbf{v} \in \mathbb{R}^3$ by choosing the vector as the vector part of the dual part of $\mathbf{Q}$ and setting the real part of $\mathbf{Q}$ to one.

Definition 1 *Let $\mathbf{v} \in \mathbb{R}^3$. The bijective operator is defined as*

$$\mathcal{D} : \mathbb{R}^3 \to \mathbb{D}_0, \quad \mathbf{v} \mapsto \mathcal{D}(\mathbf{v}) = (1 + \mathbf{0}) + \epsilon(0 + \mathbf{v}) \tag{4.12}$$

that yields the dual quaternion equivalent $\mathcal{D}(\mathbf{v})$ for any vector $\mathbf{v}$.

Using this relationship, the dual-quaternion operator that maps a given vector onto another (rotated and translated) vector is defined as follows:

Definition 2 *Let $\mathbf{v} \in \mathbb{R}^3$ and let $\mathbf{Q}$ be a unit dual quaternion. The operator*

$$\mathcal{L}(\,\cdot\,,\, \mathbf{Q}) : \mathbb{R}^3 \to \mathbb{R}^3, \quad \mathbf{v} \mapsto \mathcal{L}(\mathbf{v},\, \mathbf{Q}) = \mathcal{D}^{-1}(\, \mathbf{Q}\, \mathcal{D}(\mathbf{v})\, \mathbf{Q}^*\,) \tag{4.13}$$

is called the dual-quaternion operator.

Note that $\mathbf{v}$ is mapped to its dual-quaternion equivalent, then multiplied from both sides by $\mathbf{Q}$ and its conjugate, and then mapped back into $\mathbb{R}^3$. The geometric interpretation of this operator is given by the following theorem.

Theorem 1 *According to [308], let $\mathbf{r}, \mathbf{t} \in \mathbb{R}^3$ be unit vectors, $\theta \in [-\pi, \pi]$, $l \in \mathbb{R}$ and $\mathbf{v} \in \mathbb{R}^3$. Consider the dual quaternions*

$$\mathbf{Q}_\mathrm{r} = \cos\left(\frac{\theta}{2}\right) + \mathbf{r}\sin\left(\frac{\theta}{2}\right) + \epsilon \cdot 0 \quad =:\ \mathbf{q}_\mathrm{rr} + \epsilon\, \mathbf{q}_\mathrm{rd}, \tag{4.14}$$

$$\mathbf{Q}_\mathrm{t} = 1 + \epsilon\frac{l}{2}(0 + \mathbf{t}) \qquad\qquad\quad =:\ \mathbf{q}_\mathrm{tr} + \epsilon\, \mathbf{q}_\mathrm{td}. \tag{4.15}$$

Then, $\mathbf{Q}_\mathrm{r}$ and $\mathbf{Q}_\mathrm{t}$ are unit dual quaternions, and the dual-quaternion operation $\mathcal{L}(\mathbf{v},\, \mathbf{Q}_\mathrm{r})$ describes a rotation of $\mathbf{v}$ by θ around the rotation axis $\mathbf{r}$, and $\mathcal{L}(\mathbf{v},\, \mathbf{Q}_\mathrm{t})$ describes a translation of $\mathbf{v}$ of length l along $\mathbf{t}$.

Having described rotations and translations in the same mathematical framework, combinations of rotation and translations can now be easily described by dual-quaternion multiplication.

$$\begin{aligned}\mathbf{Q} \;&=\; \mathbf{Q}_\mathrm{r}\, \mathbf{Q}_\mathrm{t} = \;\mathbf{q}_\mathrm{rr}\, \mathbf{q}_\mathrm{tr} + \epsilon(\, \mathbf{q}_\mathrm{rr}\, \mathbf{q}_\mathrm{td} + \;\mathbf{q}_\mathrm{rd}\, \mathbf{q}_\mathrm{tr}) \\ &= \cos\left(\frac{\theta}{2}\right) + \mathbf{r}\sin\left(\frac{\theta}{2}\right) + \epsilon\frac{l}{2}\left[-\sin\left(\frac{\theta}{2}\right)\mathbf{r}\cdot\mathbf{t} + \cos\left(\frac{\theta}{2}\right)\mathbf{t} + \sin\left(\frac{\theta}{2}\right)\mathbf{r}\times\mathbf{t}\right].\end{aligned} \tag{4.16}$$

In the sequel, the special case will often occur in which a rotation is followed by a translation that is orthogonal to the rotation axis. In that case, the scalar product in the above equation, i.e., the scalar part of the dual part, becomes zero.

Note that a single unit dual quaternion can describe any combination of rotations and translations. The two unity conditions in Eqs. (4.10) and (4.11) reduce the number of DOFs from eight (general dual quaternion) to six (unit dual quaternion), which corresponds to the DOF of rotation and translation a rigid body in 3D.

Concatenation of rotations and translations is achieved by simple multiplication of the respective dual quaternions. However, attention must be paid to the order of multiplication and to whether rotations are extrinsic or intrinsic. Extrinsic rotations are rotations about (global) axes that are fixed in space, whereas intrinsic rotations are rotations about (local) body-fixed axes. Both lead to a different order of multiplication of the quaternions. In the following, concatenation of intrinsic rotations is considered to describe hand and finger kinematics. The following notation is applied: *left subscripts* denote the coordinate system in which the quaternion or vector is given, and *left superscripts* denote the object whose orientation is considered. Hence, ${}^{\mathrm{S}}_{\mathrm{G}}\mathbf{Q}$ denotes the orientation of segment S in the global coordinate system denoted by index G.

For an illustration of the concatenation, consider two segments that are linked by a joint. The orientation and position of the first segment are given by ${}^{\mathrm{S1}}_{\mathrm{G}}\mathbf{Q}$, while the orientation and position of the second segment are given relative to the first by ${}^{\mathrm{S2}}_{\mathrm{S1}}\mathbf{Q}$. The second segment's orientation and position in the global frame are then presented by ${}^{\mathrm{S2}}_{\mathrm{G}}\mathbf{Q} = {}^{\mathrm{S1}}_{\mathrm{G}}\mathbf{Q}\,{}^{\mathrm{S2}}_{\mathrm{S1}}\mathbf{Q}$.

4.3.3 Hand Sensor System Algorithms

Segment orientations, joint angles, and fingertip positions shall be determined from the inertial measurements of the HSS. Three different approaches were suggested to solve of this task: a baseline approach (method B) and two more advanced algorithms (methods M1 and M2), which exploit joint constraints to compensate errors in the attachment and the orientation estimation. In contrast to M1, the method M2 does not use measurements of the local magnetic field when estimating the segment orientations. Figure 4.3 summarizes the sub-steps of all three approaches, which are presented in detail in the following sub-sections. For each step, the methods to which the step applies is denoted in the headline.

All algorithms were implemented in *Matlab/Simulink* (MATLAB R2016b; MathWorks, Natick, MA, USA); operations on dual quaternions were performed with the *Dual Quaternion Toolbox*[25] developed by Leclercq et al. [308].

Data Recording and Sensor Fusion (B, M1, M2)

In the common first step, inertial data is recorded at a frequency of $f_\mathrm{t} = 100\,\mathrm{Hz}$ and processed by a recent sensor fusion algorithm [296]. The algorithm performs strap-down integration of the angular rates $\mathbf{g}(t)$, with t being the time, to predict the sensor orientation and uses the magnetometer readings $\mathbf{m}(t)$ and accelerometer readings $\mathbf{a}(t)$ to compensate for integration drift. The latter is done in a way that assures that magnetometer-based corrections affect only the heading of the orientation estimate but not the inclination, which overcomes a drawback of most previous algorithms. Therefore, it facilitates estimation of the full orientation (inclination and heading) while limiting the influence of magnetic field disturbances to a minimum. Details can be found in Seel et al. [296]. For the sake of compactness, the sensor fusion algorithm is

[25] `http://www.compneurosci.com/doc/DualQuaternionToolbox.zip`

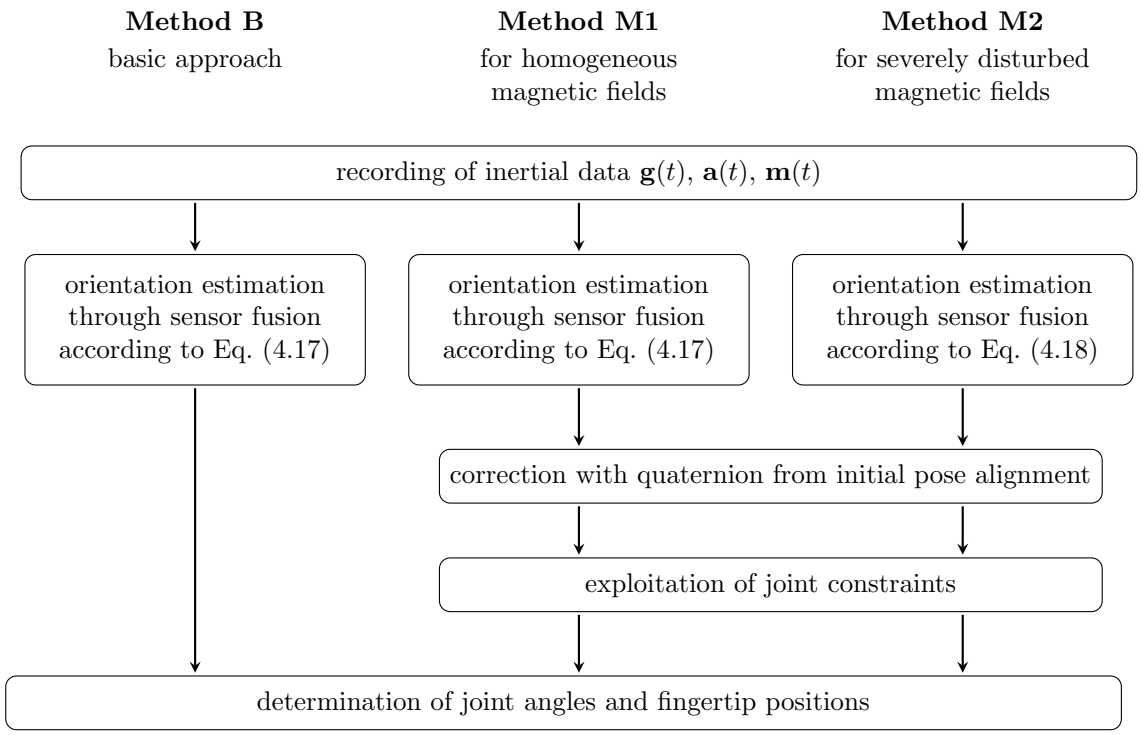

Figure 4.3: Overview of three proposed estimation methods for joint angles and fingertip positions: the baseline method (B), and two advanced methods (M1 and M2). M1 and M2 exploit joint constraints to compensate errors in the attachment and the orientation estimation. In contrast to M1, M2 is completely magnetometer-free and thus suitable for environments with severely disturbed magnetic fields.

described by the recursive function $F(\cdot)$, which yields the dual orientation quaternion for a set of given sensor readings

$$ {}^{j}_{\mathrm{G}}\mathbf{Q}_r(t) = F({}^{j}_{\mathrm{G}}\mathbf{Q}_r(t-\Delta t), \mathbf{g}^j(t), \mathbf{a}^j(t), \mathbf{m}^j(t)), \tag{4.17} $$

where $j \in \mathbb{S}$ denotes the segment to which the IMU is attached (cf. *Section* 4.3.1) and Δt denotes the sampling interval. As mentioned earlier, methods are required that work in realistic settings (e.g., clinical environment) with severe long-time or even permanent magnetic disturbances. In such situations, it is an imminent consequence that any magnetometer-based correction of the strap-down integration deteriorates the heading of the orientation estimate. To assure accurate motion tracking even in severely disturbed magnetic fields, method M2 was employed that completely avoids the use of magnetometer readings. Only accelerometer-based corrections are performed [296], and absolute heading information is instead obtained from an initial pose (cf. Fig. 4.3). In analogy to the above, the magnetometer-free sensor fusion is described by the recursive function $\tilde{F}(\cdot)$:

$$ {}^{j}_{\mathrm{G}}\mathbf{Q}_r(t) = \tilde{F}({}^{j}_{\mathrm{G}}\mathbf{Q}_r(t-\Delta t), \mathbf{g}^j(t), \mathbf{a}^j(t)), \tag{4.18} $$

where $j \in \mathbb{S}$ denotes the segment to which the IMU is attached.

Initial Pose Alignment (M1, M2)

If the local magnetic field is not perfectly homogeneous, the relative heading between inertial sensors cannot be determined from the magnetometer readings. To overcome this limitation, an initial pose period of at least three seconds was introduced during which fingers F2–F5 are straight, and the straight thumb is either abducted at a known angle or aligned with the other fingers. Any relative heading measured by the magnetometers during that pose is then removed, and the initial-pose-aligned (ipa) orientation quaternions ${}^{j}_{\mathrm{G}}\mathbf{Q}_{\mathrm{r,ipa}}(t)$ for each segment $j \in \mathbb{S}$ are obtained. Moreover, the initial-pose period is used to estimate and compensate for the gyroscope bias, which improves the accuracy of the sensor fusion.

Determine Joint Angles (B, M1, M2)

In each time step t, the relative orientation

$$
\begin{aligned}
{}^{\mathrm{a}}_{\mathrm{b}}\mathbf{Q}_{\mathrm{r,ipa}}(t) &= {}^{\mathrm{b}}_{\mathrm{G}}\mathbf{Q}^{*}_{\mathrm{r,ipa}}(t)\ {}^{\mathrm{a}}_{\mathrm{G}}\mathbf{Q}_{\mathrm{r,ipa}}(t), && (4.19)\\
&= q_0 + q_1\mathrm{i} + q_2\mathrm{j} + q_3\mathrm{k} + \epsilon\, 0, && (4.20)
\end{aligned}
$$

between two adjacent sensors a,b $\in \mathbb{S}$ is calculated. The relative quaternion ${}^{\mathrm{a}}_{\mathrm{b}}\mathbf{Q}_{\mathrm{r,ipa}}(t)$ is then converted to intrinsic zxy-Euler angles [287, 300] using

$$
\begin{aligned}
\phi_{\mathrm{z}} &= \operatorname{atan2}\left(2(q_0q_3 - q_1q_2), q_0^2 - q_1^2 + q_2^2 - q_3^2\right), && (4.21)\\
\phi_{\mathrm{x}} &= \arcsin(2(q_0q_1 + q_2q_3)), && (4.22)\\
\phi_{\mathrm{y}} &= \operatorname{atan2}\left(2(q_0q_2 - q_1q_3), q_0^2 - q_1^2 - q_2^2 + q_3^2\right). && (4.23)
\end{aligned}
$$

For each joint, only the angles according to the modeled DOFs of the corresponding joint are determined. For example, following the definitions in Fig. 4.1, ϕ_{z} is the hinge joint angle for the PIP joints of fingers F2–F5 representing extension/flexion in one DOF. In method B, the joint angles extracted at this step are provided as the output. However, for the methods M1 and M2, the joint angles are subject to another step, where physiological constraints are applied, before they are outputted, as described in the following.

Apply Joint Angle Constraints (M1, M2)

At this stage in methods M1 and M2, the modeled joint angles around physiological axes are restricted to an anatomically permissible interval before they are provided as an output (DIP: F$\in[-15°, 100°]$; PIP: F$\in[-20°, 120°]$; T-IP: F $\in$ $[-20°, 100°]$). The intervals were extracted from literature and added with a tolerance [47] (cf. Table A.1 in the *Appendix*). Moreover, non-physiological rotations around axes that are not any of the degrees of freedom of the respective biological joint model are discarded at this step. For example, in PIP joints, the angles ϕ_{x} and ϕ_{y} are set to zero. The corrected Euler angles are then transformed back into quaternion space, which yields the modified relative orientation ${}^{\mathrm{a}}_{\mathrm{b}}\tilde{\mathbf{Q}}_{\mathrm{r,ipa}}(t)$.

Determination of the Fingertip Positions (B, M1, M2)

In the final step, the relative orientations of the sensors need to be combined with the translations between the joints. Recall that the coordinate system of each distal phalanx is defined to lie at the segment's distal end, while the coordinate systems of the other segments are defined to lie in the distal joint center of those segments, as depicted in Fig. 4.2. Consequently, the location and orientation of the F3 fingertip with respect to the F3m coordinate system are given by the relative quaternion

$$\overset{\text{F3d}}{\text{F3m}}\mathbf{Q}(t) = \overset{\text{F3d}}{\text{F3m}}\tilde{\mathbf{Q}}_{\text{r,ipa}}(t) \ \overset{\text{F3d}}{\text{F3m}}\mathbf{Q}_{\text{t}}. \tag{4.24}$$

For the example of the left hand, where the constant dual quaternion $\overset{\text{F3d}}{\text{F3m}}\mathbf{Q}_{\text{t}} = 1 + \epsilon\frac{l_{\text{d}}}{2}(0 + [0,1,0]^T)$ describes the translational offset in direction of the y-axis (bone-centered axis) of the F3d segment, and l_{d} was determined in *Section* 4.3.1. Likewise, the dual quaternion $\overset{\text{F3m}}{\text{F3p}}\mathbf{Q}$ connects the F3m segment with the F3p segment:

$$\overset{\text{F3m}}{\text{F3p}}\mathbf{Q}(t) = \overset{\text{F3m}}{\text{F3p}}\tilde{\mathbf{Q}}_{\text{r,ipa}}(t) \ \overset{\text{F3m}}{\text{F3p}}\mathbf{Q}_{\text{t}}. \tag{4.25}$$

The connections between the other segments and the segments of all other fingers are made analogously. Eventually, a compact expression of the entire kinematic chain of each finger is obtained by the dual quaternion

$$\overset{\text{F}i\text{d}}{\text{WCS}}\mathbf{Q}(t) = \overset{\text{hand}}{\text{WCS}}\mathbf{Q}(t) \ \overset{\text{F}i\text{p}}{\text{hand}}\mathbf{Q}(t) \ \overset{\text{F}i\text{m}}{\text{F}i\text{p}}\mathbf{Q}(t) \ \overset{\text{F}i\text{d}}{\text{F}i\text{m}}\mathbf{Q}(t) \tag{4.26}$$

for $i \in \{2,3,4,5\}$ and by

$$\overset{\text{F1d}}{\text{WCS}}\mathbf{Q}(t) = \overset{\text{F1p}}{\text{WCS}}\mathbf{Q}(t) \ \overset{\text{F1m}}{\text{F1p}}\mathbf{Q}(t) \ \overset{\text{F1p}}{\text{F1m}}\mathbf{Q}(t) \ \overset{\text{F1d}}{\text{F1m}}\mathbf{Q}(t) \tag{4.27}$$

for the thumb (F1).

Since the fingertips are the origins of the distal segments' coordinate systems, the IMU-based fingertip positions $\mathbf{p}$ are calculated by applying the dual-quaternion operator to the zero vector

$$\overset{\text{F}i\text{d}}{\text{WCS}}\mathbf{p}_{\text{IMU}}(t) = \mathcal{L}(\mathbf{0}, \overset{\text{F}i\text{d}}{\text{WCS}}\mathbf{Q}(t)) \tag{4.28}$$

for all five fingers i. The left subscript of $\mathbf{p}$ indicates the reference coordinate frame, while the right subscript indicates that the position was calculated from inertial measurements, denoted as IMU.

4.4 Simulations and Experimental Validation

4.4.1 Overview

The accuracy of the proposed real-time hand motion tracking system was evaluated in simulations and experimental trials with four able-bodied volunteers (three female, one male, age 29.5±2.65). The experiments have been approved by the local ethical committee (Berlin Chamber of Physicians, Eth-25/15). Written informed consent was obtained from each participant before the session.

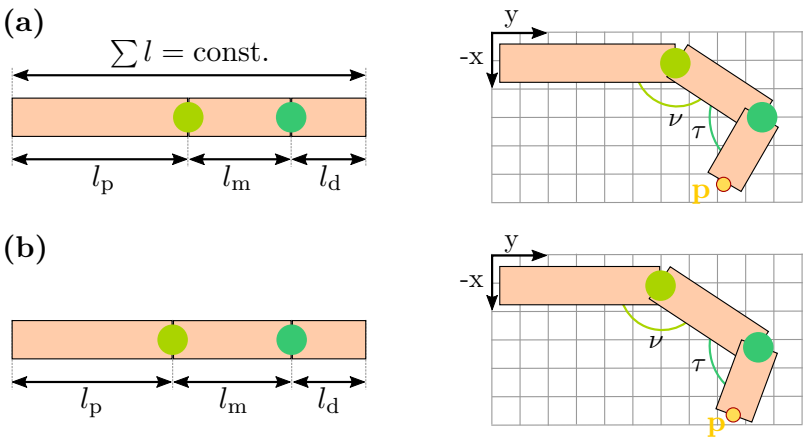

Figure 4.4: Demonstration on how functional segment length ratios influence the resulting fingertip position **p**. Here, (a) and (b) show a model of the finger F3 with the same, constant finger length but different segment ratios. When the same angles ν for the PIP joint and τ for the DIP joint flex the finger, the resulting fingertip positions **p**, here marked by the yellow circle, differ slightly.

The simulations with the hand model were conducted to estimate the influence of model assumptions and measurement noise. Experiments were performed in two different settings. First, experiments with one participant (#1) in an idealistic laboratory environment without magnetic disturbances were undertaken, as it is common in previous literature. The proposed hand motion tracking system was compared with a marker-based optical motion capture system to facilitate the comparison to earlier publications with similar setups. To avoid marker occlusion and marker swapping, isolated movements of single fingers were analyzed. For the sake of a more realistic assessment, a second setting with experiments in all four participants (#1– #4) was employed involving functional hand postures and motions in environments with disturbed magnetic fields. In these experiments, knowledge about contact or distances between fingertips and objects was utilized to assess the accuracy of the proposed methods. In both settings, only the thumb (F1) and the index and middle fingers (F2, F3) were considered because they contribute most to functional motions such as grasping, pinching or pointing.

4.4.2 Simulations

The assumptions of the biomechanical hand model regarding the finger segment ratios of F2–F5 (cf. *Section* 4.3.1) as well as the effects of measurements noise and misaligned sensors of the HSS were evaluated in simulations. A kinematic multibody framework (SimMechanics in *Matlab/Simulink* (MATLAB R2016b; MathWorks, Natick, MA, USA)) of the hand model and the inertial sensors was implemented. Thus, the performance of the developed HSS algorithms could be simulated for various hand movements, varying functional segment length ratios, sensor displacements, as well as different types and intensities of disturbances. Details to the hand SimMechanics model are provided in *Appendix* C.

The following error sources were considered in the simulations: (1) Functional segment length ratios vary by a few percents from subject to subject, as suggested by the literature on hand anthropometry (cf. *Section* 4.3.1). Therefore, the measurement of the total finger length plus the assumption of constant finger ratios is a simplification in the biomechanical hand

model which can lead to errors in the fingertip position estimation, as illustrated in Fig. 4.4. To investigate this error source, different segment ratios were simulated in the model. In particular, the results with for the mean, minimal, and maximal values of the 95% confidence intervals found by Hamilton & Dunsmuir [304] were compared. The constant overall finger lengths in the model were chosen according to Buryanov & Kotiuk [306], who averaged the length of 66 study participants. (2) In practice, sensors are not always placed in line with the finger segments' orientation. Therefore, the rotation of an IMU around the x-axis (in degree) and the relative translation in y and z direction (percent from ideal position) were modified in the model and compared with the ideal sensor placement. (3) Inertial sensor data is subject to measurement noise and bias. A disturbance model based on real sensor data of an accelerometer and gyroscope (cf. *Appendix* C) was used to quantize the influence. Furthermore, the simulations were performed for multiple angular velocities (movement speeds).

The presented simulation results focus on the MCP joints of F2–F5, as this is a joint with two DOFs in comparison to PIP and DIP joints. Pure flexion/extension, pure adduction/abduction, as well as a combination of those movements were evaluated. The maximum deviation between input joint angle and the estimated joint angle by the IMU model and proposed algorithms and the RMSEs were tracked for the time of the movement (cf. following sections).

4.4.3 Idealistic Setting with Optical Reference System (Setting 1)

Setup

The utilized optical motion capture system (Vicon Motion Systems Ltd., Oxford, UK) consists of eight infrared cameras equally distributed along the outer edge of the ceiling in a measurement chamber. Spherical optical markers with a diameter of 16 mm were applied to fingertips and MCP/T-MCP joints of all investigated fingers, as pictured in Figs. 4.5 and 4.6. Furthermore, three stationary markers on top of the measurement fixture facilitate coordinate transformation between the coordinate frames of the inertial sensor system (IMU) and the optical motion capture system (opt). The motion capture system uses triangulation to measure a time series of positions in 3D space for each optical marker. The measurements were performed in the center of the measurement chamber with an average camera distance of 3 m. For this setup, the average marker position tracking error was found to be below 1 mm.

To improve the repeatability of the experiments and to minimize the effect of forearm motion, the forearm and hand were fixed in a plaster mold with a wooden base, as shown in Fig. 4.5. When placed in the customized mold, the hand is in the initial neutral pose. The abduction angle of the wrist is zero, and the thumb is abducted in a fixed angle that assures that all bones of the thumb are aligned. The L-shaped front part of the wooden base can be hinged down in a way that the palm remains supported by the base, but the fingers (including the thumb) can be moved. The fixture prevents any translation of the forearm that would distort the optical measurement.

Alignment of the Coordinate Frames between HSS and Optical System

Recall that the WCS has its origin in the center of rotation of the wrist $\mathbf{c}$ and is aligned with the longitudinal axis of the fingers at the neutral pose. As shown in Fig. 4.6, this directly

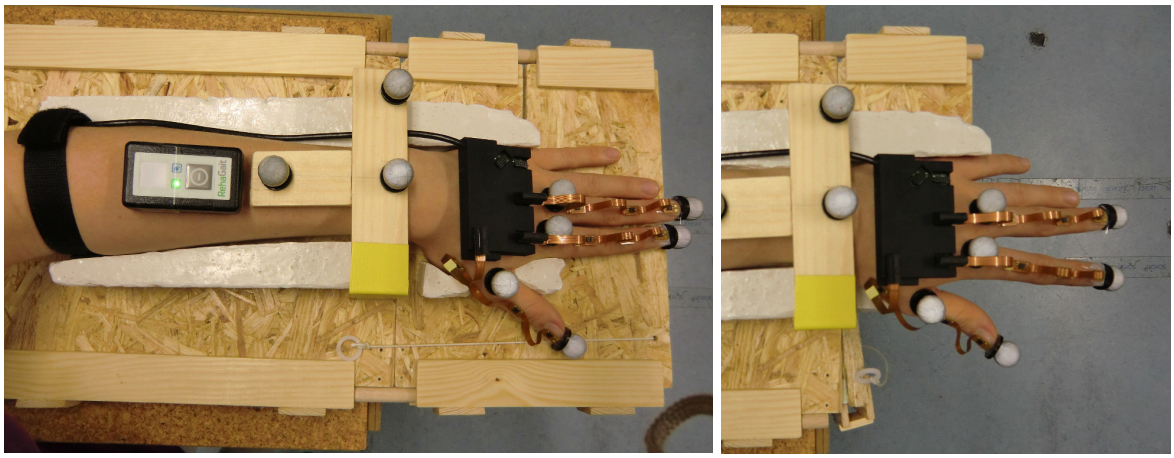

Figure 4.5: Idealistic setting with optical reference system. The customized wooden fixture assured repeatability of the experiments and unrestricted finger motion without any translation of the forearm. The markers on top of the MCP joints were used for visualization purposes. Markers on top of the fixture were used for coordinate transformation between the inertial system and the optical system.

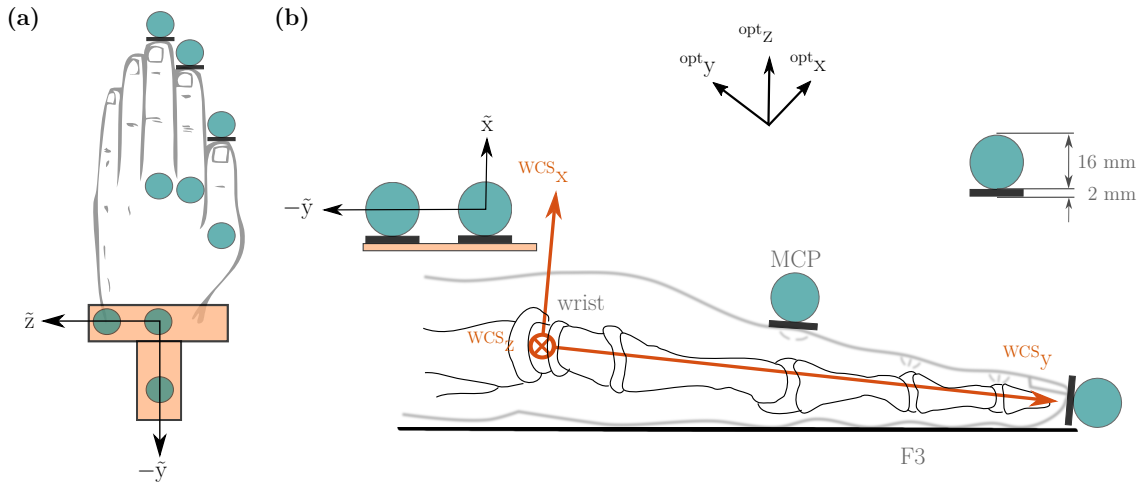

Figure 4.6: Position of the optical markers visualized as cyan circles, and definition of coordinate systems illustrated in (a) top view of wrist and hand, and (b) side view of a cut through the middle finger F3 (opt: optical system; WCS: wrist coordinate system; tilde: marker coordinate system).

Table 4.3: Overview of experiments in Setting 1 with optical reference (A: abduction, F: flexion, AF: abduction and flexion).

Experiment ID	Description
A-F1, A-F2, A-F3	Pure abduction motion of F1, F2, and F3
F-F2, F-F3	Pure flexion motion of F2 and F3
AF-F1, AF-F2, AF-F3	Combined abduction and flexion motion of F1, F2, and F3

yields the rotation ${}^{\text{opt}}_{\text{WCS}}\mathbf{q}$ between the WCS and the optical coordinate system. However, the translational offset between both coordinate systems is also required, i.e., the optical system's coordinates of the joint centers must be identified. To this end, flexion/extension and ulnar/radial deviation movements of the wrist were recorded while all other joints were stiffened voluntary by the participant. This recording yields n marker position samples ${}^{\text{F3d}}_{\text{opt}}\mathbf{p}_{\text{OPT}}(t)$ of the tip of F3, where the right subscript OPT denotes the measurement with the optical system. These n samples are used to identify the center ${}_{\text{opt}}\mathbf{c}$ of rotation of the wrist in the global coordinate frame of the optical system via the optimization problem

$$ {}_{\text{opt}}\mathbf{c} = \underset{\mathbf{c}\in\mathbb{R}^3}{\arg\min} \sum_{h=1}^{n} \Big| \| {}^{\text{F3d}}_{\text{opt}}\mathbf{p}_{\text{OPT}}(t_0 + h\Delta t) - \mathbf{c}\| - \frac{1}{n}\sum_{k=1}^{n} \| {}^{\text{F3d}}_{\text{opt}}\mathbf{p}_{\text{OPT}}(t_0 + k\Delta t) - \mathbf{c}\| \Big|. \tag{4.29} $$

The function minimizes the deviations of the individual distances to $\mathbf{c}$ from the mean distance. A coordinate transformation consisting of the calculated translational offset ${}_{\text{opt}}\mathbf{c}$ between the measurement systems and a subsequent rotation ${}^{\text{opt}}_{\text{WCS}}\mathbf{q}$ yields the marker positions in the wrist coordinate system of the inertial system:

$$ {}^{\text{F}id}_{\text{WCS}}\mathbf{p}_{\text{OPT}} = \mathcal{L}\Big({}^{\text{F}id}_{\text{opt}}\mathbf{p}\,,\, ({}^{\text{opt}}_{\text{WCS}}\mathbf{q} + \epsilon 0)(0 + \epsilon(0 - {}_{\text{opt}}\mathbf{c})) \Big) \tag{4.30} $$

with $i \in \{1, 2, 3\}$. Finally, to achieve time synchronization between both measurement systems, each recording started with a characteristic motion of one finger, which was manually identified to determine the time offset.

Conducted Experiments

Table 4.3 summarizes the motions used for validation in Setting 1. Since any functional or complex hand motion quickly leads to occlusion or swapping of optical markers, pure abduction/adduction (abbreviated as A in Table 4.3), pure flexion/extension motions (F) and a combination of both (AF) was performed with the fingers F1, F2, and F3. The abduction of F1 stands for a planar movement of the thumb, while the combination of flexion and abduction describes the opposition of the thumb to the palm. Each experiment consisted of 10–15 repetitions of the respective movement and lasted 30–50 s. All motions were performed at a comparable speed to motions caused by neuromuscular stimulation, i.e., angular rates of the finger joints remained below $2^{\text{rad}}/\text{s}$ and contained only frequencies below 2 Hz (cf. [131]).

For the analysis, the fingertip positions obtained by the inertial methods B, M1, and M2 were compared to the reference measurements obtained from the optical motion capture system. By validating the fingertip positions, the measured joint angles were indirectly confirmed as well. For each measured finger $i \in \{1, 2, 3\}$ and each time step $t \in [t_0 + \Delta t, t_0 + m\Delta t]$, the

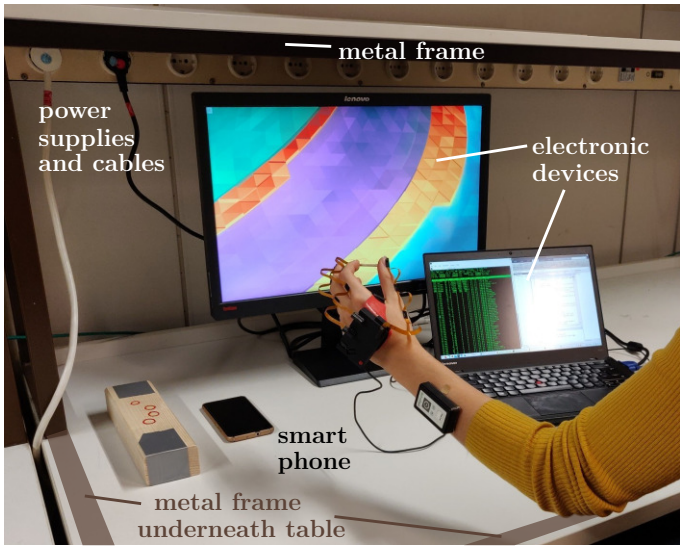

Figure 4.7: Measurement setup for Setting 2 in the direct presence of ferromagnetic materials and electronic devices.

error was calculated as

$$E_i(t) = \left\| {}^{\mathrm{Fid}}_{\mathrm{WCS}}\mathbf{p}_{\mathrm{IMU}}(t) - {}^{\mathrm{Fid}}_{\mathrm{WCS}}\mathbf{p}_{\mathrm{OPT}}(t) \right\|, \tag{4.31}$$

and for each experiment the root-mean-square error is calculated over all m time steps:

$$RMSE_i = \sqrt{\frac{1}{m}\sum_{k=1}^{m} E_i^2(t_0 + k\Delta t)}. \tag{4.32}$$

4.4.4 Realistic Setting Exploiting Characteristic Hand Poses (Setting 2)

Setup

Beyond the validation of accuracy in optical motion capture laboratories, it is likewise important to evaluate the hand motion tracking system under realistic, clinically relevant conditions. During therapy in clinics or at home, patients are indoors, and they interfere with or move in the proximity of furniture or objects containing iron or other ferromagnetic material. Hence, a homogeneous magnetic field cannot be assumed. All experiments in Setting 2 were conducted in the direct proximity of furniture containing ferromagnetic materials and electronic devices emitting electromagnetic fields, such as tables with metal legs and computers as seen in Fig. 4.7. The validation with multiple participants (four in total) allowed statements on the inter-/intra-subject reliability. Moreover, complex and functional motions of the hand such as grasping or pinching were considered, since those movements are performed in motor rehabilitation training.

Conducted Experiments

Note that such functional motions cannot be performed in an optical motion capture laboratory without causing repeated occlusion of the markers. Therefore, other strategies were employed to find a ground truth for evaluation of the results: Different points of contact around the

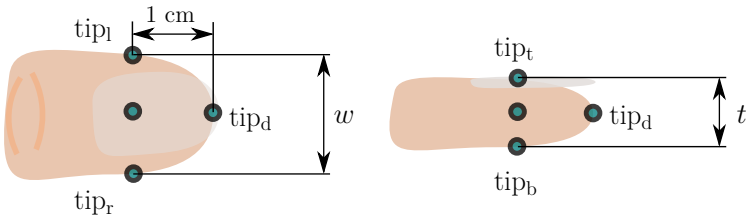

Figure 4.8: Fingertip in top view (left) and side view (right). Marked are the points of contact on the left and right ($\text{tip}_\text{l}, \text{tip}_\text{r}$), on the top and bottom ($\text{tip}_\text{t}, \text{tip}_\text{b}$) and at the distal tip (tip_d) of the finger. The parameter w is the width, t the thickness of the finger.

Table 4.4: Overview of experiments in Setting 2 with predefined postures in a magnetically disturbed environment.

Experiment ID	Description
P1	Spacer with length $d_{\text{P1}} = 3\,\text{cm}$ between F1 tip_b and F2 tip_b
P2	Spacer with length $d_{\text{P2}} = 3\,\text{cm}$ between F2 tip_l and F3 tip_r
P3	F1 tip_d and F2 tip_d in contact, distance $d_{\text{P3}} = 0\,\text{cm}$
P4	All fingers fixed on a wooden block that is moved in space, distance d_{P4} predefined for each pair of fingers ($d_{\text{P4,F1F2}} = 5.3\,\text{cm}$, $d_{\text{P4,F1F3}} = 4.6\,\text{cm}$, $d_{\text{P4,F2F3}} = 2.5\,\text{cm}$)

fingertip were defined (see Fig. 4.8) and characteristic hand poses and motions were performed during which the distances between these points were constant and known. All performed experiments are summarized in Table 4.4. For experiments P1 and P2, a spacer of known length (3 cm) was pinched between the bottom sides of the fingertips in the case of pair F1–F2 and between the left and right point of contact in the case of F2–F3, as illustrated in Fig. 4.9. The fingers as well as the entire hand were moved with translation and rotation into all directions but with the spacer remaining pinched.

In the experiment P3, a pinching grip was performed with the thumb F1 and the index finger F2 such that the distal tips (tip_d) were in contact. The pinch grip was closed and opened twice. Experiments P1 to P3 were conducted twice, and every trial lasted approximately 15–35 s. For experiment P4, a wooden block was grasped in a way that the positions of the fingertips on the surface of the block were known. The block was then moved by the participant via translation and rotation into all directions. Figure 4.9 illustrates the experimental setup.

In the analysis, the error was calculated for each time step t as

$$E_i(t) = \left| \left\| {}^{\text{T1,Fi}}_{\text{WCS}}\mathbf{p}_{\text{IMU}}(t) - {}^{\text{T2,Fi}}_{\text{WCS}}\mathbf{p}_{\text{IMU}}(t) \right\| - d_s \right| \tag{4.33}$$

with T1, T2 $\in \{\text{tip}_l, \text{tip}_r, \text{tip}_b, \text{tip}_d\}$, $i \in \{1,2,3\}$ and $s \in \{\text{P1, P2, P3, P4}\}$. For each trial, the root-mean-square error was determined according to Eq. (4.32).

4.5 Results

4.5.1 Simulative Results

The resulting fingertip positions were compared to the positions obtained when the functional finger segment lengths were set to the mean ratio-values by Hamilton & Dunsmuir [304]. In

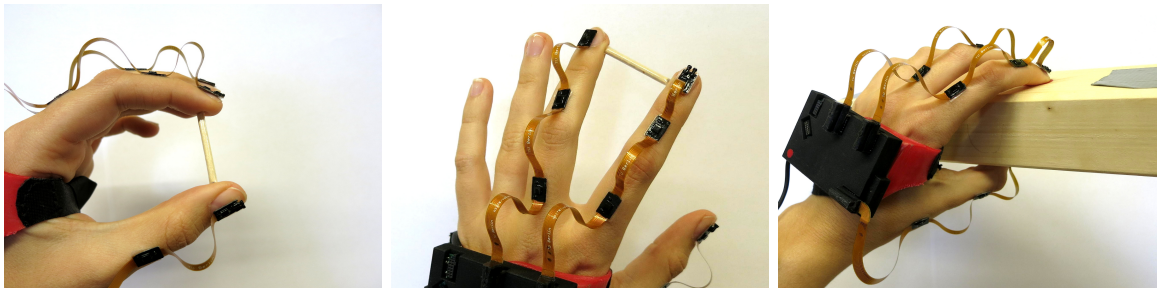

P1: Spacer between F1-F2 P2: Spacer between F2-F3 P4: Wooden block

Figure 4.9: Experimental setup for the evaluation under realistic conditions in Setting 2. The images display the hand poses with the spacer and wooden block.

the results, the error in the fingertip position relative to the length of the finger never exceeded 1%. This result is in line with the small values of the confidence intervals in the literature (cf. Table 4.1). Similarly small errors may occur if sensor orientation estimates exhibit errors of a few degrees caused by measurement noise (noise level of 10%) and bias. The simulated inaccuracies in the sensor-to-segment alignment led to errors in the order of 5 to 10 degrees in joint angles, which entails an error magnitude of approximately 0.5 cm in fingertip positions. Movement velocities in the range of physiological motion do not influence the tracking results. Only over exaggerated movements with an angular velocity amplitude bigger than 1000 °/s leads to significant deviations.

4.5.2 Results under Idealistic Conditions (Setting 1)

The results of Setting 1 for individual fingers and motions are presented in Table 4.5, and box plots for each finger and motion are displayed in Fig. 4.10. The baseline method B yields root-mean-square tracking errors between 2 cm and 6.3 cm for the different motions and fingers. In contrast, the RMSEs for the advanced methods M1 and M2 range between 0.5 cm and 1.6 cm for fingers F2 and F3 and between 1.6 cm and 2.2 cm for the anatomically more intricated thumb (F1). Even in the peak values, the tracking error never exceeds 2.5 cm for F2 and F3 and 3 cm for F1. The methods M1 and M2 were found to yield very similar results, which is not surprising since no magnetic disturbances were present.

Exemplary time series for the estimated fingertip position (top) and the error between optical and inertial system are presented in Fig. 4.11 for the experiments with the index finger (F2). For better differentiation between lines, the displayed data is low-pass filtered with 2 Hz, and the graphs are limited to 25 s. The upper subplot shows that the measurements with the two different systems (optical and HSS) were very close despite a broad range of motion. The lower subplot shows that the error E is always below 2 cm.

4.5.3 Results under Realistic Conditions (Setting 2)

Average and subject-individual results for the evaluation in Setting 2 are presented in Table 4.6 and Fig. 4.12 for all four experiments. All experiments were conducted in the direct proximity of furniture containing ferromagnetic materials and electronic devices emitting electromagnetic fields. It is therefore not surprising that the methods B and M1, which use magnetometer readings, were found to fail at yielding a reliable estimation of the fingertip positions. In fact,

Table 4.5: Mean and standard deviation (std) of error E and RMSE, both in cm, for the evaluation of methods B, M1, and M2 when compared against an optical motion capture system in Setting 1 for Subject #1. Abbreviations: A: abduction, F: flexion, AF: combined abduction and flexion motion (cf. Table 4.3).

Experiment ID	**Method B**		**Method M1**		**Method M2**	
	mean $\pm$ std(E)	**RMSE**	**mean $\pm$ std(E)**	**RMSE**	**mean $\pm$ std(E)**	**RMSE**
A-F1	6.0 ± 0.60	6.1	2.2 ± 0.36	2.2	1.8 ± 0.1	1.8
A-F2	3.6 ± 0.47	3.6	0.9 ± 0.14	0.9	0.9 ± 0.19	1.0
A-F3	4.2 ± 0.44	4.3	1.3 ± 0.26	1.4	0.6 ± 0.17	0.7
AF-F1	6.3 ± 0.52	6.3	1.6 ± 0.45	1.6	2.0 ± 0.52	2.1
AF-F2	2.2 ± 0.63	2.3	0.9 ± 0.30	0.9	0.9 ± 0.49	1.0
AF-F3	4.3 ± 0.48	4.4	1.2 ± 0.45	1.3	0.9 ± 0.45	1.0
F-F2	2.0 ± 0.75	2.1	0.5 ± 0.20	0.6	0.6 ± 0.19	0.6
F-F3	4.3 ± 0.76	4.4	1.2 ± 0.34	1.3	0.8 ± 0.34	0.8

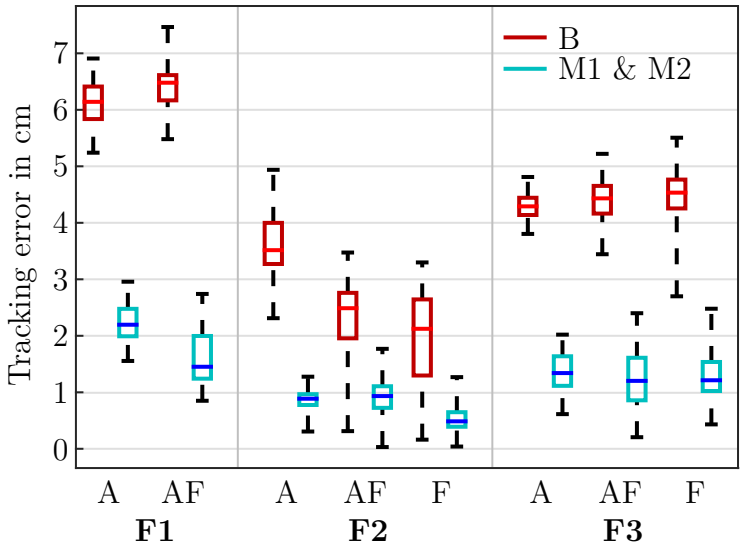

Figure 4.10: Median, 25th and 75th percentile and maximum values of the error E between the optical motion capture measurement and the HSS with method B (red) and M1 and M2 (blue) for all conducted experiments with the volunteer in Setting 1. For a better overview, methods M1 and M2 were summarized, whereby the respective higher value was illustrated. Box-plots were calculated over time intervals of 30 s with at least ten repetitions for each movement. Abbreviations: A: abduction, F: flexion, AF: combined abduction and flexion motion (cf. Table 4.3).

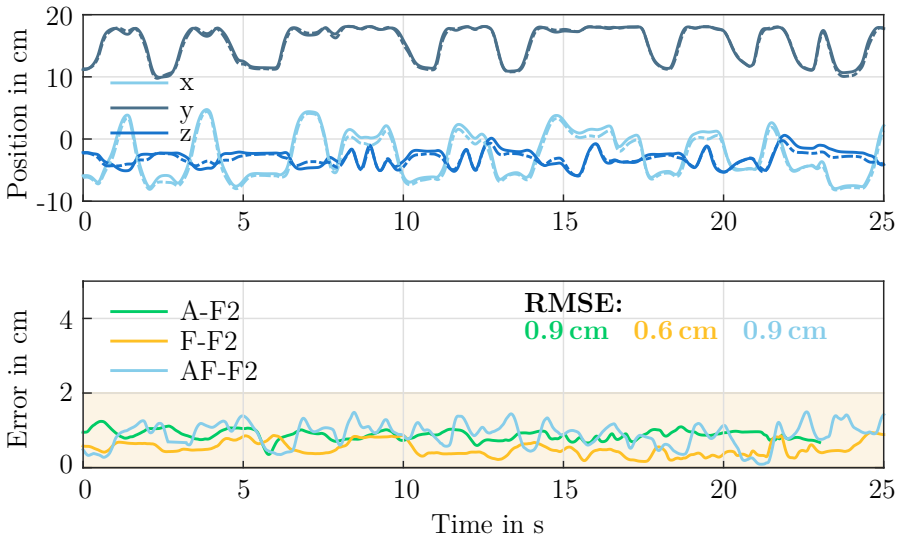

Figure 4.11: Exemplary time series of the index fingertip postion and tracking error E for Setting 1. Top: time series of x-, y-, and z-component of the fingertip position $\mathbf{p}$ in the WCS for the combined abduction and flexion motion of the index finger (AF-F2). The solid lines represent the calculated position by the HSS with method M1, the dashed lines depict the optical data. Bottom: time series of the tracking error E for all three motions of the index finger F2 between the hand sensor system with method M1 and optical system. For better illustration, the signals were low-pass filtered with a cutoff frequency of 2 Hz. The error is always below the critical value of 2 cm. Abbreviations: A: abduction, F: flexion, AF: combined abduction and flexion motion (cf. Table 4.3).

method M1 even led to considerably larger errors in most cases than method B. Moreover, the additional errors of method B and M1 when compared to M2 varied largely from subject to subject and experiment to experiment (cf. Fig. 4.12).

In contrast, the method M2, which refrains from using magnetometer readings, provided useful fingertip position estimates with RMSEs ranging between 0.5 cm and 2 cm on average. A comparison of these values with the results of Setting 1 revealed no notable differences. This means that the proposed method M2 provides accurate measurements not only under idealistic conditions but also in a far more realistic setting and for more complex functional motions. Figure 4.13 shows a representative time series with method M2 of one trial of experiment P3 (pinch of thumb and index finger while moving the hand arbitrarily in space). In this case, the distance between the fingertip position tip_d was slightly overestimated, and the positive offset contributed most to the RMSE value.

4.6 Discussion

The suggested IMU-based hand sensor system and the accompanying set of novel quaternion-based methods facilitate the measurement of joint angles and estimation of fingertip positions. Unlike gloves, the proposed HSS preserves the sense of touch. The presented methods do not rely on extensive calibration procedures or motions that must be performed precisely, both of which are challenging for patients with motor-impaired hands. Instead, the methods require only a single initial pose. The sensor system was evaluated with able-bodied subjects in two different validation settings: (1) in an optical motion capture laboratory as well as (2) in a realistic setting. In the first setting, motions were performed in an ideal magnetic environment,

Table 4.6: Mean and standard deviation (std) of error E and RMSE, both in cm, for experiments P1–P4 in the realistic environment of Setting 2. Average as well as individual results of each participant are presented.

Experiment ID	Fingers	Subject	Method B		Method M1		Method M2	
			mean $\pm$ std(E)	RMSE	mean $\pm$ std(E)	RMSE	mean $\pm$ std(E)	RMSE
P1	F1-F2	#1	3.3 ± 1.51	3.7	6.7 ± 1.85	7.0	0.8 ± 0.57	1.0
		#2	3.5 ± 1.14	3.7	12.6 ± 1.24	12.7	0.4 ± 0.25	0.5
		#3	0.8 ± 0.47	0.9	10.6 ± 1.74	10.7	1.2 ± 0.24	1.2
		#4	0.7 ± 0.45	0.8	5.1 ± 2.67	5.7	0.6 ± 0.35	0.7
		Average	$\mathbf{2.1 \pm 0.89}$	**2.3**	$\mathbf{8.8 \pm 1.88}$	**9.0**	$\mathbf{0.8 \pm 0.35}$	**0.9**
P2	F2-F3	#1	4.9 ± 1.97	5.3	1.8 ± 1.27	2.2	1.7 ± 0.65	1.8
		#2	0.9 ± 0.68	1.1	1.1 ± 1.36	1.8	0.6 ± 0.27	0.7
		#3	3.0 ± 1.14	3.2	1.8 ± 1.22	2.1	1.0 ± 0.39	1.1
		#4	1.8 ± 0.45	1.9	1.1 ± 0.59	1.3	1.4 ± 0.44	1.4
		Average	$\mathbf{2.7 \pm 1.06}$	**2.9**	$\mathbf{1.5 \pm 1.11}$	**1.9**	$\mathbf{1.2 \pm 0.44}$	**1.3**
P3	F1-F2	#1	4.5 ± 3.17	5.5	11.0 ± 2.61	11.3	1.4 ± 0.55	1.5
		#2	4.1 ± 1.19	4.3	12.5 ± 2.83	12.8	1.6 ± 0.42	1.6
		#3	4.6 ± 1.47	4.9	9.2 ± 2.34	9.5	2.6 ± 0.41	2.6
		#4	2.7 ± 1.05	2.9	7.1 ± 2.69	7.6	2.5 ± 0.44	2.5
		Average	$\mathbf{4.0 \pm 1.72}$	**4.4**	$\mathbf{10.0 \pm 2.62}$	**10.3**	$\mathbf{2.0 \pm 0.46}$	**2.0**
P4	F1–F2	#1	1.9 ± 1.59	2.5	4.0 ± 2.51	4.7	0.7 ± 0.39	0.8
		#2	0.5 ± 0.40	0.7	8.0 ± 3.48	8.8	0.2 ± 0.14	0.2
		#3	0.5 ± 0.39	0.7	5.5 ± 2.73	6.2	0.5 ± 0.32	0.6
		#4	1.6 ± 0.56	1.7	2.9 ± 1.28	3.2	0.9 ± 0.24	0.9
		Average	$\mathbf{1.1 \pm 0.74}$	**1.4**	$\mathbf{5.1 \pm 2.5}$	**5.7**	$\mathbf{0.6 \pm 0.27}$	**0.6**
P4	F1–F3	#1	4.8 ± 1.97	5.2	15.0 ± 2.52	15.2	0.4 ± 0.23	0.4
		#2	0.9 ± 0.51	1.0	9.3 ± 3.28	9.9	1.9 ± 0.26	2.0
		#3	1.2 ± 0.85	1.5	8.6 ± 3.59	9.4	2.0 ± 0.32	2.0
		#4	1.5 ± 0.89	1.8	3.8 ± 1.66	4.1	0.4 ± 0.19	0.4
		Average	$\mathbf{2.1 \pm 1.06}$	**2.4**	$\mathbf{9.2 \pm 2.76}$	**9.7**	$\mathbf{1.2 \pm 0.25}$	**1.2**
P4	F2–F3	#1	5.5 ± 1.55	5.7	11.0 ± 2.47	11.3	0.4 ± 0.40	0.6
		#2	0.5 ± 0.48	0.7	3.9 ± 1.54	4.2	1.9 ± 0.47	2.0
		#3	0.9 ± 0.54	1.0	2.8 ± 2.48	3.7	1.6 ± 0.48	1.6
		#4	0.9 ± 0.60	1.1	0.8 ± 0.43	0.9	0.5 ± 0.32	0.6
		Average	$\mathbf{2.0 \pm 0.79}$	**2.1**	$\mathbf{4.6 \pm 1.73}$	**5.0**	$\mathbf{1.1 \pm 0.42}$	**1.2**

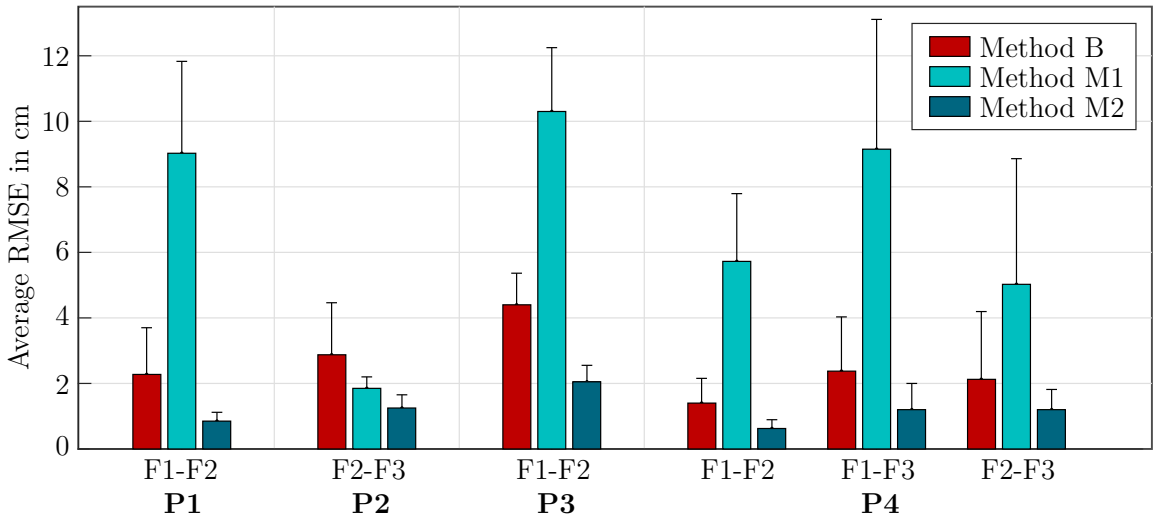

Figure 4.12: Average RMSE and standard deviations over all four participants evaluated in Setting 2 for each method. Please refer to Table 4.4 for a description of the experiments P1–P4. Method M2 always yielded the smallest RMSE with comparatively minor differences between the participants.

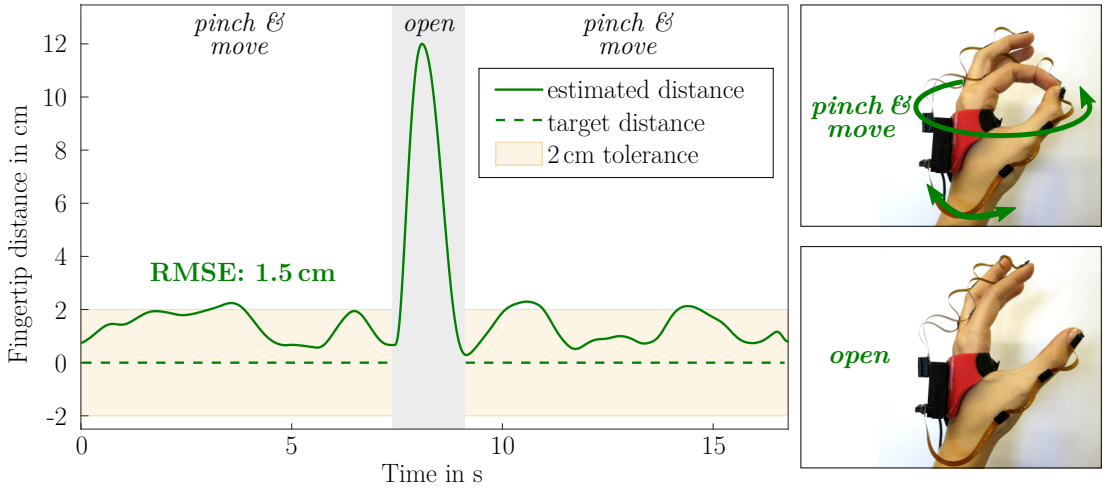

Figure 4.13: Representative time series of a pinch motion (experiment P3). The measured distance between tip_d of F1 and F2 (solid green line) is close to the true value (0 cm; dashed green line). Note that the pinch was released during the gray marked time period.

and the positions measured with the proposed system were compared with positions recorded by a marker-based optical reference system. The accuracy of the reference system itself is limited by skin (and thus markers) moving relative to the bone and by inaccuracies of marker placement. In the second setting, motions were performed in the presence of severe magnetic disturbances, and the limitations mentioned above are overcome by using functional movements with known fingertip distances.

The accuracy of the proposed methods under laboratory conditions is comparable to the accuracy reported in the literature. There are several previous contributions for IMU-based hand motion tracking that use customized rigid measurement platforms [297, 298] or blocks of wood cut to specific angles [149] instead of considering measurements in human hands. Connolly et al. performed experiments in patients but presented only coefficients of variation based on video recordings [149]. To the best of the author's knowledge, only two previous research studies evaluated kinematic measurements (angles or positions) in human subjects. These are Kortier et al. [133] and van den Noort et al. [135]. In both studies, the proposed system was compared to optical measurements recorded in laboratory environments. While Kortier et al. observed mean errors of 0.5 cm for a pure flexion/extension motion of finger F2 and 1.2 cm for a circular motion of F2, van den Noort et al. found deviations of 1–2 cm for the latter. The experiments with the new HSS showed similar results with 0.5 cm for the pure flexion/extension motion and 0.9 cm for the combined abduction and flexion motion of F2 under idealistic laboratory conditions.

In contrast to previous contributions, the proposed methods were additionally evaluated in a second setup containing magnetic disturbances as they would occur in many application scenarios. It turned out that the two methods utilizing magnetometer measurements (B and M1) are not reliable under these conditions, with RMSEs of up to 15 cm (cf. Table 4.6, subject #1). Thus, for practical applications in realistic settings, Method M2 is preferred, which achieves average RMSEs below 1.4 cm for the index and middle fingertip and below 2.1 cm for the thumb tip in all trials of all four evaluated subjects.

In favor of discussing potential sources of the remaining deviations, error propagation was investigated in simulations. As functional segment length ratios vary by a few percents from subject to subject, simulations showed that using fixed ratios can lead to fingertip position errors of a few millimeters. Similarly small errors may occur if sensor orientation estimates exhibit errors of a few degrees. Likewise, expected inaccuracies in the sensor-to-segment alignment in the order of 5–10° entail the same order of error magnitude as errors in orientation estimation. However, alignment of the thumb (F1) axes is more challenging, which might explain the slightly larger deviations found for F1. An analysis of the angles that are neglected by the application of joint constraints (Methods M1 and M2, cf. Fig. 4.3) yields average absolute values between 5–10°. For segment lengths in the range of several centimeters, such angles were found to affect the measurement results by approximately half a centimeter. In conclusion, the aforementioned remaining deviations of about 1–2 cm are most likely due to a combination of the two latter aspects.

4.7 Conclusions and Future Research

The HSS was designed to be part of the feedback-controlled hand neuroprosthesis for the rehabilitation of patients who suffer from a motor impairment of the hand after stroke. Therefore, the estimation accuracy has to match the sensitivity of the neuromuscular stimulation. The most advanced current systems are capable of generating coarse motions such as opening and closing the hand to grasp large objects. The low sensitivity and selectivity of stimulation through surface electrodes do not allow control of individual fingers to the exact centimeter. In conclusion, the achieved accuracy (RMSE of approx. 1 cm for fingertip positions) should be sufficient for feedback control of movements within the neuroprosthesis, and for registering postures during (automatic) identification of stimulation positions in the electrode arrays. The latter is performed in *Chapter* 5 using the extracted joint angles of wrist and fingers. The hypothesis that motion tracking can be correlated with other signals suitable for feedback control, such as grasp force, is evaluated in *Chapter* 6.

Method M2 completely avoids the use of magnetometer readings. Absolute heading information and a gyroscope bias estimation are obtained from the initial neutral pose. However, even the best IMUs exhibit some random bias instability, which suggests that the accuracy of Method M2 will deteriorate with time. Joint angles and fingertip positions will eventually become inaccurate. A frequent, periodic reset of the bias estimation by performing the initial pose alignment might not be practical in rehabilitation setting. Hence, future studies should include a larger number of subjects and trials and evaluate the long-time stability of Method M2. A promising direction of future research is to combine the method with recently proposed approaches that exploit kinematic constraints to compensate for heading drift in magnetometer-free sensor fusion completely [150, 311, 312, 313].

In the future, the HSS could be combined with fingertip force sensors that detect contact with an object and thus yield additional information when the patient grasps and holds an object [314, 315]. Other possible options for assessing grasp force are outlined in *Chapter* 6. Future work on the HSS should also aim at a reduction of the sensor system's weight and dimensions, to further decrease the impact of the system on movements with the motor-impaired

hand. In addition, if sufficient miniaturization of wireless IMUs is achieved henceforth, the system will no longer require flexible PCBs between the sensor units. Finally, the use of higher sampling rates to facilitate accurate and precise motion tracking of faster and less smooth motions might be advisable, especially in non-clinical application domains. The resulting challenges of large wireless communication load and accidental swapping of sensor units might be addressed by recently developed methods for event-based communication [316]. For other applications, such as the assessment of hand kinematics to track therapy progress [315], a reduced setup with a smaller number of IMUs could be sufficient [317].

5

Identification of Suitable Stimulation Sites in Electrode Arrays

5.1 Overview

The identification of suitable virtual electrodes for inducing desired hand movements is a crucial factor in the application of FES via electrode arrays on the forearm. Automatic approaches often not sufficiently reflect individual strategies by the treating health professional and the patient's sensation regarding stimulation comfort in the decision process of the algorithms. Therefore, this chapter introduces novel array identification methods of different levels of user integration and support and evaluates their usability, practicability, and acceptance in clinical, early stroke rehabilitation.

A semi-automatic identification method was developed that facilitates health professionals to continuously modify VEs via a touchscreen while the stimulation intensities are automatically controlled to maintain sufficient wrist extension. The second approach is an automatic identification procedure, which evaluates stimulation responses of various tested VEs for different intensities using a cost function and joint-angle recordings. Both methods were compared in a clinical setup with five sub-acute stroke patients with moderate hand disabilities. The experiment consisted of finding suitable VEs in the new hand neuroprostheses to generate hand opening and closing for a grasp-and-release task. Practicability and acceptance by patients and health professionals were investigated using questionnaires and interviews. The results revealed that both identification methods yield suitable VEs for hand opening and closing in patients who could tolerate the stimulation. However, the resulting stimulation positions differed for both approaches.

In the following, *Section* 5.2 briefly recaptures the challenges in electrode array technology and the drawbacks of existing identification approaches. The new methods are outlined in detail in *Section* 5.3. Subsequently, *Section* 5.4 describes the clinical experiments and the procedure of the user-centered evaluation. Results of both identification methods are presented

and compared in *Section* 5.5. The results are discussed in *Section* 5.6; the relevance for future developments is addressed in *Section* 5.7.

Copyright Statement: The text, figures, and tables in this section are based, with modifications, on the following publications:

[169] Salchow-Hömmen, C., Jankowski, N., Valtin, M., Schönijahn, L., Böttcher, S., Dähne, F., Schauer, T. "User-centered practicability analysis of two identification strategies in electrode arrays for FES induced hand motion in early stroke rehabilitation", *Journal of NeuroEngineering and Rehabilitation*, 15:123, 2018. DOI: 10.1186/s12984-018-0460-1,[26]

[318] Salchow, C., Valtin, M., Seel, T., Schauer, T. "A new semi-automatic approach to find suitable virtual electrodes in arrays using an interpolation strategy", *European Journal of Translational Myology*, 26(2):6029, 2016. DOI: 10.4081/ejtm.2016.6029,[27]

 In particular, *Section* 5.2 is based on [169]. The description of the semi-automatic identification method in *Section* 5.3.1 combines parts of both publications, [169] and [318]. Figures 5.1 and 5.4 were added. The remaining sections 5.3.2 to 5.7 are again based on [169]. Figures 5.2–5.3, 5.5–5.6, and 5.8–5.14 are included with modifications; figure 5.7 is shown without modifications. The related *Appendix* D on the semi-automatic search is adapted from [318] with modifications in text and figures (Fig. D.3).

5.2 Motivation

The usage of standard hydro-gel surface electrodes for transcutaneous FES has several disadvantages, such as lacking selectivity of the stimulation, long placement times, and static electrode positions during therapy sessions [319]. These listed drawbacks are especially relevant for the application of FES on the forearm for generating complex movements in impaired hands [320]. Proper manipulation of objects requires coordinated, synergistic activation of wrist and finger extensors and wrist flexors [244]. Stroke survivors often exhibit an overactivity of wrist and finger flexors combined with weakness of the extensor muscles [244, 321, 322]. Inaccurate stimulation results and elaborate setup times combined with non-adaptable, open-loop stimulation patterns result in a lack of acceptance and little application of this technology in clinical practice. Electrode arrays (or multi-pad electrodes) were introduced to overcome these problems and have become popular in hand neuroprostheses within the last two decades (cf. *Section* 2.4) [173]. The application of EAs yields new challenges regarding setup times, VE identification strategies, and user integration. The standard, intuitive manual approach

[26] ***Author's contribution***: The author's contribution to [169] includes reviewing the literature, developing the novel methods, implementing the algorithms, designing the study, conducting and evaluating the experiments, visualizing methods and results, writing the manuscript, and revising the manuscript based on annotations and suggestions of the co-authors.

[27] ***Author's contribution***: The author's contribution to [318] includes reviewing the literature, developing the novel methods, implementing the algorithms, conducting and evaluating the experiments, visualizing methods and results, writing the manuscript, and revising the manuscript based on annotations and suggestions of the co-authors.

[28] https://creativecommons.org/licenses/by/4.0/

[29] https://creativecommons.org/licenses/by-nc/4.0/

for finding suitable VEs in EAs consists of testing single elements or element combinations iteratively [92]. However, a manual, brute-force search for suitable VEs within electrode arrays with numerous elements is laborious and time-consuming and additionally may lead to muscle fatigue.

Many approaches have been introduced to automatically find the optimal stimulation point(s) for defined movements within an EA and were reviewed in detail in *Section* 2.4. In summary, automatic search algorithms usually combine a stimulation and element testing strategy with a predefined selection criterion or cost function. In most approaches, the evoked motion via twitch or step stimulation is registered and evaluated in a cost function for each tested element or element combination. Such a function can be the fit with a reference trajectory, which was derived from the movement of healthy people [170], the achievement of predefined constraints for the joint angles [179], or the maximum registered joint angle amplitude [151] together with additional restrictions [177]. Besides, electro-physiologically based identification approaches [172] and the use of feedback-controlled strategies [153, 171] were suggested. Still, the existing methods often evaluate only a small number of (low) stimulation intensities [151, 182] and interpolate the outcome for higher intensities. Thereby, the search space is reduced, but higher intensities may induce movement in underlying and neighboring muscles as well, which is not considered.

Another missing aspect in existing approaches is the integration of the users' expertise and the individual opinion of health professional and patient in the VE selection process. Together with extensive setup procedures, lack of customization, and non-user-evaluated interfaces, this may lead to poor acceptance of existing EA-based neuroprostheses in clinical practice. The involvement of users in development processes turned out to increase the usability and acceptance of health care systems such as rehabilitation technologies and is recommended already in early stages [323]. However, systematic usability analyses are rare in current research in the field of EA-based FES (e.g., [40]). One way to overcome these problems is to establish new user array-interfaces and dynamic stimulation adaptation via the feedback of integrated sensors, as suggested in [324]. There, individual elements in the EA can be activated and deactivated via an overlying touch layer. This allows a unique adaptation by the caregiver but can be quite time-consuming.

In this work, novel array identification methods of different levels of user integration and support were established and evaluated regarding usability, practicality, and acceptance of such methods in clinical practice. Both approaches aim to assist the therapist in finding individual stimulation areas and stimulation parameters according to a patient's needs and personal training strategy in a convenient way. The first approach is a semi-automatic identification procedure which allows the caregiver to continuously modify VEs to find a good stimulation area. The purpose of the semi-automatic search was to provide an identification framework that a) is faster and more convenient than manual search and b) overcomes the lack of user integration and acceptance of fully automatic identification procedures for EAs. In the presented framework, the center of a VE can be modified by the therapist to arbitrary positions within the array, and individual stimulation intensities of involved elements are determined automatically with feedback-control.

The second approach is an automatic identification procedure that finds stimulation positions as well as parameters via iterative testing of VEs and a cost function. The fully automatic search might be more appropriate for home use because it provides more assistance in the decision process. This support is especially important for independent usage by patients. The presented automatic search strategy was examined as an example of the practicability of such approaches in everyday clinical practice. It is an extension and combination of algorithm features from existing methods [151, 182] for hand movements.

The goal was to validate the two methods for finding suitable VEs with the hand neuroprosthesis and to assess the practicability, effectiveness, and acceptance of the different approaches concerning their varying degree of user integration in a clinical environment. Therefore, both methods—the semi-automatic and the automatic approach—were evaluated and compared in a clinical setup with sub-acute stroke patients for the identification of suitable VEs for hand closing and hand opening. Physicians and therapists were instructed to find up to three suitable VEs with each approach for a grasp-and-release task. After the VE identification, a predefined stimulation pattern was repeatedly applied, and the generated hand movement was assessed. Both methods were tested one after another on the same patient with a short break in between, to allow a direct comparison of the results.

For the first time, the application of array search techniques was accompanied by user-centered methods. Face-to-face user acceptance and satisfaction surveys were conducted using standardized and system specific questionnaires and interviews. 'Users' in the context of rehabilitation systems might refer to patients and health professionals such as physicians and therapists as well [325]. The interests of both user groups need to be considered for the successful integration of new technologies. The following research questions, regarding the functionality and acceptance of the tested array identification strategies, were in the center of the investigations: i) were both array identification approaches appropriate to find suitable VEs, ii) which approach needed more time, iii) which method was favored by clinicians and patients regarding practicability, outcome, comfort, and fun, and iv) what are the essential key-factors for future HNPs to gain high impact and acceptance in clinical practice?

5.3 Methods

5.3.1 Semi-Automatic Search Strategy

The Interpolation Problem

Conventional approaches for finding suitable VEs in electrode arrays assess the motion or force that is caused by applying stimulation to discrete positions. Single array elements are either deactivated or stimulated at the same (global) stimulation intensity, forming a virtual electrode as illustrated in Fig. 5.1. The following novel search strategy aims to overcome the restriction of discrete VE positions by applying a virtual electrode model in combination with a smooth interpolation function. The interpolation function determines whether an element should be activated and which individual intensity is applied depending on the position and dimensions of the VE model in the given array layout (cf. Fig. 5.1) and the global stimulation intensity.

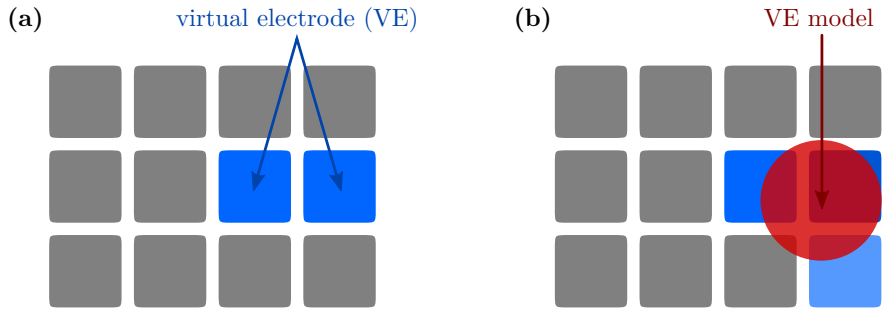

Figure 5.1: Comparison of (a) the classical virtual electrode definition and (b) the virtual electrode model established for the semi-automatic identification method. In general, VEs are formed by EA-elements activated at the same time or in a close timely relationship (asynchronous activation). Here, active EA elements are depicted in blue; the shades of blue symbolize different stimulation intensities. The VE model, shown in red, serves as an aid to define VEs: An interpolation function, suited to the shape of the VE model, determines which elements are included in the active VE depending on the position of the model in the array and its dimensions.

For a circular VE model, consider the following: Imagine an array with a matrix of m elements, which covers a defined two-dimensional area. Within this area, the center point $\mathbf{z} \in \mathbb{R}^2$ of a VE can be placed arbitrarily. The VE model is circular and parametrized by a diameter h. The global stimulation intensity $\hat{u}$ is assigned to the VE. For each array element, an individual stimulation intensity u_i, $i = 1...m$ with m being the number of available elements, is then applied, which is related to the global intensity $\hat{u}$ by the interpolation function $f_{s,i}(\hat{u}, \mathbf{z}, h)$. This function determines whether an element should be activated and which individual intensity u_i is applied depending on the parameters $\mathbf{z}$, h, and $\hat{u}$. For the case of a circular VE shape s, a quadratic relationship is assumed between VE position $\mathbf{z}$ and stimulation intensity $\hat{u}$, yielding the weight function $w_i(\mathbf{z}, h)$ given in Eq. (5.1). The resulting virtual electrode consists of active elements within the area of the VE model and its vicinity depending on the chosen weight function, which also determines the individual stimulation intensities according to the distance between the element's center and the VE center $\mathbf{z}$.

$$w_i(\mathbf{z}, h) = \frac{1}{2.5 \cdot \sigma \cdot h} \cdot (2.5 \cdot \sigma \cdot h - ||\mathbf{z}_i - \mathbf{z}||_2^2) \tag{5.1}$$

$$f_{s,i}(\hat{u}, \mathbf{z}, h) = \begin{cases} w_i(\mathbf{z}, h) \cdot \hat{u}, & \text{if } w_i(\mathbf{z}, h) > 0, \\ 0, & \text{otherwise.} \end{cases} \tag{5.2}$$

Here $\mathbf{z}_i \in \mathbb{R}^2$ marks the position vector for the center of the i^{th} element. σ is the size (diameter) of the electrode element in mm, assuming the element shape is symmetric. Figure 5.2 exemplifies the quadratic weight function of Eq. (5.1) for four neighboring elements in one dimension. In this example, the VE partly covers the elements two and three. As a result, both elements account for the VE and achieve high stimulation intensities u_i according to their weight function values close to one. Three different shapes s have been realized until now: circle, ellipse, and rectangle. Those shapes were found to show similar stimulation characteristics regarding selectivity and comfort [326]. Note that in the favor of a clear presentation, only the interpolation function for the circular VE model was specified above. For shapes not being rotationally symmetric, as for example an ellipse, the interpolation and weight functions are

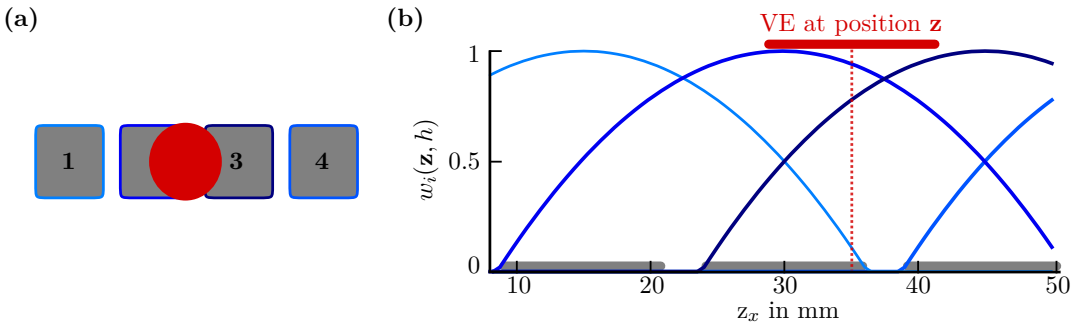

Figure 5.2: Exemplary one-dimensional weight function $w_i(\mathbf{z}, h)$ of four neighboring elements for $\mathbf{z} = [8...50, z_y]^\intercal$, where z_y is a fixed position value. (a) Layout of four elements of size $\sigma = 12$mm with the circular VE model marked in red. (b) The colors of the weight functions of each element match the colors in (a). The red bar marks the size of the VE of $h = 12$ mm with the center at $\mathbf{z} = [35, z_y]^\intercal$.

different. The position of the center of the VE model as well as the dimensions can be changed in real-time by the user.

Feedback-Control

In the semi-automatic search strategy, the system supports the user in choosing the applied stimulation intensities via the interpolation function and closed-loop control. The system constantly controls the global stimulation intensity $\hat{u}$, such that a predefined reference joint angle y_{ref} is achieved in a major degree of freedom y. The remaining DOFs ($\tilde{\mathbf{y}}$) can be observed by the user, who can also influence the generated motion by changing shape, size, and position of the VE. The principle of this closed-loop system is depicted in Fig. 5.3. A controller K_1 adjusts the global intensity $\hat{u}$ based on the fed-back error e between the measured joint angle y and the reference angle y_{ref}. The individual stimulation intensities u_i of the elements are assigned based on the interpolation function $f_{s,i}(\hat{u}, \mathbf{z}, h)$ and can be equal to or less than $\hat{u}$ (cf. Eq. (5.2)).

For the application within the HNP, the controlled DOF is the wrist extension/flexion angle α ($y = \alpha$). The stimulation $\hat{u}$ is adjusted such that the desired wrist extension is achieved (default: $\alpha_{\text{ref}} = -20°$). In this way, the automatic adaption of the stimulation intensity enables the treating health professional to search manually for a sufficient stimulation area, while entirely focusing on the current hand posture. The level of automatically applied intensity also serves as information for the search: Some VEs may require less stimulation intensity compared to other VEs for achieving the same degree of wrist extension. The user will probably select those VEs as a lower intensity is more convenient for the patient, and remains a higher margin for closed-loop control of the stimulation intensity during the subsequent therapy.

Finding a controller K_1 that adjusts the stimulation intensity $\hat{u}$ robustly throughout the searched electrode array is a non-trivial task because the stimulation response varies strongly between single elements. Therefore, the FES response is quantified throughout the EA by identifying a first-order model with delay given in Eq. (5.3). The model is determined by recording step responses of three predefined elements, which are distributed across the EA. The stimulation intensity during the step starts at the motor-threshold level u_{mot} and jumps up to a preset stimulation level u_{step}. The threshold u_{mot} is estimated from one single element

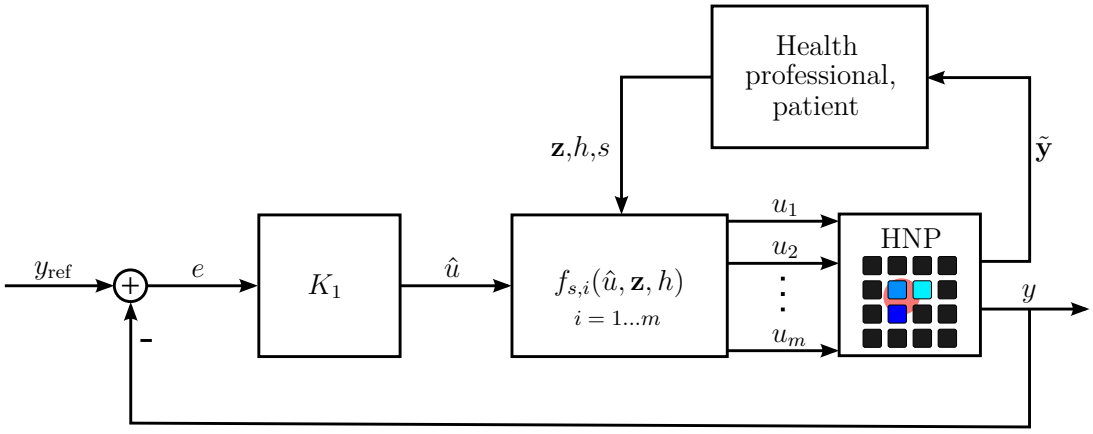

Figure 5.3: Overview of the closed-loop system for the semi-automatic search. The controller K_1 adjusts the global intensity $\hat{u}$ based on the fed-back error e between the recorded movement of one DOF y and the reference angle y_{ref} (loop one). The interpolation function $f_{s,i}$, with s being the shape of the VE model, assigns an individual intensity to each array element i, which is then applied. In this pictogram, a circular VE model is displayed exemplarily. Additionally, patient and health professional perceive the other DOFs (e.g., individual finger movements) and control the VE model parameters shape s, size h, and position $\mathbf{z}$ (loop two).

as the highest stimulation intensity which still does not cause a movement (cf. *Section* 1.4). At the same element, u_{step} is determined as 90% of the maximum stimulation intensity tolerated by the user (u_{tol}). The identified model parameters are averaged and then used to adjust the controller parameters. Through measurements in four healthy volunteers, it was shown that averaging the model parameters of three elements distributed across the array leads to similar model parameters compared to averaging all model parameters when testing each array element [318] (see *Appendix* D).

$$G(s) = \frac{k}{Ts + 1} e^{T_d s} \tag{5.3}$$

A PID controller in its parallel form (Eq. (5.4)) is utilized as a controller K_1 due to its simplicity. The controller parameters are adjusted according to the Chien, Hrones, and Reswick set-point method [327] given in Eq. (5.5). An anti-windup is realized with a gain of '1'. Furthermore, a dead-band of $\pm 1°$–$\pm 5°$ is applied to the PID controller input to avoid oscillations.

$$K(s) = K_P + K_I \cdot \frac{1}{s} + K_D \cdot \frac{Ns}{s + N} \tag{5.4}$$

$$\begin{aligned} K_P &= 0.6 \cdot \frac{k}{T \cdot T_d} \\ K_I &= K_P \cdot \frac{1}{T} \\ K_D &= K_P \cdot \frac{T_d}{2} \end{aligned} \tag{5.5}$$

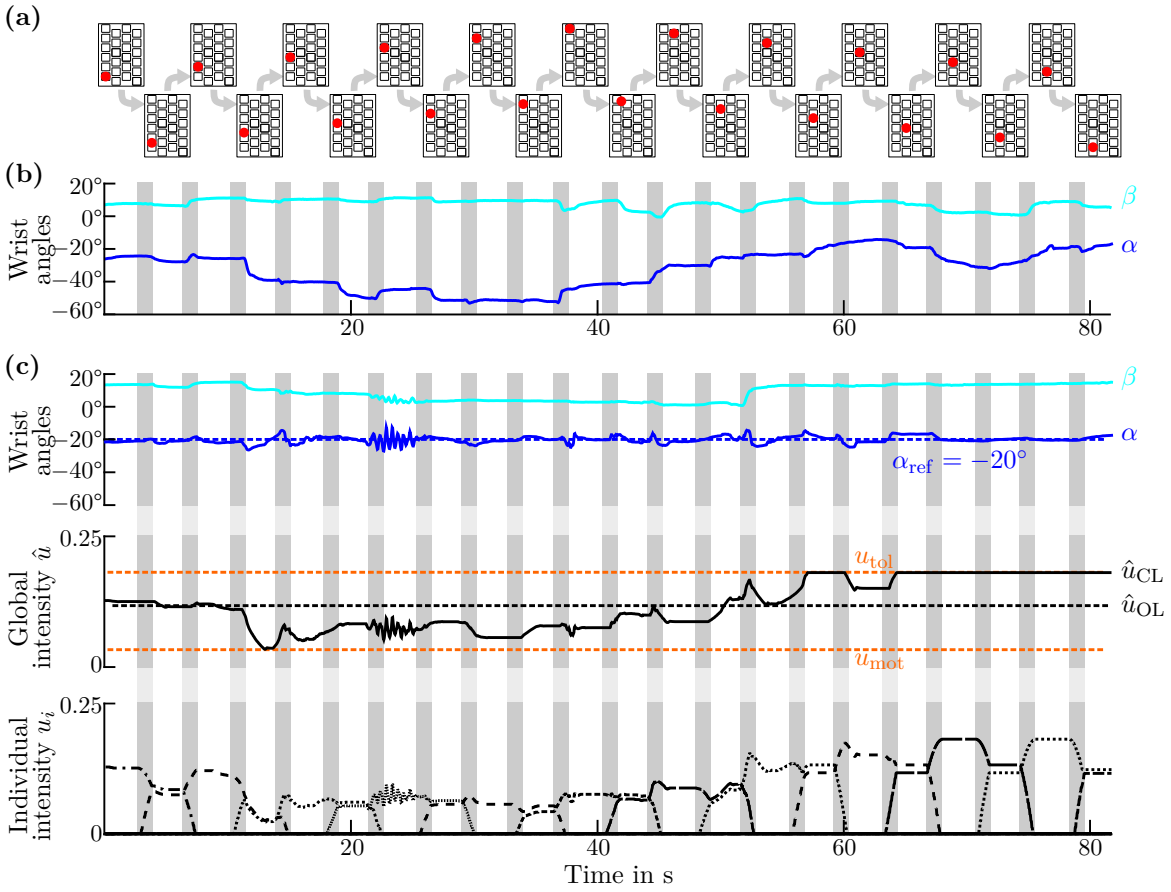

Figure 5.4: Representative measurement results of one unimpaired volunteer when testing (a) a predefined VE path with a stimulation intensity applied either in (b) open-loop or (c) closed-loop. (a) A circular VE model of fixed size $h = 12\,\text{mm}$, which equals the size of a single element and is displayed in red, moved from array element to array element on a predefined path. The VE center $\mathbf{z}$ stayed for 2.5 s on each element and then shifted within 5 s to the neighboring element with a stop of 2.5 s midway between elements. The movement periods of the VE model are marked by the gray bars in (b) and (c). (b) Measured wrist extension/flexion (α) and wrist deviation angle (β) when testing the VE path with a constant stimulation intensity (open-loop; $\hat{u}_{\text{OL}}$) applied. (c) Joint angles and resulting global and element-individual stimulation intensities when closed-loop control is applied such that α matches the reference of $\alpha_{\text{ref}} = -20°$ (dotted blue line). For a better comparison, both, the stimulation intensity of the open- ($\hat{u}_{\text{OL}}$) and closed-loop ($\hat{u}_{\text{CL}}$), are displayed. The stimulation intensity $\hat{u}_{\text{CL}}$ required for achieving the desired wrist extension α_{ref} varies visibly between the different VE positions in the EA.

To demonstrate the feasibility of the feedback-control concept, measurements in healthy volunteers were performed investigating whether the controller K_1 is able to track a desired wrist extension α_{ref} throughout an EA on the dorsal forearm. Details on the experimental setup and procedure are presented in *Appendix* D. Instead of having a user adjusting the VE position $\mathbf{z}$, paths for $\mathbf{z}$ through the whole array were defined with two different sizes h. This allowed comparing the results of all volunteers. Each path was stimulated twice in each subject: first in open-loop with a constant $\hat{u}$ and afterward in closed-loop. The results of testing the VE path with a circular VE in one volunteer are exemplarily shown for open- and closed-loop in Fig. 5.4. The measurements revealed that the stimulation intensity $\hat{u}$, required for the desired wrist extension, varies for the different positions in the EA. In every tested volunteer, the implemented PID controller was able to adjust to the changing conditions after a certain period (≈1 s) leading to RMSEs between measured angle α and reference of α_{ref} of 2°–8°.

The Procedure in Practice

The whole procedure of VE identification with the semi-automatic approach as performed in the user-centered evaluation is illustrated in Fig. 5.5. First, motor (u_{mot}) and pain (u_{tol}) thresholds have to be identified for the individual patient by stimulating any arbitrary element, representative of the sensation of pain on the forearm [66]. Afterward, step responses of 2 s are recorded, and PID controller parameters are calculated based on the identified models. The user, in this case the physician or physical therapist, can then manipulate the shape, size, and position of the applied VE and observe the evoked motion in the patient for DOFs that are not under feedback control. Any position and size within an array can be tested and saved as a suitable VE for the desired motion. It is possible to combine VEs of different positions $\mathbf{z}$ to one active VE; they can vary in shape s and size h. In this way, active VEs with branched patterns can be realized, which might be necessary for generating a uniform movement of all fingers [92].

In the subsequent experiments with the HNP, the search with the semi-automatic approach was performed twice: first in the extensor array to find VEs for hand opening and wrist stabilization with feedback control, and then in the flexor array to find a VE for finger flexion (grasping; see details in the following *Section* 5.4). For the latter, the stimulation intensity applied to the VE in the flexor array was modified manually (open-loop), whereas the already identified VE for wrist stabilization in the extensor array could be stimulated simultaneously in closed-loop mode, to guarantee sufficient wrist extension.

5.3.2 Automatic Search Strategy

Parallel to the semi-automatic approach, an automatic search strategy was developed and tested as an alternative, which aims to identify suitable VEs and matching stimulation parameters (stimulation current and pulse width). The approach explores the array(s) automatically and suggests VEs for different reference postures. This kind of intelligent procedure might be the right choice when it comes to FES systems in home-use, as it assists the patient in the decision-making. The presented automatic search strategy combines algorithm features of previous methods by Hoffmann et al. [151] and Schill et al. [182]. Those previous algorithms aimed at finding VEs for stability in the wrist joint [151, 182] and simultaneous extension and flexion of the fingers [151] by comparing generated and desired joint angles, and showed promising results in healthy volunteers.

The new algorithm consists of two phases, as illustrated in Fig. 5.6: In phase I, all single elements of an EA are sequentially stimulated in random order with a staircase like intensity profile (*single element mode*). The induced movement by the electrical stimulation strongly depends on the stimulation parameters (f_{s}, I, and pw). The algorithm automatically increases the stimulation intensity (normalized charge u) step-wise for each element until a predefined threshold is reached, such that the induced motion is recorded for varying intensities. The stimulation frequency is set to a fixed value. A cost function $J(i, n)$ based on the observed steady-state joint angle recordings is calculated online after each stimulated element i and

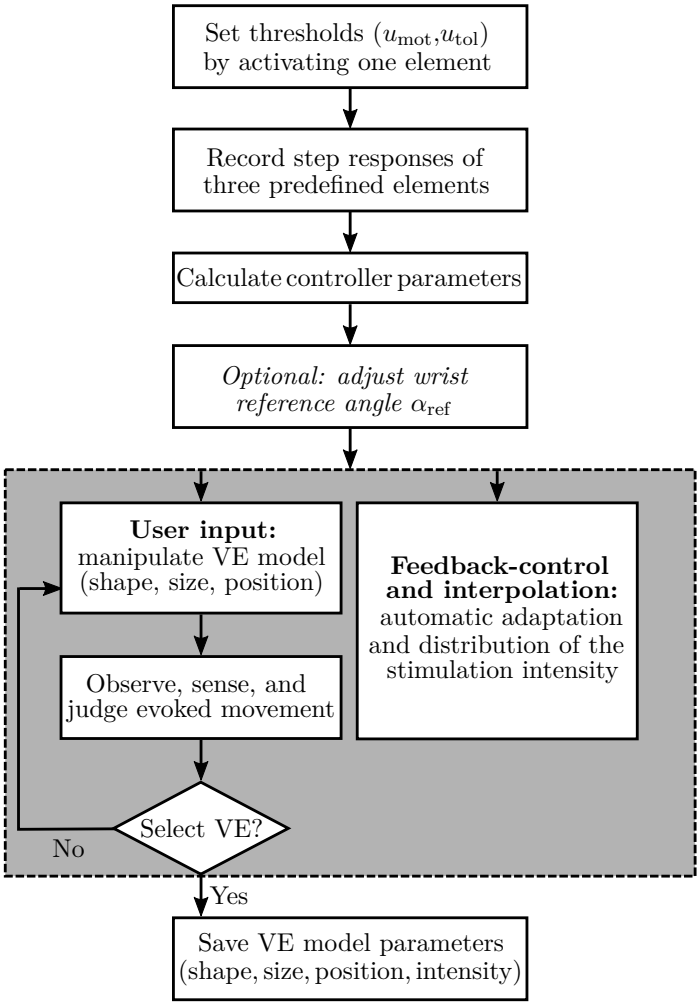

Figure 5.5: The course of action for the VE identification with the semi-automatic search. After the initialization steps, the user can manipulate the active VE model and observe the resulting motion, while the system automatically adapts and distributes the stimulation intensity (gray box).

for each applied intensity level $n \in \mathbb{Z}_+^*$. For each element i, the algorithm determines the minimum value

$$L(i) = \min_n J(i, n) \tag{5.6}$$

of the cost function over all applied stimulation intensities. The result of phase I are the four best elements with the lowest value of L. In phase II, element combinations with those elements are formed according to two heuristics and are stimulated in the same manner in an arbitrary order (*combined element mode*). Finally, the five VEs with the lowest cost function values L of all applied stimulation intensities are suggested as suitable VEs with corresponding stimulation parameters for a given reference movement.

The developed cost function $J(i, n)$ for each element or element combination i is defined as follows:

$$J(i, n) = \frac{100}{\sum_{j=1}^{M} g_j} \cdot \sum_{j=1}^{M} g_j \cdot \|\bar{a}_j(i, n) - a_{j,\mathrm{ref}}\|. \tag{5.7}$$

The function $J(i, n)$ is calculated separately for each of the applied stimulation intensity steps n ($n = 1 \dots N$). With a delay of 60 ms, the recorded joint angles are averaged over the remaining steady-state time interval after each increase of the stimulation intensity yielding $\bar{a}_j(i, n)$. The measured and reference joint angles are normalized to the anatomical range of motion of the specific hand and finger joints. The resulting averages $\bar{a}_j(i, n)$ are compared with the corresponding reference joint angles $a_{j,\mathrm{ref}}$ for each considered joint $j = 1 \dots M$. The deviation of each joint can be weighted individually with the weight $g_{j\,j}$.

For each desired motion, different reference joint angles and weights can be chosen. It is possible to adapt these values to individual patients. For the experiments conducted in this thesis, reference angles have been extracted from recorded hand movements of five healthy volunteers during a grasp-and-release task. The desired movements and matching reference angles can be found in *Section* 5.4.

Two different heuristics were established to build candidate element combinations for phase II. In heuristic a), the element combinations for testing consists of all eleven possible combinations of the four best single elements (cf. [151]). The maximum number of elements in an element combination selected with heuristic a) thus is four. In heuristic b), the three best single elements are combined with their neighboring elements. Combinations of two elements (good element plus direct neighbor), three elements (best element plus two direct neighbors in a row), and four elements are considered. Combinations with four elements consist of one of the three best elements plus two directly neighboring elements and one direct neighbor of those elements. To limit the number of combinations with heuristic b) and thereby the required time of phase II, an additional selection criterion is applied. Combinations which hold neighbor elements with comparatively high cost-function values L are excluded. The cost function of an element counts as comparatively high if its value is larger than the mean cost function value of all tested elements of phase I. The number of all tested combinations of phase II for one cost function is limited to 22, so eleven combinations are selected by each heuristic. For heuristic b), those element combinations are selected which hold the lowest mean cost function over the included elements.

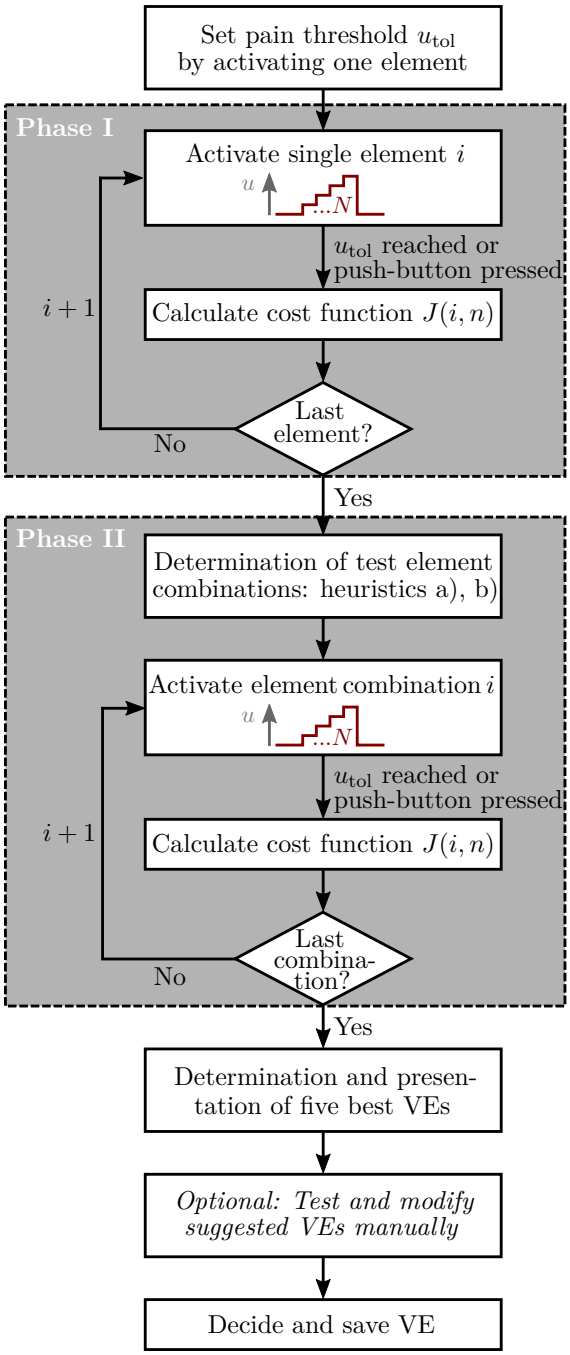

Figure 5.6: The course of action for the VE identification with the automatic search. First, the maximum tolerated stimulation intensity u_{tol} of the individual patient is determined exemplarily by stimulating one array element manually. Then, each element and element combination is stimulated sequentially with a staircase-like profile from zero until u_{tol} (default step-size for the applied normalized charge u: 0.01; default step-duration: 120 ms). A push-button was given to the patient, such that he/she was enabled to stop the stimulation at any time. The next element (phase I)/element combination (phase II) is stimulated automatically after 1.5 s of break (adjustable), or the patient pushing the button (user input) starts the next stimulation. During phase I, uncomfortable elements can be marked and are excluded for phase II.

At the end of phase II, the five best VEs of phase I and II are presented to the user (see Fig. 5.6). Additionally, an array map is displayed showing the distribution of the cost function values L of the single elements, in other words, the results of phase I. The user is allowed to reexamine the suggested VEs regarding their evoked movement. This manual phase can be necessary because not all DOFs are considered, and to guarantee that the evoked movement matches the expectations of the patient and the treating health professional. However, the users can also decide to trust the system's decision and simply accept the suggested VEs. Furthermore, new VEs can be built manually by combining elements if necessary. If more than one cost function is investigated, for example, to find matching positions for different movements, the last three steps of Fig. 5.6 are repeated for each function.

5.4 User-Centered Validation

5.4.1 Participants

Five sub-acute stroke patients (female = 1, male = 4, age 53–69 (59 ± 6.5), 6–14 days after stroke (8.4 ± 3.2), right-side paralyzed = 3) with moderate to moderately severe hemiparesis of the upper extremity were included in the pilot study. The local ethical committee approved the study (Berlin Chamber of Physicians, Eth-25/15). Written informed consent was obtained from each participant before the session. Exclusion criteria were severe communication limitations, cognitive dysfunction, and no response toward electrical stimulation at a comfortable stimulation level. The included patients had a *modified Rankin Scale*[30] (mRS) value of 3–4 (3.2 ± 0.4) and a muscle strength in hand and forearm of 0–3 (2.2 ± 1.3) from 5 according to Janda [329]. All patients needed support for performing grasp-and-release tasks with the paralyzed hand.

In addition to the stroke patients as one user group, also the second user group—the health professionals—were included in the user-centered evaluation. The second user group consisted of n = 5 (female = 1) health professionals (physicians = 3, occupationaltherapist = 1, medicalstudent = 1). Three of five health professionals stated their age with an age range between 33–45 years (39.3 ± 4.9). None of the health professionals had previously used FES in the treatment.

5.4.2 Setup

For the clinical validation, the HNP with the components described in *Chapter* 3 was utilized. In summary, the applied system consisted of the RehaMovePro stimulator with science adapter and demultiplexer, two customized electrode arrays with separate counter electrodes, the modular hand sensor system with sensor strips for four fingers F1–F4, a laptop with touchscreen and GUI (version 1; cf. Fig. 3.7a), as well as an external push-button. The extensor array with 35 available elements was placed above the extensor muscle group; the flexor array with 24 available active elements was applied above the finger flexor muscles on the forearm, as shown in Figs. 3.1 and 3.3 in *Chapter* 3.

[30]The mRS is a standardized measure for describing the level of impairment after stroke on a scale from 0–5 [328]. '0' applies to patients showing no symptoms at all; '5' describes a severe disability requiring constant nursing care and attention.

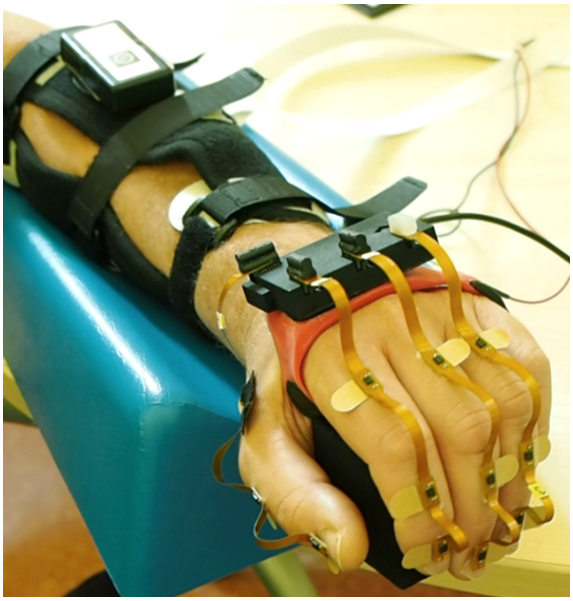

Figure 5.7: Experimental setup. The HNP is displayed in action on a patient, showing the hand sensor system with four sensor strips on the fingers, base unit, and wireless sensor. The two EAs are placed on the forearm and fixated with the arm cuff. The patient grasps a cube under stimulation. Not seen in this picture is the push-button the patient holds in his other hand, which allows to control or interrupt the stimulation at any time.

The mounted HNP is shown exemplarily in Fig. 5.7. In total, 19 joint angles were measured with the HSS: extension (negative; cf. defined coordinate systems in Fig. 4.2) and flexion (positive) angle of the wrist (α), of the metacarpalphalangeal joints (mcp_α), proximal interphalangeal joints (pip), and distal interphalangeal joints (dip) of the fingers F1–F4, as well as the deviation angle of wrist (β) and abduction of the MCP joints (mcp_β), and the five joint angles of the thumb (F1). The measurement of the little finger F5 was omitted as there exists a coupling to the ring finger. At the beginning of each experiment, the hand with mounted HSS had to remain in an initial neutral pose for a few seconds during which the heading of all sensor units was aligned (cf. *Section* 4.3.3). In patients, this pose could be taken up with the help of the health professional. Note that for the semi-automatic search a more reduced setup of the modular HSS would have been possible (i.e., only capturing the wrist angle), but, for the analysis and better comparison, all 19 joint angles were measured for both search approaches.

Stimulation was applied at 33 Hz as biphasic pulses of asymmetric shape (pulse width, current) but charge balanced. Elements were activated asynchronously, successively after another. Asynchronous stimulation in EAs has been shown to be stable regarding discomfort [66] and to provide benefits on fatigue and selectivity compared to synchronous stimulation [72] (see *Section* 2.4). The stimulation pulse intensity u or $\hat{u}$ equals the normalized charge, as described in *Section* 3.2.

5.4.3 User-Centered Evaluation

Both quantitative and qualitative research methods were used to evaluate the functionality and acceptance of the tested array identification strategies as well as the hardware setup from the user's perspective. Therefore, interviews, questionnaires, and the thinking-aloud technique

were utilized to receive a broad insight into their perception of the system and the identification methods. A questionnaire for the patients, tailored to the HNP and research questions, was developed in cooperation with the institute for rehabilitation science at Humboldt Universität zu Berlin [325]. The questionnaire contained open-ended and closed questions to gain qualitative and quantitative data. Closed questions were mainly rated on five-point Likert scales from '1' (entirely disagree) to '5' (entirely agree). The questionnaire for the patients was conducted as an interview and covered sociodemographic data, the personal attitude to technology (measure of technology commitment, [330]), experience with technology in general, usage experience with the system (e.g., problems, understanding, motivation, safety, pain in dealing with the system) and the acceptance of the system via the *Technology Acceptance Model* (TAM) by Davis [331]. The TAM is one of the most widely used acceptance models. The acceptance and actual use of a technology can be explained in terms of internal beliefs, attitudes, and intentions of the user, which are decisively influenced by the perceived usefulness and perceived ease of use of the technology.

The concurrent thinking aloud method was used to gain direct information from the health professionals about the interaction with the system. With this method, the participating physicians and therapists are encouraged to verbalize their thoughts continuously while handling tasks with the system (cf. [332]). The recordings should provide access to their thoughts, feelings, intentions, and expectations and reveal their perception of the actual system use [333].

5.4.4 Procedure

Measurements were performed at the clinic for neurology with stroke unit and early rehabilitation at the Unfallkrankenhaus Berlin (Germany). If possible, the experiments were conducted with the patient sitting in a chair at a table. Otherwise, the measurements were performed with the patient in a comfortable upright position in their bed. During the identification procedures, patients had their paralyzed forearm in an arm mount and were instructed to prevent voluntary hand movements.

At the beginning of each experiment, the health professionals were familiarized with the thinking-aloud method. To gain information about the underlying reasons for their preferred identification method, the health professionals were instructed to express all their thoughts on the system and especially the identification method during the whole session. All sessions were recorded with an audio device. The health professionals had been familiarized with the usage of the HNP in previous workshops and experiments.

The experimental procedure is outlined in Fig. 5.8. After the setup of the HNP, both array identification methods—the semi-automatic and the automatic—were used one after another to find suiting stimulation positions for a grasp-and-release task. A suitable stimulation position was defined in accordance with [94] ("functional point"): the VE in the array for which sufficient strength of contraction can be generated in the target muscles with minimum overflow to non-synergistic muscles. The first method applied was always the semi-automatic search, as the knowledge of the health professional on the stimulation responses gained during the automatic search would have distorted the results regarding search time and positions.

Following [177], three VEs needed to be identified for the grasp-and-release task evoking the following movements: (1) Hand and finger extension for a hand opening (VE_1), (2) wrist

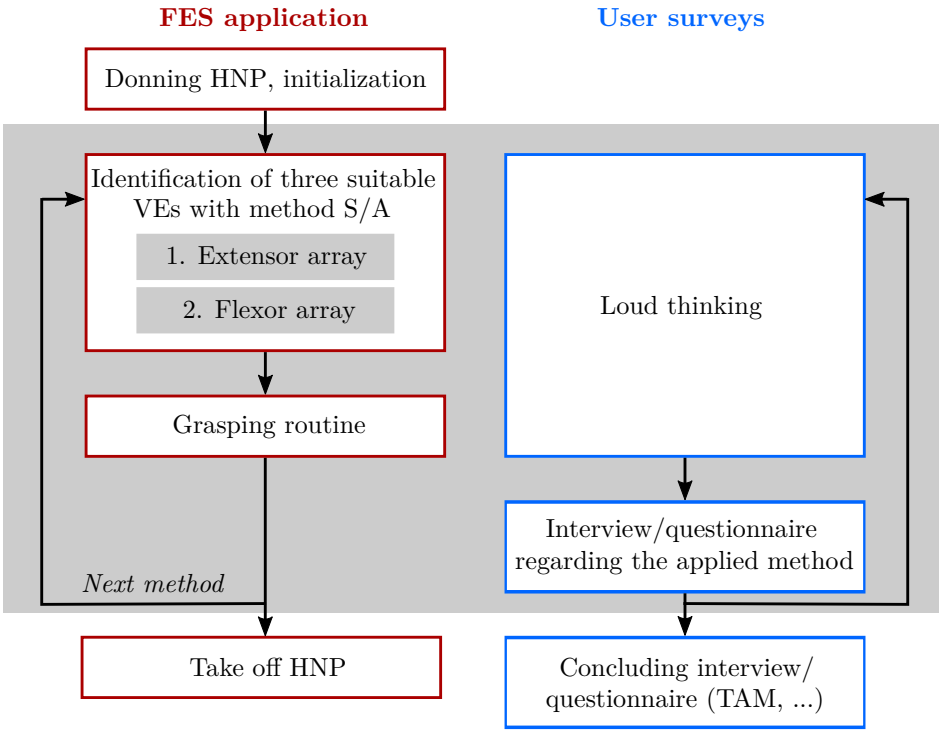

Figure 5.8: Overview of the experimental procedure, where the FES application is evaluated in parallel by the users. Method S and A refer to the semi-automatic and automatic search strategy.

stabilization (wrist extended, fingers in rest or flexed; VE_2), and (3) functional finger flexion (power/spherical grasp; VE_3). The corresponding reference joint angles and weights for the cost function of the automatic search strategy are listed in Table 5.1. VE_1 and VE_2 were searched for in the extensor array (cf. Fig. 3.1). After successful identification of these VEs, the flexor array was tested to evoke finger flexion. It was possible to simultaneously stimulate VEs in the extensor array for wrist stabilization, even with feedback control for the semi-automatic search. The identified positions, applied stimulation intensities, recorded joint angles, and the duration of each step of the identification procedures were saved for the subsequent analysis.

If successful, each identification procedure was followed by a grasping routine, which was performed with and without an object (wooden cube, $5 \times 5\,\mathrm{cm}$). The predefined stimulation sequence consisted of 4 s of stimulating a hand opening via VE_1, then 4 s of stimulating finger flexors (grasping; VE_3) and extensors for stabilizing the wrist (VE_2; if identified), and ended with 4 s of hand opening (VE_1). The patient was able to initialize and pause the stimulation sequence via the push-button. It was also possible that the patient controlled the onset and offset of each stimulation phase via the push-button to synchronize it with his/her voluntary effort, which was wanted in this state of the experiment. Thereby, different timings within the stimulation sequence ($> 4\,\mathrm{s}$ or $< 4\,\mathrm{s}$) were possible. If the patient was unable to reach the object due to severe arm palsy, the therapist gave the object to the patient, or the object was placed on the table next to the patient's hand. After each identification approach, the patients were asked about their experiences in a short interview, as outlined in Fig. 5.8.

Table 5.1: Default joint-angle references for the cost function J of the automatic search for three different movements (VE_1–VE_3). The reference joint angles are displayed in degree; the corresponding weights (g) have no dimension.

VE	**Joint Angle References & Weights**									
	α_{ref}	g_α	β_{ref}	g_β	$MCP_{\alpha,ref}$	g_{MCP}	PIP_{ref}	g_{PIP}	DIP_{ref}	g_{DIP}
VE_1	-20°	1	0°	0.50	-5°	0.25	0°	0.25	5°	0.25
VE_2	-15°	1	0°	0.25	20°	0.50	52°	0.50	40°	0.50
VE_3	-15°	1	0°	0.25	20°	0.50	52°	0.50	40°	0.50

5.4.5 Data Analysis

The subsequent, quantitative data analysis of recorded joint angles, system parameters, and applied stimulation parameters was conducted with *Matlab* (MATLAB R2016b; MathWorks, Natick, MA, USA). Identified VEs were compared between methods and patients. The quantitative data from the interviews of the patients were analyzed with the statistic software 'SPSS Statistics' (Version 22; IBM, Armonk, NY, USA) using methods of descriptive and nonparametric statistics. To examine if the identification methods cause significant differences in the user's experience of the system and the stimulation effect, Wilcoxon signed-rank tests were performed. Furthermore, nonparametric correlation analyses according to Spearman were carried out to test if the user experience is related to age, date, and the severity of stroke.

To examine the feedback from the health professionals on the identification methods, qualitative data analysis was performed using strategies of qualitative content analysis by Mayring [334]. The sound material was transcribed according to Dresing & Pehl [335]. Positive and negative feedback to the system and the identification methods, as well as positive and negative feedback to the stimulation outcome, was analyzed with the software 'MAXQDA' (Version 12; VERBI GmbH, Berlin, Germany).

5.5 Results

Identified VEs

The identified VEs for all three desired movements in each patient are summarized for both search methods in Fig. 5.9. Details on the corresponding, identified stimulation parameters are given in Table 5.2. In all five stroke patients, suitable VEs were identified to evoke the movement *hand opening* (VE_1) with the semi-automatic and the automatic approach. The VEs varied in number and position of the active elements for the two methods. VE_1 consisted on average of 4.2 elements for the semi-automatic search, and of 1.6 elements for the automatic search (cf. Table 5.2). In general, the VEs identified with the semi-automatic search consisted of more active elements than VEs identified with the automatic search for all three desired movements. For patient #2 and #4, in which the locations of the chosen VEs were apart for the two methods, the measured hand postures are illustrated in Fig. 5.9 for stimulating VE_1 found with the automatic approach (top pictogram) and with the semi-automatic search (bottom pictogram). For both cases, the observed hand posture was similar revealing minor differences in the joint angles of the index finger. It should be noted that the VE_1 for *hand*

Table 5.2: Details on the identified VEs and corresponding stimulation parameters for both search methods. The number of involved array elements (m) of the VEs for hand opening (VE_1) and finger flexion (VE_3) are listed. The applied stimulation current I, found during the identification, is presented in mA; the corresponding pulse width pw is given in μs. For the semi-automatic method, also the shape s of the utilized VE model is listed, where 'circ' corresponds to a circular shape, and 'rect' marks a rectangular shape. An 'x' marks cases where no suitable VE was identified.

Patient	VE_1							VE_3						
	Semi-automatic				*Automatic*			*Semi-automatic*				*Automatic*		
	m	I	pw	s	m	I	pw	m	I	pw	s	m	I	pw
#1	4	24.0	244	circ	1	28.5	289	2	24.9	257	rect	1	15.5	161
#2	4	23.0	240	circ	1	25.0	260	x	x	x	x	x	x	x
#3	4	18.3	188	circ	3	22.0	227	x	x	x	x	x	x	x
#4	4	22.0	222	circ	1	24.0	250	2	19.1	200	rect	1	17.0	176
#5	5	29.5	300	circ	2	28.5	289	x	x	x	x	x	x	x

opening identified with the semi-automatic approach always utilized a VE model of circular shape.

In two patients (#2 and #5) suitable VEs were identified to generate a wrist stabilization (VE_2) with the semi-automatic and the automatic approach. In patient #1, VE_2 was found with the semi-automatic search. During its stimulation in the subsequent grasp-and-release pattern, it turned out to hinder a precise finger flexion and was turned off. Hence, a VE for wrist stabilization was not considered in the automatic search. Besides the extension of the wrist, the stimulation in the extensor array often led to a small degree of finger extension, which hindered the grasping function.

The identification of a position for finger flexion (VE_3) was successful in two patients (#1 and #4, see Fig. 5.9). Patient #3 showed sufficient remaining finger flexion such that no FES-support via the flexor array was necessary. The main reason for not finding a suitable VE_3 in patients #2 and #5 was the low tolerance toward the electrical stimulation in the flexor array. All patients reported the stimulation to be more unpleasant in the flexor array than in the extensor array. This feeling resulted in a lower stimulation intensity maximum, as seen when comparing intensities for VE_1 and VE_3 in Table 5.2, which was sometimes insufficient to evoke a strong finger flexion. Furthermore, parallel induced wrist flexion when stimulating finger flexors was a problem that could not always be compensated by stimulation of VE_2. In line with the findings for VE_1, the identified VEs (VE_3) in patients #1 and #4 varied in number and positions of the active elements for the two identifications methods. For patient #4, the resulting hand posture is depicted when stimulating VE_3 found with the automatic approach (top) and with the semi-automatic search (bottom) in Fig. 5.9. VE_3 of the semi-automatic search led to less flexion in the wrist. It should be noted that the VE for finger flexion found with the semi-automatic approach always utilized a VE model of rectangular shape (cf. Table 5.2).

The difference between the identified VEs with both methods was further analyzed by considering the cost function value. For this, the cost function value was calculated offline for the VE of the semi-automatic approach as well. The time frames where the saved VEs were stimulated during the identification process were determined and used for the calculation. The resulting cost function values of both methods are presented in Table 5.3. Illustrated scales

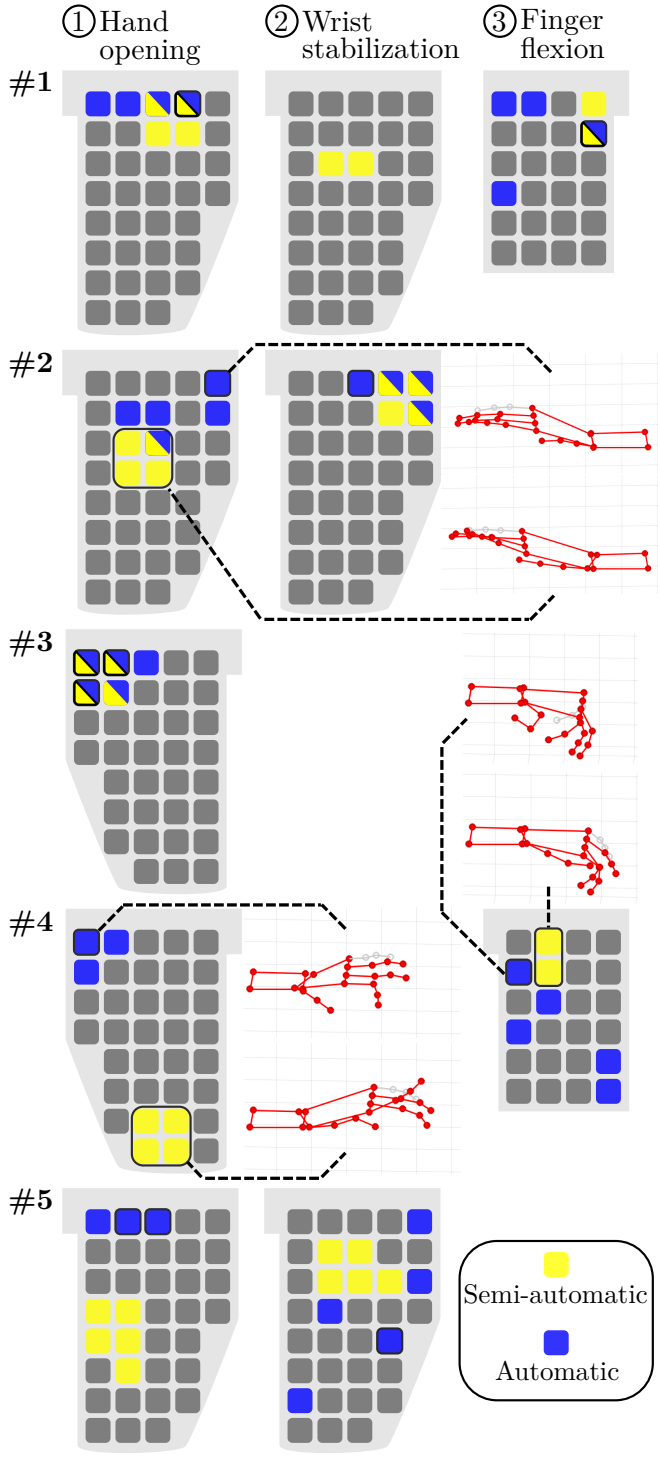

Figure 5.9: Identified VEs with the two search methods for each patient. Each row represents the results of one patient for all desired movements, as indicated in the headline. EA layouts are displayed in top view, as positioned on the forearm with gel layer at the bottom. Different array layout orientations are due to the treatment of different arms: right arm for patients #1, #2, and #5; left arm for patients #4 and #5. Search results are labeled in yellow for the semi-automatic search and in blue for the automatic search (top five VEs). A black frame marks the finally chosen VE from the automatic search. Elements identified with both search methods are colored in yellow and blue. For patients and movements, where the results of semi-automatic and automatic search are located quite differently in the array, the evoked hand motion is depicted (see patient #2 and #3) with the measured hand segments colored in red. If an array layout is not given for defined motion it means that either no suitable VE was found for that motion (patient #2, #4 and #5), or that the patient could perform the movement on his/her own with the remaining hand function (patient #3).

Table 5.3: Cost function values L for each identified VE with each method for each patient. Here, the abbreviation S refers to VEs identified with the semi-automatic search, and A refers to the automatic search. If the element combination of the semi-automatic VE was tested during the automatic search, the corresponding cost function value is displayed in the column *S in A*. If not, this column holds an '-.' An 'x' marks cases where no suitable VE was identified. The average across subjects is calculated for columns containing at least three values.

Patient	**VE_1**			**VE_2**			**VE_3**		
	S	*S in A*	*A*	*S*	*S in A*	*A*	*S*	*S in A*	*A*
#1	1.8	10.4	3.5	11.5	-	x	12.1	-	10.3
#2	12.0	-	3.1	13.1	8.0	7.9	x	x	x
#3	1.6	1.6	1.4	x	x	x	x	x	x
#4	9.9	-	6.0	x	x	x	11.4	-	9.6
#5	2.3	-	1.6	3.5	-	8.1	x	x	x
Average	5.5	-	3.1	9.4	-	-	-	-	-

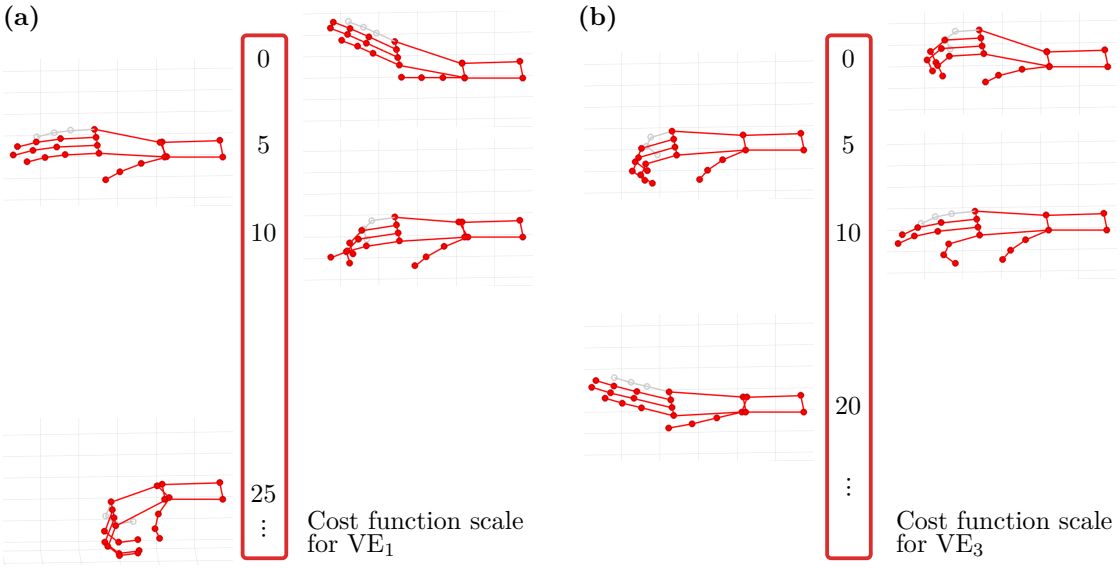

Figure 5.10: Cost function scale for the references for VE_1 (hand opening) and VE_3 (finger flexion). Exemplary hand postures are depicted with corresponding cost function values (cf. Eq. (5.7)). For the cost function value $J = 0$, the shown hand posture is the desired reference postures for both scales, because a value of '0' means that the generated hand posture equals the reference exactly. The little finger is drawn in gray as it was not utilized in the experiments nor in the cost function. For better visualization, it was assigned the same joint angles as the ring finger.

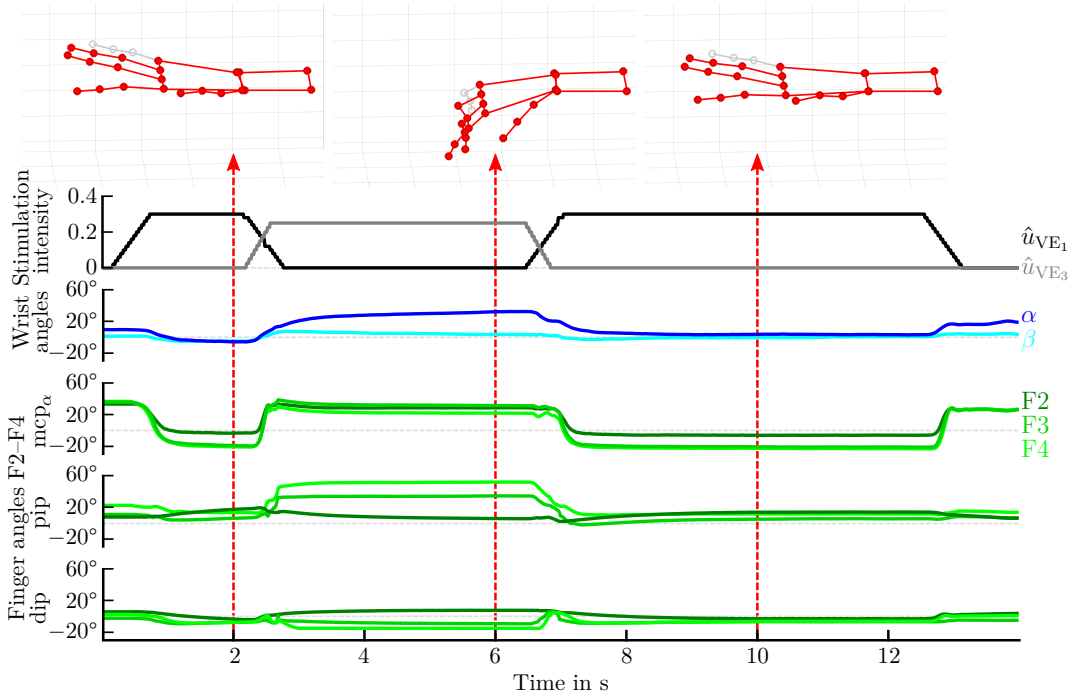

Figure 5.11: Exemplary grasp-and-release cycle with FES support in patient #1. For this trial, the VEs identified with the semi-automatic search were stimulated. The applied stimulation intensities for hand opening ($\hat{u}_{VE_1}$) and grasping ($\hat{u}_{VE_3}$) are displayed in the first graph. The second graph shows the flexion/extension (α) and abduction (β) angles of the wrist. Flexion/extension angles of the finger joints (mcp$_\alpha$, pip, dip) for fingers F2–F4 are plotted in shades of green in the last three graphs. The measured hand posture, including the thumb, is visualized at discrete times during the three phases of the grasp-and-release cycle: hand opening, grasp of wooden cube, release. The little finger F5 is drawn in gray because it was not measured in the experiments. In the interest of good visualization, F5 was assigned the same joint angles as F4.

for the references of VE_1 and VE_3 are provided in Fig. 5.10 to increase the interpretability of the results. For VE_1 and VE_2 in the extensor array, there is no clear tendency that one method outperforms the other one in terms of the cost function values. The differences were sometimes minor (patients #3 and #5). In patient #1, VE_1 of the semi-automatic search was also stimulated during the automatic search, resulting in a different movement with a larger cost function value (10.4 to 1.8; cf. Table 5.3), which is why this combination was not chosen in that approach.

Grasp-and-Release Task

Three out of five patients were able to perform the grasp-and-release task with a wooden cube successfully at the end of the experiment (patients #1, #2, and #3). Figure 5.11 exemplarily shows the course of one grasp-and-release cycle of patient #1 with resulting joint angles and hand postures when stimulating the VEs from the semi-automatic search. The patient used the push-button to control the timing of the stimulation pattern. This patient was not able to hold the object without the stimulation: Finger flexors were stimulated (VE_3). Patients #2 and #3 were sometimes able to grasp the object without FES-support.

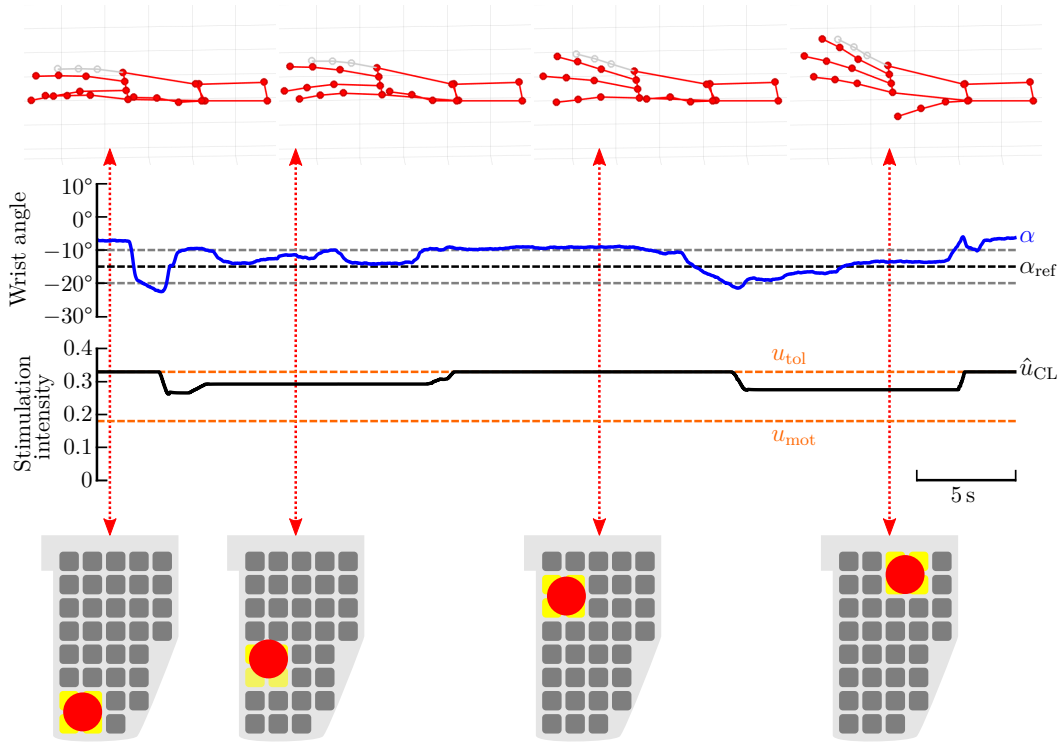

Figure 5.12: Semi-automatic search in the extensor array with feedback-control for patient #1. The feedback controlled wrist extension/flexion angle α (blue) is displayed over time together with the applied global stimulation intensity $\hat{u}$ (black; actuating variable). The reference angle α_{ref} was set to 15° (black dotted line) and the tolerated error bound (gray, dotted line) was ±5°. An error smaller $\alpha_{\text{ref}} \pm 5°$ equaled zero at the input of the controller. In the displayed time frame, the location of the VE model was changed by the caregiver. The resulting position of the VE model in the array (red circle) and the corresponding active elements, marked in yellow, are exemplarily shown for four times, together with the measured hand posture. As in the previous figure, the little finger F5 is depicted in gray, and assigned the same joint angles as F4 for better visualization.

Search Parameters

Also, the search process itself was analyzed. Exemplary results of the feedback control of the wrist angle α during the semi-automatic search in the extensor array are depicted in Fig. 5.12. While the VE model position changed, the controller automatically adjusted the global stimulation intensity $\hat{u}$. As can be seen in this example, there existed positions in the array, where the same degree of wrist extension was achieved with less stimulation intensity. For the depicted patient, a position for hand opening (VE_1) was chosen that needed a lower stimulation intensity than the other positions and led to a strong finger extension. Details on the search settings used in each patient are summarized in Table 5.4. All provided VE model shapes—circle, ellipse, rectangle—were used during the semi-automatic search, whereby not every shape was tested in every patient or every array. For the interpretation, it is to be noted that the circular shape was selected by default when starting the identification procedure. The option of combining VEs of different locations to one active VE was not utilized. The feedback control was not applied in patient #4 because the tolerated level of stimulation was too small to allow closed-loop adaptation. The wrist stabilization via VE_2 was only used in patient #5 during the search for VE_3.

For the experimental results of the automatic search, it occurred that single elements were chosen more frequently than element combinations as the final VE. However, the average cost

Table 5.4: Used options in the semi-automatic search and automatic search for each patient. The term 'combined VEs' refers to the option of combining VEs with different positions to one active VE. The term 'VE_2 on' relates to the option of using the identified VE_2 for wrist stabilization during the search in the flexor array. In the automatic search, there exists the option on defining 'customized VE,' which were not ranked in the top five VEs for a desired hand posture. For patient #3, the flexor array was not utilized. An 'x' therefore marks the corresponding entries.

Patient	**Semi-Automatic**					**Automatic**
	Tested shapes E	*Tested shapes F*	*Combined VEs*	*Feedback control (E)*	VE_2 *on*	*Customized VE*
#1	circular	circular, rectangular	no	yes	no	no
#2	circular	circular	no	yes/no	no	no
#3	circular, ellipsoid, rectangular	x	no	yes	x	no
#4	circular	circular, rectangular	no	no	no	no
#5	circular	circular	no	yes	yes	yes (VE_2)

function value of phase I of the algorithm was always higher or almost equal to the average value of phase II, indicating that the applied heuristics worked sufficiently. The option of defining customized VEs, which were not rated in the top five by the algorithm for the desired posture, was used once, as seen in Table 5.4.

Search Duration

The donning of the HNP, including stimulation electrodes and inertial sensor network, took between 2–4 minutes. The average time needed for the search with each identification method is summarized in Fig. 5.13. The total duration of the search method included the initialization of the method (e.g., adjustment of parameters), the search for VE_1 and VE_2 in the extensor array, and the search for VE_3 in the flexor array. On average, the total time of the semi-automatic method (7.5 minutes) was smaller than the time needed with the automatic approach (10.3 minutes). The search in the extensor array took longer compared to the other periods of the search procedure, which was due to the larger number of elements in that array and the search for two different induced movements (VE_1 and VE_2).

Evaluation by Patients

The survey of the patients after each identification method held similar answers for both methods. Patients were asked regarding the perceived pain on a scale from '0' (no pain) until '10' (highest conceivable pain) for the identified VEs. When stimulating in the extensor array, average values of 1.2 ± 0.45 were reported by the patients for both methods, stating that only slight discomfort was perceived. For the stimulation of the flexor array, the semi-automatic approach led to higher pain values (3.8 ± 3) compared to the automatic approach (2.8 ± 3.5). However, this difference was not significant. In addition, patients were asked after each

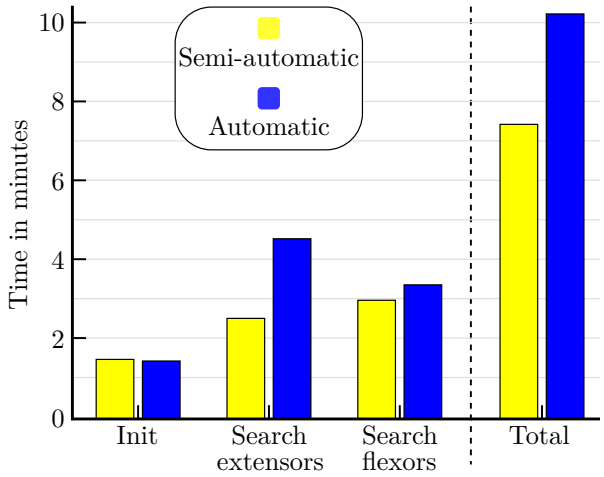

Figure 5.13: The average duration for the VE search with both identification methods. The time required for the identification procedure is displayed for each period: (i) initialization of the sensors, stimulation thresholds, and for the semi-automatic search the estimation of the controller parameters (*Init*), (ii) search in the extensor array for VE_1 and VE_2 , and (iii) search in the flexor array for VE_3. The sum of all periods leads to the total time needed for each approach (right column).

identification method regarding their perception, such as anxiety and fun. They answered the questions on a five-stage Likert scale, as seen in the results in Fig. 5.14. Again, no significant differences were found between the two methods. When interpreting the results, it has to be kept in mind, that the semi-automatic approach was the first method applied and often was the very first FES treatment of the patients.

The general concept of the HNP was also assessed on a five-stage Likert. On average, the patients agreed that the HNP is comfortable (4.25) and to some extent enjoyable (3.5). The answers regarding technology acceptance were summarized in the dimensions intention of use (4.6), ease of use (4.9), and perceived benefit (5) according to the TAM.

Evaluation by Health Professionals

The qualitative analysis of the audio data from the health professionals revealed positive and negative comments regarding the identification methods and the HNP in general. One physician stated the duration of both identification methods as relatively fast but rated the automatic search faster as the semi-automatic. In the automatic identification method, one physician also indicated to like the random order of the stimulation locations, because of the relieving effect for the muscles. The health professionals made further positive comments, which can be related to both identification methods. In this context, the graphical visualization of the array electrodes and their attachment, as well as the visualization of the current stimulation location in the GUI and the system by itself gained positive feedback. The negative feedback only pertains to the usability of the GUI in both identification methods.

The health professionals gave positive and negative feedback regarding the outcome of the FES. In the semi-automatic approach, nine statements with positive feedback on the stimulation outcome were determined. The physicians were especially pleased with the stimulated wrist movement. In overall five times, they rated the stimulation effect from ‘good’ to ‘nearly perfect.’ Furthermore, in one test session, the outcome for the index finger was

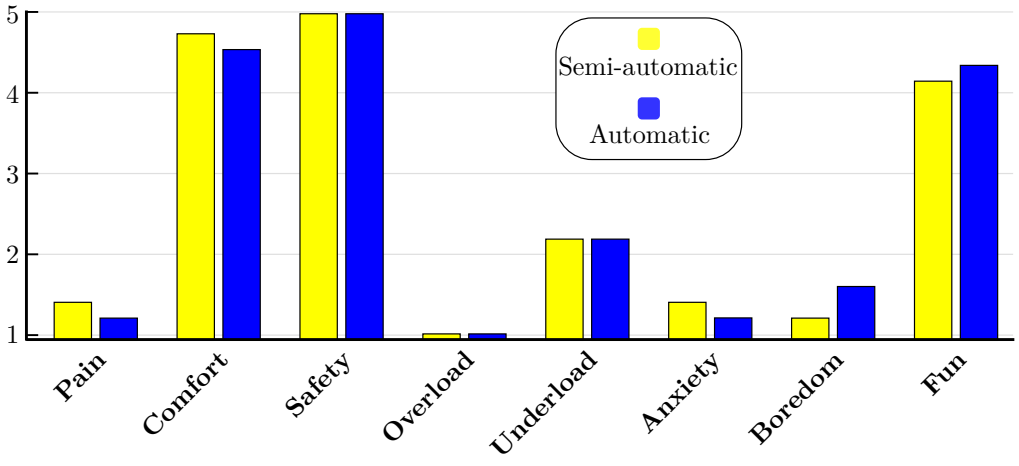

Figure 5.14: The average patients' perception of the two search strategies. After each identification method, the patients ranked their perception in the experiment on a five-stage Likert scale: '1' = strongly disagree, '2' = disagree, '3' = neutral, '4' = agree, and '5' = strongly agree. No significant differences were found between the methods.

assessed as effective and, in another test session, the physician positively valued the stimulation outcome because of the holistic movement of all digits. In the automatic approach, 20 positive comments on the stimulation outcome were counted. Four positive statements were related to the overall stimulation outcome; three comments were explicitly about efficient electrode positions. Furthermore, the physicians and therapists remarked in three statements each a good movement effect of 1) the thumb, 2) the index finger and 3) the wrist, and gave positive comments on the stimulated hand opening. In two cases, they annotated that the stimulated single elements are more efficient than the electrode combinations.

In the semi-automatic approach, four statements, including one negative feedback on the stimulation outcome, were counted. The physicians indicated the movement of the fingers and especially the thumb as quite weak and stated to see only a small stimulation effect. In the automatic approach, seven statements with negative feedback on the stimulation outcome were found. In two patients, the physicians complained—as well as in the semi-automatic condition—about the missing stimulation effect on the thumb. On the contrary, one participating physician noticed in another patient the opposite effect and criticized that only the thumb and the middle finger showed stimulation effects. Further negative feedback was related to the fact that the stimulation produced a non-physiological rotation of the wrist.

The participating health professionals gave further clinical indications, which can be used to optimize the system and its handling. Two statements of the importance and the difficulty of the stimulation of the thumb movement were determined. In this context, one physician suggested to move or enlarge the stimulation field closer to the direction of the hand.

5.6 Discussion

Summary

Two array identification procedures with different degrees of user integration, which both aim to assist in finding suitable stimulation areas and stimulation parameters, were evaluated for a new hand neuroprosthesis. The results in five sub-acute stroke patients showed that both identification methods—semi-automatic and fully automatic—yield suitable VEs for hand opening and with limitation for hand closing in patients who could tolerate the stimulation. To the best of the author's knowledge, this was the first time that array identification procedures were directly compared in a clinical setup and the user's perspective was considered systematically to improve the usability of future FES systems.

Comparison of VEs

The preferred VEs for hand opening, wrist stabilization, and finger flexion differed among patients, probably due to inter-individual physiological variability and slightly varying array locations on the individual forearm. This finding is in line with other studies (e.g., [170, 177]) and motivates the application of electrode arrays. It also indicates that identification methods need to be applied at least one time for each placed EA on the forearm for each patient. Furthermore, in half the cases of the conducted measurements, the preferred VEs with the semi-automatic and automatic approach were found in different areas of the EAs within one patient. Several reasons might contribute to this observation. When considering the generated hand postures with both methods displayed in Fig. 5.9, and the corresponding cost function values of each VE presented in Table 5.3, often similar values and postures can be observed. This observation indicates that there exist multiple activation areas covered by the array which evoke comparable functional movements. Popović-Maneski et al. [94] discovered similar phenomena when they identified functional points in hemiplegic patients for a grasp-and-release task. Therefore, one reason for the inconsistent results of the two identification methods is the existence of multiple, equally good solutions in the search space. During the semi-automatic search, the clinician chose a different solution than the automatic algorithm. In addition, it could have an impact that the two methods do not search the same parameter space. While the automatic search always tests all individual elements and then combines a maximum of four, in the semi-automatic approach, the user decides on the location and extent of the search. As a result, the two identification methods often do not evaluate and select the same VEs. The term "optimal stimulation point," as used in other studies on VE identification on the forearm (e.g., [170, 171]) can be misleading.

Another reason for the diverging results of the two methods might be the patient-individual time-variance of the response toward electrical stimulation. This assumption is supported by the cost function values of the VEs identified with the semi-automatic approach. For example, in patient #1, the identified VE_1 by the semi-automatic search was tested within both search procedures, and cost function values can be compared. This comparison revealed that the VE_1 matched the reference nearly perfectly (1.8) during the semi-automatic search, but during the automatic search the same VE configuration yielded a higher cost function value (10.4) indicating a change in the patient's muscular responsiveness. The duration of

the experiment with one identification procedure, including explanations, search, grasp-and-release test, and interview/questionnaire regarding the applied method, was approximately 25 minutes. After this time, when considering the HNP and the patient's forearm as a system, characteristics might have changed due to reasons such as electrode-skin interface impedance changes, increased muscle tone, or muscle fatigue. The changing conditions might have led to different selected VEs in the second approach, the automatic search.

Besides the differences in the location of the identified VEs with both methods, the selected VEs also varied in the number of active elements, the shape those elements formed, and in the applied stimulation intensity, as presented in Fig. 5.9 and Table 5.2. One reason for this could be the design of the two methods. In the automatic approach, all single elements were tested and thereby also available as VEs to choose. During the semi-automatic search, it was preferred by the users to use a VE model of larger size activating several elements at the same time. In this way, possible activation zones in the EA could be manually explored at a shorter time. This strategy led to a higher number of elements included in the VEs of the semi-automatic search, 4.2 elements on average, compared to the automatic search with 1.6 elements. It is still an unanswered question whether a lower or higher number of active elements and thereby a smaller or larger VE is beneficial in the treatment. Different array layouts in research prevented a direct comparison with findings in other studies. Nevertheless, others identified VEs with a branched pattern [92, 94], which the new results do not reflect. Both methods allow to build a branched active pattern, but the automatic approach requires less effort.

Regarding the stimulation intensities, the values were similar for both identification methods, even though the number of activated elements differed a lot for hand opening (VE_1; cf. Table 5.2). A reason for this might be the asynchronous stimulation of VEs with multiple elements. The applied intensities varied between arrays. Stimulation on the ventral side of the forearm was perceived as more painful in general, which was one of the reasons for not finding suitable stimulation points for grasping in all patients. Sometimes, the tolerated intensity was not sufficient to evoke strong finger flexion as required for manipulating objects. Another reason was the parallel induced but unintended wrist flexion. The stabilization of the wrist by stimulating VE_2 was often not possible because no stimulation point could be found to elicit the wrist extensors exclusively. Finger extensors were excited as well, which would hinder a successful grasp. Closed-loop control for both VEs (VE_2 and VE_3) might be a future solution here, to balance the intensities and thereby the induced motions of both VEs [152, 153]. Yet, closed-loop control requires that patients tolerate sufficiently large stimulation intensities.

Practicability Analysis

The results regarding induced motion as well as clinician's and patient's feedback indicated no clear preference for one of the two methods. Neither of the identification methods was perceived as painful by the patients, whereby the value of the fully-automatic method was insignificantly better. This finding might be explained by the fact that the semi-automatic search was always the first method performed, and the patients were not used to the sensation of the stimulation at that point. However, the patients felt safe, comfortable, and appropriately challenged during the experiments (cf. Fig. 5.14). Regarding the HNP, the comparatively

poorer rating of the item "enjoyable" to the item "comfortable" concerning the wearing of the HNP at the end of the experiment could indicate that wearing comfort should be increased for prolonged use of the prosthesis.

The automatic approach received more positive feedback but also more negative feedback than the semi-automatic from the health professionals. The higher amount of comments on the automatic search could be related to the longer duration of the procedure, with the health professional being less involved. The evaluation of the health professional's statements on the procedure further revealed that the visualization in the GUI played an essential role in the acceptance of the methods. Uncertainties were identified regarding the current state of the system, visualization, and operation. A user-friendly GUI, tailored to the particular method and system, turned out to be essential for perception by the users. Since the GUIs of both investigated methods were based on the same concept, the interfaces should not have had a significant impact on the comparison of the methods. In conclusion, future algorithms should always be evaluated in combination with their operation interface for clinical use to deduce their usability and duration in clinical practice, even in early development stages [336].

The average time needed for the VE search was lower for the semi-automatic search than for the automatic. With the donning of the HNP taking between 2–4 minutes and average total identification time of 7.5 minutes for the semi-automatic search, total setup time for the FES-supported grasp-and-release task of 10 minutes could be achieved. Most published studies on VE identification did not hold detailed information on the required time of the search procedure in the conducted experiments (e.g., [42, 177, 179, 182]), although it is of high practical relevance. Furthermore, many studies have evaluated only the methodology itself under specific test conditions and not the actual clinical course of action, making it impossible to estimate the needed search time. Bijelić et al. [92] with a manual search (push-button control box) and Popović & Popović [170] with an automatic approach reported a search time of approximately 5 minutes per 24-element EA, which would sum up to > 12 minutes in the new HNP with 59 elements. Freeman [153] achieved about 8 minutes per posture when using a 40-element EA and an iterative learning control approach. Counting hand opening and hand closing as one posture each, this would sum up to 16 minutes in the suggested setup. According to [170], a duration of < 10 minutes for the phase of electrode-determination is within the level of tolerance for clinical applications. Compared to the mentioned methods, the achieved results with the semi-automatic search for two movements—hand opening and grasping—are faster. However, additional time is needed if different grasp types (e.g., tip grasp; cf. Fig. 1.6) have to be identified and if an automatic adaptation to varying underarm postures (pronation/supination) should be realized.

In rehabilitation therapy, repetitive training with FES is best practice [8, 10]. In literature, it was observed that size and shape of individually identified VEs remained the same from day to day in the same patient if the electrode array is placed at the same forearm position (e.g., [170, 177]). In a recent study by Malešević et al. [168], which analyzed the temporal and spatial variability of surface motor activation zones in EAs in 20 FES sessions in stroke patients, it was reported that changes in the VE configuration for wrist, finger, and thumb extension were required each session for all patients. The authors concluded that an experimental (re-)calibration procedure is necessary for each therapy session. They suggested using the

results of the previous session as a priori knowledge to reduce the search space in the following session(s). In this application scenario, the presented semi-automatic identification approach would be a suitable tool to gradually modify stored VEs of previous sessions if necessary, which is a benefit in comparison with the suggested and other fully automatic approaches. For the future, one could also think of a combination of both methods as a suitable approach for clinical practice: In the first session, the whole EA is scanned with the automatic search, and the information is saved for the following sessions. Then, the semi-automatic approach is used to modify the VEs individually in the regions of interest.

Limitations

Changes from day to day in VE configurations could not be tested in the presented study as the sub-acute stroke patients were only measured once, which is a major limitation of the presented results. Follow-up experiments would have been desirable, but could not be performed due to the limited time the patients stayed in the neurology department. As most patients used FES for the first time, they were cautious regarding the stimulation intensity and unprepared for the pricking feeling of the stimulation. Nevertheless, the methods were tested in this early stage of the rehabilitation process, because early intervention after stroke is one of the key factors for successful rehabilitation [39, 244]. Therefore, array identification methods need to prove suitable under these conditions.

Another limitation is that the identification methods were tested under controlled conditions, with the forearm lying in pronation on an arm mount. The grasp-and-release task following the identification phase solely included one object without supporting the upper arm via FES. For patients with insufficient, remained voluntary activity in the upper arm, reaching the object had to be supported manually by the caregiver. These restrictions have partly been necessary to limit the length of the experiment, allowing a direct comparison of two different methods. As a result, some essential features and aspects of EA-based FES could not be investigated. Multiple publications mentioned the need for a dynamic VE relocation in the array during forearm movements, which occur in many tasks in ADL (e.g., [92, 94, 337]). The rotation of the forearm between pronation and supination yields a relative shift between the active electrode position on the skin and underlying tissue, changing which muscles or motor units are recruited (see *Chapter* 2). A real-time adaptation of the active VE in EAs can compensate resulting changes in the generated hand movement, as suggested in [324] or as presented in the following chapter of this thesis. A clinical validation of this feature is an important aspect of future studies.

That the suitability of the identified VEs was solely assessed in a simplified grasp-and-release task with one object is another drawback of the presented assessment. Thereby, the applicability of the method for the identification of different grasp types and strengths cannot be estimated. The results in patients #2 and #5, in which it was not possible to select a suitable VE for grasping, suggest that a re-design of the EAs or an individual design may be needed.

5.7 Conclusions and Recommendations

Both presented array identification methods—semi-automatic and fully automatic—enable for finding suitable VEs in the proposed hand neuroprosthesis. However, the resulting VEs differed for both approaches in three of five patients. The novel semi-automatic approach should be slightly preferred as the search strategy in arrays on the forearm because it is comparatively faster. Its observed search duration would further reduce when applying the system repeatedly on a patient as only small position adjustments for VEs from previous sessions are required. Nevertheless, the search duration will increase significantly, when different grasping types shall be generated, or an adaptation to varying forearm conditions shall be realized. It remains to be seen whether this constraint precludes the use in short exercise sessions or whether the repeated use of the system from day-to-day will speed up the identification significantly due to a priori knowledge.

None of the two methods was preferred over the other by the interviewed clinicians and patients regarding practicability, outcome, comfort, and fun. Therefore, it can be concluded that both levels of user integration should be provided in future FES systems such that the applied method can be chosen individually based on the users' preferences and the application scenario. The gained results underline the need for personalization of the search procedure as, for example, different VE model shapes were utilized during the semi-automatic search and closed-loop support was applied in some patient but not in all.

It was found that the design of the GUI influences the acceptance of the methods in general. This finding initiated the optimization of the utilized GUI through subsequent user-tests following usability engineering standards [293] (cf. *Section* 3.5, GUI version 2). Further, the patient surveys regarding acceptance and engagement indicate that the motivation of patients at this stage of rehabilitation is particularly high. This observation encourages the application of FES-based neuroprostheses in early rehabilitation interventions. It follows that the hard- and software must also be evaluated clinically for this type of use. Due to these findings, the incorporation of end-users in research and product development processes is recommended. Future studies in this area should include more detailed questions regarding setup time, handling of the equipment, and desired options in the algorithms for personalization.

In future work, patient measurements with multiple sessions are necessary to review and maybe re-design the EAs of the HNP to generate finger flexion. An additional single surface electrode for the stimulation of the thumb (to support grasp) shall be added for prospective measurements, as health professionals complained about the lack of induced thumb movement in some patients. Furthermore, it is necessary for patients without voluntary muscle contractions in the upper arm to support the reaching motion as well.

6

Real-Time Adaptation of Virtual Electrodes for Safe Grasping

6.1 Overview

In this chapter, a new method for automatic real-time adaptation of active electrode configurations in EAs to compensate forearm movements during grasping is presented. The technique combines motion tracking using the hand sensor system with motion-dependent interpolation of the VE position, size, and stimulation intensity. Additionally, feedback control is applied to maintain a desired level of grasp force, which is also estimated from the inertial sensors. Experiments in able-bodied volunteers revealed that the new method generates a strong, stable grasp force regardless of the rotational state of the forearm, which is not the case when applying FES via static VEs. In conclusion, automatic adaptation methods are crucial for FES applications on hand and forearm in clinical and home-based rehabilitation.

In the remainder of this chapter, a brief motivation for dynamic VEs is provided in *Section* 6.2. The new adaptation strategy is outlined in detail in *Section* 6.3. *Section* 6.4 describes the conduction of the measurements. Results of all volunteers are presented in *Section* 6.5 and are discussed in *Section* 6.6. Conclusions and perspectives for future work are addressed in *Section* 6.7.

Copyright Statement: The methods and results presented in this chapter have been previously published in:

[288] Salchow-Hömmen, C., Thomas, T., Valtin, M., Schauer, T. "Automatic control of grasping strength for functional electrical stimulation in forearm movements via electrode arrays", *at – Automatisierungstechnik*, 66(12):1027–1036, 2018. DOI: 10.1515/auto-2018-0068,[31]

[31] ***Author's contribution***: The author's contribution to [288] includes reviewing the literature, developing the novel methods, implementing the algorithms, conducting and evaluating the experiments, visualizing the methods and results, writing the manuscript, and revising the manuscript based on annotations and suggestions of the co-authors.

[338] Thomas, T., Salchow, C., Valtin, M., Schauer, T. "Automatic real-time adaptation of electrode positions for grasping with FES during forearm movements", In *Automed Workshop*, Villingen-Schwenningen, March 2018.[32]

The text, tables, and figures in this chapter are extracted with slight modifications from those publications. Specifically, Figures 6.1–6.3 and Figures 6.6–6.9 are included with modifications from [288]. Written permission has been granted to include figures, text, and tables from [288] in this thesis; the copyright remains with the original publisher Walter de Gruyter GmbH (Berlin/Boston). Figures 6.4 and 6.5 as well as *Appendix* E were added.

6.2 Motivation

One of the present shortcomings in hand neuroprostheses is the diminished performance of the electrical stimulation during the rotation of the forearm, namely pronation or supination, illustrated in Fig. 6.1. For example, when a person grasps an object lying on a table and presents or hands over the object to another person, the forearm rotation changes from pronation to supination. The relative movement between the skin surface and the underlying muscular and neural tissue results in a shift of the transcutaneous stimulation point, which leads to changes regarding which muscles or motor units are recruited and to what extent they are activated [92]. Lawrence [54] tracked the transcutaneous functional points for recruiting middle and ring finger in five healthy volunteers during pronation, neutral forearm, and supination, finding individual displacements of up to 40 mm. In the case of grasping with FES, this shift may result in varying accuracy and stronger or weaker grasp strength when stimulating with static electrodes.

The use of EAs was proposed to overcome this problem by allowing the definition and dynamic adaptation of several, situation-related virtual electrodes [92, 94, 166, 182]. Popović & Popović [170] suggested in their outlook to determine suitable VEs for various positions of the forearm and then adjust the active VE dynamically depending on the forearm status. However, a real-time setup allowing a dynamic repositioning of VEs in EAs with respect to the forearm rotation to maintain sufficient grasp strength has not been reported so far [173].

Changes in the response toward FES are not exclusively the result of voluntary hand and arm movements, but can also be caused by changes of the time-variant system of ES and target muscles, such as electrode-skin interface impedance changes, increased or decreased muscle tone, or muscle fatigue [241]. A way to compensate those changes in the evoked response can be closed-loop control with the applied stimulation intensity as actuating variable (e.g., [13, 131, 152, 241, 339]; see *Section* 2.5). Besides the difficult choice of the control structure and parameters of this complex, nonlinear system, the selection of a relevant controlled variable can be challenging as well (cf. *Section* 2.5.2). When it comes to grasping, the control of the grasp force seems to be essential, even though the generated force can be tough to acquire in task-oriented therapy or ADL.

The scope of this chapter is the development and evaluation of a real-time adaptation method for the VE position, size, and stimulation intensity for HNPs for upper limb

[32] ***Author's contribution***: The author's contribution to [338] includes reviewing the literature, developing the novel methods, overseen the algorithm implementation, the experiments, and the data evaluation, visualizing the methods and results, and writing the manuscript.

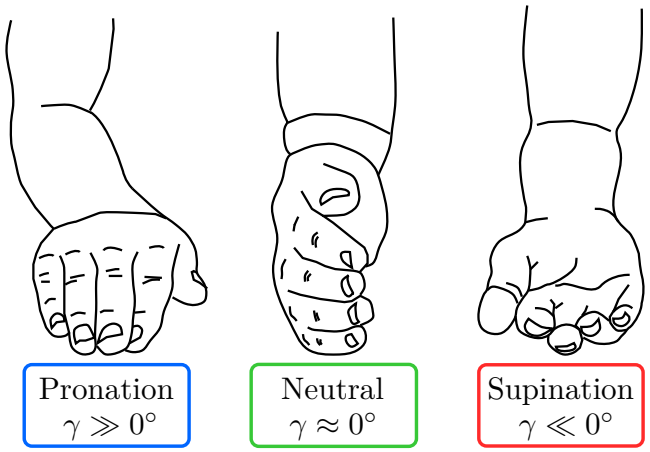

Figure 6.1: Three forearm states classified by the rotation angle γ. The color scheme is used for the remainder of this chapter. The figure is reproduced from [288] with minor modifications.

rehabilitation, to compensate the changes of the muscular response toward the ES due to forearm movements. The presented solution combines the IMU-based motion tracking from *Chapter* 4, the interpolation of the VE size and position as proposed in the semi-automatic identification in *Chapter* 5, and optional closed-loop control of the global stimulation intensity. For the latter, an innovative approach for grasping strength assessment based on the estimated finger joint angles is proposed. The hypothesis is that the new adaptation strategy yields a higher, and more stable grasp strength than non-adaptive stimulation during rotation of the forearm. Measurements in four able-bodied volunteers were performed, in which finger flexion (grasp) was tracked during varying forearm states.

6.3 Method

In a preliminary study, it was analyzed whether pronation and supination of the forearm (cf. Fig. 6.1) and also the posture of the upper arm—elbow extended or flexed—influence the quality of the FES-induced hand movement. It turned out that only the rotational state of the forearm has a significant impact on the generated hand posture, the upper arm posture does not. Details on this investigation are provided in *Appendix* E. Based on these findings, the new method adapts the location of the VE in real-time depending on the rotation angle γ of the forearm. Within the HNP, γ can be measured in real-time by extending the existing hand sensor system: An additional wireless IMU is placed proximally on the forearm near the elbow, as shown in Fig. 6.2. The angle γ is measured as the rotation between the two IMUs on the forearm. Three discrete rotational states of the forearm are differentiated: Neutral (N) forearm position is defined as $\gamma \approx 0°$, pronation (P) equals $\gamma \gg 0°$, and supination (S) corresponds to $\gamma \ll 0°$, as illustrated in Fig. 6.1. The concrete values depend on the achievable range of motion of each person.

Stimulation points or VEs in electrode arrays are usually identified in one defined forearm position, as performed in *Chapter* 5. The basis of the new adaptation approach is the identification of suitable stimulation points for the three discrete rotational states of the forearm (P, N, S) using the semi-automatic search. The semi-automatic search method facilitates a quick, smooth adjustment of stimulation positions: A VE model can be manipulated via a GUI,

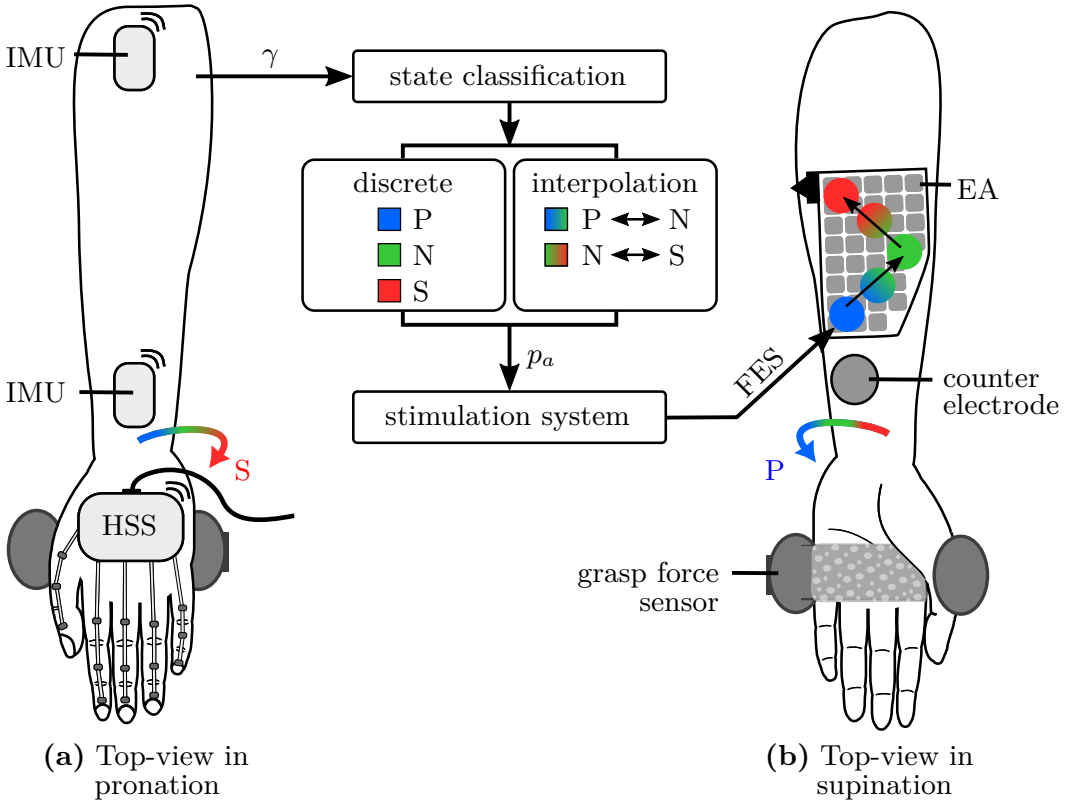

Figure 6.2: Scheme of the real-time adaptation of the VE with the HNP for finger flexion in dependence of the forearm rotation γ. (a) Forearm and hand are depicted in top-view with the HSS and an additional IMU sensor for measuring γ. The algorithm classifies the measured rotation angle γ into the discrete states P, N, and S, which are determined individually for each user. If none of the discrete states can be assigned, the active VE is interpolated according to Eq. (6.1). (b) The stimulation setup consists of a 35-element EA and a circular counter electrode. A course of VEs adapted to the forearm rotation are illustrated exemplarily. For the validation, a grasp force sensor covered in foam foil was utilized. The figure is reproduced from [288] with minor modifications.

while an interpolation function determines the active array elements (refer to *Section* 5.3.1 for details). Here, the circular VE model is utilized with the adjustable parameters location $\mathbf{z}$ in the quantized array, and size h (diameter). In the identification phase, suitable stimulation points (VEs) for three discrete rotational states of the forearm (pronation, neutral, supination) are identified. First, the forearm is placed in pronation and a suitable VE for grasping is identified by testing different VE model configurations in the EA above the finger flexors. A virtual electrode is considered suitable if a firm lateral grasp (power grasp) with almost all fingers flexed is achieved, and only a minor flexion in the wrist occurs. A claw grasp is not accepted. Once a suitable VE is found in pronation, the search is repeated with the forearm being in neutral position and supination. The VE identified in pronation is only modified if necessary. For the most satisfactory VE in each state $z \in \{\mathrm{P}, \mathrm{N}, \mathrm{S}\}$, stimulation parameters $p_z(\mathbf{z}, h, \hat{u})$ and the corresponding rotation angle γ_z are saved.

In the following execution phase, the automatic adaptation is realized via an almost continuous shift of the active VE model as a function of the rotation angle γ. This process is illustrated in Fig. 6.2. The online-adapted electrode configuration p_a is given as

$$p_a = \begin{cases} p_{\mathrm{P}}, & \gamma > \gamma_{\mathrm{P}} - \rho \\ p_{\mathrm{N}} + (\gamma - \gamma_{\mathrm{N}}) \frac{p_{\mathrm{P}} - p_{\mathrm{N}}}{\gamma_{\mathrm{P}} - \gamma_{\mathrm{N}}}, & \gamma_{\mathrm{N}} + \rho \leq \gamma \leq \gamma_{\mathrm{P}} - \rho \\ p_{\mathrm{N}}, & \gamma_{\mathrm{N}} - \rho < \gamma < \gamma_{\mathrm{N}} + \rho \\ p_{\mathrm{S}} + (\gamma - \gamma_{\mathrm{S}}) \frac{p_{\mathrm{N}} - p_{\mathrm{S}}}{\gamma_{\mathrm{N}} - \gamma_{\mathrm{S}}}, & \gamma_{\mathrm{S}} + \rho \leq \gamma \leq \gamma_{\mathrm{N}} - \rho \\ p_{\mathrm{S}}, & \gamma < \gamma_{\mathrm{S}} + \rho. \end{cases} \tag{6.1}$$

The parameter $\rho >= 0^\circ$ defines a vicinity for the three discrete forearm states, in which the active VE is set to the corresponding stimulation parameter set p_z ($z \in \{\mathrm{P}, \mathrm{N}, \mathrm{S}\}$). Those regions are introduced to keep the stimulation constant, while the most common forearm positions are recognized. Thereby, oscillations in p_a are avoided. The default value $\rho = 5^\circ$ can be adjusted online if required. When the measured angle γ lies in between the discrete states, the parameter set p_a of the adapted VE is interpolated between the saved parameter sets of the neighboring states, as stated in Eq. (6.1). More precisely, the parameters $\mathbf{z}$, h, and $\hat{u}$ are linearly interpolated based on the angular difference between the measured angle γ and neighboring forearm states. If the described linear interpolation is applied to all stimulation parameters, including the stimulation intensity $\hat{u}$, the adaptation is applied in open-loop ($\hat{u}_{\mathrm{OL}}$).

In closed-loop, the interpolation of VE position $\mathbf{z}$ and size h is performed as described above, but the global stimulation intensity $\hat{u}$ is feedback controlled instead of interpolated ($\hat{u}_{\mathrm{OL}} \rightarrow \hat{u}_{\mathrm{CL}}$). As a signal for feedback-control, a new variable is defined that correlates with the overall grasp force F and utilizes the HSS: the grasp index C. C is a dimensionless value that describes the flexion/extension of the T-IP joint of the thumb (F1) and the joints MCP, PIP, and DIP of fingers F2–F5. The measured joint angles are normalized to the anatomical range of motion of the specific finger joints (see *Appendix* A) and are notated as mcp_α, pip, dip, and tip. The grasp index $C(t)$ for a time point t is then defined as the weighted sum of all normalized finger flexion angles averaged over all N fingers ($N = 4$) and the thumb, as formulated in Eq. (6.2). The weights g_j ($j = 1...N$) were optimized empirically such that the difference between an extended and flexed hand had maximum difference in C ($g_1 = 1$, $g_2 = 0.8$, $g_3 = 0.5$, $g_4 = 0.2$).

$$C(t) \;=\; \sum_{n=2}^{N+1} \frac{g_1 \cdot \mathrm{mcp}_{\alpha,n}(t) + g_2 \cdot \mathrm{pip}_n(t) + g_3 \cdot \mathrm{dip}_n(t)}{N \cdot (g_1 + g_2 + g_3 + g_4)} \;+\; \frac{g_4 \cdot \mathrm{tip}(t)}{g_1 + g_2 + g_3 + g_4} \tag{6.2}$$

By definition, the grasp index C holds different values for different hand postures, which gives information on the grasp force if the fingers enclose an object. From the time point on at which complete enclosure of the object is first achieved, a further increase of the grasp index C correlates with an increase in grasp strength F. This is possible because of the further flexion of the finger joints and the elasticity of the finger's tissue. The measurement can be enhanced by using an object's surface that provides additional elasticity (e.g., the grasp of a soft ball or sponge), such that a greater flexion of the finger joints corresponds to a stronger force. In that case, feedback control of the grasp index C correlates with the control of the force F. For the

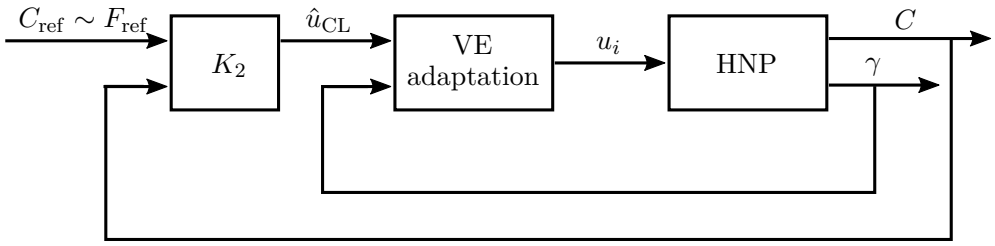

Figure 6.3: Feedback control of the grasping strength. The reference C_{ref} for the grasp index is chosen such that it corresponds to a suitable force (F_{ref}) for holding a specific object. The actuating variable $\hat{u}_{\text{CL}}$ is fed into the VE adaptation, which selects the active elements i, depending on the measured forearm angle γ, and adjusts the corresponding stimulation intensities $u(i)$ depending on $\hat{u}_{\text{CL}}$. The figure is reproduced from [288] with minor modifications.

new approach, a controller K_2 adjusts the global stimulation intensity $\hat{u}_{\text{CL}}$, which is then fed into to the VE adaptation, as depicted in Fig. 6.3.

As in the semi-automatic identification (cf. *Section* 5.3.1), a PID controller in its parallel form is utilized for K_2. For the controller parameters, first-order models with delay (cf. Eq. (5.3)) need to be experimentally identified, here for the VE position of each forearm state z. The estimated model parameters T and T_d are averaged over all states and used together with the obtained maximal gain k to tune the PID controller according to the Chien, Hrones, and Reswick response set-point method [327] with minor, empirically established modifications, as seen in the following equations.

$$K_P = 0.9 \cdot \frac{k}{T \cdot T_d} \tag{6.3}$$

$$K_I = K_P \cdot \frac{1}{3T} \tag{6.4}$$

$$K_D = K_P \cdot \frac{T_d}{3}. \tag{6.5}$$

An integrator anti-windup is realized. The working range of the controller is from u_C to u_{tol}, where u_C is the minimal stimulation intensity that causes a complete enclosure of the object by the fingers and thumb for the individual user, and u_{tol} is the maximum tolerated intensity by the user (e.g., patient, volunteer).

6.4 Experimental Validation

For evaluation of the adaptation method, the hypothesis was tested whether a stronger, more stable grasp can be achieved when stimulating with adaptive VEs rather than with one static VE during forearm rotations. Additionally, open-loop adaptation was compared with closed-loop adaptation of the stimulation intensity.

The stimulator with demultiplexer was used together with the 35-element EA placed over the finger flexors and one counter electrode, as seen in Fig. 6.2. Because only one EA was utilized in this test setup, all 35 elements on the flexor-array were available (cf. *Section* 3.3).

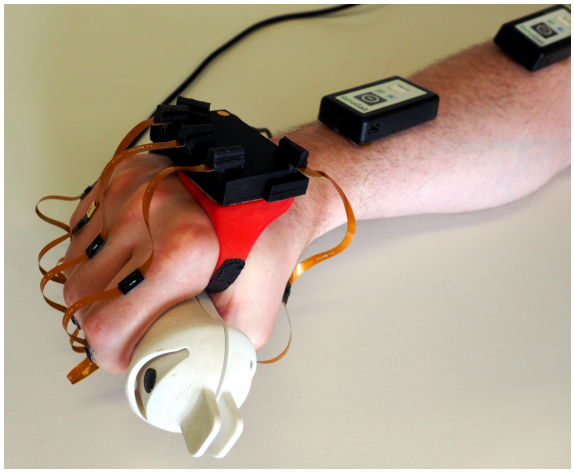

Figure 6.4: The utilized sensor setup with HSS and *Pablo* sensor handle. Five sensor strips, one on each finger, were utilized together with two IMUs on the forearm.

The HSS was employed with two wireless sensors on the forearm to track forearm rotation, as shown in the picture in Fig. 6.4. Additionally, a force sensor was used for measuring the strength of grasp and hand opening (*Pablo*; Tyromotion GmbH, Graz, Austria). The force sensor handle was covered with foam foil to increase the elasticity of the surface. Active element configurations (i.e., the VE) were changed with the frequency of the stimulation, here 33 Hz. The other stimulation settings were applied accordingly to *Section* 3.2. The complete experimental setup is illustrated in Fig. 6.2.

The joint angles were assessed in real-time via the HSS and Method M2 (cf. *Chapter* 4, *Section* 4.3.3). As the measurements were conducted in indoor environments, in the presence of magnetic disturbances, initial pose alignment had to be performed at the beginning of each measurement and was repeated in intervals of three minutes (cf. *Section* 4.3.3). The pose consisted of fingers F2–F5 and wrist being straight (angle ≈ 0) and the thumb abducted at a known angle (50°). It was possible to execute the alignment pose with the *Pablo* sensor handle being attached.

Four healthy volunteers participated in the experiments (female $= 1$, male $= 3$, age 31.8 ± 8.4). Written informed consent was obtained. All measurements were performed on the right forearm. The volunteers were instructed to avoid voluntary hand movements if not otherwise requested. They could not watch the measured force and grasp index during the measurement.

Each measurement consisted of an identification phase, where VEs for each forearm state (P, N, S) were selected, and an execution phase. In the latter, the volunteers were instructed to rotate their forearm continuously between the states pronation and supination for at least three iterations under different conditions: (i) without adaptation by steadily applying the VE identified in pronation (open-loop; standard approach), (ii) using the adaptation method with interpolated VEs with the initially identified, fixed stimulation intensity (open-loop), and (iii) using the adaptation method with interpolated VEs and feedback controlled stimulation intensity (closed-loop). The conditions were tested in random order, and volunteers were not informed about the applied condition during testing. Three volunteers performed conditions (i) and (ii), volunteer #4 performed all three conditions.

The performance in the execution phase was analyzed by calculating the mean and standard deviation of grasp force F measured with the *Pablo* handle over the measurement period of each condition. Furthermore, it was examined how often (in percent) the force F was lower than a critical value of 3 N, that corresponds to the possible release of an object.

To control the grasp force F by utilizing the grasp index C in condition (iii), it was necessary to identify the point of complete enclosure (PCE) of the object online in each measurement session, as the value will be slightly different for each subject and object. In the measurements, the *Pablo* sensor handle with foam foil served as the training object and could simultaneously measure the produced force to validate the grasp index. After the identification phase, electrical pulses with a ramp profile in the stimulation intensity are applied, starting from zero until the maximum tolerated intensity u_{tol}. The grasp index C is recorded for identified VEs in each forearm state to determine the PCE. Once the stimulation intensity is reached for the (PCE), there is a phase of smaller slope in C due to the resistance of the object. The beginning of this slope-change defines the starting value for the correlation range of grasp force F and grasp index C. The PCE and the corresponding stimulation intensity u_C were determined online from the recorded ramp profiles by calculating the curvature of C.

After initialization and determination of the PCEs for measurement condition (iii), three step responses of 2 s were recorded for the corresponding VE in each state z, to identify the first-order models G for each forearm state. The step consisted of a jump from the identified grasp stimulation level u_C up to the saved stimulation intensity of that VE. The data of each step was offset-removed before the model was fitted. Based on the identified model parameters, the PID controller K_2 was tuned as outlined in *Section* 6.3.

6.5 Results

Virtual electrodes were identified successfully for all volunteers in all three forearm states (P, N, and S). The identified VEs of each volunteer are presented in Fig. 6.5. No common pattern or path regarding the VE position $\mathbf{z}$ was found in this small group of subjects. The resulting grasp forces of all volunteers are compared for the standard approach (condition (i)) and the suggested VE adaptation method (condition (ii)) in Table 6.1. For each volunteer, the application of the VE adaptation led to the generation of a higher grasp force F compared to the standard approach. Furthermore, the automatic adaptation prevented F from falling beneath the critical value of 3 N for three of the volunteers.

Figure 6.6 displays the time courses of forearm rotation γ and grasp force C for the two conditions(i) and (ii) for one volunteer. For condition (i) in Fig. 6.6, the produced hand motion varies between grasp ($F > 0$) and hand opening ($F < 0$) when the standard stimulation is applied during rotation of the forearm. Besides, the generated response got unpredictable, as the VE determined in pronation did not always lead to the strongest force. Figure 6.6 for condition (ii) reveals that the adaptation of the VE parameters led to a stronger grasp force F. However, it seems that the achievable force decreased slowly over time in both conditions.

The hypothesis that compensation of decreasing response toward the electrical stimulation might be achieved via feedback-control was tested in volunteer #4 with measurement condition (iii). Figure 6.7 shows the results of the identification of the correlation range of grasp force F

Table 6.1: Comparison of stimulation intensity and generated grasp force F between the measurement conditions (i)–static VE and (ii)–real-time VE adaptation (open-loop). Mean and standard deviation of grasp force F are determined for the entire measurement period of each condition. F is given in Newton (N). Furthermore, the amount of time where the grasp force F was above the critical value of 3 N is presented in percentage of the measurement period. The lower the percentage, the better was the performance of the FES.

Subject	**Condition (i)—no adaptation**			**Condition (ii)—with adaptation**		
	$\hat{u}_{\mathrm{OL}}$	F	$F < 3\,\mathrm{N}$	$\hat{u}_{\mathrm{OL}}$	F	$F < 3\,\mathrm{N}$
#1	0.11	0.9 ± 1.9	87.5 %	0.11	9.1 ± 1.9	0.6 %
#2	0.19	1.4 ± 8.1	67.7 %	0.19	33.8 ± 5.1	0.0 %
#3	0.13	-0.5 ± 0.5	100.0 %	0.13	2.5 ± 1.4	63.9 %
#4	0.16	5.0 ± 3.0	32.0 %	0.18	10.1 ± 3.3	0.0 %
Average	**0.15**	**1.7±3.4**	**71.8 %**	**0.15**	**13.9±2.9**	**16.1 %**

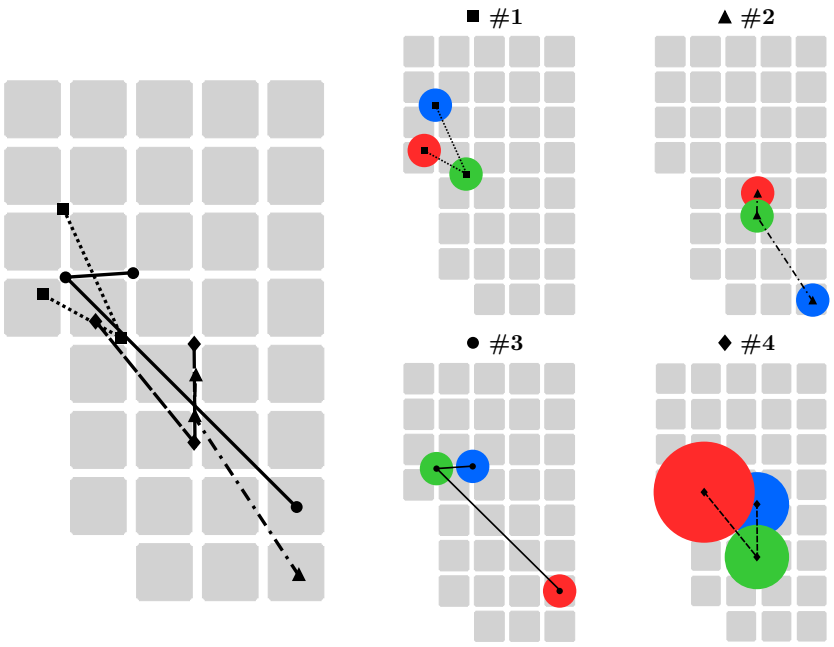

Figure 6.5: Identified VEs for grasping in the forearm states pronation (blue), neutral (green), and supination (red) for all four volunteers. The EA is displayed in top view when placed on the forearm (gel-layer at the bottom). The EA on the left summarizes the resulting VE paths of all volunteers when applying automatic VE adaptation. The feature of adjusting the size h of the VE was only utilized in volunteer #4.

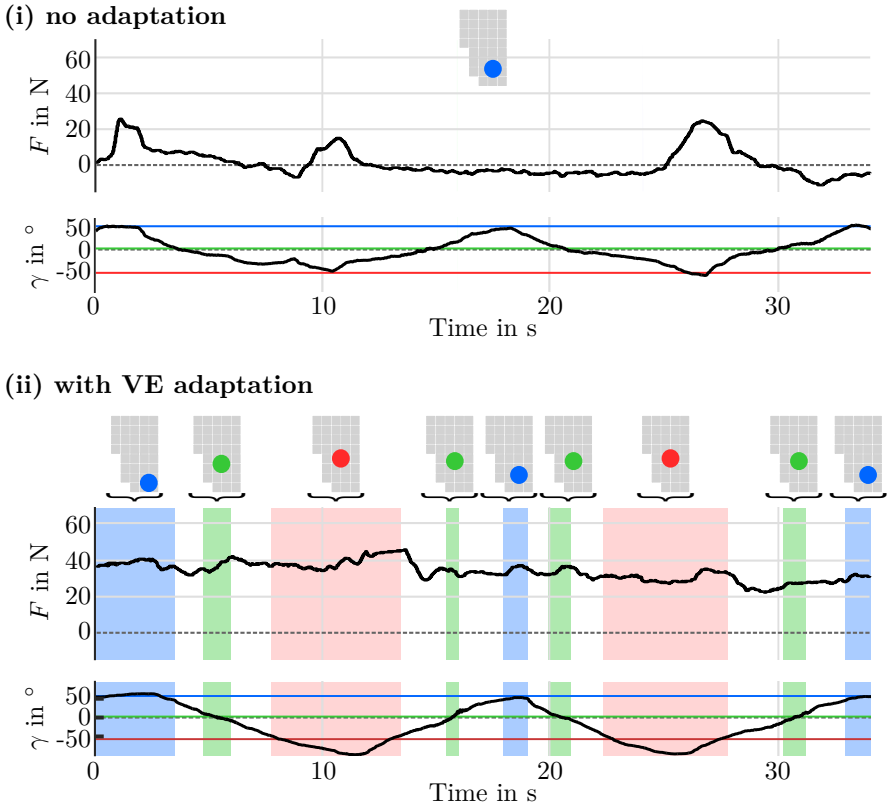

Figure 6.6: Results of volunteer #2 with conditions (i) constant VE ($p_a = p_\mathrm{P}$, green) and (ii) real-time VE adaptation. In the latter, the color blocks illustrate the classified forearm rotation states as introduced in Figs. 6.1 and 6.2. The applied VEs are depicted exemplarily in the top line for the discrete forearm states. The applied stimulation intensity $\hat{u}_\mathrm{OL}$ was constant in both cases (open-loop). Through the adaptation in (ii), the generated force F stayed positive, indicating grasping, at all times. The figure is reproduced from [288] with modifications.

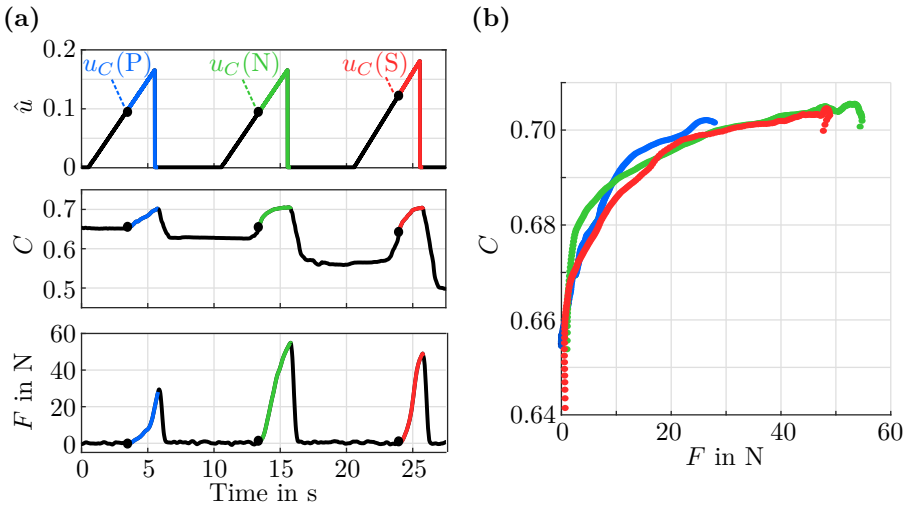

Figure 6.7: Identification measurement for the correlation range between grasp force F and grasp index C for all three VEs of volunteer #4. (a) The relevant sectors of the correlation range are marked according to the stimulated VE and forearm state: blue for pronation (P), green for neutral (N), and red for supination (S). The black dots indicate the PCEs and equal u_C. (b) The resulting relationship between grasp force F and grasp index C is nonlinear. The figure is reproduced from [288] with minor modifications.

and grasp index C using ramp profiles. The stimulation intensity u_C for complete enclosure of the object varied for the three forearm states, as seen in Fig. 6.7(a). Figure 6.7(b) reveals that a nonlinear relationship exists between F and C. Moreover, the relationship slightly differs for the three forearm states. For example, a force value of F=13 N corresponds with a grasp index of C=0.695 for p_a=p_P and of C=0.689 for p_a=p_S. This variance in the correlation between F and C is caused by small errors in the joint angle measurements, that especially arise when the forearm is in neutral position or close to it. These errors have been confirmed by placing the HSS on a static hand model that has been rotated in space.

The feedback control concept was therefore only tested for the static forearm state P, in which a drift-less grasp index measurement was possible. In contrast to the proposed procedure in *Sections* 6.3 and 6.4, only one step response with the forearm in pronation was recorded, and model parameters were estimated for condition (iii). The resulting model is depicted in Fig. 6.8. For the closed-loop experiment, the volunteer had his forearm in pronation and was instructed to relax arm and hand muscles. At distinct time points, the volunteer was asked to produce voluntary grasps, such that the feedback controller was forced to react. Exemplary results of this experiment are shown in Fig. 6.9. The controller responded to the voluntary grasping by decreasing the applied stimulation intensity $\hat{u}_\mathrm{CL}$ to its lower bound u_C. As soon as the volunteer released the handle, the controller increased the stimulation intensity to maintain the grasp by FES.

6.6 Discussion

For the first time in literature, an automatic real-time adaptation strategy for VEs in electrode arrays was successfully developed and evaluated for compensating variation in grasp strength due to forearm rotation. The generated grasp strength could be enhanced through open-

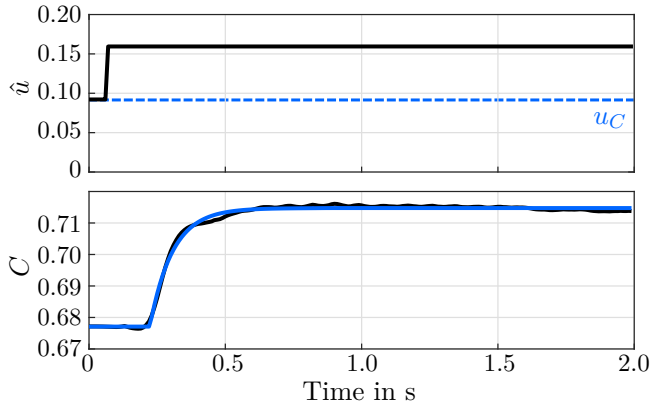

Figure 6.8: One step response and identified first-order model (solid blue line) for volunteer #4 in pronation. The determined model parameters were: $k = 0.39$, $T = 0.16$, $T_d = 0.09$. The figure is reproduced from [288] with minor modifications.

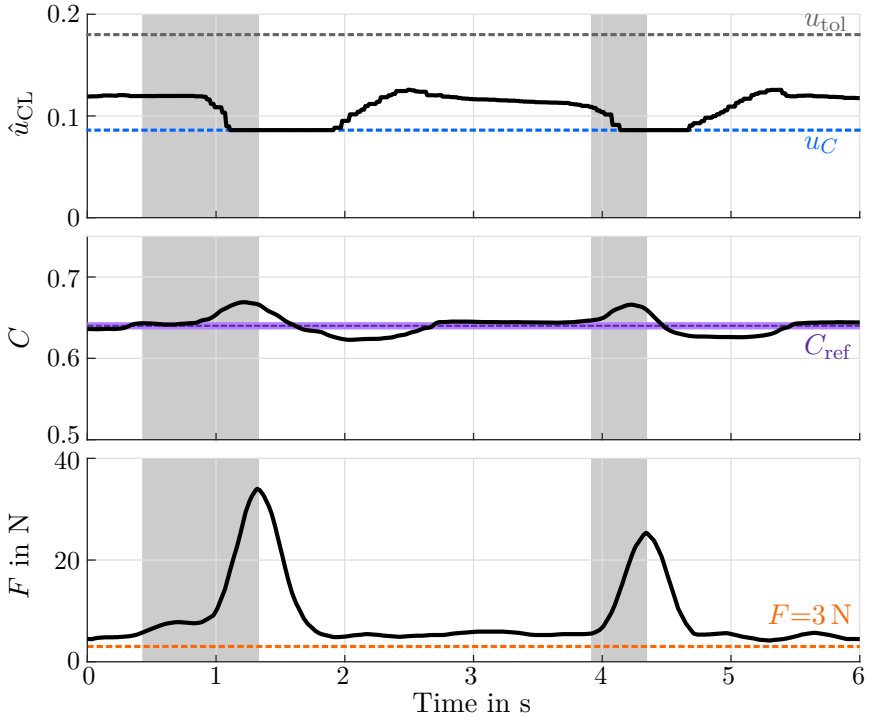

Figure 6.9: Closed-loop experiment for volunteer #4 with the forearm in pronation. The controller aims at keeping the grasp index C within the purple boundaries of the reference C_{ref}. The gray areas mark periods of voluntary grasp motion appearing as disturbances to the controller. The measured force F never fell below the critical value of 3 N (orange line). The figure is reproduced from [288] with minor modifications.

loop adaptation by about 800% on average, from 1.7 N to 13.9 N, compared to the standard stimulation with one constant VE at similar stimulation intensities. These results substantiate the reported necessity for an adaptation of the stimulation position in relation to the forearm rotation [182]. However, a slow decrease in the generated force was observed over time with adaptive open-loop stimulation, which might be due to the rapid onset of muscle fatigue [72].

It was further found that the response toward the stimulation with the VE identified in pronation (p_{P}) changed within states over time in condition (i). The generated grasp was sometimes stronger for other forearm states (N, S) than in state P, although it was stimulated with p_{P}. The reason for this is most likely the shift of muscles due to the evoked contractions and thereby differences in recruited motor units through stimulation over time [94].

In therapeutic and everyday applications of the HNP, it is necessary to guarantee that the grasping strength is sufficient over time, for example, when transporting an object from one location to another. Therefore, closed-loop control was employed to compensate changes of the time-variant system of FES and forearm, relying on the new control variable grasp index C representative for the grasp force F. A nonlinear correlation between C and F was obtained for each forearm state, but a lack in consistency over the whole range of forearm states occurred. The latter is caused by small errors in the measured flexion angles. In neutral forearm position, these angles are mainly determined by integration of the gyroscope outputs which possess a time-varying bias. Compensation of these errors by the acceleration measurements is not possible, as the gravitational vector is almost parallel to the flexion related joint axis. Therefore, the initial pose alignment (cf. *Section* 4.3.3), during which the bias is estimated, needs to be repeated more frequently, approximately every 30–60 s, in order to compensate a heading drift and gain a higher precision in the joint angles. This high frequency in alignment is, however, not practical. Currently, new methods are employed determining the relative heading of the IMUs in real time by optimization approaches in two-DOF joints [340].

Due to the limitation in the grasp index measurement, a proof-of-concept of the proposed closed-loop approach was presented only in pronation with one volunteer. The results revealed that the closed-loop approach could be integrated into a rehabilitation concept using a HNP, in which a dynamic change of the stimulation intensity will stabilize the generated force over longer tasks. Hence, effects such as muscle fatigue might be compensated up to the limit of the tolerated stimulation intensity (u_{tol}). Once the grasp index estimation via the HSS is improved, the measurement protocol should be repeated with more participants and patients to confirm the results. Another limitation of the conducted measurements is the inability of the suggested grasp index C to differentiate between active and passive finger movements. Changes in the grasp pattern over time (e.g., from power grasp to claw grasp) cannot be determined from the grasp index alone. Thus, an additional classifier that utilizes pattern recognition over all individual joint angles needs to be developed.

6.7 Conclusions and Future Research

To conclude, automatic adaptation methods are crucial for applications supporting therapeutic training and assistance in ADL with HNPs. The presented results revealed that an automatic real-time adaptation of virtual electrodes (size, position) and stimulation intensity in EAs

can be used to guarantee a sufficient grasp strength during forearm movements. The large variance in the found VE positions between subjects underlines the need for electrode arrays and individual VE identification for FES-induced hand movements [320]. Using real-time motion tracking as a measurement for grasp strength in feedback-control was shown to be a promising approach. However, the precision of the HSS needs to be further improved before this correlation of force and motion can be used in hand therapy.

In the future, the experimental setup should be extended to stimulate wrist extensors in parallel with finger flexors to generate a more natural grasp pattern [39]. An in-depth study with patients could provide more insights into the relation of the shift in stimulation point and forearm rotation.

Besides the further development of the HSS, it is planned to integrate an intelligent touch object into the setup of the HNP. The object, a wooden cube of size $5 \times 5\,\text{cm}$, detects via five capacitive touch sensors which faces of the cube are in contact with the human hand and communicates this wirelessly to the HSS. The touch sensors can detect small changes in the electrical capacitance of an isolated metal surface that occur when a human finger is near the metal surface. The detection can be tuned to work even through 3 mm thick plywood, which covers the exterior of the cube. This information might be used in the future to determine the onset and offset of feedback-control (PCE).

7

General Discussion and Conclusion

7.1 Summary

This dissertation aimed at deriving a novel adaptive hand neuroprosthesis using transcutaneous FES technology that increases the acceptance and usage of this technology in clinical practice. Automation, closed-loop control, and user-centered design were identified as crucial and utilized to achieve this goal. The target patient group are stroke survivors suffering from partial or complete paralysis in hand function. The subsequent paragraphs briefly summarize the achievements of this thesis.

A broad literature review was performed, revealing the challenges with existing systems in clinical practice. Selective stimulation with electrode arrays suffers from exhaustive setup times or insufficient user integration, hindering the use in FES-assisted rehabilitation so far. Flexibility in control strategies, adaptive levels of support with regard to the patient's capabilities, as well as the continuous adaptation of the ES during operation to guarantee the completion of movements still lack in available systems.

Precise hand motion tracking in real time was identified as a key element for automatic adaptation and feedback-control of HNPs. Therefore, this work suggested a novel hand sensor system based on inertial sensors with algorithms for the robust measurement of joint angles and fingertip positions in indoor environments. The modular design of the sensor system facilitates an individual adaption to diverse therapy setups. The HSS was evaluated on four able-bodied subjects in different scenarios and utilized for virtual electrode identification and automatic adaptation for grasping.

Chapter 5 of this thesis offered two array identification procedures to address the challenge of selectively activating desired motor nerves by surface FES for generating functional hand motion. For the first time, identification methods with different levels of user integration were realized and directly compared: The semi-automatic search facilitates a convenient, supported manual search in which the decision on the selected virtual electrodes stayed with the users; the fully automatic search evaluates suitable VEs autonomously and makes suggestions from which the users can choose. A user-centered evaluation in early-stroke rehabilitation with patients and

health professionals allowed the assessment of the clinical practicability of the two approaches. The results showed that both identification methods—semi-automatic and automatic—yield suitable VEs for hand opening and, with limitation, for hand closing. The users accepted both methods. A possible combination of both methods appears particularly promising to improve the initial setup of the system and to deal with subsequent daily fluctuations in the stimulation parameters in a convenient way.

Problems with ensuring a sufficient grasping strength during exercises with the HNPs under varying forearm conditions were often discussed in the literature to be solved with EA technology. Yet, complete solutions with matching hard- and software were never presented. In this thesis, a method for automatic real-time adjustment of electrode positions was developed in *Chapter* 6. The rotation angle of the forearm is assessed via two inertial sensors. Depending on this angle, the active VE is adjusted through linear interpolation between previously identified VEs in pronation, neutral forearm rotation, and supination. Experiments in healthy volunteers, blinded to the stimulation, revealed that the generated grasp strength could be enhanced through open-loop adaptation by about 800% on average compared to the standard stimulation with one constant VE. Closed-loop control of the stimulation intensity was employed to stabilize the evoked grasp strength throughout sessions. A correlation between the measured joint angles with the HSS and grip force was accomplished but was limited to static forearm postures. Nevertheless, the results revealed that closed-loop control should be integrated into FES rehabilitation systems to establish assist-as-needed support.

In summary, a set of new methods for hand rehabilitation with HNPs are provided within this thesis addressing customization of electrical stimulation and automatic adaptation. By increasing the convenience in usage and the accuracy of FES-induced motion, the presented methods have the potential to improve patients' motivation for using FES in rehabilitation of hand function.

Several, method-specific questions have already been considered in the discussion sections of the individual chapters. The same applies to recommendations and future perspectives mentioned in the conclusion sections. In this final chapter, these aspects are summarized and discussed in a broader sense with respect to the overarching topic of the dissertation, the use of neuroprostheses for supporting and assisting rehabilitation exercises in regaining hand function.

7.2 General Discussion

The requirements on HNPs from users' perspectives are manifold and often possess contradictory characteristics. However, some demands are essential for the noninvasive application in clinical practice, such as an easy and fast donning of the system, quick initialization, low costs, and hygiene aspects. The established HNP takes many aspects into account. For example, the sensor system can be used with spastic hands, it preserves the sense of touch, it fits all average hand sizes, and its modular design facilitates adaptation to different therapy setups. The EAs can be applied on the left and right arm to reduce manufacturing and thereby overall application costs. Usability engineering techniques were used to increase the ease of use of selective stimulation with EAs. The automatic VE adaptation will improve the

performance in FES grasping in tasks requiring forearm rotations and may thereby raise the patient's motivation. All these factors promote acceptance of FES technology in clinical hand rehabilitation.

In favor of establishing a reliable and adaptive system, not all requirements could be met. The new HNP comprises many wires connecting the electrodes with the stimulator, the sensor system with the computer, etc. The wires simplify the communication between the different system components, but they also restrict the range of motion. Wireless data connections between stimulator, sensor system, and a smart device might solve this issue in the future. Other approaches in the literature suggest the use of optical, contact-free motion tracking to reduce the setup time of the sensor system at the expense of the system's portability (e.g., [131, 143]). The decision for incorporating motion tracking as a control signal contradicts the requirement on the HNP reacting at a temporal resolution as close as possible to physiological motion generation. However, a combination with other biological signals, such as EMG or EEG, would further expand the hardware setup and would require additional initialization steps. The balance between a high degree of automation and low effort in the sensor setup remains the subject of future research.

The precision and accuracy of the proposed methods for IMU-based hand motion tracking under laboratory conditions are comparable to the accuracy reported in the literature [133, 135]. Nevertheless, it is not yet adequate to establish a stable relationship with grasping strength under varying forearm conditions in indoor environments. Small errors in the measured joint angles were the result of a time-varying bias of the IMUs' gyroscopes. These errors do not pose a problem for the automatic identification of appropriate VEs in *Chapter* 5 or motion-based feedback-control. However, they did not allow closed-loop control of grasped force based on the HSS for varying measurement conditions through rotation of the forearm in *Chapter* 6. A frequent, periodic reset of the bias estimation by performing the initial pose alignment approximately every minute as a solution for this issue seems not practical in clinical setups. Therefore, magnetometer measurements would be necessary for compensation in specific forearm orientations. However, the results in *Chapter* 4 proved that magnetometer-based methods are not reliable in magnetically disturbed environments found in practice.

An important feasibility aspect of FES on the forearm is the required search time for individual stimulation positions. The results of multiple studies (e.g., [54, 92, 168]) and of this thesis underline the existence of inter-subject variability in neuroanatomy and tolerance. Consequently, the individual adjustment of spatial and temporal stimulation parameters is obligatory. The required search time of approximately ten minutes with the presented VE identification methods for hand opening and grasping might still be too long in the context of clinical therapy sessions, usually taking between 30–45 minutes in Germany. Additionally, the identification effort increases when multiple forearm positions shall be tested as necessary for the established automatic VE adaptation to forearm movements. This effort can only be justified if the identification does not need to be repeated in every therapy session of an individual patient. It was suggested that stimulation parameters from previous measurements of a patient should be used as a priori knowledge or as starting points for following interventions [168]. In this application scenario, the presented semi-automatic identification approach would be a suitable tool to gradually modify stored VEs of previous sessions if necessary. The gradual,

convenient modification is a benefit in comparison with existent, fully automatic methods. Therefore, future investigations on VE identification strategies should have a study design with multiple sessions in each subject.

In general, the lack in synchronization and adaptation of the ES in the sense of a natural motor control lead to a limited acceptance of available HNPs by affected patients. A quick and easy adjustment of stimulation parameters in real time can compensate motion-dependent and time-variant changes of the neuromuscular system. This adaptation is necessary to guarantee sufficient FES-support of motion in diverse situations and over time. Only by improving the reliability of HNPs and thereby offering benefits to conventional therapy, therapists and patients will be motivated to actually use the technology. The automatic VE adaptation to forearm movements established in this thesis will guarantee sufficient grasping strength for holding objects with HNPs. Although the proposed grasp index cannot differentiate between active and passive finger movements, this new degree of automation will increase the performance in FES grasping. Additional measurements such as pressure/force sensors placed on the fingertips or intelligent objects might help to improve the precision in the future.

As the synchronization of the onset and offset of the stimulation was addressed by numerous researchers before (e.g., [24, 109, 123, 265]; see *Section* 2.5.3), it was not treated in this thesis. Future progress on this topic is most likely achieved through hybrid control with a combination of various sensor and signal types. In the presented system, this could be obtained by adding intelligent touch objects, measuring contact information, and force. This information could be used to determine the onset of FES support for patients with remaining, weak volitional hand function. First own attempts were made to combine motion tracking with the HSS and biological signals, namely EMG, to establish intention recognition for FES control via a state machine [285]. Preliminary results revealed that a combination of motion tracking and EMG yields higher reliability and temporal resolution of the classification, possibly enabling physiological control of FES-induced movements. The development of such strategies will be necessary to engage patients in FES-based rehabilitation actively.

Besides the discussed aspects, the presented work is subject to limitations of different nature, which are listed in the following paragraphs. First of all, this work focuses on FES solutions for rehabilitation and assistance of wrist and finger motion and neglects disabilities in shoulder and elbow function. A holistic rehabilitation approach to increase the performance of patients in ADL, and thereby encourage their independence, should include a combination with support systems for the upper arm [282], for example, through additional FES or robotics (e.g., [40, 131, 269]). Consequently, the total setup time of such a multi-support system will increase, due to donning and initialization of the extra components.

A second limitation is the reduced number of neurologically impaired subjects included in the experiments. It turned out that scheduling experiments in early stroke rehabilitation is an especially challenging process. At this stage, patients are in a physically bad, new situation and are only available for measurements on short notice. Furthermore, the experiments disturb the clinical routine of both patients and health professionals. After approximately 7–21 days, the stroke patients of the collaborating hospital—Unfallkrankenhaus Berlin—went to rehabilitation at different institutions across the country, making follow-up experiments on the recruited patients unworkable. For these reasons, only five patients were included in this thesis. Further

measurements were conducted exclusively in healthy volunteers to evaluate the feasibility and advantages of the new methods. Nevertheless, these investigations have laid the foundation for future clinical studies by uncovering and correcting problems of the first generation.

The recruited patients received FES for the first time. The tolerance of the ES was a problem when stimulating on the ventral side of the forearm, limiting the analysis of suitable stimulation points for grasping. Moreover, stabilization of the wrist could not always be achieved with the utilized electrode setup and suggested identification methods. These observations indicate that other methods for pain management and different electrode array layouts should be explored in the future. Noninvasive proximal nerve stimulation of the ulnar and median nerve has recently been demonstrated as an alternative for eliciting various hand grasp patterns with low, tolerable current intensities of less than 5 mA [341].

7.3 General Conclusions and Future Research

The presented thesis has shown that advanced hand motion tracking, electrode array technologies, and automated adaptation of stimulation parameters can increase the benefits and applicability of noninvasive, state-of-the-art hand neuroprostheses. The new system facilitates the automatic adjustment of stimulation parameters regarding electrode configuration and intensity to the individual patient and forearm movements. Furthermore, the flexibility in system components allows overcoming inter-individual physiological variability. Thereby, the thesis addressed the central question of how the acceptance of EA-based HNPs can be improved in clinical practice. The derived recommendations for future FES systems are presented in the following three paragraphs.

Methods are recommended that are, on the one hand, simple to apply, in the sense that they can be used intuitively and without much effort. On the other hand, they should apply FES physiologically and task-specifically. The latter requires a high degree of automation and closed-loop control, which consequently yields a more intensive setup. Solutions in which the load is shared between the users and the technical system, as it is the case in the presented semi-automatic VE identification, are most promising to increase the acceptance through the balance of user integration and support. It is necessary to keep the final decision authority on system parameters to patients and treating health professionals.

Customization and high flexibility of rehabilitation systems are essential for the future of FES-based therapy. For example, the user-centered evaluation of the two identification methods revealed that patients and health professionals accept both methods. However, each person may favor the one over the other. This finding supports the statement made earlier that various grasping and command strategies should be available in new HNPs to adapt to individual needs and therapy goals of a patient. Future feasibility studies on practical FES approaches should always include detailed information on the required time for donning/doffing and initialization of the system in the clinical course of action. Besides, the term “functional point,” introduced in [94], is recommended for future investigations of suitable stimulation positions in EA technology. It was found that multiple activation areas exist on the forearm evoking comparable functional movements, and they are subject to change depending on the forearm rotation. Hence, the term “optimal stimulation point” can be misleading.

The visualization in the GUI turned out to play an important role in the users' perception of the methods. Hence, an intuitive, user-friendly GUI, tailored to the particular purpose, is crucial for their acceptance. It is recommended that future FES technologies are always evaluated in combination with their operation interface for clinical use, even in early development stages [336]. User workshops and training with GUI prototypes ("click prototypes") are tools that help to identify misleading workflows and instructions at this stage [325].

The presented methods provide a good proof-of-concept for an adaptive HNP. Yet, the results of the preliminary validation pose particular demands toward a stable and reliable setup for clinical rehabilitation. In the following, suggestions are given on how the presented FES system can be enhanced in the future. For the hand sensor system, the improvement of the accuracy and long-time stability of magnetometer-free motion tracking should be in the focus of future investigations. First efforts regarding this issue have already been made at the Control Systems Group at Technische Universität Berlin [150, 312, 340]. Further, the optimization of sensor hardware in terms of dimensions, weight, wireless IMUs, and higher sampling rates will increase the usability of inertial motion tracking for HNPs. Despite the provided grasp index to access grasping strength, the force could be measured by integrating force sensors in the HSS. However, first attempts revealed that it is a non-trivial task to interpret the measured force due to nonlinear relationships and varying contact points depending on the grasping type.

Once the grasp index estimation via the HSS is improved, the VE adaptation with closed-loop control should be studied with stroke and SCI patients to confirm the achieved results. Besides, the experimental setup should be extended to stimulate wrist extensors in parallel with finger flexors to generate a more natural grasp pattern [39]. An in-depth study with patients could provide more insights into the relation of the shift in stimulation point and forearm rotation, which could help to speed up the identification phase. The employed closed-loop control approach utilizes static controller parameters. In the future, strategies such as iterative learning control to continuously improve the controller performance could be explored [248].

In conclusion, the presented concepts and methods in this thesis contribute to a higher degree of automation, adaptation, and usability of HNPs. Thereby, the accuracy of FES-induced motion will be improved, potentially raising the acceptance of HNPs in clinical practice. Through future efforts in the demonstrated areas of flexible system design, closed-loop control of motion, and user integration, the appeal of incorporating FES-based technology in neurorehabilitation will be further enhanced. In this way, automated HNPs may facilitate a higher intensity and frequency of therapy and, thus, promote the motor recovery of stroke survivors.

References

[1] M. A. Busch and R. Kuhnert, "12-Monats-Prävalenz von Schlaganfall oder chronischen Beschwerden infolge eines Schlaganfalls in Deutschland", *Journal of Health Monitoring*, vol. 2, no. 1, pp. 70–76, 2017. DOI: 10.17886/RKI-GBE-2017-010.

[2] Robert-Koch-Institut, Ed., *Gesundheit in Deutschland. Gesundheitsberichterstattung des Bundes. Gemeinsam getragen von RKI und Destatis*. Berlin, Germany: RKI, 2015, ISBN: 978-3-89606-225-3. DOI: 10.17886/rkipubl-2015-003.

[3] D. Plass, T. Vos, C. Hornberg, C. Scheidt-Nave, H. Zeeb, and A. Krämer, "Trends in disease burden in Germany: Results, implications and limitations of the global burden of disease study", *Deutsches Ärzteblatt International*, vol. 111, no. 38, pp. 629–638, 2014. DOI: 10.3238/arztebl.2014.0629.

[4] N. J. Kassebaum, M. Arora, R. M. Barber, Z. A. Bhutta, J. Brown, A. Carter, *et al.*, "Global, regional, and national disability-adjusted life-years (dalys) for 315 diseases and injuries and healthy life expectancy (hale), 1990–2015: A systematic analysis for the global burden of disease study 2015", *The Lancet*, vol. 388, no. 10053, pp. 1603–1658, 2016. DOI: 10.1016/S0140-6736(16)31460-X.

[5] G. J. Hankey, "Stroke", *The Lancet*, vol. 389, no. 10069, pp. 641–654, 2017. DOI: 10.1016/S0140-6736(16)30962-X.

[6] T. Truelsen, B. Piechowski-Jóźwiak, R. Bonita, C. Mathers, J. Bogousslavsky, and G. Boysen, "Stroke incidence and prevalence in Europe: A review of available data", *European Journal of Neurology*, vol. 13, no. 6, pp. 581–598, 2006. DOI: 10.1111/j.1468-1331.2006.01138.x.

[7] B. B. Johansson, "Brain plasticity and stroke rehabilitation: The Willis lecture", *Stroke*, vol. 31, no. 1, pp. 223–230, 2000. DOI: 10.1161/01.STR.31.1.223.

[8] S. Knecht, S. Hesse, and P. Oster, "Rehabilitation after stroke", *Deutsches Ärzteblatt International*, vol. 108, no. 36, pp. 600–606, 2011. DOI: 10.3238/arztebl.2011.0600.

[9] G. Kwakkel, R. van Peppen, R. C. Wagenaar, S. W. Dauphinee, C. Richards, A. Ashburn, *et al.*, "Effects of augmented exercise therapy time after stroke", *Stroke*, vol. 35, no. 11, pp. 2529–2539, 2004. DOI: 10.1161/01.STR.0000143153.76460.7d.

[10] G. E. Conti and S. L. Schepens, "Changes in hemiplegic grasp following distributed repetitive intervention: A case series", *Occupational Therapy International*, vol. 16, no. 3–4, pp. 204–217, 2009. DOI: 10.1002/oti.276.

[11] P. Langhorne, F. Coupar, and A. Pollock, "Motor recovery after stroke: A systematic review", *The Lancet Neurology*, vol. 8, no. 8, pp. 741–754, 2009. DOI: 10.1016/S1474-4422(09)70150-4.

[12] T. Platz and S. Roschka, *Rehabilitative Therapie bei Armlähmungen nach einem Schlaganfall: Patientenversion der Leitlinie der Deutschen Gesellschaft für Neurorehabilitation*. Bad Honnef, Germany: Hippocampus-Verlag, 2011, ISBN: 978-3-936817-82-9.

[13] T. Schauer, "Sensing motion and muscle activity for feedback control of functional electrical stimulation: Ten years of experience in Berlin", *Annual Reviews in Control*, vol. 44, pp. 355–374, 2017. DOI: 10.1016/j.arcontrol.2017.09.014.

[14] D. Statistisches Bundesamt, Ed., *Statistik der schwerbehinderten Menschen 2015 - Kurzbericht*. Wiesbaden, Germany: Destatis, Feb. 2017.

[15] T. Platz, "Evidenzbasierte Konzepte der motorischen Rehabilitation: Ergotherapie und Physiotherapie", in *Die neurologisch-neurochirurgische Frührehabilitation*, J. D. Rollnik, Ed., Berlin/Heidelberg, Germany: Springer, 2013, pp. 131–154. DOI: 10.1007/978-3-642-24886-3_10.

[16] A. Curt, "Neurotraumatologie und Erkrankungen von Wirbelsäule und Nervenwurzel– Querschnittlähmung", in *Leitlinien für Diagnostik und Therapie in der Neurologie*, H. C. Diener, C. Weimar, P. Berlit, G. Deuschl, C. Elger, R. Gold, *et al.*, Eds., 5th. Stuttgart, Germany: Thieme, 2012, pp. 878–886. DOI: 10.1055/b-0034-37854.

[17] A. Bryden, A. Sinnott, and M. J. Mulcahey, "Innovative strategies for improving upper extremity function in tetraplegia and considerations in measuring functional outcomes", *Topics in Spinal Cord Injury Rehabilitation*, vol. 10, no. 4, pp. 75–93, 2005. DOI: 10.1310/LN94-NMVK-59V3-CC1F.

[18] R. Rupp and H. J. Gerner, "Neuroprosthetics of the upper extremity–clinical application in spinal cord injury and future perspectives", *Biomedizinische Technik/Biomedical Engineering*, vol. 49, no. 4, pp. 93–98, 2004. DOI: 10.1515/BMT.2004.019.

[19] A. M. Bryden, A. E. Peljovich, H. A. Hoyen, G. Nemunaitis, K. L. Kilgore, and M. W. Keith, "Surgical restoration of arm and hand function in people with tetraplegia", *Topics in Spinal Cord Injury Rehabilitation*, vol. 18, no. 1, pp. 43–49, 2012. DOI: 10.1310/sci1801-43.

[20] K. E. Musselman, M. Shah, and J. Zariffa, "Rehabilitation technologies and interventions for individuals with spinal cord injury: Translational potential of current trends", *Journal of NeuroEngineering and Rehabilitation*, vol. 15, no. 1, p. 40, 2018. DOI: 10.1186/s12984-018-0386-7.

[21] J. M. Veerbeek, E. van Wegen, R. van Peppen, P. J. van der Wees, E. Hendriks, M. Rietberg, and G. Kwakkel, "What is the evidence for physical therapy poststroke? A systematic review and meta-analysis", *PLOS ONE*, vol. 9, no. 2, e87987, 2014. DOI: 10.1371/journal.pone.0087987.

[22] H. F. M. van der Loos, D. J. Reinkensmeyer, and E. Guglielmelli, "Rehabilitation and health care robotics", in *Springer Handbook of Robotics*, B. Siciliano and O. Khatib, Eds., Cham, Switzerland: Springer, 2016, pp. 1685–1728. DOI: 10.1007/978-3-319-32552-1_64.

[23] H. I. Krebs and B. T. Volpe, "Chapter 23 - Rehabilitation robotics", in *Neurological Rehabilitation*, ser. Handbook of clinical neurology, M. P. Barnes and D. C. Good, Eds., vol. 110, Amsterdam, Netherlands: Elsevier, 2013, pp. 283–294. DOI: 10.1016/B978-0-444-52901-5.00023-X.

[24] T. Keller, "Surface functional electrical stimulation (FES) neuroprostheses for grasping", PhD thesis, Swiss Federal Institute of Technology Zürich, Zürich, Switzerland, 2002. DOI: 10.3929/ethz-a-004278166.

[25] B. M. Doucet, A. Lam, and L. Griffin, "Neuromuscular electrical stimulation for skeletal muscle function", *The Yale Journal of Biology and Medicine*, vol. 85, no. 2, p. 201, 2012.

[26] P. H. Peckham and J. S. Knutson, "Functional electrical stimulation for neuromuscular applications", *Annual Review of Biomedical Engineering*, vol. 7, pp. 327–360, 2005. DOI: 10.1146/annurev.bioeng.6.040803.140103.

[27] M. W. Keith, P. H. Peckham, G. B. Thrope, K. C. Stroh, B. Smith, J. R. Buckett, K. L. Kilgore, and J. W. Jatich, "Implantable functional neuromuscular stimulation in the tetraplegic hand", *The Journal of Hand Surgery*, vol. 14, no. 3, pp. 524–530, 1989. DOI: 10.1016/S0363-5023(89)80017-6.

[28] M. J. Ijzerman, T. S. Stoffers, M. A. P. Klatte, G. J. Snoek, J. H. C. Vorsteveld, R. H. Nathan, and H. J. Hermens, "The NESS handmaster orthosis: Restoration of hand function in C5 and stroke patients by means of electrical stimulation", *Journal of Rehabilitation Sciences*, vol. 9, no. 3, pp. 86–89, 1996.

[29] R. Rupp, A. Kreilinger, M. Rohm, V. Kaiser, and G. R. Müller-Putz, "Development of a non-invasive, multifunctional grasp neuroprosthesis and its evaluation in an individual with a high spinal cord injury", in *Proceedings 34th International Conference IEEE Engineering in Medicine and Biology Society (EMBC)*, (San Diego, CA, USA), IEEE, Aug. 2012, pp. 1835–1838. DOI: 10.1109/EMBC.2012.6346308.

[30] J. S. Petrofsky, H. Heaton III, and C. A. Phillips, "Outdoor bicycle for exercise in paraplegics and quadriplegics", *Journal of Biomedical Engineering*, vol. 5, no. 4, pp. 292–296, 1983. DOI: 10.1016/0141-5425(83)90003-1.

[31] M. Maležić, S. Hesse, H. Schewe, and K.-H. Mauritz, "Restoration of standing, weight-shift and gait by multichannel electrical stimulation in hemiparetic patients", *International Journal of Rehabilitation Research*, vol. 17, no. 2, pp. 169–179, 1994.

[32] T. Seel, S. Schäperkötter, M. Valtin, C. Werner, and T. Schauer, "Design and control of an adaptive peroneal stimulator with inertial sensor-based gait phase detection", in *Proceedings 18th Annual Conference of the International FES Society (IFESS)*, (Donostia-San Sebastián, Spain), 2013, pp. 6–8.

[33] T. Keller, N. Malešević, and G. Bijelić, *System for functional electrical stimulation*, EU Patent EP 3 154 627 B1, Apr. 2017.

[34] P. L. Melo, M. T. Silva, J. M. Martins, and D. J. Newman, "Technical developments of functional electrical stimulation to correct drop foot: Sensing, actuation and control strategies", *Clinical Biomechanics*, vol. 30, no. 2, pp. 101–113, 2015. DOI: 10.1016/j.clinbiomech.2014.11.007.

[35] J. H. Burridge and M. Ladouceur, "Clinical and therapeutic applications of neuromuscular stimulation: A review of current use and speculation into future developments", *Neuromodulation: Technology at the Neural Interface*, vol. 4, no. 4, pp. 147–154, 2001. DOI: 10.1046/j.1525-1403.2001.00147.x.

[36] A. Basteris, S. M. Nijenhuis, A. H. A. Stienen, J. H. Buurke, G. B. Prange, and F. Amirabdollahian, "Training modalities in robot-mediated upper limb rehabilitation in stroke: A framework for classification based on a systematic review", *Journal of NeuroEngineering and Rehabilitation*, vol. 11, no. 1, p. 111, 2014. DOI: 10.1186/1743-0003-11-111.

[37] C. Sicuri, G. Porcellini, and G. Merolla, "Robotics in shoulder rehabilitation", *Muscles, Ligaments and Tendons Journal*, vol. 4, no. 2, pp. 207–213, 2014.

[38] L. Pignolo, "Robotics in neuro-rehabilitation", *Journal of Rehabilitation Medicine*, vol. 41, no. 12, pp. 955–960, 2009. DOI: 10.2340/16501977-0434.

[39] M. R. Popović, D. B. Popović, and T. Keller, "Neuroprostheses for grasping", *Neurological Research*, vol. 24, no. 5, pp. 443–452, 2002. DOI: 10.1179/016164102101200311.

[40] A. Pedrocchi, S. Ferrante, E. Ambrosini, M. Gandolla, C. Casellato, T. Schauer, *et al.*, "MUNDUS project: Multimodal neuroprosthesis for daily upper limb support", *Journal of NeuroEngineering and Rehabilitation*, vol. 10, no. 1, p. 66, 2013. DOI: 10.1186/1743-0003-10-66.

[41] G. R. Müller-Putz, P. Ofner, A. Schwarz, J. Pereira, G. Luzhnica, C. di Sciascio, *et al.*, "MoreGrasp: Restoration of upper limb function in individuals with high spinal cord injury by multimodal neuroprostheses for interaction in daily activities", in *Proceedings 7th Graz Brain-Computer Interface Conference*, (Graz, Austria), Sep. 2017, pp. 338–343. DOI: 10.3217/978-3-85125-533-1-62.

[42] A. Crema, N. Malešević, I. Furfaro, F. Raschellà, A. Pedrocchi, and S. Micera, "A wearable multi-site system for NMES-based hand function restoration", *IEEE Transactions on Neural Systems and Rehabilitation Engineering*, vol. 26, no. 2, pp. 428–440, 2018. DOI: 10.1109/TNSRE.2017.2703151.

[43] K. D. Anderson, "Targeting recovery: Priorities of the spinal cord-injured population", *Journal of Neurotrauma*, vol. 21, no. 10, pp. 1371–1383, 2004. DOI: 10.1089/neu.2004.21.1371.

[44] J. McCabe, M. Monkiewicz, J. Holcomb, S. Pundik, and J. J. Daly, "Comparison of robotics, functional electrical stimulation, and motor learning methods for treatment of persistent upper extremity dysfunction after stroke: A randomized controlled trial", *Archives of Physical Medicine and Rehabilitation*, vol. 96, no. 6, pp. 981–990, 2015. DOI: 10.1016/j.apmr.2014.10.022.

[45] O. A. Howlett, N. A. Lannin, L. Ada, and C. McKinstry, "Functional electrical stimulation improves activity after stroke: A systematic review with meta-analysis", *Archives of Physical Medicine and Rehabilitation*, vol. 96, no. 5, pp. 934–943, 2015. DOI: 10.1016/j.apmr.2015.01.013.

[46] C. R. Mason, J. E. Gomez, and T. J. Ebner, "Hand synergies during reach-to-grasp", *Journal of Neurophysiology*, vol. 86, no. 6, pp. 2896–2910, 2001. DOI: 10.1152/jn.2001.86.6.2896.

[47] G. Aumüller, G. Aust, A. Doll, J. Engele, J. Kirsch, S. Mense, *et al.*, *Anatomie*, 1st, ser. Duale Reihe. Stuttgart, Germany: Thieme, 2007, ISBN: 978-3-13136-043-4.

[48] S. Cobos, M. Ferre, M. S. A. Uran, J. Ortego, and C. Pena, "Efficient human hand kinematics for manipulation tasks", in *Proceedings IEEE/RSJ International Conference International Conference on Intelligent Robots and Systems (IROS)*, (Nice, France), 2008. DOI: 10.1109/IROS.2008.4651053.

[49] S. Cobos, M. Ferre, R. Aracil, J. Ortego, and M. Angel, "Simplified Human Hand Models for Manipulation Tasks", in *Cutting Edge Robotics 2010*, V. Kordic, Ed., InTech, 2010. DOI: 10.5772/10326.

[50] H. Gray and W. H. Lewis, *Anatomy of the human body*, 20th. Philadelphia / New York, USA: Lea & Febiger / Bartleby.com, 1918.

[51] C. Salchow-Hömmen, L. Callies, L. Daniel, M. Valtin, T. Schauer, and T. Seel, "A tangible solution for hand motion tracking in clinical applications", *Sensors*, vol. 19, no. 1, p. 208, 2019. DOI: 10.3390/s19010208.

[52] C. L. Taylor and R. J. Schwarz, "The anatomy and mechanics of the human hand", *Artificial Limbs*, vol. 2, no. 2, pp. 22–35, 1955.

[53] T. L. McIsaac and A. J. Fuglevand, "Motor-unit synchrony within and across compartments of the human flexor digitorum superficialis", *Journal of Neurophysiology*, vol. 97, no. 1, pp. 550–556, 2007. DOI: 10.1152/jn.01071.2006.

[54] M. Lawrence, "Transcutaneous electrode technology for neuroprostheses", PhD thesis, Swiss Federal Institute of Technology Zürich, Zürich, Switzerland, 2009. DOI: 10.3929/ethz-a-005828341.

[55] C. Long, P. W. Conrad, E. A. Hall, and S. L. Furler, "Intrinsic-extrinsic muscle control of the hand in power grip and precision handling: An electromyographic study", *The Journal of Bone & Joint Surgery*, vol. 52, no. 5, pp. 853–867, 1970.

[56] V. M. Zatsiorsky, Z.-M. Li, and M. L. Latash, "Enslaving effects in multi-finger force production", *Experimental Brain Research*, vol. 131, no. 2, pp. 187–195, 2000. DOI: 10.1007/s002219900261.

[57] C. Häger-Ross and M. H. Schieber, "Quantifying the independence of human finger movements: Comparisons of digits, hands, and movement frequencies", *Journal of Neuroscience*, vol. 20, no. 22, pp. 8542–8550, 2000. DOI: 10.1523/JNEUROSCI.20-22-08542.2000.

[58] S. W. Kim, J. K. Shim, V. M. Zatsiorsky, and M. L. Latash, "Finger inter-dependence: Linking the kinetic and kinematic variables", *Human Movement Science*, vol. 27, no. 3, pp. 408–422, 2008. DOI: 10.1016/j.humov.2007.08.005.

[59] M. Santello and J. F. Soechting, "Gradual molding of the hand to object contours", *Journal of Neurophysiology*, vol. 79, no. 3, pp. 1307–1320, 1998. DOI: 10.1152/jn.1998.79.3.1307.

[60] M. Santello, M. Flanders, and J. F. Soechting, "Patterns of hand motion during grasping and the influence of sensory guidance", *Journal of Neuroscience*, vol. 22, no. 4, pp. 1426–1435, 2002. DOI: 10.1523/JNEUROSCI.22-04-01426.2002.

[61] C. Sollerman and A. Ejeskär, "Sollerman hand function test: A standardised method and its use in tetraplegic patients", *Scandinavian Journal of Plastic and Reconstructive Surgery and Hand Surgery*, vol. 29, no. 2, pp. 167–176, 1995. DOI: 10.3109/02844319509034334.

[62] C. M. Light, P. H. Chappell, and P. J. Kyberd, "Establishing a standardized clinical assessment tool of pathologic and prosthetic hand function: Normative data, reliability, and validity", *Archives of Physical Medicine and Rehabilitation*, vol. 83, no. 6, pp. 776–783, 2002. DOI: 10.1053/apmr.2002.32737.

[63] C. J. Heckman and R. M. Enoka, "Physiology of the motor neuron and the motor unit", in *Clinical Neurophysiology of Motor Neuron Diseases*, ser. Handbook of Clinical Neurophysiology, A. Eisen, Ed., vol. 4, Elsevier, 2004, pp. 119–147. DOI: 10.1016/S1567-4231(04)04006-7.

[64] S. Silbernagl and A. Despopoulos, *Taschenatlas Physiologie*, 7th. Stuttgart, Germany: Thieme, 2007, ISBN: 9783135677071.

[65] R. F. Schmidt and H.-G. Schaible, Eds., *Neuro- und Sinnesphysiologie*, 5th. Heidelberg, Germany: Springer Medizin, 2006, ISBN: 978-3-540-25700-4.

[66] E. Imatz Ojanguren, "Neuro-fuzzy modeling of multi-field surface neuroprostheses for hand grasp", PhD thesis, University of the Basque Country, Bilbao, Spain, 2016.

[67] T. Schauer, "Funktionelle Elektrostimulation in der Rehabilitation nach Schlaganfall und Querschnittlähmung", in *Automatisierte Therapiesysteme*, ser. Biomedizinische Technik, J. Werner, Ed., 1st, vol. 9, Berlin, Germany: Walter de Gruyter, 2014, ISBN: 9783110252132.

[68] C. L. Lynch and M. R. Popović, "Functional electrical stimulation: Closed-loop control of induced muscle contractions", *IEEE Control System Magazine*, vol. 28, no. 2, pp. 40–50, 2008. DOI: 10.1109/MCS.2007.914689.

[69] C. Lynch, "Closed-loop control of electrically stimulated skeletal muscle contractions", PhD thesis, University of Toronto, Toronto, ON, Canada, 2011.

[70] E. Henneman, "The size-principle: A deterministic output emerges from a set of probabilistic connections", *Journal of Experimental Biology*, vol. 115, no. 1, pp. 105–112, 1985.

[71] T. Schauer, K.-P. Hoffmann, and J. Szecsi, "Funktionelle Elektro- und Magnetstimulation in der Rehabilitation", in *Rehabilitationstechnik*, ser. Biomedizinische Technik, M. Kraft and C. Disselhorst-Klug, Eds., vol. 10, Berlin, Germany: Walter de Gruyter, 2015, ISBN: 9783110252262.

[72] L. Popović-Maneski, N. M. Malešević, A. M. Savić, T. Keller, and D. B. Popović, "Surface-distributed low-frequency asynchronous stimulation delays fatigue of stimulated muscles", *Muscle & Nerve*, vol. 48, no. 6, pp. 930–937, 2013. DOI: 10.1002/mus.23840.

[73] J. T. Mortimer, "Motor prostheses", *Comprehensive Physiology*, pp. 155–187, 2011. DOI: 10.1002/cphy.cp010205.

[74] S. Salmons, Z. Ashley, H. Sutherland, M. F. Russold, F. Li, and J. C. Jarvis, "Functional electrical stimulation of denervated muscles: Basic issues", *Artificial Organs*, vol. 29, no. 3, pp. 199–202, 2005. DOI: 10.1111/j.1525-1594.2005.29034.x.

[75] P. Gargiulo, P. J. Reynisson, B. Helgason, H. Kern, W. Mayr, P. Ingvarsson, T. Helgason, and U. Carraro, "Muscle, tendons, and bone: Structural changes during denervation and FES treatment", *Neurological Research*, vol. 33, no. 7, pp. 750–758, 2011. DOI: 10.1179/1743132811Y.0000000007.

[76] T. Schauer, "Feedback control of cycling in spinal cord injury using functional electrical stimulation", PhD thesis, University of Glasgow, Glasgow, UK, 2006.

[77] M. R. Popovic, A. Curt, T. Keller, and V. Dietz, "Functional electrical stimulation for grasping and walking: Indications and limitations", *Spinal Cord*, vol. 39, pp. 403–412, 2001. DOI: 10.1038/sj.sc.3101191.

[78] P. E. Crago, R. F. Kirsch, and R. J. Triolo, "Movement synthesis and regulation in neuroprostheses", in *Biomechanics and Neural Control of Posture and Movement*, New York, NY, USA: Springer, 2000, pp. 573–589. DOI: 10.1007/978-1-4612-2104-3_43.

[79] D. M. Durand, W. M. Grill, and R. Kirsch, "Electrical stimulation of the neuromuscular system", in *Neural Engineering*, Springer, 2005, pp. 157–191. DOI: 10.1007/0-306-48610-5_5.

[80] A. Botter, G. Oprandi, F. Lanfranco, S. Allasia, N. A. Maffiuletti, and M. A. Minetto, "Atlas of the muscle motor points for the lower limb: Implications for electrical stimulation procedures and electrode positioning", *European Journal of Applied Physiology*, vol. 111, no. 10, p. 2461, 2011. DOI: 10.1007/s00421-011-2093-y.

[81] M. Gobbo, N. A. Maffiuletti, C. Orizio, and M. A. Minetto, "Muscle motor point identification is essential for optimizing neuromuscular electrical stimulation use", *Journal of NeuroEngineering and Rehabilitation*, vol. 11, no. 1, p. 17, 2014. DOI: 10.1186/1743-0003-11-17.

[82] J. P. Reilly and A. M. Diamant, *Electrostimulation: Theory, applications, and computational model*. Norwood, MA, USA: Artech House, 2011, ISBN: 978-1-60807-108-1.

[83] M. C. Kutlu, "A home-based functional electrical stimulation system for upper-limb stroke rehabilitation", PhD thesis, University of Southhampton, Southhampton, UK, 2017.

[84] G. Alon, G. Kantor, and H. S. Ho, "Effects of electrode size on basic excitatory responses and on selected stimulus parameters", *Journal of Orthopaedic & Sports Physical Therapy*, vol. 20, no. 1, pp. 29–35, 1994. DOI: 10.2519/jospt.1994.20.1.29.

[85] M. Solomonow, J. Lyman, and A. Freedy, "Electrotactile two-point discrimination as a function of frequency, body site, laterality, and stimulation codes", *Annals of Biomedical Engineering*, vol. 5, no. 1, pp. 47–60, 1977. DOI: 10.1007/BF02409338.

[86] N. M. Malešević, L. Z. Popović, L. Schwirtlich, and D. B. Popović, "Distributed low-frequency functional electrical stimulation delays muscle fatigue compared to conventional stimulation", *Muscle & Nerve*, vol. 42, no. 4, pp. 556–562, 2010. DOI: 10.1002/mus.21736.

[87] K. A. Sluka and D. Walsh, "Transcutaneous electrical nerve stimulation: Basic science mechanisms and clinical effectiveness", *The Journal of Pain*, vol. 4, no. 3, pp. 109–121, 2003. DOI: 10.1054/jpai.2003.434.

[88] T. Kesar and S. Binder-Macleod, "Effect of frequency and pulse duration on human muscle fatigue during repetitive electrical stimulation", *Experimental Physiology*, vol. 91, no. 6, pp. 967–976, 2006. DOI: 10.1113/expphysiol.2006.033886.

[89] A. Elsaify, "A self-optimising portable FES system using an electrode array and movement sensors", PhD thesis, University of Leicester, Leicester, UK, 2005.

[90] T. Keller and A. Kuhn, "Electrodes for transcutaneous (surface) electrical stimulation", *Journal of Automatic Control*, vol. 18, no. 2, pp. 35–45, 2008. DOI: 10.2298/JAC0802035K.

[91] A. Kuhn, T. Keller, M. Lawrence, and M. Morari, "The Influence of Electrode Size on Selectivity and Comfort in Transcutaneous Electrical Stimulation of the Forearm", *IEEE Transactions on Neural Systems and Rehabilitation Engineering*, vol. 18, no. 3, pp. 255–262, 2010. DOI: 10.1109/TNSRE.2009.2039807.

[92] G. Bijelić, A. Popović-Bijelić, N. Jorgovanović, D. Bojanić, and D. B. Popović, "E actitrode: The new selective stimulation interface for functional movements in hemiplegics patients", *Serbian Journal of Electrical Engineering*, vol. 1, no. 3, pp. 21–28, 2004. DOI: 10.2298/SJEE0403021B.

[93] T. Keller, M. Lawrence, A. Kuhn, and M. Morari, "New multi-channel transcutaneous electrical stimulation technology for rehabilitation", in *Conference Proceedings IEEE Engineering in Medicine and Biology Society (EMBC)*, (New York, NY, USA), Aug. 2006, pp. 194–197. DOI: 10.1109/IEMBS.2006.259399.

[94] L. Popović-Maneski, M. Kostić, G. Bijelić, T. Keller, S. Mitrović, L. Konstantinović, and D. B. Popović, "Multi-pad electrode for effective grasping: Design", *IEEE Transactions on Neural Systems and Rehabilitation Engineering*, vol. 21, no. 4, pp. 648–654, 2013. DOI: 10.1109/TNSRE.2013.2239662.

[95] L. R. Sheffler and J. Chae, "Neuromuscular electrical stimulation in neurorehabilitation", *Muscle & Nerve*, vol. 35, no. 5, pp. 562–590, 2007. DOI: 10.1002/mus.20758.

[96] M. Thomsen and P. H. Veltink, "Influence of synchronous and sequential stimulation on muscle fatigue", *Medical and Biological Engineering and Computing*, vol. 35, no. 3, pp. 186–192, 1997. DOI: 10.1007/BF02530036.

[97] J. S. Petrofsky, "Control of the recruitment and firing frequencies of motor units in electrically stimulated muscles in the cat", *Medical and Biological Engineering and Computing*, vol. 16, no. 3, pp. 302–308, 1978. DOI: 10.1007/BF02442432.

[98] D. Graupe, P. Suliga, C. Prudiant, and K. H. Kohn, "Stochastically-modulated stimulation to slow down muscle fatigue at stimulated sites in paraplegics using functional electrical stimulation for leg extension", *Neurological Research*, vol. 22, no. 7, pp. 703–704, 2000. DOI: 10.1080/01616412.2000.11740743.

[99] A. Thrasher, G. M. Graham, and M. R. Popović, "Reducing muscle fatigue due to functional electrical stimulation using random modulation of stimulation parameters", *Artificial Organs*, vol. 29, no. 6, pp. 453–458, 2005. DOI: 10.1111/j.1525-1594.2005.29076.x.

[100] K. T. Ragnarsson, "Functional electrical stimulation after spinal cord injury: Current use, therapeutic effects and future directions", *Spinal Cord*, vol. 46, no. 4, pp. 255–274, 2008. DOI: 10.1038/sj.sc.3102091.

[101] F. Quandt and F. C. Hummel, "The influence of functional electrical stimulation on hand motor recovery in stroke patients: A review", *Experimental & Translational Stroke Medicine*, vol. 6, no. 1, p. 9, 2014. DOI: 10.1186/2040-7378-6-9.

[102] N. M. Kapadia, M. K. Nagai, V. Zivanovic, J. Bernstein, J. Woodhouse, P. Rumney, and M. R. Popovic, "Functional electrical stimulation therapy for recovery of reaching and grasping in severe chronic pediatric stroke patients", *Journal of Child Neurology*, vol. 29, no. 4, pp. 493–499, 2014. DOI: 10.1177/0883073813484088.

[103] H. K. Shin, S. H. Cho, H.-S. Jeon, Y.-H. Lee, J. C. Song, S. H. Jang, C.-H. Lee, and Y. H. Kwon, "Cortical effect and functional recovery by the electromyography-triggered neuromuscular stimulation in chronic stroke patients", *Neuroscience Letters*, vol. 442, no. 3, pp. 174–179, 2008. DOI: 10.1016/j.neulet.2008.07.026.

[104] C. A. Coste, W. Mayr, M. Bijak, A. Musarò, and U. Carraro, "FES in Europe and beyond: Current translational research", *European Journal of Translational Myology*, vol. 26, no. 4, 2016. DOI: 10.4081/ejtm.2016.6369.

[105] G. Alon, A. F. Levitt, and P. A. McCarthy, "Functional electrical stimulation (FES) may modify the poor prognosis of stroke survivors with severe motor loss of the upper extremity: A preliminary study", *American Journal of Physical Medicine & Rehabilitation*, vol. 87, no. 8, pp. 627–636, 2008. DOI: 10.1097/PHM.0b013e31817fabc1.

[106] N. M. M. Gharib, A. M. Aboumousa, A. A. Elowishy, S. S. Rezk-Allah, and F. S. Yousef, "Efficacy of electrical stimulation as an adjunct to repetitive task practice therapy on skilled hand performance in hemiparetic stroke patients: A randomized controlled trial", *Clinical Rehabilitation*, vol. 29, no. 4, pp. 355–364, 2015. DOI: 10.1177/0269215514544131.

[107] C. Marquez-Chin, S. Bagher, V. Zivanovic, and M. R. Popovic, "Functional electrical stimulation therapy for severe hemiplegia: Randomized control trial revisited", *Canadian Journal of Occupational Therapy*, vol. 84, no. 2, pp. 87–97, 2017. DOI: 10.1177/0008417416668370.

[108] S. Hamid and R. Hayek, "Role of electrical stimulation for rehabilitation and regeneration after spinal cord injury: An overview", *European Spine Journal*, vol. 17, no. 9, pp. 1256–1269, 2008. DOI: 10.1007/s00586-008-0729-3.

[109] S. Saxena, S. Nikolic, and D. B. Popović, "An EMG-controlled grasping system for tetraplegics", *Journal of Rehabilitation Research & Development*, vol. 32, no. 1, pp. 17–24, 1995.

[110] J. Jonsdottir, R. Thorsen, I. Aprile, S. Galeri, G. Spannocchi, E. Beghi, *et al.*, "Arm rehabilitation in post stroke subjects: A randomized controlled trial on the efficacy of myoelectrically driven FES applied in a task-oriented approach", *PLOS ONE*, vol. 12, no. 12, e0188642–e0188642, 2017. DOI: 10.1371/journal.pone.0188642.

[111] R. Shalaby, "Development of an electromyography detection system for the control of functional electrical stimulation in neurological rehabilitation", PhD thesis, Technische Universität Berlin, Berlin, Germany, 2011.

[112] C. Klauer, J. Raisch, and T. Schauer, "Linearisation of electrically stimulated muscles by feedback control of the muscular recruitment measured by evoked EMG", in *Proceedings 17th International Conference Methods and Models in Automation and Robotics (MMAR)*, (Miedzyzdrojie, Poland), IEEE, 2012, pp. 108–113. DOI: 10.1109/MMAR.2012.6347902.

[113] R. Merletti and P. Parker, *Electromyography: Physiology, engineering, and non-invasive applications*. Hoboken, NJ, USA: John Wiley & Sons, 2004, ISBN: 9780471675808.

[114] C. J. De Luca and M. Knaflitz, *Surface electromyography: What's new?* Torino, Italy: CLUT, 1992.

[115] E. Ambrosini, S. Ferrante, T. Schauer, C. Klauer, M. Gaffuri, G. Ferrigno, and A. Pedrocchi, "A myocontrolled neuroprosthesis integrated with a passive exoskeleton to support upper limb activities", *Journal of Electromyography and Kinesiology*, vol. 24, no. 2, pp. 307–317, 2014. DOI: 10.1016/j.jelekin.2014.01.006.

[116] C. Klauer, S. Ferrante, E. Ambrosini, U. Shiri, F. Dähne, I. Schmehl, A. Pedrocchi, and T. Schauer, "A patient-controlled functional electrical stimulation system for arm weight relief", *Medical Engineering & Physics*, vol. 38, no. 11, pp. 1232–1243, 2016. DOI: 10.1016/j.medengphy.2016.06.006.

[117] C. Frigo, M. Ferrarin, W. Frasson, E. Pavan, and R. Thorsen, "EMG signals detection and processing for on-line control of functional electrical stimulation", *Journal of Electromyography and Kinesiology*, vol. 10, no. 5, pp. 351–360, 2000. DOI: 10.1016/S1050-6411(00)00026-2.

[118] R. Thorsen, R. Spadone, and M. Ferrarin, "A pilot study of myoelectrically controlled FES of upper extremity", *IEEE Transactions on Neural Systems and Rehabilitation Engineering*, vol. 9, no. 2, pp. 161–168, 2001. DOI: 10.1109/7333.928576.

[119] J. M. Heasman, T. R. D. Scott, V. A. Vare, R. Y. Flynn, C. R. Gschwind, J. W. Middleton, and S. B. Butkowski, "Detection of fatigue in the isometric electrical activation of paralyzed hand muscles of persons with tetraplegia", *IEEE Transactions on Rehabilitation Engineering*, vol. 8, no. 3, pp. 286–296, 2000. DOI: 10.1109/86.867870.

[120] G. Pfurtscheller, G. R. Müller, J. Pfurtscheller, H. J. Gerner, and R. Rupp, "'Thought' – control of functional electrical stimulation to restore hand grasp in a patient with tetraplegia", *Neuroscience Letters*, vol. 351, no. 1, pp. 33–36, 2003, ISSN: 0304-3940. DOI: 10.1016/S0304-3940(03)00947-9.

[121] B. Mijovic, M. B. Popović, and D. B. Popović, "Synergistic control of forearm based on accelerometer data and artificial neural networks", *Brazilian Journal of Medical and Biological Research*, vol. 41, no. 5, pp. 389–397, 2008. DOI: 10.1590/S0100-879X2008005000019.

[122] E. A. Corbett, N. A. Sachs, K. P. Körding, and E. J. Perreault, "Multimodal decoding and congruent sensory information enhance reaching performance in subjects with cervical spinal cord injury", *Frontiers in Neuroscience*, vol. 8, p. 123, 2014. DOI: 10.3389/fnins.2014.00123.

[123] M. Štrbac, S. Kočović, M. Marković, and D. B. Popović, "Microsoft Kinect-based artificial perception system for control of functional electrical stimulation assisted grasping", *BioMed Research International*, vol. 2014, 2014. DOI: 10.1155/2014/740469.

[124] T. Seel, C. Werner, J. Raisch, and T. Schauer, "Iterative learning control of a drop foot neuroprosthesis – generating physiological foot motion in paretic gait by automatic feedback control", *Control Engineering Practice*, vol. 48, no. 1, pp. 87–97, 2016. DOI: 10.1016/j.conengprac.2015.11.007.

[125] H.-R. Kobravi and A. Erfanian, "Decentralized adaptive robust control based on sliding mode and nonlinear compensator for the control of ankle movement using functional electrical stimulation of agonist–antagonist muscles", *Journal of Neural Engineering*, vol. 6, no. 4, p. 046 007, 2009. DOI: 10.1088/1741-2560/6/4/046007.

[126] M. Valtin, T. Seel, J. Raisch, and T. Schauer, "Iterative learning control of drop foot stimulation with array electrodes for selective muscle activation", *IFAC Proceedings Volumes*, vol. 47, no. 3, pp. 6587–6592, 2014. DOI: 10.3182/20140824-6-ZA-1003.01991.

[127] T. Seel, C. Werner, and T. Schauer, "The adaptive drop foot stimulator – multivariable learning control of foot pitch and roll motion in paretic gait", *Medical Engineering Physics*, vol. 38, no. 11, pp. 1205–1213, 2016, ISSN: 1350-4533. DOI: 10.1016/j.medengphy.2016.06.009.

[128] C. T. Freeman, *Control system design for electrical stimulation in upper limb rehabilitation*. Cham, Switzerland: Springer International Publishing, 2016. DOI: 10.1007/978-3-319-25706-8.

[129] E. Ambrosini, N. C. Bejarano, and A. Pedrocchi, "Sensors for motor neuroprosthetics: Current applications and future directions", in *Emerging Theory and Practice in Neuroprosthetics*, G. Naik and Y. Guo, Eds., Hershey, PA, USA: IGI Global, 2014, pp. 38–64. DOI: 10.4018/978-1-4666-6094-6.ch003.

[130] M. Sun, L. Kenney, C. Smith, K. Waring, H. Luckie, A. Liu, and D. Howard, "A novel method of using accelerometry for upper limb FES control", *Medical Engineering & Physics*, vol. 38, no. 11, pp. 1244–1250, 2016. DOI: 10.1016/j.medengphy.2016.06.005.

[131] M. Kutlu, C. Freeman, A.-M. Hughes, and M. Spraggs, "A home-based FES system for upper-limb stroke rehabilitation with iterative learning control", *IFAC-PapersOnLine*, vol. 50, no. 1, pp. 12 089–12 094, 2017. DOI: 10.1016/j.ifacol.2017.08.2153.

[132] D. A. Nowak, "The impact of stroke on the performance of grasping: Usefulness of kinetic and kinematic motion analysis", *Neuroscience & Biobehavioral Reviews*, vol. 32, no. 8, pp. 1439–1450, 2008. DOI: 10.1016/j.neubiorev.2008.05.021.

[133] H. G. Kortier, V. I. Sluiter, D. Roetenberg, and P. H. Veltink, "Assessment of hand kinematics using inertial and magnetic sensors", *Journal of NeuroEngineering and Rehabilitation*, vol. 11, no. 1, p. 70, 2014. DOI: 10.1186/1743-0003-11-70.

[134] J. van den Noort, K. van Dijk, H. Kortier, N. van Beek, R. Verhagen, L. Bour, and P. Veltink, "Applications of the PowerGlove for measurement of finger kinematics", in *Proceedings 11th International Conference Wearable and Implantable Body Sensor Networks Workshops*, (Zürich, Switzerland), IEEE, 2014. DOI: 10.1109/BSN.Workshops.2014.19.

[135] J. C. van den Noort, H. G. Kortier, N. van Beek, D. H. E. J. Veeger, P. H. Veltink, and S. J. Bensmaia, "Measuring 3D hand and finger kinematics—a comparison between inertial sensing and an opto-electronic marker system", *PLOS ONE*, vol. 11, no. 11, 2016. DOI: 10.1371/journal.pone.0164889.

[136] B. Stenger, A. Thayananthan, P. H. S. Torr, and R. Cipolla, "Model-based hand tracking using a hierarchical bayesian filter", *IEEE Transactions on Pattern Analysis and Machine Intelligence*, vol. 28, no. 9, pp. 1372–1384, 2006. DOI: 10.1109/TPAMI.2006.189.

[137] A. Erol, G. Bebis, M. Nicolescu, R. D. Boyle, and X. Twombly, "Vision-based hand pose estimation: A review", *Computer Vision and Image Understanding*, vol. 108, no. 1, pp. 52–73, 2007. DOI: 10.1016/j.cviu.2006.10.012.

[138] A. I. Cuesta-Vargas, A. Galán-Mercant, and J. M. Williams, "The use of inertial sensors system for human motion analysis", *Physical Therapy Reviews*, vol. 15, no. 6, pp. 462–473, 2010. DOI: 10.1179/1743288X11Y.0000000006.

[139] W. Y. Wong, M. S. Wong, and K. H. Lo, "Clinical applications of sensors for human posture and movement analysis: A review", *Prosthetics and Orthotics International*, vol. 31, no. 1, pp. 62–75, 2007. DOI: 10.1080/03093640600983949.

[140] K. Khoshelham and S. O. Elberink, "Accuracy and resolution of Kinect depth data for indoor mapping applications", *Sensors*, vol. 12, no. 2, pp. 1437–1454, 2012. DOI: 10.3390/s120201437.

[141] F. Weichert, D. Bachmann, B. Rudak, and D. Fisseler, "Analysis of the accuracy and robustness of the Leap Motion controller", *Sensors*, vol. 13, no. 5, pp. 6380–6393, 2013. DOI: 10.3390/s130506380.

[142] Y.-J. Chang, S.-F. Chen, and J.-D. Huang, "A Kinect-based system for physical rehabilitation: A pilot study for young adults with motor disabilities", *Research in Developmental Disabilities*, vol. 32, no. 6, pp. 2566–2570, 2011. DOI: 10.1016/j.ridd.2011.07.002.

[143] M. Štrbac, M. Marković, and D. B. Popović, "Kinect in neurorehabilitation: Computer vision system for real time hand and object detection and distance estimation", in *Proceedings 11th Symposium on Neural Network Applications in Electrical Engineering (NEUREL)*, (Belgrade, Serbia), IEEE, Sep. 2012, pp. 127–132. DOI: 10.1109/NEUREL.2012.6419983.

[144] L. Dipietro, A. M. Sabatini, and P. Dario, "A survey of glove-based systems and their applications", *IEEE Transactions on Systems, Man, and Cybernetics, Part C*, vol. 38, no. 4, pp. 461–482, 2008. DOI: 10.1109/TSMCC.2008.923862.

[145] G. Saggio, S. Bocchetti, C. A. Pinto, G. Orengo, and F. Giannini, "A novel application method for wearable bend sensors", in *Proceedings 2nd International Symposium on Applied Sciences in Biomedical and Communication Technologies (ISABEL)*, (Bratislava, Slovakia), IEEE, 2009, pp. 1–3. DOI: 10.1109/ISABEL.2009.5373625.

[146] J. L. Hernandez-Rebollar, N. Kyriakopoulos, and R. W. Lindeman, "The acceleglove: A whole-hand input device for virtual reality", in *Conference Abstracts and Applications, ACM SIGGRAPH 2002*, ACM, 2002, pp. 259–259. DOI: 10.1145/1242073.1242272.

[147] A. Filippeschi, N. Schmitz, M. Miezal, G. Bleser, E. Ruffaldi, and D. Stricker, "Survey of motion tracking methods based on inertial sensors: A focus on upper limb human motion", *Sensors*, vol. 17, no. 6, p. 1257, 2017. DOI: 10.3390/s17061257.

[148] A. M. Sabatini, "Quaternion-based extended Kalman filter for determining orientation by inertial and magnetic sensing", *IEEE Transactions on Biomedical Engineering*, vol. 53, no. 7, pp. 1346–1356, 2006. DOI: 10.1109/TBME.2006.875664.

[149] J. Connolly, J. Condell, B. O'Flynn, J. T. Sanchez, and P. Gardiner, "IMU sensor-based electronic goniometric glove for clinical finger movement analysis", *IEEE Sensors Journal*, vol. 18, no. 3, pp. 1273–1281, 2018. DOI: 10.1109/JSEN.2017.2776262.

[150] D. Laidig, T. Schauer, and T. Seel, "Exploiting kinematic constraints to compensate magnetic disturbances when calculating joint angles of approximate hinge joints from orientation estimates of inertial sensors", in *Proceedings 15th IEEE International Conference on Rehabilitation Robotics (ICORR)*, (London, UK), 2017, pp. 971–976. DOI: 10.1109/ICORR.2017.8009375.

[151] U. Hoffmann, M. Deinhofer, and T. Keller, "Automatic determination of parameters for multipad functional electrical stimulation: Application to hand opening and closing", in *Conference Proceedings IEEE Engineering in Medicine and Biology Society (EMBC)*, (San Diego, CA, USA), Aug. 2012, pp. 1859–1863. DOI: 10.1109/EMBC.2012.6346314.

[152] A. J. Westerveld, A. Kuck, A. C. Schouten, P. H. Veltink, and H. van der Kooij, "Grasp and release with surface functional electrical stimulation using a model predictive control approach", in *Proceedings 34th International Conference IEEE Engineering in Medicine and Biology Society (EMBC)*, (San Diego, CA, USA), Aug. 2012, pp. 333–336. DOI: 10.1109/EMBC.2012.6345937.

[153] C. T. Freeman, "Iterative learning control with restricted input subspace for electrode array-based FES", in *Conference Proceedings of American Control Conference (ACC)*, (Portland, OR, USA), 2014, pp. 4243–4248. DOI: 10.1109/ACC.2014.6858712.

[154] A. Prochazka, "Neuroprosthetics", in *Spinal Cord Injury Rehabilitation*, E. Field-Fote, Ed., Philadephia, PA, USA: FA Davis Company, 2009, ch. 5, pp. 87–99, ISBN: 9780803623194.

[155] B. Smith, P. H. Peckham, M. W. Keith, and D. D. Roscoe, "An externally powered, multichannel, implantable stimulator for versatile control of paralyzed muscle", *IEEE Transactions on Biomedical Engineering*, no. 7, pp. 499–508, 1987. DOI: 10.1109/TBME.1987.325979.

[156] K. L. Kilgore, H. A. Hoyen, A. M. Bryden, R. L. Hart, M. W. Keith, and P. H. Peckham, "An implanted upper-extremity neuroprosthesis using myoelectric control", *The Journal of Hand Surgery*, vol. 33, no. 4, pp. 539–550, 2008.

[157] W. D. Memberg, K. H. Polasek, R. L. Hart, A. M. Bryden, K. L. Kilgore, G. A. Nemunaitis, *et al.*, "Implanted neuroprosthesis for restoring arm and hand function in people with high level tetraplegia", *Archives of Physical Medicine and Rehabilitation*, vol. 95, no. 6, pp. 1201–1211, 2014.

[158] A. B. Ajiboye, F. R. Willett, D. R. Young, W. D. Memberg, B. A. Murphy, J. P. Miller, *et al.*, "Restoration of reaching and grasping in a person with tetraplegia through brain-controlled muscle stimulation: A proof-of-concept demonstration", *Lancet*, vol. 389, no. 10081, pp. 1821–1830, 2017. DOI: 10.1016/S0140-6736(17)30601-3.

[159] A. Prochazka, M. Gauthier, M. Wieler, and Z. Kenwell, "The Bionic Glove: An electrical stimulator garment that provides controlled grasp and hand opening in quadriplegia", *Archives of Physical Medicine and Rehabilitation*, vol. 78, no. 6, pp. 608–614, 1997. DOI: 10.1016/S0003-9993(97)90426-3.

[160] R. H. Nathan, "Functional electrical stimulation of the upper limb: Charting the forearm surface", *Medical and Biological Engineering and Computing*, vol. 17, p. 729, 1979. DOI: 10.1007/BF02441554.

[161] R. H. Nathan and A. Ohry, "Upper limb functions regained in quadriplegia: A hybrid computerized neuromuscular stimulation system.", *Archives of Physical Medicine and Rehabilitation*, vol. 71, no. 6, pp. 415–421, 1990.

[162] K. M. Kohlmeyer, J. P. Hill, G. M. Yarkony, and R. J. Jaeger, "Electrical stimulation and biofeedback effect on recovery of tenodesis grasp: A controlled study.", *Archives of Physical Medicine and Rehabilitation*, vol. 77, no. 7, pp. 702–706, 1996. DOI: 10.1016/S0003-9993(96)90011-8.

[163] M. R. Popović and T. A. Thrasher, "Neuroprostheses", in *Encyclopedia of Biomaterials and Biomedical Engineering*, Taylor & Francis, 2004, pp. 1056–1065.

[164] D. Popović and T. Sinkjaer, *Control of movement for the physically disabled: Control for rehabilitation technology*, 1st. London, UK: Springer-Verlag, 2000, ISBN: 978-1-4471-1141-2. DOI: 10.1007/978-1-4471-0433-9.

[165] A. Elsaify, J. Fothergill, and W. Peasgood, "A portable FES system incorporating an electrode array and feedback sensors", in *Conference Proceedings 8th Vienna International Workshop on FES*, (Vienna, Austria), Sep. 2004.

[166] M. Lawrence, T. Kirstein, and T. Keller, "Electrical stimulation of the finger flexors using 'virtual electrodes'", in *Conference Proceedings 8th Vienna International Workshop on FES*, (Vienna, Austria), Sep. 2004.

[167] R. Velik, N. M. Malešević, L. Popović, U. Hoffmann, and T. Keller, "INTFES: A multi-pad electrode system for selective transcutaneous electrical muscle stimulation", in *Proceedings Annual Conference of the International FES Society (IFESS)*, (São Paulo, Brasil), Sep. 2011.

[168] J. Malešević, M. Štrbac, M. Isaković, V. Kojić, L. Konstantinović, A. Vidaković, *et al.*, "Temporal and spatial variability of surface motor activation zones in hemiplegic patients during functional electrical stimulation therapy sessions", *Artifical Organs*, vol. 41, no. 11, 2017. DOI: 10.1111/aor.13057.

[169] C. Salchow-Hömmen, N. Jankowski, M. Valtin, L. Schönijahn, S. Böttcher, F. Dähne, and T. Schauer, "User-centered practicability analysis of two identification strategies in electrode arrays for FES induced hand motion in early stroke rehabilitation", *Journal of NeuroEngineering and Rehabilitation*, vol. 15, p. 123, 2018. DOI: 10.1186/s12984-018-0460-1.

[170] D. B. Popović and M. B. Popović, "Automatic determination of the optimal shape of a surface electrode: Selective stimulation", *Journal of Neuroscience Methods*, vol. 178, pp. 174–181, 2009. DOI: 10.1016/j.jneumeth.2008.12.003.

[171] T. Exell, C. Freeman, K. Meadmore, A.-M. Hughes, E. Hallewell, and J. Burridge, "Optimisation of hand posture stimulation using an electrode array and iterative learning control", *Journal of Automatic Control*, vol. 21, no. 1, pp. 1–5, 2013. DOI: 10.2298/JAC1301001E.

[172] C. De Marchis, T. S. Monteiro, C. Simon-Martinez, S. Conforto, and A. Gharabaghi, "Multi-contact functional electrical stimulation for hand opening: Electrophysiologically driven identification of the optimal stimulation site", *Journal of NeuroEngineering and Rehabilitation*, vol. 13, no. 1, p. 22, 2016. DOI: 10.1186/s12984-016-0129-6.

[173] A. D. Koutsou, J. C. Moreno, A. J. del Ama, E. Rocon, and J. L. Pons, "Advances in selective activation of muscles for non-invasive motor neuroprostheses", *Journal of NeuroEngineering and Rehabilitation*, vol. 13, no. 1, p. 56, 2016. DOI: 10.1186/s12984-016-0165-2.

[174] A. Kuhn, T. Keller, S. Micera, and M. Morari, "Array electrode design for transcutaneous electrical stimulation: A simulation study", *Medical Engineering & Physics*, vol. 31, pp. 945–951, 2009. DOI: 10.1016/j.medengphy.2009.05.006.

[175] L. M. Livshitz, J. Mizrahi, and P. D. Einziger, "Interaction of array of finite electrodes with layered biological tissue: Effect of electrode size and configuration", *IEEE Transactions on Neural Systems and Rehabilitation Engineering*, vol. 9, no. 4, pp. 355–361, 2001. DOI: 10.1109/7333.1000115.

[176] F. Gracanin and A. Trnkoczy, "Optimal stimulus parameters for minimum pain in the chronic stimulation of innervated muscle", *Archives of Physical Medicine and Rehabilitation*, vol. 56, no. 6, pp. 243–249, 1975.

[177] N. M. Malešević, L. Z. Maneski, V. Ilić, N. Jorgovanović, G. Bijelić, T. Keller, and D. B. Popović, "A multi-pad electrode based functional electrical stimulation system for restoration of grasp", *Journal of NeuroEngineering and Rehabilitation*, vol. 9, no. 1, p. 66, 2012. DOI: 10.1186/1743-0003-9-66.

[178] A. Popović-Bijelić, G. Bijelić, N. Jorgovanović, D. Bojanić, M. B. Popović, and D. B. Popović, "Multi-field surface electrode for selective electrical stimulation", *Artificial Organs*, vol. 29, no. 6, pp. 448–452, 2005. DOI: 10.1111/j.1525-1594.2005.29075.x.

[179] S. B. O'Dwyer, D. T. O'Keeffe, S. Coote, and G. M. Lyons, "An electrode configuration technique using an electrode matrix arrangement for FES-based upper arm rehabilitation systems", *Medical Engineering & Physics*, vol. 28, no. 2, pp. 166–176, 2006. DOI: 10.1016/j.medengphy.2005.03.010.

[180] T. Keller, B. Hackl, M. Lawrence, and A. Kuhn, "Identification and control of hand grasp using multi-channel TES", in *Proceedings Annual Conference of the International FES Society (IFESS)*, (Zao, Japan), Sep. 2006, pp. 29–31.

[181] T. Keller, M. R. Popovic, and C. Dumont, "A dynamic grasping assessment system for measuring finger forces during wrist motion", in *Proceedings 18th Congress of the International Society of Biomechanics*, (Zürich, Switzerland), Jul. 2001, pp. 230–231.

[182] O. Schill, R. Rupp, C. Pylatiuk, S. Schulz, and M. Reischl, "Automatic adaptation of a self-adhesive multi-electrode array for active wrist joint stabilization in tetraplegic SCI individuals", in *Proceedings IEEE International Conference Science and Technology for Humanity*, (Toronto, ON, Canada), IEEE, 2009, pp. 708–713. DOI: 10.1109/TIC-STH.2009.5444408.

[183] N. Malešević, L. Popović, G. Bijelić, and G. Kvaščev, "Classification of muscle twitch response using ANN: Application in multi-pad electrode optimization", in *10th Symposium on Neural Network Applications in Electrical Engineering (NEUREL), 23–25 Sep 2010*, IEEE, 2010, pp. 11–13. DOI: 10.1109/NEUREL.2010.5644042.

[184] N. M. Malešević, L. Popović, G. Bijelić, and G. Kvaščev, "Muscle twitch responses for shaping the multi-pad electrode for functional electrical stimulation", *Journal of Automatic Control*, vol. 20, pp. 53–58, 2010. DOI: 10.2298/JAC1001053M.

[185] M. Kutlu, C. T. Freeman, E. Hallewell, A.-M. Hughes, and D. S. Laila, "Upper-limb stroke rehabilitation using electrode-array based functional electrical stimulation with sensing and control innovations", *Medical Engineering & Physics*, vol. 38, no. 4, pp. 366–379, 2016. DOI: 10.1016/j.medengphy.2016.01.004.

[186] M. Valtin, T. Schauer, C. Behling, M. Daniel, and M. Weber, "Combined stimulation and measurement system for array electrodes", in *Proceedings Biodevices*, (Vilamoura, Portugal), Feb. 2012, pp. 345–349.

[187] A. Crema, E. Guanziroli, N. Malešević, M. Colombo, D. Liberali, D. Proserpio, *et al.*, "Helping hand grasp rehabilitation: Preliminary assessment on chronic stroke patients", in *Proceedings 8th International IEEE/EMBS Conference on Neural Engineering (NER)*, (Shanghai, China), IEEE, 2017, pp. 146–149. DOI: 10.1109/NER.2017.8008313.

[188] F. Molteni, M. Rossini, G. Gasperini, P. Davide, K. Krakow, I. Nancy, *et al.*, "A wearable hand neuroprosthesis for hand rehabilitation after stroke: Preliminary results of the RETRAINER S2 randomized controlled trial", in *Converging Clinical and Engineering Research on Neurorehabilitation III, Proceedings INCR Biosystems & Biorobotics*, (Pisa, Italy), L. Masia, S. Micera, M. Akay, and J. Pons, Eds., Springer, 2018, pp. 3–7. DOI: 10.1007/978-3-030-01845-0_1.

[189] A. Crema, I. Furfaro, F. Raschellà, and S. Micera, "Development of a hand neuroprosthesis for grasp rehabilitation after stroke: State of art and perspectives", in *Converging Clinical and Engineering Research on Neurorehabilitation III; Proceedings INCR Biosystems & Biorobotics*, (Pisa, Italy), L. Masia, S. Micera, M. Akay, and J. Pons, Eds., Springer, 2018, pp. 89–93. DOI: 10.1007/978-3-030-01845-0_17.

[190] M. Valtin, K. Kociemba, C. Behling, B. Kuberski, S. Becker, and T. Schauer, "RehaMovePro: A versatile mobile stimulation system for transcutaneous FES applications", *European Journal of Translational Myology*, vol. 26, no. 3, p. 6076, 2016. DOI: 10.4081/ejtm.2016.6076.

[191] L. Popović-Maneski, I. Topalović, N. Jovičić, S. Dedijer, L. Konstantinović, and D. B. Popović, "Stimulation map for control of functional grasp based on multi-channel EMG recordings", *Medical Engineering & Physics*, vol. 38, no. 11, pp. 1251–1259, 2016, ISSN: 1350-4533. DOI: 10.1016/j.medengphy.2016.06.004.

[192] N. S. Jovičić, L. V. Saranovac, and D. B. Popović, "Wireless distributed functional electrical stimulation system", *Journal of NeuroEngineering and Rehabilitation*, vol. 9, no. 1, p. 54, 2012. DOI: 10.1186/1743-0003-9-54.

[193] K. Yang, K. Meadmore, C. Freeman, N. Grabham, A.-M. Hughes, Y. Wei, *et al.*, "Development of user-friendly wearable electronic textiles for healthcare applications", *Sensors*, vol. 18, no. 8, 2018. DOI: 10.3390/s18082410.

[194] C. K. Häger-Ross, C. S. Klein, and C. K. Thomas, "Twitch and tetanic properties of human thenar motor units paralyzed by chronic spinal cord injury", *Journal of Neurophysiology*, vol. 96, pp. 165–174, 2006. DOI: 10.1152/jn.01339.2005.

[195] S. A. Binder-Macleod, E. E. Halden, and K. A. Jungles, "Effects of stimulation intensity on the physiological responses of human motor units", *Medicine and Science in Sports and Exercise*, vol. 27, no. 4, pp. 556–565, 1995.

[196] L. Z. Popović and N. M. Malešević, "Muscle fatigue of quadriceps in paraplegics: Comparison between single vs. multi-pad electrode surface stimulation", in *Annual International Conference IEEE Engineering in Medicine and Biology Society (EMBC)*, (Minneapolis, MN, USA), IEEE, Sep. 2009, pp. 6785–6788. DOI: 10.1109/IEMBS.2009.5333983.

[197] N. Miljković, N. Malešević, V. Kojić, G. Bijelić, T. Keller, and D. B. Popović, "Recording and assessment of evoked potentials with electrode arrays", *Medical & Biological Engineering & Computing*, vol. 53, no. 9, pp. 857–867, 2015. DOI: 10.1007/s11517-015-1292-9.

[198] J. C. Loitz, A. Reinert, A. K. Neumann, F. Quandt, D. Schroeder, and W. H. Krautschneider, "A flexible standalone system with integrated sensor feedback for multi-pad electrode FES of the hand", *Current Directions in Biomedical Engineering*, vol. 2, no. 1, pp. 391–394, 2016. DOI: 10.1515/cdbme-2016-0087.

[199] M. Isaković, J. Malešević, M. Kostić, M. Štrbac, L. Konstantinović, O. Dordević, E. Imatz Ojanguren, and T. Keller, "Pilot clinical trial of novel multi-pad based FES grasping system and two treatment modalities", in *Proceedings Annual Conference of the International FES Society (IFESS)*, (Toronto, ON, Canada), IFESS, Jun. 2019.

[200] A.-M. Hughes, T. Ward, C. T. Freeman, N. Grabham, C. Power, K. Meadmore, *et al.*, "Electrical stimulation for upper limb rehabilitation post stroke applied using a wearable electronic array", in *Proceedings Annual Conference of the IFESS*, (Toronto, ON, Canada), IFESS, Jun. 2019.

[201] K. Y. Tong, A. F. T. Mak, and W. Y. Ip, "Command control for functional electrical stimulation hand grasp systems using miniature accelerometers and gyroscopes", *Medical and Biological Engineering and Computing*, vol. 41, no. 6, pp. 710–717, 2003. DOI: 10.1007/BF02349979.

[202] H. S. Milner-Brown and R. B. Stein, "The relation between the surface electromyogram and muscular force", *The Journal of Physiology*, vol. 246, no. 3, pp. 549–569, 1975. DOI: 10.1113/jphysiol.1975.sp010904.

[203] G. Francisco, J. Chae, H. Chawla, S. Kirshblum, R. Zorowitz, G. Lewis, and S. Pang, "Electromyogram-triggered neuromuscular stimulation for improving the arm function of acute stroke survivors: A randomized pilot study", *Archives of Physical Medicine and*

Rehabilitation, vol. 79, no. 5, pp. 570–575, 1998. DOI: 10.1016/S0003-9993(98)90074-0.

[204] J. Cauraugh, K. Light, S. Kim, M. Thigpen, and A. Behrman, "Chronic motor dysfunction after stroke: Recovering wrist and finger extension by electromyography-triggered neuromuscular stimulation", *Stroke*, vol. 31, pp. 1360–1364, 2000. DOI: 10.1161/01.STR.31.6.1360.

[205] J. d. R. Millán, F. Renkens, J. Mourino, and W. Gerstner, "Noninvasive brain-actuated control of a mobile robot by human EEG", *IEEE Transactions on Biomedical Engineering*, vol. 51, no. 6, pp. 1026–1033, 2004. DOI: 10.1109/TBME.2004.827086.

[206] R. Leeb, F. Lee, C. Keinrath, R. Scherer, H. Bischof, and G. Pfurtscheller, "Brain–computer communication: Motivation, aim, and impact of exploring a virtual apartment", *IEEE Transactions on Neural Systems and Rehabilitation Engineering*, vol. 15, no. 4, pp. 473–482, 2007. DOI: 10.1109/TNSRE.2007.906956.

[207] J. J. Daly and J. R. Wolpaw, "Brain–computer interfaces in neurological rehabilitation", *The Lancet Neurology*, vol. 7, no. 11, pp. 1032–1043, 2008. DOI: 10.1016/S1474-4422(08)70223-0.

[208] J. d. R. Millán, R. Rupp, G. Müller-Putz, R. Murray-Smith, C. Giugliemma, M. Tangermann, *et al.*, "Combining brain-computer interfaces and assistive technologies: State-of-the-art and challenges", *Frontiers in Neuroscience*, vol. 4, p. 161, 2010. DOI: 10.3389/fnins.2010.00161.

[209] A. M. Savić, N. M. Malešević, and M. B. Popović, "Feasibility of a hybrid brain-computer interface for advanced functional electrical therapy", *The Scientific World Journal*, vol. 2014, p. 797 128, 2014. DOI: 10.1155/2014/797128.

[210] R. T. Lauer, P. H. Peckham, and K. L. Kilgore, "EEG-based control of a hand grasp neuroprosthesis", *NeuroReport*, vol. 10, no. 8, pp. 1767–1771, 1999.

[211] E. Hortal, D. Planelles, F. Resquin, J. M. Climent, J. M. Azorín, and J. L. Pons, "Using a brain-machine interface to control a hybrid upper limb exoskeleton during rehabilitation of patients with neurological conditions", *Journal of NeuroEngineering and Rehabilitation*, vol. 12, no. 1, p. 92, 2015. DOI: 10.1186/s12984-015-0082-9.

[212] A. Schwarz, P. Ofner, J. Pereira, A. I. Sburlea, and G. R. Müller-Putz, "Decoding natural reach-and-grasp actions from human EEG", *Journal of Neural Engineering*, vol. 15, no. 1, p. 016 005, 2017. DOI: 10.1088/1741-2552/aa8911.

[213] C. H. Blabe, V. Gilja, C. A. Chestek, K. V. Shenoy, K. D. Anderson, and J. M. Henderson, "Assessment of brain-machine interfaces from the perspective of people with paralysis", *Journal of Neural Engineering*, vol. 12, no. 4, p. 043 002, 2015. DOI: 10.1088/1741-2560/12/4/043002.

[214] N. Sharma, J.-C. Baron, and J. B. Rowe, "Motor imagery after stroke: Relating outcome to motor network connectivity", *Annals of Neurology*, vol. 66, no. 5, pp. 604–616, 2009. DOI: 10.1002/ana.21810.

[215] J. J. Daly, R. Cheng, J. Rogers, K. Litinas, K. Hrovat, and M. Dohring, "Feasibility of a new application of noninvasive brain computer interface (BCI): A case study of training for recovery of volitional motor control after stroke", *Journal of Neurologic Physical Therapy*, vol. 33, no. 4, pp. 203–211, 2009. DOI: 10.1097/NPT.0b013e3181c1fc0b.

[216] C. Marquez-Chin, I. Bolivar-Tellería, and M. R. Popovic, "Chapter 18 - Brain–Computer interfaces for neurorehabilitation: Enhancing functional electrical stimulation", in *Smart Wheelchairs and Brain–Computer Interfaces*, P. Diez, Ed., Academic Press, 2018, pp. 425–451, ISBN: 978-0-12-812892-3. DOI: 10.1016/B978-0-12-812892-3.00018-2.

[217] H. Nahrstaedt, T. Schauer, R. Shalaby, S. Hesse, and J. Raisch, "Automatic control of a drop-foot stimulator based on angle measurement using bioimpedance", *Artificial Organs*, vol. 32, no. 8, pp. 649–654, 2008. DOI: 10.1111/j.1525-1594.2008.00617.x.

[218] H. Nahrstaedt and T. Schauer, "A bioimpedance measurement device for sensing force and position in neuroprosthetic systems", in *Proceedings 4th European Conference of the International Federation for Medical and Biological Engineering (IFMBE)*, J. Vander Sloten, P. Verdonck, M. Nyssen, and J. Haueisen, Eds., ser. IFMBE Proceedings, Berlin/Heidelberg, Germany: Springer, 2009, pp. 1642–1645. DOI: 10.1007/978-3-540-89208-3_390.

[219] A. Duchowski, *Eye Tracking Methodology*, 2nd. London, UK: Springer, 2007, ISBN: 978-1-84628-608-7.

[220] G. Mann, P. Taylor, and R. Lane, "Accelerometer-triggered electrical stimulation for reach and grasp in chronic stroke patients: A pilot study", *Neurorehabilitation and Neural Repair*, vol. 25, no. 8, pp. 774–780, 2011. DOI: 10.1177/1545968310397200.

[221] M. D. Štrbac, N. M. Malešević, R. Čobeljić, and L. Schwirtlich, "Feedback control of the forearm movement of tetraplegic patient based on Microsoft Kinect and multi-pad electrodes", *Journal of Automatic Control*, vol. 21, no. 1, pp. 7–11, 2013. DOI: 10.2298/JAC1301007S.

[222] T. Seel, "Learning control and inertial realtime gait analysis in biomedical applications", PhD thesis, Technische Universität Berlin, Berlin, Germany, 2016. DOI: 10.14279/depositonce-4973.

[223] M. Kok, J. D. Hol, T. B. Schön, F. Gustafsson, and H. Luinge, "Calibration of a magnetometer in combination with inertial sensors", in *Proceedings 15th International Conference on Information Fusion (FUSION)*, (Singapore, Singapore), IEEE, Jul. 2012, pp. 787–793, ISBN: 978-0-9824438-5-9.

[224] T. Exell, C. Freeman, K. Meadmore, M. Kutlu, E. Rogers, A.-M. Hughes, E. Hallewell, and J. Burridge, "Goal orientated stroke rehabilitation utilising electrical stimulation, iterative learning and Microsoft Kinect", in *Proceedings IEEE 13th International Conference on Rehabilitation Robotics (ICORR)*, (Seattle, WA, USA), IEEE, Jun. 2013, p. 6. DOI: 10.1109/ICORR.2013.6650493.

[225] R. B. Ambar, H. B. M. Poad, A. M. B. M. Ali, M. S. B. Ahmad, and M. M. B. A. Jamil, "Multi-sensor arm rehabilitation monitoring device", in *Proceedings International Conference on Biomedical Engineering (ICoBE)*, (Penang, Malaysia), IEEE, Feb. 2012, pp. 424–429. DOI: 10.1109/ICoBE.2012.6179051.

[226] A. S. Sadun, J. Jalani, and J. A. Sukor, "Force sensing resistor (FSR): A brief overview and the low-cost sensor for active compliance control", in *Proceedings SPIE First International Workshop on Pattern Recognition*, (Tokyo, Japan), International Society for Optics and Photonics, vol. 10011, May 2016, p. 1 001 112. DOI: 10.1117/12.2242950.

[227] A. Inmann, M. Haugland, J. Haase, F. Biering-Sörensen, and T. Sinkjaer, "Signals from skin mechanoreceptors used in control of a hand grasp neuroprosthesis", *Neuroreport*, vol. 12, no. 13, pp. 2817–2820, 2001. DOI: 10.1097/00001756-200109170-00013.

[228] W. Baccinelli, F. Molteni, and M. Bulgheroni, "Smart objects in rehabilitation", in *Converging Clinical and Engineering Research on Neurorehabilitation III; Proceedings INCR Biosystems & Biorobotics*, (Pisa, Italy), L. Masia, S. Micera, M. Akay, and J. Pons, Eds., Springer, 2018, pp. 12–15. DOI: 10.1007/978-3-030-01845-0_3.

[229] V. Gritsenko and A. Prochazka, "A functional electric stimulation–assisted exercise therapy system for hemiplegic hand function", *Archives of Physical Medicine and Rehabilitation*, vol. 85, no. 6, pp. 881–885, 2004. DOI: 10.1016/j.apmr.2003.08.094.

[230] L. Schmalfuss, R. Rupp, M. R. Tuga, A. Kogut, M. Hewitt, J. Meincke, *et al.*, "Steer by ear: Myoelectric auricular control of powered wheelchairs for individuals with spinal cord injury", *Restorative Neurology and Neuroscience*, vol. 34, no. 1, pp. 79–95, 2016. DOI: 10.3233/RNN-150579.

[231] J. Kim, H. Park, J. Bruce, E. Sutton, D. Rowles, D. Pucci, *et al.*, "The tongue enables computer and wheelchair control for people with spinal cord injury", *Science Translational Medicine*, vol. 5, no. 213, 213ra166, 2013. DOI: 10.1126/scitranslmed.3006296.

[232] A. I. Sburlea and G. R. Müller-Putz, "Exploring representations of human grasping in neural, muscle and kinematic signals", *Scientific Reports*, vol. 8, no. 1, p. 16 669, 2018. DOI: 10.1038/s41598-018-35018-x.

[233] I. Herrera-Luna, E. J. Rechy-Ramirez, H. V. Rios-Figueroa, and A. Marin-Hernandez, "Sensor fusion used in applications for hand rehabilitation: A systematic review", *IEEE Sensors Journal*, vol. 19, no. 10, pp. 3581–3592, 2019. DOI: 10.1109/JSEN.2019.2897083.

[234] P. U. Lima and G. N. Saridis, "Intelligent controllers as hierarchical stochastic automata", *IEEE Transactions on Systems, Man, and Cybernetics, Part B (Cybernetics)*, vol. 29, no. 2, pp. 151–163, 1999. DOI: 10.1109/3477.752790.

[235] A. Fougner, E. Scheme, A. D. C. Chan, K. Englehart, and Ø. Stavdahl, "Resolving the limb position effect in myoelectric pattern recognition", *IEEE Transactions on Neural Systems and Rehabilitation Engineering*, vol. 19, no. 6, pp. 644–651, 2011. DOI: 10.1109/TNSRE.2011.2163529.

[236] J. G. Hincapie and R. F. Kirsch, "Feasibility of EMG-based neural network controller for an upper extremity neuroprosthesis", *IEEE Transactions on Neural Systems and Rehabilitation Engineering*, vol. 17, no. 1, pp. 80–90, 2009. DOI: 10.1109/TNSRE.2008.2010480.

[237] D. Blana, R. F. Kirsch, and E. K. Chadwick, "Combined feedforward and feedback control of a redundant, nonlinear, dynamic musculoskeletal system", *Medical & Biological Engineering & Computing*, vol. 47, no. 5, pp. 533–542, 2009. DOI: 10.1007/s11517-009-0479-3.

[238] T. Roux-Oliveira, L. R. Costa, A. V. Pina, and P. Paz, "Extremum seeking-based adaptive PID control applied to neuromuscular electrical stimulation", *Anais da Academia Brasileira de Ciências*, vol. 91, 2019. DOI: 10.1590/0001-3765201820180544.

[239] T. A. Thrasher, V. Zivanovic, W. McIlroy, and M. R. Popovic, "Rehabilitation of reaching and grasping function in severe hemiplegic patients using functional electrical stimulation therapy", *Neurorehabilitation and Neural Repair*, vol. 22, no. 6, pp. 706–714, 2008. DOI: 10.1177/1545968308317436.

[240] E. d. L. d. Santos, M. C. Gelain, E. Krueger, G. N. Nogueira-Neto, and P. Nohama, "Artificial motor control for electrically stimulated upper limbs of plegic or paretic people", *Research on Biomedical Engineering*, vol. 32, no. 2, pp. 199–211, 2016. DOI: 10.1590/2446-4740.03415.

[241] P. E. Crago, R. J. Nakai, and H. J. Chizeck, "Feedback regulation of hand grasp opening and contact force during stimulation of paralyzed muscle", *IEEE Transactions on Biomedical Engineering*, vol. 38, no. 1, pp. 17–28, 1991. DOI: 10.1109/10.68205.

[242] R. Thorsen, E. Occhi, S. Boccardi, and M. Ferrarin, "Functional electrical stimulation reinforced tenodesis effect controlled by myoelectric activity from wrist extensors", *Journal of Rehabilitation Research & Development*, vol. 43, no. 2, pp. 247–256, 2006. DOI: 10.1682/JRRD.2005.04.0068.

[243] R. Thorsen, D. D. Costa, S. Chiaramonte, L. Binda, T. R. Beghi, E. Occhi, and M. Ferrarin, "A noninvasive neuroprosthesis augments hand grasp force in individuals with cervical spinal cord injury: The functional and therapeutic effects", *The Scientific World Journal*, vol. 2013, p. 836 959, 2013. DOI: 10.1155/2013/836959.

[244] R. Thorsen, M. Cortesi, J. Jonsdottir, I. Carpinella, D. Morelli, A. Casiraghi, *et al.*, "Myoelectrically driven functional electrical stimulation may increase motor recovery of upper limb in poststroke subjects: A randomized controlled pilot study", *Journal of Rehabilitation Research & Development*, vol. 50, no. 6, pp. 785–794, 2013. DOI: 10.1682/JRRD.2012.07.0123.

[245] R. C. Lyle, "A performance test for assessment of upper limb function in physical rehabilitation treatment and research", *International Journal of Rehabilitation Research*, vol. 4, no. 4, pp. 483–492, 1981.

[246] J. H. van der Lee, V. De Groot, H. Beckerman, R. C. Wagenaar, G. J. Lankhorst, and L. M. Bouter, "The intra- and interrater reliability of the action research arm test: A practical test of upper extremity function in patients with stroke", *Archives of Physical Medicine and Rehabilitation*, vol. 82, no. 1, pp. 14–19, 2001. DOI: 10.1053/apmr.2001.18668.

[247] R. C. Salbert, T. Schauer, S. Schmidt, and J. Raisch, "Funktionelles handöffnen und -schließen mittels EMG-gesteuerter elektrischer stimulation", in *Proceedings of the 4th Wismar Symposium on Automatic Control (AUTSYM)*, (Wismar, Germany), 2005, pp. 1–4.

[248] A. L. Cologni, M. G. Madaschi, F. Previdi, C. Werner, and T. Schauer, "Automatic adjustment of electromyography-based FES control", in *Proceedings 18th Annual Conference of the International FES Society (IFESS)*, (Donostia-San Sebastián, Spain), IFESS, 2013.

[249] J. L. Emken, J. E. Bobrow, and D. J. Reinkensmeyer, "Robotic movement training as an optimization problem: Designing a controller that assists only as needed", in *Proceedings 9th International Conference on Rehabilitation Robotics (ICORR)*, (Chicago, IL, USA), IEEE, Jun. 2005, pp. 307–312. DOI: 10.1109/ICORR.2005.1501108.

[250] R. Riener, L. Lunenburger, S. Jezernik, M. Anderschitz, G. Colombo, and V. Dietz, "Patient-cooperative strategies for robot-aided treadmill training: First experimental results", *IEEE Transactions on Neural Systems and Rehabilitation Engineering*, vol. 13, no. 3, pp. 380–394, 2005. DOI: 10.1109/TNSRE.2005.848628.

[251] M. Lotze, C. Braun, N. Birbaumer, S. Anders, and L. G. Cohen, "Motor learning elicited by voluntary drive", *Brain*, vol. 126, no. 4, pp. 866–872, 2003. DOI: 10.1093/brain/awg079.

[252] A. Kaelin-Lang, L. Sawaki, and L. G. Cohen, "Role of voluntary drive in encoding an elementary motor memory", *Journal of Neurophysiology*, vol. 93, no. 2, pp. 1099–1103, 2005. DOI: 10.1152/jn.00143.2004.

[253] K. J. Åström and B. Wittenmark, *Computer-Controlled Systems: Theory and Design*, 3rd. Upper Saddle River, NJ, USA: Prentice Hall, 1997, ISBN: 978-0-486-48613-0.

[254] Y.-X. Zhou, H.-P. Wang, X.-P. Cao, Z.-Y. Bi, Y.-J. Gao, X.-B. Chen, X.-Y. Lü, and Z.-G. Wang, "Electromyographic bridge–a multi-movement volitional control method for functional electrical stimulation: Prototype system design and experimental validation", in *Proceedings 39th Annual International Conference of the IEEE Engineering in Medicine and Biology Society (EMBC)*, (Seogwipo, South Korea), IEEE, Jul. 2017, pp. 205–208. DOI: 10.1109/EMBC.2017.8036798.

[255] H.-P. Wang, Z.-Y. Bi, Y. Zhou, Y.-X. Zhou, Z.-G. Wang, and X.-Y. Lv, "Real-time and wearable functional electrical stimulation system for volitional hand motor function control using the electromyography bridge method", *Neural Regeneration Research*, vol. 12, no. 1, pp. 133–142, 2017. DOI: 10.4103/1673-5374.197139.

[256] M. Gandolla, S. Ferrante, G. Ferrigno, D. Baldassini, F. Molteni, E. Guanziroli, *et al.*, "Artificial neural network EMG classifier for functional hand grasp movements prediction", *Journal of International Medical Research*, vol. 45, no. 6, pp. 1831–1847, 2017. DOI: 10.1177/0300060516656689.

[257] N. Jiang, S. Dosen, K.-R. Muller, and D. Farina, "Myoelectric control of artificial limbs—is there a need to change focus?", *IEEE Signal Processing Magazine*, vol. 29, no. 5, pp. 152–150, 2012. DOI: 10.1109/MSP.2012.2203480.

[258] A. Ramos-Murguialday, E. García-Cossio, A. Walter, W. Cho, D. Broetz, M. Bogdan, L. G. Cohen, and N. Birbaumer, "Decoding upper limb residual muscle activity in severe chronic stroke", *Annals of Clinical and Translational Neurology*, vol. 2, no. 1, pp. 1–11, 2015. DOI: 10.1002/acn3.122.

[259] A. Sarasola-Sanz, N. Irastorza-Landa, F. Shiman, E. López-Larraz, M. Spüler, N. Birbaumer, and A. Ramos-Murguialday, "EMG-based multi-joint kinematics decoding for robot-aided rehabilitation therapies", in *Proceedings IEEE International Conference on Rehabilitation Robotics (ICORR)*, (Singapore, Singapore), IEEE, Aug. 2015, pp. 229–234. DOI: 10.1109/ICORR.2015.7281204.

[260] Y. Geng, Y. Ouyang, O. W. Samuel, S. Chen, X. Lu, C. Lin, and G. Li, "A robust sparse representation based pattern recognition approach for myoelectric control", *IEEE Access*, vol. 6, pp. 38 326–38 335, 2018. DOI: 10.1109/ACCESS.2018.2851282.

[261] S. W. Lee, K. M. Wilson, B. A. Lock, and D. G. Kamper, "Subject-specific myoelectric pattern classification of functional hand movements for stroke survivors", *IEEE Transactions on Neural Systems and Rehabilitation Engineering*, vol. 19, no. 5, pp. 558–566, 2011. DOI: 10.1109/TNSRE.2010.2079334.

[262] M. Rohm, M. Schneiders, C. Müller, A. Kreilinger, V. Kaiser, G. R. Müller-Putz, and R. Rupp, "Hybrid brain–computer interfaces and hybrid neuroprostheses for restoration of upper limb functions in individuals with high-level spinal cord injury", *Artificial Intelligence in Medicine*, vol. 59, no. 2, pp. 133–142, 2013. DOI: 10.1016/j.artmed.2013.07.004.

[263] J. Likitlersuang, R. Koh, X. Gong, L. Jovanovic, I. Bolivar-Telleria, M. Myers, J. Zariffa, and C. Márquez-Chin, "EEG-controlled functional electrical stimulation therapy with automated grasp selection: A proof-of-concept study", *Topics in Spinal Cord Injury Rehabilitation*, vol. 24, no. 3, pp. 265–274, 2018. DOI: 10.1310/sci2403-265.

[264] R. W. Bohannon and M. B. Smith, "Interrater reliability of a modified Ashworth Scale of muscle spasticity", *Physical Therapy*, vol. 67, no. 2, pp. 206–207, 1987. DOI: 10.1093/ptj/67.2.206.

[265] P. A. Tresadern, S. B. Thies, L. P. J. Kenney, D. Howard, and J. Y. Goulermas, "Rapid prototyping for functional electrical stimulation control", *IEEE Pervasive Computing*, vol. 7, no. 2, pp. 62–69, 2008. DOI: 10.1109/MPRV.2008.35.

[266] A. J. Westerveld, A. C. Schouten, P. H. Veltink, and H. van der Kooij, "Passive reach and grasp with functional electrical stimulation and robotic arm support", in *Proceedings 36th International Conference IEEE Engineering in Medicine and Biology Society (EMBC)*, (Chicago, IL, USA), IEEE, Aug. 2014, pp. 3085–3089. DOI: 10.1109/EMBC.2014.6944275.

[267] M. D. Štrbac and D. B. Popović, "Computer vision with Microsoft Kinect for control of functional electrical stimulation: ANN classification of the grasping intentions", in *Proceedings 12th Symposium on Neural Network Applications in Electrical Engineering (NEUREL)*, (Belgrade, Serbia), IEEE, Nov. 2014, pp. 153–156. DOI: 10.1109/NEUREL.2014.7011491.

[268] D. Simonsen, E. G. Spaich, J. Hansen, and O. K. Andersen, "Design and test of a closed-loop FES system for supporting function of the hemiparetic hand based on automatic detection using the Microsoft Kinect sensor", *IEEE Transactions on Neural Systems and Rehabilitation Engineering*, vol. 25, no. 8, pp. 1249–1256, 2017. DOI: 10.1109/TNSRE.2016.2622160.

[269] J. S. Knutson, M. Y. Harley, T. Z. Hisel, N. S. Makowski, and J. Chae, "Contralaterally controlled functional electrical stimulation for recovery of elbow extension and hand opening after stroke: A pilot case series study", *American Journal of Physical Medicine & Rehabilitation*, vol. 93, no. 6, pp. 528–539, 2014. DOI: 10.1097/PHM.0000000000000066.

[270] M. Sun, C. Smith, D. Howard, L. Kenney, H. Luckie, K. Waring, *et al.*, "FES-UPP: A flexible functional electrical stimulation system to support upper limb functional activity practice", *Frontiers in Neuroscience*, vol. 12, 2018. DOI: 10.3389/fnins.2018.00449.

[271] M. Sun, L. Kenney, C. Smith, K. Waring, H. Luckie, and D. Howard, "A flexible finite state controller for upper limb functional electrical stimulation", in *Proceedings 20th Annual Conference of the International FES Society (IFESS)*, (La Grande-Motte, France), IFESS, Jun. 2016.

[272] C. Smith, M. Sun, L. Kenney, D. Howard, H. Luckie, K. Waring, *et al.*, "A three-site clinical feasibility study of a flexible functional electrical stimulation system to support functional task practice for upper limb recovery in people with stroke", *Frontiers in Neurology*, vol. 10, p. 227, 2019. DOI: 10.3389/fneur.2019.00227.

[273] H. Luckie, K. Waring, C. Smith, M. Sun, L. Kenney, D. Howard, *et al.*, "Clinicians' perspectives on the usability of a flexible functional electrical stimulation system to support upper limb task practice in people with stroke", in *Proceedings Annual Conference of the International FES Society (IFESS)*, (Toronto, ON, Canada), IFESS, Jun. 2019.

[274] A. Reinert, J. C. Loitz, F. Quandt, D. Schroeder, and W. H. Krautschneider, "Smart control for functional electrical stimulation with optimal pulse intensity", *Current Directions in Biomedical Engineering*, vol. 2, no. 1, pp. 395–398, 2016. DOI: 10.1515/cdbme-2016-0088.

[275] E. F. Hodkin, Y. Lei, J. Humby, I. S. Glover, S. Choudhury, H. Kumar, *et al.*, "Automated FES for upper limb rehabilitation following stroke and spinal cord injury", *IEEE Transactions on Neural Systems and Rehabilitation Engineering*, vol. 26, no. 5, pp. 1067–1074, 2018. DOI: 10.1109/TNSRE.2018.2816238.

[276] A. J. Westerveld, A. C. Schouten, P. H. Veltink, and H. van der Kooij, "Control of thumb force using surface functional electrical stimulation and muscle load sharing", *Journal of NeuroEngineering and Rehabilitation*, vol. 10, no. 1, p. 104, 2013. DOI: 10.1186/1743-0003-10-104.

[277] F. Grimm and A. Gharabaghi, "Closed-loop neuroprosthesis for reach-to-grasp assistance: Combining adaptive multi-channel neuromuscular stimulation with a multi-joint arm exoskeleton", *Frontiers in Neuroscience*, vol. 10, p. 284, 2016. DOI: 10.3389/fnins.2016.00284.

[278] C. Klauer, T. Schauer, W. Reichenfelser, J. Karner, S. Zwicker, M. Gandolla, *et al.*, "Feedback control of arm movements using neuro-muscular electrical stimulation (NMES) combined with a lockable, passive exoskeleton for gravity compensation", *Frontiers in Neuroscience*, vol. 8, p. 262, 2014. DOI: 10.3389/fnins.2014.00262.

[279] A.-M. Hughes, C. T. Freeman, J. H. Burridge, P. H. Chappell, P. L. Lewin, and E. Rogers, "Feasibility of iterative learning control mediated by functional electrical stimulation for reaching after stroke", *Neurorehabilitation and Neural Repair*, vol. 23, no. 6, pp. 559–568, 2009. DOI: 10.1177/1545968308328718.

[280] K. L. Meadmore, A.-M. Hughes, C. T. Freeman, Z. Cai, D. Tong, J. H. Burridge, and E. Rogers, "Functional electrical stimulation mediated by iterative learning control and 3D robotics reduces motor impairment in chronic stroke", *Journal of NeuroEngineering and Rehabilitation*, vol. 9, no. 1, p. 32, 2012. DOI: 10.1186/1743-0003-9-32.

[281] C. T. Freeman, A.-M. Hughes, J. H. Burridge, P. H. Chappell, P. L. Lewin, and E. Rogers, "Iterative learning control of FES applied to the upper extremity for rehabilitation", *Control Engineering Practice*, vol. 17, no. 3, pp. 368–381, 2009. DOI: 10.1016/j.conengprac.2008.08.003.

[282] K. L. Meadmore, T. A. Exell, E. Hallewell, A.-M. Hughes, C. T. Freeman, M. Kutlu, *et al.*, "The application of precisely controlled functional electrical stimulation to the shoulder, elbow and wrist for upper limb stroke rehabilitation: A feasibility study", *Journal of NeuroEngineering and Rehabilitation*, vol. 11, no. 1, p. 105, 2014. DOI: 10.1186/1743-0003-11-105.

[283] C. T. Freeman, "Electrode array-based electrical stimulation using ILC with restricted input subspace", *Control Engineering Practice*, vol. 23, pp. 32–43, 2014. DOI: 10.1016/j.conengprac.2013.11.006.

[284] C. T. Freeman, K. L. Meadmore, A.-M. Hughes, N. Grabham, J. Tudor, and K. Yang, "Multiple model adaptive ILC for human movement assistance", in *Proceedings European Control Conference (ECC)*, (Limassol, Cyprus), IEEE, Jun. 2018, pp. 2405–2410. DOI: 10.23919/ECC.2018.8550450.

[285] C. Salchow, A. Dorn, M. Valtin, and T. Schauer, "Intention recognition for FES in a grasp-and-release task using volitional EMG and inertial sensors", *Current Directions in Biomedical Engineering*, vol. 3, no. 2, pp. 161–165, DOI: 10.1515/cdbme-2017-0034.

[286] C. Salchow, M. Valtin, T. Seel, and T. Schauer, "Development of a feedback-controlled hand neuroprosthesis: FES-supported mirror training", in *AUTOMED Workshop*, (Wismar, Germany), Sep. 2016.

[287] M. Valtin, C. Salchow, T. Seel, D. Laidig, and T. Schauer, "Modular finger and hand motion capturing system based on inertial and magnetic sensors", *Current Directions in Biomedical Engineering*, vol. 3, no. 1, pp. 19–23, 2017. DOI: 10.1515/cdbme-2017-0005.

[288] C. Salchow-Hömmen, T. Thomas, M. Valtin, and T. Schauer, "Automatic control of grasping strength for functional electrical stimulation in forearm movements via electrode arrays", *At-Automatisierungstechnik*, vol. 66, no. 12, pp. 1027–1036, 2018. DOI: 10.1515/auto-2018-0068.

[289] R. Rupp, M. Rohm, M. Schneiders, A. Kreilinger, and G. R. Müller-Putz, "Functional rehabilitation of the paralyzed upper extremity after spinal cord injury by noninvasive hybrid neuroprostheses", *Proceedings of the IEEE*, vol. 103, no. 6, pp. 954–968, 2015. DOI: 10.1109/JPROC.2015.2395253.

[290] C. E. Clauser, J. T. McConville, and J. W. Young, "Weight, volume, and center of mass of segments of the human body", Antioch College, Yellow Springs, OH, USA, Tech. Rep., 1969.

[291] R. Zhang, F. Hoflinger, and L. M. Reind, "Calibration of an IMU using 3-D rotation platform", *IEEE Sensors Journal*, vol. 14, no. 6, pp. 1778–1787, 2014. DOI: 10.1109/JSEN.2014.2303642.

[292] M. Sojka and P. Píša, "Usable Simulink embedded coder target for Linux", in *Proceedings 16th Real Time Linux Workshop*, (Düsseldorf, Germany), Oct. 2014, pp. 1–6.

[293] L. Schönijahn, "Funktionelle Elektrostimulation in der Schlaganfallbehandlung: Nutzerzentrierte Entwicklung einer grafischen Benutzeroberfläche", Master thesis, Technische Universität Berlin, Berlin, Germany, 2017.

[294] R. Colombo and V. Sanguineti, *Rehabilitation Robotics: Technology and Application*, 1st. Academic Press, 2018, ISBN: 9780128119969. DOI: 10.1016/C2016-0-02285-4.

[295] W. H. K. de Vries, H. E. J. Veeger, C. T. M. Baten, and F. C. T. van der Helm, "Magnetic distortion in motion labs, implications for validating inertial magnetic sensors", *Gait & Posture*, vol. 29, no. 4, pp. 535–541, 2009. DOI: 10.1016/j.gaitpost.2008.12.004.

[296] T. Seel and S. Ruppin, "Eliminating the effect of magnetic disturbances on the inclination estimates of inertial sensors", *IFAC-PapersOnLine*, vol. 50, no. 1, pp. 8798–8803, 2017. DOI: 10.1016/j.ifacol.2017.08.1534.

[297] Y. Choi, K. Yoo, S. J. Kang, B. Seo, and S. K. Kim, "Development of a low-cost wearable sensing glove with multiple inertial sensors and a light and fast orientation estimation algorithm", *The Journal of Supercomputing*, pp. 1–14, 2018. DOI: 10.1007/s11227-017-2021-y.

[298] B.-S. Lin, I. Lee, S.-Y. Yang, Y.-C. Lo, J. Lee, J.-L. Chen, *et al.*, "Design of an inertial-sensor-based data glove for hand function evaluation", *Sensors*, vol. 18, no. 5, p. 1545, 2018. DOI: 10.3390/s18051545.

[299] D. A. Winter, *Biomechanics and Motor Control of Human Movement*, 4th. Hoboken, NJ, USA: John Wiley & Sons, 2009, ISBN: 978-0-470-39818-0.

[300] G. Wu, F. C. T. van der Helm, H. E. J. Veeger, M. Makhsous, P. van Roy, C. Anglin, *et al.*, "ISB recommendation on definitions of joint coordinate systems of various joints for the reporting of human joint motion–Part II: Shoulder, elbow, wrist and hand", *Journal of Biomechanics*, vol. 38, no. 5, pp. 981–992, 2005. DOI: 10.1016/j.jbiomech.2004.05.042.

[301] B. Goislard de Monsabert, J. M. A. Visser, L. Vigouroux, F. C. T. van der Helm, and H. E. J. Veeger, "Comparison of three local frame definitions for the kinematic analysis of the fingers and the wrist", *Journal of Biomechanics*, vol. 47, no. 11, pp. 2590–2597, 2014. DOI: 10.1016/j.jbiomech.2014.05.025.

[302] A. Gustus, G. Stillfried, J. Visser, H. Jörntell, and P. van der Smagt, "Human hand modelling: Kinematics, dynamics, applications", *Biological Cybernetics*, vol. 106, no. 11–12, pp. 741–755, 2012. DOI: 10.1007/s00422-012-0532-4.

[303] B. Buchholz, T. J. Armstrong, and S. A. Goldstein, "Anthropometric data for describing the kinematics of the human hand", *Ergonomics*, vol. 35, no. 3, pp. 261–273, 1992. DOI: 10.1080/00140139208967812.

[304] R. Hamilton and R. A. Dunsmuir, "Radiographic assessment of the relative lengths of the bones of the fingers of the human hand", *The Journal of Hand Surgery*, vol. 27, no. 6, pp. 546–548, 2002. DOI: 10.1054/jhsb.2002.0822.

[305] A. E. Park, J. J. Fernandez, K. Schmedders, and M. S. Cohen, "The Fibonacci sequence: Relationship to the human hand", *The Journal of Hand Surgery*, vol. 28, no. 1, pp. 157–160, 2003. DOI: 10.1053/jhsu.2003.50000.

[306] A. Buryanov and V. Kotiuk, "Proportions of hand segments", *International Journal of Morphology*, vol. 28, pp. 755–758, 2010.

[307] L. Radavelli, R. Simoni, E. R. De Pieri, and D. Martins, "A comparative study of the kinematics of robots manipulators by Denavit-Hartenberg and dual quaternion", *Mecánica Computacional*, vol. 31, no. 15, pp. 2833–2848, 2012.

[308] G. Leclercq, P. Lefèvre, and G. Blohm, "3D kinematics using dual quaternions: Theory and applications in neuroscience", *Frontiers in Behavioral Neuroscience*, vol. 7, p. 7, 2013. DOI: 10.3389/fnbeh.2013.00007.

[309] W. R. Hamilton, "II. on quaternions; or on a new system of imaginaries in algebra", *The Philosophical Magazine Series 3*, vol. 25, no. 163, 1844. DOI: 10.1080/14786444408644923.

[310] B. Kenwright, "A beginners guide to dual-quaternions: What they are, how they work, and how to use them for 3D", in *Communication Proceedings of 20th International Conference on Computer Graphics, Visualization and Computer Vision (WSCG)*, (Plzen, Czech Republic), Jun. 2012, pp. 1–13.

[311] M. Kok, J. D. Hol, and T. B. Schön, "An optimization-based approach to human body motion capture using inertial sensors", in *IFAC Proceedings Volumes*, vol. 47, 2014, pp. 79–85. DOI: 10.3182/20140824-6-ZA-1003.02252.

[312] P. Müller, M. A. Bégin, T. Schauer, and T. Seel, "Alignment-free, self-calibrating elbow angles measurement using inertial sensors", *IEEE Journal of Biomedical and Health Informatics*, vol. 21, no. 2, pp. 312–319, 2017, ISSN: 2168-2194. DOI: 10.1109/JBHI.2016.2639537.

[313] W. Teufl, M. Miezal, B. Taetz, M. Fröhlich, and G. Bleser, "Validity, test-retest reliability and long-term stability of magnetometer free inertial sensor based 3D joint kinematics", *Sensors*, vol. 18, no. 7, 2018. DOI: 10.3390/s18071980.

[314] H. G. Kortier, H. M. Schepers, and P. H. Veltink, "Identification of object dynamics using hand worn motion and force sensors", *Sensors*, vol. 16, no. 12, p. 2005, 2016. DOI: 10.3390/s16122005.

[315] J. Malešević, M. Isaković, M. Štrbac, M. Kostić, V. Kojić, L. Konstantinović, O. Dordević, and T. Keller, "Wireless glove for estimation of hand functions and tracking movement amplitudes during FES therapy", in *Proceedings Annual Conference of the International FES Society (IFESS)*, (Toronto, ON, Canada), IFESS, Jun. 2019.

[316] D. Laidig, S. Trimpe, and T. Seel, "Event-based sampling for reducing communication load in realtime human motion analysis by wireless inertial sensor networks", *Current Directions in Biomedical Engineering*, vol. 2, no. 1, pp. 711–714, 2016, ISSN: 2364-5504. DOI: 10.1515/cdbme-2016-0154.

[317] K. Hrabia C.-E.and Wolf and M. Wilhelm, "Whole hand modeling using 8 wearable sensors: Biomechanics for hand pose prediction", in *Proceedings 4th Augmented Human International Conference*, (Stuttgart, Germany), ACM, Mar. 2013, pp. 21–28. DOI: 10.1145/2459236.2459241.

[318] C. Salchow, M. Valtin, T. Seel, and T. Schauer, "A new semi-automatic approach to find suitable virtual electrodes in arrays using an interpolation strategy", *European Journal of Tranlational Myology*, vol. 26, no. 2, p. 6029, 2016. DOI: 10.4081/ejtm.2016.6029.

[319] S. Micera, T. Keller, M. Lawrence, M. Morari, and D. B. Popović, "Wearable neural prostheses", *IEEE Engineering in Medicine and Biology Magazine*, vol. 29, no. 3, pp. 64–69, 2010. DOI: 10.1109/MEMB.2010.936547.

[320] A. J. Westerveld, A. C. Schouten, P. H. Veltink, and H. van der Kooij, "Selectivity and resolution of surface electrical stimulation for grasp and release", *IEEE Transactions on Neural Systems and Rehabilitation Engineering*, vol. 20, no. 1, pp. 94–101, 2012. DOI: 10.1109/TNSRE.2011.2178749.

[321] K. B. Petropoulou, I. G. Panourias, C.-A. Rapidi, and D. E. Sakas, "The phenomenon of spasticity: A pathophysiological and clinical introduction to neuromodulation therapies", in *Operative Neuromodulation*, 1, D. E. Sakas, B. A. Simpson, and E. S. Krames, Eds., vol. 97, Vienna, Austria: Springer, 2007, pp. 137–144. DOI: 10.1007/978-3-211-33079-1_19.

[322] D. G. Kamper, H. C. Fischer, E. G. Cruz, and W. Z. Rymer, "Weakness is the primary contributor to finger impairment in chronic stroke", *Archives of Physical Medicine and Rehabilitation*, vol. 87, no. 9, pp. 1262–1269, 2006. DOI: 10.1016/j.apmr.2006.05.013.

[323] A. E. Jackson, R. J. Holt, P. R. Culmer, S. G. Makower, M. C. Levesley, R. C. Richardson, *et al.*, "Dual robot system for upper limb rehabilitation after stroke: The design process", *Proceedings of the Institution of Mechanical Engineers, Part C: Journal of Mechanical Engineering Science*, vol. 221, no. 7, pp. 845–857, 2007. DOI: 10.1243/0954406JMES561.

[324] D. Popović, N. Malešević, and T. Keller, "Apparatus for external activation of paralyzed body parts by stimulation of peripheral nerves", Patent EP 2 519 312 B1, Nov. 2012.

[325] N. Jankowski, L. Schönijahn, C. Salchow, E. Ivanova, and M. Wahl, "User-centred design as an important component of technological development", *Current Directions in Biomedical Engineering*, vol. 3, no. 1, pp. 69–73, 2017. DOI: 10.1515/cdbme-2017-0015.

[326] N. Ravichandran, K. Aw, and A. McDaid, "Influence of electrode geometry on selectivity and comfort for functional electrical stimulation", in *Proceedings Annual Conference of the International FES Society (IFESS)*, (Toronto, ON, Canada), IFESS, Jun. 2019.

[327] K. J. Åström and T. Hägglund, *PID controllers: Theory, design, and tuning*, 2nd. Durham, NC, USA: Instrument Society of America, 1995, ISBN: 978-1-55617-516-9.

[328] J. C. Van Swieten, P. J. Koudstaal, M. C. Visser, H. J. A. Schouten, and J. van Gijn, "Interobserver agreement for the assessment of handicap in stroke patients", *Stroke*, vol. 19, no. 5, pp. 604–607, 1988.

[329] V. Janda, Ed., *Manuelle Muskelfunktionsdiagnostik*, 4th. München, Germany: Urban & Fischer, 2000, ISBN: 978-3437464300.

[330] F. J. Neyer, J. Felber, and C. Gebhardt, "Development and validation of a brief measure of technology commitment", *Diagnostica*, vol. 58, no. 2, pp. 87–99, 2012. DOI: 10.1026/0012-1924/a000067.

[331] F. D. Davis, "Perceived usefulness, perceived ease of use, and user acceptance of information technology", *MIS quarterly*, vol. 13, no. 3, pp. 319–340, 1989. DOI: 10.2307/249008.

[332] J. Nielsen. (2012). Thinking aloud: The #1 usability tool, [Online]. Available: https://www.nngroup.com/articles/thinking-aloud-the-1-usability-tool/ (visited on 08/29/2017).

[333] M. W. Van Someren, Y. F. Barnard, and J. Sandberg, *The Think aloud method. A practical guide to modelling cognitive processes*. London, UK: Academic Press, 1994, ISBN: 0-12-714270-3.

[334] P. Mayring, *Qualitative Inhaltsanalyse. Grundlagen und Techniken*, 11th. Weinheim, Germany: Beltz, 2010.

[335] T. Dresing and T. Pehl, "Transkription", in *Handbuch qualitative Forschung in der Psychologie*, G. Mey and K. Mruck, Eds., Wiesbaden, Germany: Springer, 2010, pp. 723–733.

[336] A. K. Forshaug and J. B. Sigurjónsson, "User involvement in the design of health care devices", in *Proceedings 17th International Conference on Engineering and Product Design Education*, (Loughborough, UK), Sep. 2015.

[337] S.-C. Chen, C.-H. Yu, C.-L. Liu, C.-H. Kuo, and S.-T. Hsu, "Design of surface electrode array applied for hand functional electrical stimulation in the variation of forearm gesture", in *Proceedings 12th Annual Conference of the International FES Society (IFESS)*, (Philadelphia, PA USA), IFESS, Nov. 2007.

[338] T. Thomas, C. Salchow, M. Valtin, and T. Schauer, "Automatic real-time adaptation of electrode positions for grasping with FES during forearm movements", in *AUTOMED Workshop*, (Villingen-Schwenningen, Germany), Mar. 2018.

[339] C. T. Freeman, E. Rogers, A.-M. Hughes, J. H. Burridge, and K. L. Meadmore, "Iterative learning control in health care: Electrical stimulation and robotic-assisted upper-limb stroke rehabilitation", *IEEE Control Systems Magazine*, vol. 32, no. 1, pp. 18–43, 2012. DOI: 10.1109/MCS.2011.2173261.

[340] D. Laidig, D. Lehmann, M.-A. Bégin, and T. Seel, "Magnetometer-free realtime inertial motion tracking by exploitation of kinematic constraints in 2-DOF joints", in *Proceedings 41st IEEE Engineering in Medicine and Biology Conference (EMBC)*, (Berlin, Germany), To appear, IEEE, Jul. 2019.

[341] H. Shin, Z. Watkins, and X. Hu, "Exploration of hand grasp patterns elicitable through non-invasive proximal nerve stimulation", *Scientific Reports*, vol. 7, no. 1, p. 16 595, 2017. DOI: 10.1038/s41598-017-16824-1.

A

Range of Hand Motion

Table A.1: Average range of motion of each joint of the human hand for healthy individuals excerpted from [47]. The values hold for the functional joint axes and with the forearm being in pronation with a right angle in the elbow joint. For the joints MCP, PIP, and DIP, average values over all four fingers F2–F5 are provided.

Joint	**Motion**	**Range**	
		Lower Bound	Upper Bound
wrist	extension/flexion	-60°	80°
	radial/ulnar deviation	-20°	40°
T-CMC	extension/flexion	-30°	40°
	abduction/adduction	0°	50°
	rotation	0°	30°
T-MCP	extension/flexion	0°	50°
T-IP	extension/flexion	-5°	80°
MCP	extension/flexion	-45°	90°
	abduction/adduction	-20°	10°
PIP	extension/flexion	0°	110°
DIP	extension/flexion	-5°	80°

B

Stimulator RehaMovePro

Table B.1: Technical details of the RehaMovePro stimulator (Hasomed GmbH, Magdeburg, Germany).

Stimulator type	constant-current regulated
Number of available stimulation channels	4
Supply voltage	max. 150 V
Pulse amplitude	0–130 mA
Pulse amplitude resolution	0.5 mA
Pulse width	10–4096 μs
Pulse width resolution	1 μs
Pulse shape	adjustable (16 characteristic points)
Stimulation frequency	max. 500 Hz(one channel)

C

Hand Model for Simulations

The biomechanical hand model with 23 DOF together with 17 IMUs of the HSS were implemented as a kinematic multibody framework in *SimMechanics*, as seen in Fig. C.1. Forearm, palm/handback, and finger segments were represented by 'Solid' objects. The implemented standard lengths of the finger segments are provided in Table C.1. The solid's coordinate systems correspond with the defined orientations in Fig. 4.2. All joints were simulated using the 'Revolute Joint' block, which acts as a hinge joint. For joints with more than one DOF (e.g., wrist and MCP), multiple hinge joints were placed after another with different rotation axes. The joints were actuated by angular input (degree).

Each IMU of the HSS was modeled as a 'Solid' object. Via the block 'Transform Sensor,' global acceleration and angular velocity of all three axes of the object were extracted together with the 'true' quaternion for the sensor object. These values were then transformed into a local sensor coordinate system, as they are sensed in real-world measurements. Gravitation was added to the acceleration data. Magnetometer data was simulated for the case of a homogeneous magnetic field in z-direction. The IMU disturbance model consisted of measurement noise and time-invariant plus time-variant bias, which values were based on real sensor data of accelerometers and gyroscopes. The maximum noise derivation from the mean value found in the measured data was $0.05\,{}^{\mathrm{m}}/_{s^2}$ for the accelerometer and $0.0004\,{}^{\mathrm{rad}}/_{s^2}$ for the gyroscope. A histogram of both sensor data showed that the noise is Gaussian distributed. A time-varying bias can be defined with a specific amplitude and frequency in form of a sinusoid.

Table C.1: Assumed finger length in the *Simulink* hand model. Values were extracted from Buryanov & Kotiuk [306].

	F1	**F2**	**F3**	**F4**	**F5**
Length in cm	5.32	7.78	8.84	8.43	6.68

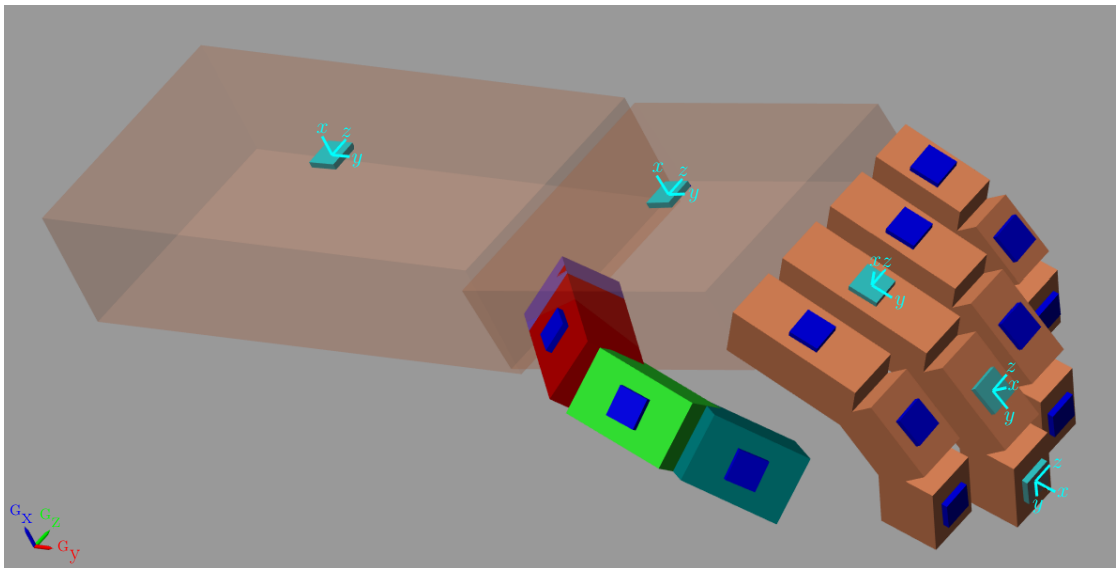

Figure C.1: Visualization ('Mechanics Explorer') of the implemented biomechanic hand model. IMUs of the hand sensor system are modeled by the dark blue boxes.

D

Feedback Controller Experiments

Participants

Measurements for evaluating the performance of the feedback controller for wrist extension were performed in on four unimpaired volunteers (one female, 1 male, age 31 ± 9 years). Written informed consent was obtained. During the experiments, they were instructed to keep their forearm muscles relaxed and not to watch their own hand motion during testing.

Hardware Setup

As these experiments were performed at an early-stage during the research for this thesis, a different stimulator and electrode array setup were utilized for these experiments. FES was applied via the RehaStim1 stimulator (HASOMED GmbH, Magdeburg, Germany) together with a customized demultiplexer from the Control Systems Group. Both parts of the system are displayed in Fig. D.1. Technical details on the stimulator are summarized in Table D.1. The stimulator has a custom firmware (*DeltaMode*) for communication with the demultiplexer and the use of EAs. The demultiplexer is connected with the stimulator via a synchronization channel and one stimulation channel. Together with a customized adapter, it supports EAs with up to 64 elements. The system is able to apply up to ten different stimuation pulses asynchronously to the active elements of a connected electrode array. Please refer to [186] for more information.

Table D.1: Technical details of the RehaStim stimulator.

Stimulator type	current-controlled
Number of available stimulation channels	8
Pulse amplitude	0–130 mA
Pulse amplitude resolution	2 mA
Pulse width	10–500 μs
Pulse width resolution	1 μs
Pulse shape	biphasic, symmetric

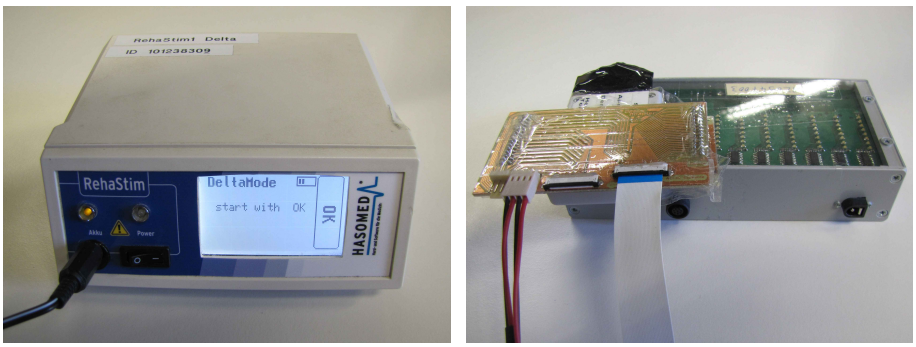

Figure D.1: RehaStim stimulator (left) and customized demultiplexer (right).

The EA which was used in combination with the aforementioned stimulation system is shown in Fig. D.2. It consists of 24 elements of size 12×12 mm in a 6 × 4 arrangement printed on a flexible PCB. The EA was originally designed by Valtin et al. to be used in a drop-foot stimulation setup [126]. A common, self-adhesive hydro-gel layer (7×10 cm; AG702 Gel, Axelgaard Manufacturing Co., Ltd., Fallbrook, CA, USA) over the array elements established contact between the EA and the skin. In the experiments, the EA was placed over hand and finger extensors on the upper half of the forearm. All EA elements serve as active elements. A common counter electrode was placed at approximately 1 cm distance in distal direction. Stimulation was applied with f_s =25 Hz.

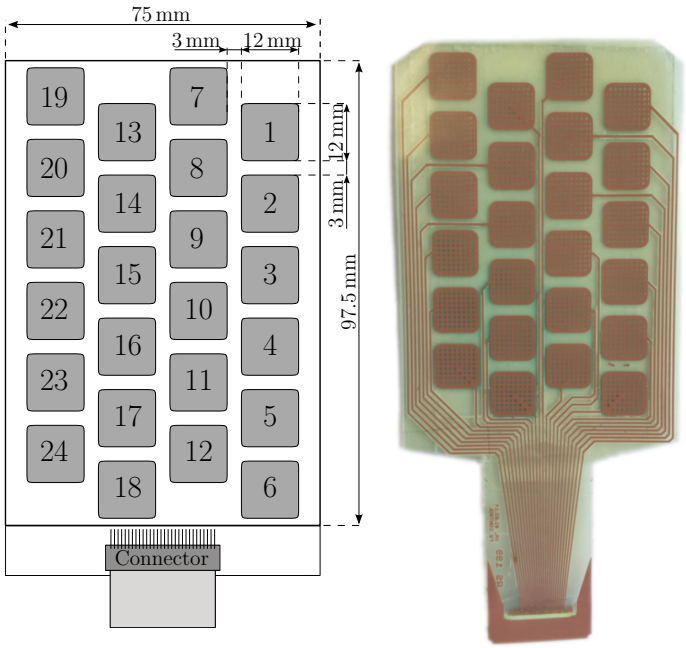

Figure D.2: Customized electrode array with 24 elements in top view (gel-layer at the bottom).

Two inertial measurement units (MTx; Xsens Technologies B.V., Enschede, Netherlands), one placed on the forearm and one of the back of the hand, were used to track the wrist extension (negative) and flexion (positive) angle α, as well as the wrist deviation angle β.

Procedure

Participants were seated at a table in a comfortable chair. All experiments started with the hand and forearm lying flat on a table (α=0°). After the values u_{mot}, u_{step}, and u_{tol} were

determined by testing one single element, step responses were recorded for every element. Model parameters were identified for each element and averaged before calculating the PID controller parameters.

To demonstrate that the suggested controller K is able to track a desired wrist extension throughout the array, two paths of positions $\mathbf{z}$ covering the whole array were defined with two different VE models. Those paths are illustrated in Fig. D.3. Each VE path was tested at least twice in each volunteer: first in open-loop with a constant global stimulation intensity $\hat{u}$ and afterwards in closed-loop.

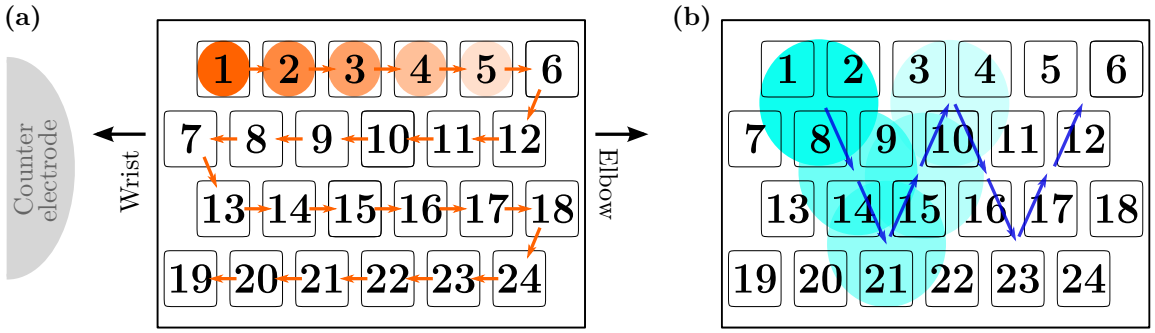

Figure D.3: VE models and tested paths of positions $\mathbf{z}$ through the 24-element EA. (a) A VE model of the size h=12 mm, which equals the size of a single EA element, started at with $\mathbf{z}$ at the center of element 1. The VE stayed on each element for 2.5 s and slowly shifted from one element to the next through the whole array along the orange arrows. (b) A larger VE model of h=30 mm was applied along the path marked by the blue arrows. The path started with $\mathbf{z}$ between elements 1, 2, and 8. The center $\mathbf{z}$ stopped for 2.5 s at every arrowhead.

E

Influence of the Upper Arm Position

Experimental Design

Measurements were performed with different arm postures to obtain the influence of the elbow joint angle on the FES response when stimulating on the forearm. Three postures of elbow flexion of 90°, 45°, and 0° were tested. Furthermore, it was considered that, in a vertical position, the rotation of the hand also comes with a change in the direction of gravity, which could influence the stimulated posture. In order to eliminate the effects of gravity in the analysis, a fourth posture was examined in which the arm hangs vertically, extended next to the body. As a result, the gravitational vector acts along the arm in the distal direction. The tested arm postures are from now on referred to as 90° *flexion*, 45° *flexion*, 0° *horizontal*, and 0° *vertical*, as depicted in Fig. E.1. In each arm position, the same VE was stimulated for hand opening with the forearm in pronation, neutral, and supination. In total, twelve combinations were investigated.

The experimental setup consisted of the following parts of the HNP: RehaMovePro stimulator with demultiplexer, 35-element electrode array above the wrist and finger extensors (extensor array), one single counter electrode, the hand sensor system with two sensor strips (fingers F2–F3), as well as a measurement laptop. At the beginning of each measurement, a VE for hand opening was initially determined with the automatic search (cf. *Section* 5.3.2) with the arm lying in an arm mount (forearm in pronation, upper arm in 45° *flexion*). Then, the identified VE was tested in each of the twelve arm postures. For each posture, FES was applied three times, each trial consisting of a trapezoidal stimulation intensity profile (0.5 s ramp up → 1 s with determined stimulation intensity u (plateau) → 0.5 s ramp down). The pause between each trial was 6 s. The sequence of the tested arm postures was carried out pseudo-randomized. The resulting hand motions were recorded on video. All trials were recorded on video. Six able-bodied volunteers (female = 3, male = 3, age 25.5 ± 1.6) participated in the measurements. Written informed consent was obtained.

In the analysis, the cost function value J for hand opening was determined for each investigated arm posture. For this, the measured angles in the last third of the stimulation

phase (plateau) were averaged for each trial, as seen in Fig. E.2. This analysis window was chosen to avoid falsification by the delay of the muscular response. The hypothesis that either the rotation of the forearm, the upper arm posture, or a combination of both yield significant differences in the FES response was evaluated statistically by calculating a two-factor ANOVA[33] on the gathered cost function values. The null hypotheses were that for the two parameters—forearm rotation and upper arm posture—and their interaction, the distributions of J are equal. The level of significance was $p = 0.05$. The similarity of the variance distributions was approved in advance by applying the Levene test.

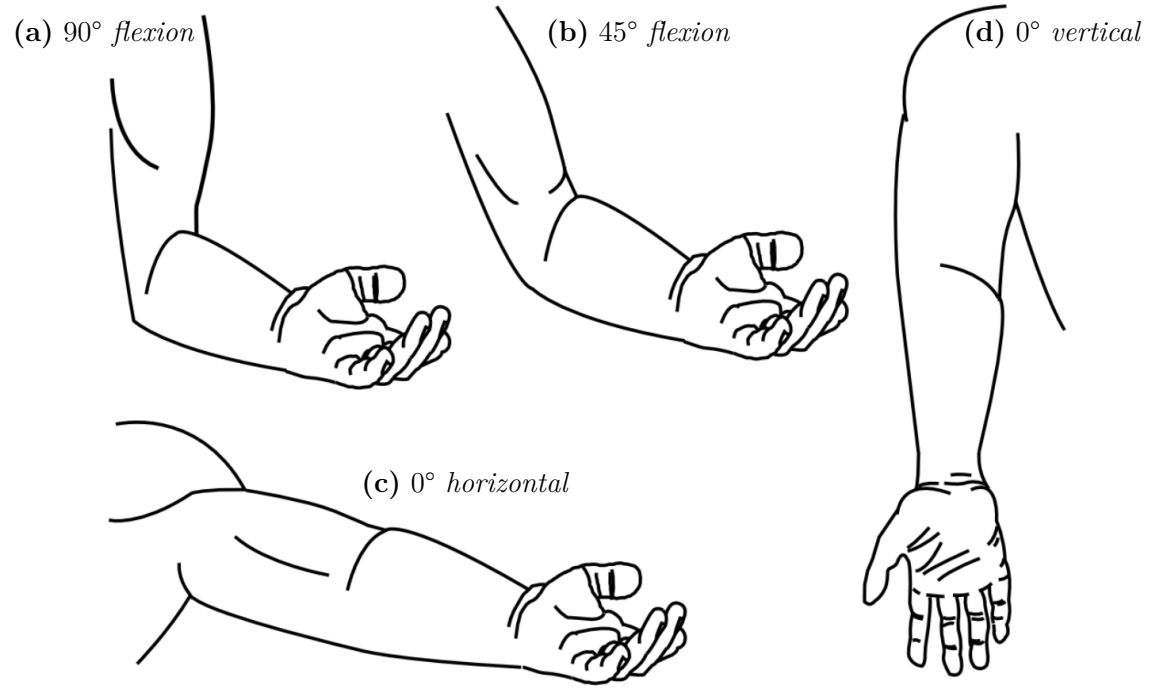

Figure E.1: Investigated upper arm positions.

Results

The results of the ANOVA are presented in Table E.1. The statistical analysis revealed that the rotational state of the forearm had a highly significant impact ($p \ll 0.05$) on the FES results for hand opening. The other tested variables, namely upper arm posture and its combination with the rotational state of the forearm, had no significant effect on the calculated quality criterion ($p > 0.05$).

A visual comparison of the measured angles and recorded videos showed that the influence of the rotational state of the forearm varied between the evaluated participants. While equally good simulation results could be achieved in subject #1 independent of the tested arm posture, the FES response of subject #6 changed entirely with the forearm being in supination. Instead of finger extension, finger flexion and non-voluntary induced, additional forearm rotation were observed. In three subjects (#1, #2, and #4), a strong radial deviation of the wrist was recognized when the forearm was in supination, as, for example, seen in Fig. E.2. This

[33]The analysis of variance, short ANOVA, refers to a collection of statistical methods for analyzing the differences among group means in a sample. Usually, the variance of one or more target variables is tested to be explained by the influence of one or more influencing variables (factors).

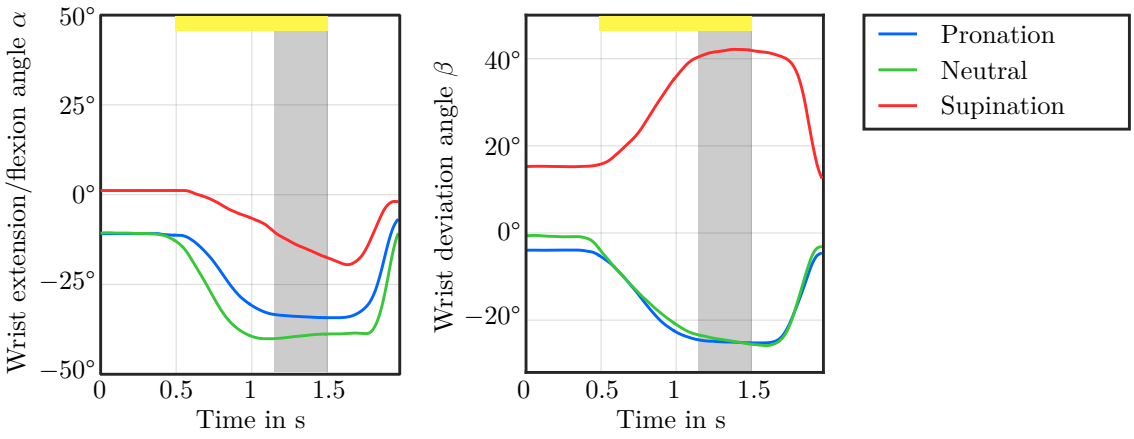

Figure E.2: Exemplarily recorded wrist angles of participant #4 over the stimulation period with the upper arm in posture 0° *vertical*. The average trials are shown for each tested forearm state, namely pronation, neutral, and pronation. The yellow bar indicates the period of maximal applied stimulation intensity (plateau; 1 s length). The gray area marks the utilized analysis window.

observation is in line with anatomical structure: Pronation/supination of the forearm is promoted unevenly on the neuromuscular structures and the covering skin. The electrode attached to the skin rotates less with the rotation of the forearm than the underlying tissue creating a relative movement of the stimulation point. In the described case of radial deviation, the stimulation point moves from the wrist and finger extensor (*E. digitorum communis*) to the radial wrist extensors (*E. carpi radialis brevis / longus*; cf. Fig. 1.4).

In summary, the existence of changes in hand movement related to the rotational state of the forearm could be proven by the analysis of the quality criterion and video recordings. It turned out that pronation and supination of the forearm significantly influence the FES-induced hand posture. Furthermore, it was found that neither the upper arm posture nor its interaction with the forearm state has a significant impact on the quality criterion. With regard to developing an automatic adaptation strategy with electrode arrays, it can be concluded that the active stimulation point—virtual electrode—should be changed in real-time with regard to the current forearm state. The posture of the upper arm does not have to be taken into account.

Table E.1: Results of the ANOVA for testing the influence of the rotational forearm state, the upper arm posture, and their combination.

Variable	Degrees of freedom	F-value	p-value
(a) Rotation of the forearm	2	7.6363	0.0006
(b) Upper arm posture	3	2.1135	0.0997
Combination of (a) and (b)	6	1.8342	0.0940

Dissertation

Christina Salchow-Hömmen